Summer 2011

Nitrate metabolism in the Epsilonproteobacteria: Campylobacter jejuni and Sulfurospirillum barnesii

Courtney Sparacino-Watkins

NITRATE METABOLISM IN THE EPSILONPROTEOBACTERIA: *CAMPYLOBACTER JEJUNI* AND *SULFUROSPIRILLUM BARNESII*

A Dissertation

Submitted to the Bayer School of Natural and Environmental Sciences

Duquesne University

In partial fulfillment of the requirements for

the degree of Doctor of Philosophy

By

Courtney E. Sparacino-Watkins

August 2011

NITRATE METABOLISM IN THE EPSILONPROTEOBACTERIA:
CAMPYLOBACTER JEJUNI AND *SULFUROSPIRILLUM BARNESII*

By

Courtney E. Sparacino-Watkins

Approved June 30, 2011

Partha Basu, PhD Professor of Chemistry and Biochemistry (Committee Chair)	Michael Cascio, PhD Associate Professor of Chemistry and Biochemistry (Committee Member)
Mihaela Rita Mihailescu, PhD Associate Professor of Chemistry and Biochemistry (Committee Member)	John F. Stolz, PhD Director, Center for Environmental Research and Education Professor of Biological Science (Outside Reader)
David W. Seybert, PhD Dean, Bayer School of Natural and Environmental Sciences Professor of Chemistry and Biochemistry	Ralph A. Wheeler, PhD Chair, Chemistry and Biochemistry Professor of Chemistry and Biochemistry

ABSTRACT

NITRATE METABOLISM IN THE EPSILONPROTEOBACTERIA:

CAMPYLOBACTER JEJUNI AND *SULFUROSPIRILLUM BARNESII*

By

Courtney E. Sparacino-Watkins

August 2011

Dissertation supervised by Partha Basu

The molecular mechanisms employed by *Campylobacter jejuni* and *Sulfurospirillum barnesii* during nitrate metabolism will be examined, specifically the periplasmic nitrate reductase (Nap) enzyme which transforms nitrate into nitrite. The catalytic subunit, NapA, is a molybdenum dependent enzyme. Isolation of molybdenum containing enzymes is not straightforward as co-factor can be lost during protein purification procedures. This study explored two protein purification methods to isolate NapA. First, NapA was isolated directly from *S. barnesii* using protein fractionation and anion exchange chromatography. Second, molecular cloning was used to express the recombinant affinity-tagged *S.barnesii* and *C. jejuni* NapA proteins from *E. coli*. Immobilized metal affinity chromatography was used to isolate the recombinant proteins. NapD was co-expressed with NapA to aid in post-translational modifications. The reduced methyl viologen assay was used to study the kinetics of nitrate reduction.

Comparison of the native and recombinant NapA kinetic properties suggests that the recombinant enzyme have attenuated activity. The theoretical structure of *C. jejuni* NapA was calculated using homology modeling techniques. Comparison of the *C. jejuni* NapA with structures of NapA from other organisms indicates that *C. jejuni* NapA has large sequence inserts on the outside of the protein. Furthermore, the *napA* operon of *C. jejuni* and *S. barnesii* display distinct gene content and organization.

DEDICATION

This dissertation is dedicated to:

- My mother, Linda Sparacino, who has always encouraged and supported my educational goals. Thank you for believing in my abilities.
- My first son, Tyler, who initially inspired me to pursue a career in the sciences. You, and your siblings, are my motivation to be successful.
- My father, Jim Sparacino, and my husband, William Watkins, for keeping me grounded and thinking practical.
- My family and close friends for their unwavering support.

ACKNOWLEDGEMENTS

First and foremost, I must thank my PhD advisor and mentor, Dr. Partha Basu. Your encouragement, guidance, and motivation over the years have facilitated me in achieving my educational goals and directed me onto the path to accomplish my career goals. I appreciate your dedication, and thank you for pushing me to strive for excellence.

I thank my current committee members, Dr. Rita Mihailescu, Dr. Michael Cascio, and Dr. John Stolz, for their guidance and time. Your ideas and suggestions have been invaluable. Dr. Stolz, your passion for research was particularly inspiring. As well, I would like to thank my past committee members, Dr. Charles Dameron and Dr. Mitch Johnson, for their guidance during my initial years. Thank you to my undergrad research advisor, Dr. Paul Birckbichler, for encouraging me to continue my chemistry education, at a graduate level. I am grateful to you for introducing me to scientific research.

A special thanks to Dr. Günter Schwarz at the University of Cologne, Germany for inviting me work in his laboratory. I appreciate the opportunity to work with you and your lab members: Dr. Jose Santamaria, Jens Herweg, Sita Arjune, Abdel Ali Belaidi, Jen-Chih Chi, Simona Jansen, Juliane Röper, Oliver Schwiese, Julika Csaszar, Julian Klein, Borislav Dejanovic. I am especially thankful to Nastassia Havarushka and Natalie Keib for helping me enjoy Germany, moreover making me feel welcome abroad. I am particularly grateful to Dr. Katrin Schrader, who provided me with countless hours of one-on-one training and guidance on molecular biology and cloning.

I graciously thank Drs. Axel Magalon and A. Andrew Pacheco for valuable discussions. A special thanks to the individuals of the research community, who guided me through the more practical aspects of my dissertation research, especially Dr. Peter

Chovanec and Claudia Almaguer. Following written protocols could not serve as a substitution for your experimental know-how.

Also I am grateful for Dr. William Miller, who provided the *C. jejuni* RM1221genomic DNA, Dr. Rishu Dheer and Shrabani Basu for *S. barnesii* SES-3 DNA. I am thankful to Lina Bird and Dr. Ganesh Naik for preliminary work on NapA. Many thanks to my good friend Dr. Peter Chovanec for performing mass spectroscopy

I thank the present and past Basu lab members for their support: Brain Kail, Barbra Serli, Bernd Hammond, Benjamin Mogesa, Eranda Perera, Indrajit Saha, Igor Pimkov, John Thomas, Kiran Venna, Samih Nassif, Lauren Marbella and Lawrence Blume. My fellow graduate students, especially Tim Evans, Suma Shetty, Anna Blice-Baum, Rachael Palchesko, Kelly Keller, Chelsee Donelan, Valerie Scott, Erin Divito, Bonnie Merchant, Meirelle Balili, Will Eckenhoff, Raj Kaur, Johanna Burnett, Chris Kabana, Matt Purzycki, Dinesh Nath, Shankar Manepalli, for supporting me both professionally and personally.

I appreciated the encouragement of the Duquesne University community, especially Dr. Paul Johnson, Dr. Alicia Paterno-Parsi, Alcira Chapman, Amy Stroyne, Dr. Jane Cavanaugh, Dr. Jennifer Aitken, Dr. Jelena Janjic, Dr. Rita Mihailescu, Sandy Russell, and Dr. Sarah Woodley. Thanks to the entire faculty and staff within the Department of Chemistry and Biochemistry at Duquesne University. In the department of Biological Sciences, I thank Dr. Peter Castric, Dr. Jana Patton-Vogt, and Dr. Nancy Turn, who always made time for my biology questions.

I would like to express my gratitude to Dean Seybert and Provost Ralph Pearson at Duquesne University, for their part in facilitating my trip to the University of Cologne.

I would like to acknowledge the Bayer School of Natural and Environmental Sciences funding my graduate education and providing teaching assistantship. The partial financial support of this work by the Office of Science (BER), U.S. Department of Energy, Grant No. DE-FG02-07ER64372 is gratefully acknowledged.

TABLE OF CONTENTS

Page

LIST OF TABLES

Page

LIST OF FIGURES

Page

LIST OF ABBREVIATIONS

SO: sulfite oxidase

XO: xanthine oxidase

DMSOR: dimethyl sulfoxide reductase

mARC: mitochondrial amidoxime reducing component

PPT: Pyranopterin

PGD: Pyranopterin guanidine dinucleotide

PCD: Pyranopterin cytosine dinucleotide

C. jejuni: *Campylobacter jejuni*

S. barnesii: *Sulfurospirillum barnesii*

E. coli: *Escherichia coli*

D. desulfuricans: *Desulfovibrio desulfuricans*

W. succinogenes: *Wolinella succinogenes*

C. necator: *Cupriavidus necator*

R. sphaeroides*: Rhodobacter sphaeroides*

nap**:** Periplasmic nitrate reductase gene

Aox: Arsenite oxidase

Arr: Arsenate respiratory reductase

Bis: Biotin sulfoxide reductase

Clr: Chlorate reductase

Ddh: Dimethyl sulfide dehydrogenase

Dor: Dimethyl sulfoxide reductase

Dms: Respiratory dimethyl sulfoxide reductase

Ebd: Ethylbenzene dehydrogenase

Fdh_H: Formate dehydrogenase-H

Fdn_N: Formate dehydrogenase-N

Pcr: Perchlorate reductase

Nap: Periplasmic nitrate reductase

pNar: Periplasmic respiratory nitrate reductase

Psr: Polysulfide reductase

Pgt: Pyrogallol–phloroglucinol transhydroxylase

Nar: Respiratory nitrate reductase

Ser: Selenate reductase

Ttr: Tetrathionate reductase

Phs: Thiosulfate reductase

Tor: Trimethylamine-N-oxide reductase

EukNR: Eukaryotic nitrate reductase

RarA: Metalloid reductase

NasA: Assimilatory nitrate reductase A

NarB: Assimilatory nitrate reductase B

Fdh: Formate dehydrogenase

DNRA: dissimilatory nitrate reduction to ammonia

TAT: Twin arginine translocase

SEC: Secretory translocase

DNA: Deoxyribonucleic acid

EDTA: Ethylene diamine tetra acetic acid

RE: Restriction endonucleases

Amp^R: Ampicillin resistance

Kan^R: Kanamycin resistance

bp: Base pair

Da: Dalton

PCR: Polymerase chain reaction

CHAPS: 3-[(3-cholamidopropyl)dimethylammonio]-1-propanesulfonate

OBGP: *n*-octyl-*β*-D-glucopyranoside

SDS-PAGE: Sodium dodecyl sulfate-polyacrylamide gel electrophoresis

CN-PAGE: CHAPS native-polyacrylamide gel electrophoresis

MQH_2: Menaquinone

UQH_2: Ubiquinone

DEAE: Diethylaminoethyl cellulose

V_{max}: Maximum velocity

K_m: Michaelis-Menten constant

K_{cat}: Catalytic constant

LB: Lysogeny broth

IPTG: Isopropyl-b-D-thiogalactopyranoside

MWCO: Molecular weight cut off

Moco: Molybdenum cofactor

DH5α: *Escherichia coli* strain DH5α

His_{6x}: Hexahistidine tag

Ni-NTA: Nickel-nitrilotriacetic acid

RNR: Ribonucleotide reductase

MV: Methyl viologen

BV: Benzyl viologen

TCA: Trichloroacetic acid

Crp: Cyclic AMP receptor protein

IscR: Iron-sulfur cluster regulator

FNR: fumarate and nitrate reductase

ModE: Molybdate-Responsive transcriptional regulator protein

NRases: Nitrate reductases

AMP: Adenosine monophosphate

VMD: Visual Molecular Dynamics

MOE: Molecular Operating Environment

PDB: Protein data bank

CHAPTER 1: Introduction

1.1. Molybdenum enzymes

1.1.1. Importance of molybdenum enzymes

Molybdenum is considered to be an essential micronutrient [4] as it is a vital component of nearly all organisms. Incorporation of the metal into the active site of metabolically essential enzymes gives rise to the necessity for molybdenum. Enzymes which are dependent on molybdenum for catalysis are generally referred to as molybdenum enzymes. Molybdenum enzymes catalyze a variety of transformations in all domains of life (i.e., eukarya, bacteria and archaea).

Sulfite oxidase, arguably the most important human molybdenum enzyme, is responsible for converting sulfite (toxic in high concentrations) into sulfate (a vital component of sulfur amino acid metabolism).[5, 6] Molybdenum cofactor deficiency hinders the enzymatic conversion of sulfite, which eventually will cause neurological damage and death. In humans, three additional molybdenum enzymes are expressed: xanthine oxidoreductase, aldehyde oxidase and the mitochondrial amidoxime reducing component (mARC). mARC, the most recently identified molybdenum enzyme, has been garnering the attention of many researchers, as it is the first non-cytochrome enzyme exclusively involved in drug metabolism. mARC is capable of reducing an assortment of N-hydroxylated compounds, [7] therefore playing an important role in pro-drug metabolism. While the physiological role of mARC is not completely defined, mARC has been implemented in nitric oxide generation and the reduction of Nω-hydroxy-L-arginine. [8] To date, more than fifty molybdenum enzymes have been identified. [9] The number of unidentified molybdenum enzymes may be comparable. [10] While only a

handful of eukaryotic molybdenum enzymes have been identified, prokaryotic molybdenum enzymes are numerous. To stay within the context of this study, prokaryotic molybdenum enzymes will be discussed in detail within the subsequent sections.

1.1.2. Classification of molybdenum enzymes

Molybdenum enzymes have been divided into two groups according to the active site architecture: multinuclear or mononuclear molybdenum enzymes. [11-13] The multinuclear molybdenum enzyme, nitrogenase (EC 1.18.6.1), catalyzes fixation of nitrogen gas (N_2) into ammonia. [14] Nitrogenase has an iron-molybdenum cofactor active site. Mononuclear molybdenum enzymes are far more abundant. A basic pterin structure, known as the pyranopterin (PPT) (**Figure 1.1**) has been identified in all mononuclear molybdenum enzyme isolates. The PPT is located in the interior of the enzyme, clenched by multiple non-covalent interactions. Over 40 hydrogen bonds are formed between the PPT and protein. Consequently no consensus sequence exists for PPT binding.

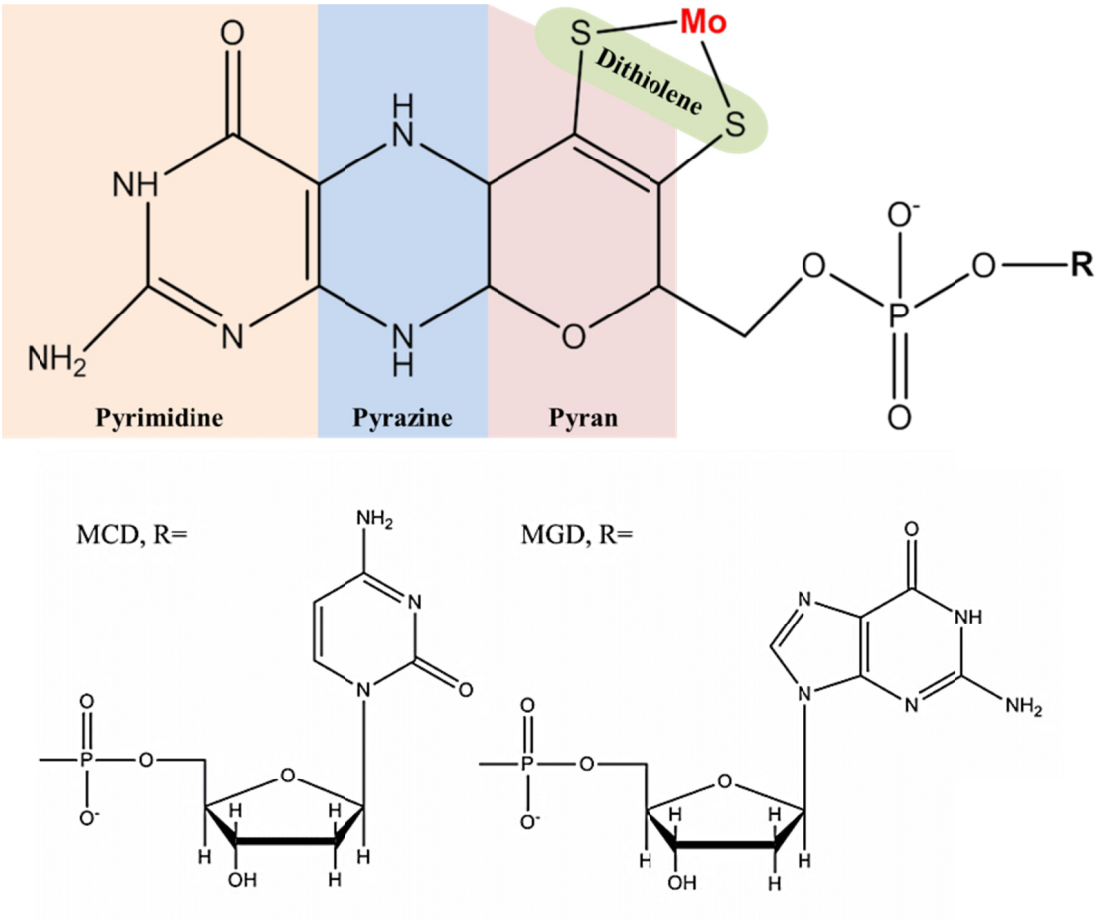

Figure 1.1: The structure of pyranopterin (PPT) with bound molybdenum: the basic pterin unit conserved in all mononuclear molybdopterin enzymes. R = H, monophosphate, guanidine dinucleotide (PGD) or cytosine dinucleotide (PCD).

Pyranopterin- containing enzymes have been categorized by Hille into three families based on the active site structure: sulfite oxidase (SO), xanthine oxidase (XO) and dimethyl sulfoxide reductase (DMSOR) (**Figure 1.2**). [15] Recently a fourth family, referred to as the mARC family hereon, has been proposed following the characterization of mARC. [16] Enzymes in the SO, mARC, and XO families contain one PPT molecule per mole of protein. DMSOR family enzymes contain two (**Figure 1.3**), the PPT molecules are arranged anti-parallel around the molybdenum center. In addition to the PPT dithiolene sulfur donors, the oxidized molybdenum is coordinated by additional ligands. In the SO family, two oxo ligands and a protein derived cysteinyl sulfur; in the

XO family, an oxo, a hydroxyl and a sulfide; in the mARC family, two oxo ligands and sulfur or oxygen are contributed by an unidentified protein residue. In lieu of detailed spectroscopic and crystallographic data, mARC is proposed to have a similar coordination as the SO family, except that cysteine is not involved in covalent bonding.[16] In the DMSOR family four dithiolene sulfurs, provided by two PPT molecules, coordinate molybdenum in the active site. Typically, a protein derived sulfur, oxygen or selenocysteine also coordinate molybdenum. The identity of the amino acid ligands varies greatly within the DMSOR family and is dependent on the chemistry of the reaction catalyzed.

In general, molybdopterin enzymes function either via oxygen atom transfer reactions or hydroxylation. The two electron oxidation or reduction of the substrate is coupled to the reduction or the oxidation of molybdenum. During the catalysis molybdenum shuttles between the fully oxidized (+6) and reduced (+4) oxidation states. In some cases, the molybdenum center is also associated other redox centers (e.g. iron sulfur clusters or heme) for electron transfer. [17]

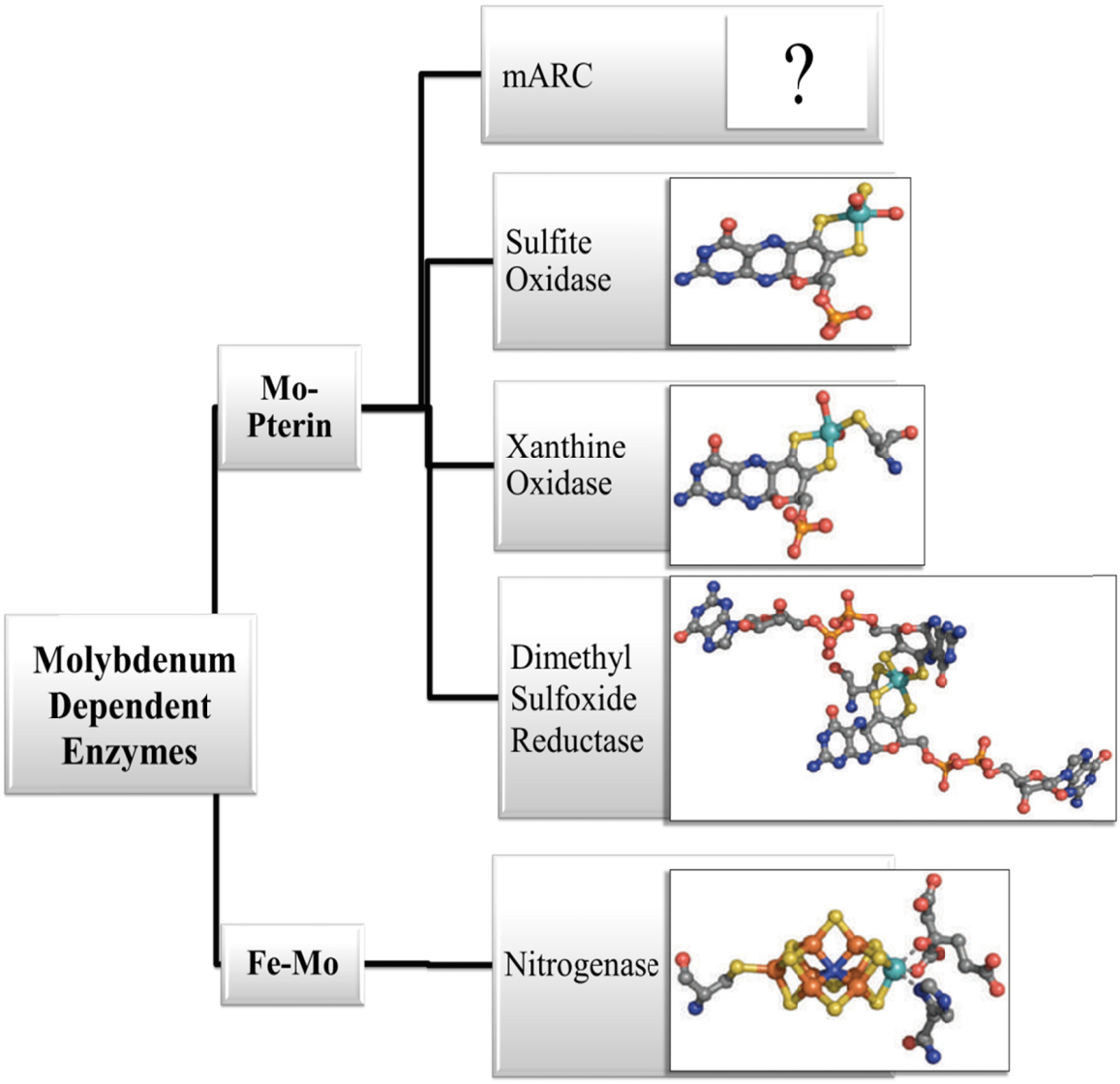

Figure 1.2: Categorization of molybdenum enzymes. Cofactor inserts from Schwarz *et al.* [18] Used with permission from the publisher (license number 2707751006623).

1.1.3. Diversity and functional significance of the molybdopterin (PPT)

Eukaryotes contain an unmodified PPT. Prokaryotes contain an amended PPT with a dinucleotide group (the "R" group in **Figure 1.1**). Either a guanidine dinucleotide (pyranopterin guanidine dinucleotide, PGD) or cytosine dinucleotide (pyranopterin cytosine dinucleotide, PCD) are attached to the PPT via a phosphate linkage. [19] In the DMSOR family, two PGD molecules are arranged anti-parallel around the molybdenum center (**Figure 1.3**). When bound to molybdenum, the entire cofactor is referred to as the *bis*pyranopterin guanine dinucleotide (Mo-*bis*PGD).

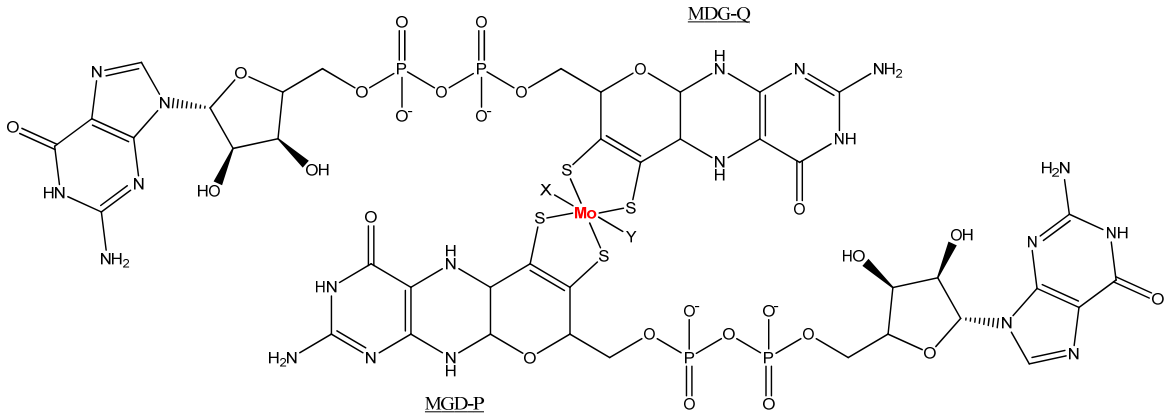

Figure 1.3: The *bis*pyranopterin guanine dinucleotide (*bis*PGD) molybdenum cofactor. Only mononuclear molybdenum enzymes within the DMSOR family contain the *bis*PGD cofactor.

In general PPT biosynthesis is conserved in eukaryotes and prokaryotes, although prokaryotes are capable of an additional step which transforms the basic pterin into the more complex nucleoside cofactor (**Figure 1.3**). [18, 20] Eukaryotes do not encode the genes responsible for nucleoside bound PPT synthesis, as the modified PPT containing enzymes have only been identified in prokaryotes.[18, 21] In humans mutation of the PPT biosynthesis pathway has fatal consequences. Due to the unavailability of PPT all

molybdopterin enzymes (e.g., sulfite oxidase, aldehyde, and xanthine oxidoreductase) are inactivated. Fortunately reconstitution of the PPT cofactor into the inactive enzymes is possible for some forms of molybdopterin biosynthesis deficiencies. [22]

In addition to acting as a scaffold for molybdenum the PPT is thought to be involved in enzyme catalysis. The dithiolene ligand (**Figure 1.3**) may play a role in the substrate transformation mechanism. [23] The dithiolene ligands are located in the first coordination sphere around molybdenum. Additionally, the pyrimidine may provide a route for intermolecular electron transfer between the active site and additional redox centers. [24], [25] A conserved amino acid residue unites the iron sulfur cluster and molybdopterin active site (**Figure 1.4**). Mutagenesis of this residue, for instance the lysine in formate dehydrogenase (**Figure 1.4**), inactivates the enzyme. [26]

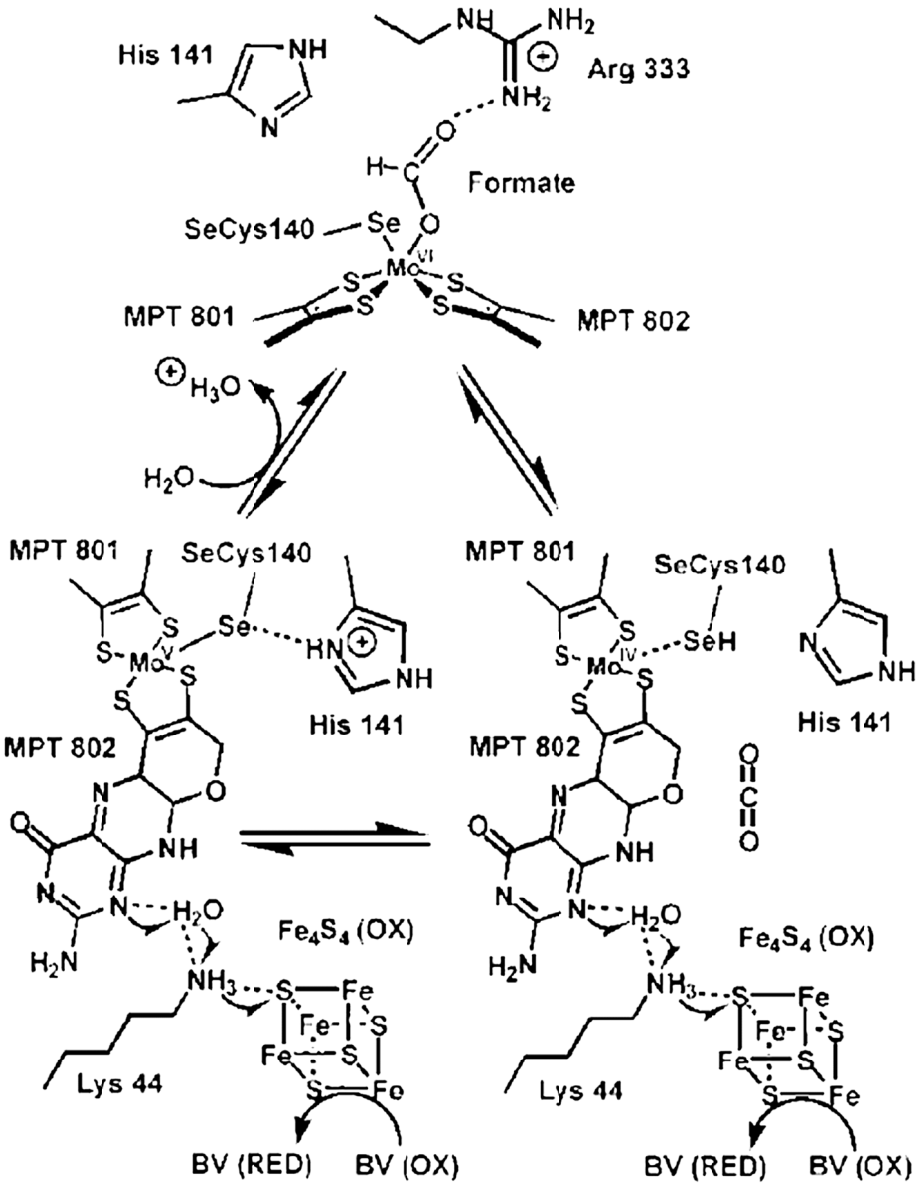

Figure 1.4: The hypothesized route of intermolecular electron transport within DMSOR enzymes. In formate dehydrogenase (Fdh), the substrate, formate, transfers electrons to the molybdenum active site, then, via the PGD-P (labeled "MPT 802") and a lysine (Lys 44) residue the electrons are sent to the iron sulfur cluster. An external electron acceptor, in this figure, benzyl viologen (BV). This figure, originally published by Boyington *et al.* in Science (1997), [24] was used with permission by the publisher. License Number: 2659110526821.

The pyranopterin ring, which is also redox active, has been proposed by Enemark to provide a route of proton transfer. [27] The properties of the natural enzyme bound PPTs are not completely understood. Although synthetic models of the PPT demonstrate that the pyran ring is capable of scission and condensation. The closed, pyran ring is illustrated in **Figure 1.1**. Most structurally characterized DMSOR enzymes are reported to harbor closed pyran rings in the *bis*PGD cofactor (**Figure 1.3**). However two DMSOR enzyme structures, ethylbenzene dehydrogenase (Ebd) and respiratory nitrate reductase (Nar), contain an open pyran ring. In the crystal structure of *Aromatoleum aromaticum* Ebd the PGD-P pyran ring is open. [28] The PGD-P pyranopterin is relatively closer, compared to the PGD-Q, to the iron sulfur cluster and is believed to aid in electron transfer from the iron sulfur cofactor to the molybdenum cofactor. Conversely, the PGD-Q, which is distal to the iron sulfur cofactor, is open in the structure of respiratory nitrate reductase from *E. coli*. PGD-Q is proposed to be involved in proton translocation from the active site to the external environment.[29] **Figure 1.4** illustrates the proposed route of electron transport from the molybdenum active site to the iron sulfur cluster via proximal pyranopterin (PPT-P) in formate dehydrogenase. Crystal structures cannot verify if the PGD-P and PGD-Q are redox active, although these observations do raise the possibility of a functional advantage of the *bis*PGD cofactor in the DMSOR family enzymes. In any case, the *bis*PGD does not have an experimentally demonstrated role in catalysis. The question remains: could the two PGD moieties (designated PGD-P and PGD-D in **Figure 1.3**) confer discrete functions? This question can only be addressed though purification and characterization of the enzymes.

1.1.4. The DMSOR family of molybdopterin enzymes

Molybdopterin containing enzymes in DMSOR family participate in a diverse collection of reactions. The majority are involved in the global cycling of nitrogen, sulfur and carbon.[30] To date, several enzymes of the DMSOR family have been identified and many have been structurally characterized (**Table 1.1**). In general the DMSOR family enzymes exhibit a high degree of structural similarity:[17] an alpha and beta (α/β) type fold with four domains, and a *bis*PGD cofactor, which is buried in the core of the protein and accessible through a large (over 14 Å deep) catalytic funnel in the center of the enzyme. However the differences among the DMSOR family enzymes are more noteworthy, such as active site heterogeneity, iron sulfur cofactor content, and oligomeric state. The following sections will describe the differences among the DMSOR family enzymes, and exactly how these somewhat subtle modifications can extrapolate into catalytic diversity.

Almost all molybdopterin enzymes in the DMSOR family catalyze redox reactions (**Table 1.2**). Molybdenum, which transitions between oxidation states (+4 and +6), must receive and export electrons from the active site in order to achieve catalytic turnover. The route of electron transport, either to or from the active site, involves additional redox centers (e.g. iron sulfur clusters), amino acid residues and other redox active proteins.

Table 1.1: Structurally characterized, DMSOR molybdopterin enzymes. All enzymes have the *bis*PGD, which provides four dithiolene sulfur ligands.

Enzyme name	α subunit		β subunit redox centers	γ subunit redox centers	Organism	PDB ID
	Mo-*bis*PGD)	redox center				
Dimethyl sulfoxide reductase (Dor)	(Oγ)Ser, =O	–	–	–	*Rhodobacter capsulatus*	1H5N[31]
					Rhodobacter sphaeroides	1EU1[32]
Pyrogallol-Phloroglucinol Transhydroxylase	(Oγ)Ser, =O	–	3x[4Fe-4S]	–	*Pelobacter acidigallici*	1VLD[33]
Trimethylamine N-oxide reductase (Tor)	(Oγ)Ser,=O	–	–	–	*Shewanella massilia*	1TMO[34]
Arsenite oxidase	=O, –OH	[3Fe-4S]	[2Fe-2S]	-	*Alcaligenes faecalis*	1G8J[35]
Formate Dehydrogenase (Fdh)	(Seγ)SeCys, –OH	[4Fe-4S]	-	-	*Escherichia coli*	1FDO[24]
						2IV2[36]
W - Formate Dehydrogenase (W-Fdh)	(Seγ)SeCys, =S	[4Fe-4S]	3x[4Fe-4S]	–	*Desulfovibrio gigas*	1HOH[37]
Periplasmic nitrate reducatase (Nap)	(Sγ)Cys, =S	[4Fe-4S]	–	–	*Desulfovibrio desulfuricans*	2JIM[38]
						2Nap[39]
			2 x heme *c*	–	*Cupriavidus necator*	3ML1[40]
					Rhodobacter sphaeroides	1OGY[41]
					Escherichia coli	2NYA[42]
Polysulfide reductase (Psr)	(Sγ)Cys, (O)water	[4Fe-4S]	4x[4Fe-4S]	no cofactor	*Thermus thermophilus*	2VPZ[43]
Formate dehydrogenase (Fdh_N)	(Seγ)SeCys, –OH	[4Fe-4S]	4x[4Fe-4S]	2x heme *b*	*Escherichia coli*	1KQG[44]
Respiratory nitrate reductase (Nar)	(Oδ1) (Oδ2)Asp	[4Fe-4S]	3x [4Fe-4S], [3Fe-4S]	2x heme b	*Escherichia coli*	1R27[45]
	(Oδ2)Asp					1Q16[29]
Ethylbenzene dehydrogenase (Ebd)	(Oδ2)Asp, (O)acetate	[4Fe-4S]	3x [4Fe-4S], [3Fe-4S]	heme *b*	*Aromatoleum aromaticum*	2IVF[28]

Cofactor content varies significantly among enzymes in the DMSOR family. To generalize, the DMSOR enzymes are categorized into four sub-categories (labeled as groups in **Table 1.3**) based on the iron sulfur cluster content in the Mo-enzyme and oligomeric state. The method of organization was proposed by Magalon *et al.* [46]. In group I the molybdopterin subunit only contains the *bis*PGD cofactor. No iron sulfur cluster binding motif is present in the catalytic subunit, confirmed by the structures of dimethyl sulfoxide reductase (DorA), Pyrogallol-Phloroglucinol Transhydroxylase and Trimethylamine N-oxide reductase (TorA) (**Table 1.1**). The remaining three groups contain iron sulfur binding motifs which are located at the peptide N-terminus. In the three dimensional enzyme structures the iron sulfur cluster is situated roughly 12 Å from the PGD-P. [46] Two types of iron sulfur cluster (i.e. [3Fe-4S] and [4Fe-4S]) have been identified in the structurally characterized enzymes, providing a second degree of categorization. Group II enzymes encode a [3Fe-4S] binding motif (i.e. C-X_2-C-X_3-C), as found in arsenite oxidase (Aox). Groups III and IV encode a [4Fe-4S] binding motif (i.e. C/H-X_2-C-X_3-C-$X_{24\text{-}26}$-C). Group IV, referred to as the "complex iron-sulfur molybdoenzymes" by Magalon *et al.*, form a stable tetramer (αβγ subunits), as exemplified by the structures of polysulfide reductase (Par), respiratory nitrate reductase (Nar), and formate dehydrogenase-N (Fdh_N). Conversely, the group III enzymes do not have strong interactions with membrane bound subunits.

Table 1.2: The reactions catalyzed by mononuclear molybdenum enzymes of the DMOSR family.

Enzymes	Reaction catalyzed	$E^{o\prime}$ (V)
Arsenite oxidase (Aro & Aox)	$As^{(V)}O_2^- + 2H_2O \rightarrow As^{(III)}O_4^{3-} + 4H^+ + 2e^-$	+ 0.56
Arsenate reductase (Arr)	$AsO_4^{3-} + 4H^+ + 2e^- \rightarrow AsO_2^- + 2H_2O$	- 0.71
Biotin sulfoxide reductase (Bis)	$C_{10}H_{16}N_2O_4S + 2H^+ + 2e^- \rightarrow C_{10}H_{16}N_2O_3S + H_2O$	
Chlorate reductase (Clr)	$ClO_3^- + 3H^+ + 2e^- \rightarrow HClO_2 + H_2O$	+ 1.18
dimethyl sulfide dehydrogenase (Ddh)	$Me_2S + H_2O \rightarrow Me_2SO + 2H^+ + 2e^-$	+ 0.16
Dimethyl sulfoxide reductase (Dor & Dsm)	$Me_2SO + 2H^+ + 2e^- \rightarrow Me_2S + H_2O$	- 0.16
Ethylbenzene dehydrogenase (Ebd)	$C_8H_{10} + H_2O \rightarrow C_8H_{10}O + 2H^+ + 2e^-$	
Formate dehydrogenase (Fdh &Fdn)	$HCOOH \rightarrow CO_2 + 2H^+ + 2e^-$	- 0.42
Nitrate reductases (Nap, pNar & Nar)	$NO_3^- + 2H^+ + 2e^- \rightarrow NO_2^- + H_2O$	+ 0.42
perchlorate reductase (Pcr)	$ClO_4^- + 2H^+ + 2e^- \rightarrow ClO_3^- + H_2O$	+ 1.19
polysulfide reductase (Psr)	$S_n^{2-} + 2H^+ + 2e^- \rightarrow S_{(n-1)}^{2-} + H_2S$	
pyrogallol–phloroglucinol transhydroxylase (Pgt)	$C_6H_6O_3 \rightarrow C_6H_6O_3$	
Selenate reductase (Ser)	$SeO_4^{2-} + 2H^+ + 2e^- \rightarrow SeO_3^{2-} + H_2O$	+ 1.15
tetrathionate reductase (Ttr)	$S_4O_6^{2-} + 2H^+ + 2e^- \rightarrow 2S_2O_3^{2-} + H_2O$	+ 0.08 + 0.17
thiosulfate reductase (Phs)	$S_2O_3^{2-} + 2H^+ + 2e^- \rightarrow SO_3^{2-} + H_2S^2$	- 0.40
Trimethylamine N-oxide reductase (Tor)	$Me_3NO + 2H^+ + 2e^- \rightarrow Me_3N + H_2O$	+ 0.13

Table 1.3: The iron sulfur content and subunit composition of DMSOR family enzymes. Cytoplasmic molybdopterin proteins are denoted within the table with **bold text**. The redox active cofactors are denoted as follows: iron sulfur clusters ([4Fe-4S], [3Fe-4S], [2Fe-2S], or [Fe-S]); c-type cytochrome (***c***); *b*-type cytochrome (***b***), no redox cofactor motif (**-NA-**), W-*bis*PGD (ǂ); Mo-*bis*PGD. If more than one co-factor is present the total amount in each enzyme is indicated by an Arabic number and an "x" (*i.e.* 2 x).

DMSOR group	Alpha subunit Mo-*bis*PGD		Beta subunit					Gamma subunit			
			c	3 x[4Fe-4S] [3Fe-4S]	3x [4Fe-4S]	rieske [2Fe- 2S]	4 x [4Fe-4S]	4-5 x *c*	2 x *b*	-NA-	[Fe-S]
I		TorA						TorC			
		DorA						DorC			
		BisC									
		PgtL			**PgtS**						
II	[3Fe-4S]	AoxB				AoxA					
		AroA				AroB					
III	[4Fe-4S]	NapA	NapB					NapC			
		ArrA		ArrB							
		EbdA		EbdB					EbdC		
		DdhA		DdhB					DdhC		
		SerA		SerB					SerC		
		ClrA		ClrB					ClrC		
		PcrA		PcrB					PcrC		
		pNarG		pNarH							
		FdhAǂ			FdhB			CytC			
		FdhF					**HycB**				**FHL**
IV	[4Fe-4S]	FdnG					FdnH		FdnI		
		PhsA					PhsB		PhsC		
		TtrA					TtrB			TtrC	
		PsrA					PsrB			PsrC	
		DmsA					DmsB			DmsC	
		NarG		**NarH**				**NarI**			
		NarZ		**NarY**				**NarV**			

Enzyme abbreviations: arsenite oxidase (**AoxAB**), arsenate respiratory reductase (**ArrA**), biotin sulfoxide reductase (**BisC**), chlorate reductase(**ClrABC**), dimethyl sulfide dehydrogenase (**DdhABC**), dimethyl sulfoxide reductase (**DorAC**), dimethyl sulfoxide reductase (**DmsABC**), ethylbenzene dehydrogenase (**EbdABC**), formate dehydrogenase-H (**FdhAB**), formate dehydrogenase-N (**FdnGHI**), perchlorate reductase (**PcrABC**), periplasmic nitrate reductase (**NapABC**), periplasmic respiratory nitrate reductase (**pNarGH**), polysulfide reductase (**PsrABC**), pyrogallol–phloroglucinol transhydroxylase (**PgtLS**), respiratory nitrate reductase (**NarGHI**), selenate reductase(**SerABC**), tetrathionate reductase (**TtrABC**), thiosulfate reductase (**PhsABC**), trimethylamine-N-oxide reductase (**TorAC**).

Cofactor content is an important part of understanding the physiological function and mechanism of each enzyme. Each cofactor confers a different redox potential, thereby affecting the overall electron transport and catalysis. For example, many of the group III and IV enzyme complexes are involved in electron transport from membranous quinone pools. Electron transport can be coupled to respiration and therefore energy conservation. Functionally homologous enzymes, which catalyze the same reactions but are structurally different (i.e. cofactor content and subunit composition) may confer a selective advantages in preforming their respective physiological function.

For example, the periplasmic nitrate reductase (NapABC) and respiratory nitrate reductases (NapGHI) use nitrate reduction for very different roles in the cell. The periplasmic nitrate reductase, which in some organisms is a NapA monomer, is linked to detoxification or redox balance. Conversely, the Nar complex is always employed for nitrate respiration. NarG has a tight association with the redox active NarHI and is capable of coupling nitrate reduction to respiration. NarI is a quinone oxidase that transports electrons from the membrane to the molybdenum catalytic site. In some organisms the NapABC complex has been linked to nitrate respiration, [47] however NapAB interacts more transiently with NapC. Before discussing the significance of the cofactor content and presence (or absence) of additional redox proteins in nitrate reductase enzymes, the physiological functions nitrate reduction (**section 1.2**) and the difference in the Nap system (**section 1.3**) will be introduced. The Nap subunit content varies immensely among organisms, thus generalizations in regard to the relationship between the Nap subunit composition and the function of Nap are not straightforward.

A second aspect in which the DMSOR enzymes differ is the active site structure, which confers more obvious effects on the chemistry of each catalyzed reaction. In addition to the substrate selectivity provided by surface exposed amino acid residues, the catalytic diversity demonstrated by the DMSOR family is a result of variations within the active site. Specifically, the surrounding residues (non-covalently bound) and metal coordination sphere. **Figure 1.5** [13] illustrates the differences in the non- covalently bound residues that are located directly above the molybdopterin active site. The superimposition of the formate dehydrogenase (Fdh) and periplasmic nitrate reductase (Nap) structures in **Figure 1.5** reveals the structural conservation of the *bis*PGD. The residues surrounding the active site, although not covalently bound to molybdenum, play a crucial role in catalysis. In formate dehydrogenase a conserved histidine is responsible for proton abstraction during formate oxidation (**Figure 1.4**). [24] Similarly non-covalently bound active site residues are involved in catalysis, alanine in arsenate oxidase, tyrosine in Dms, lysine in Ebd.

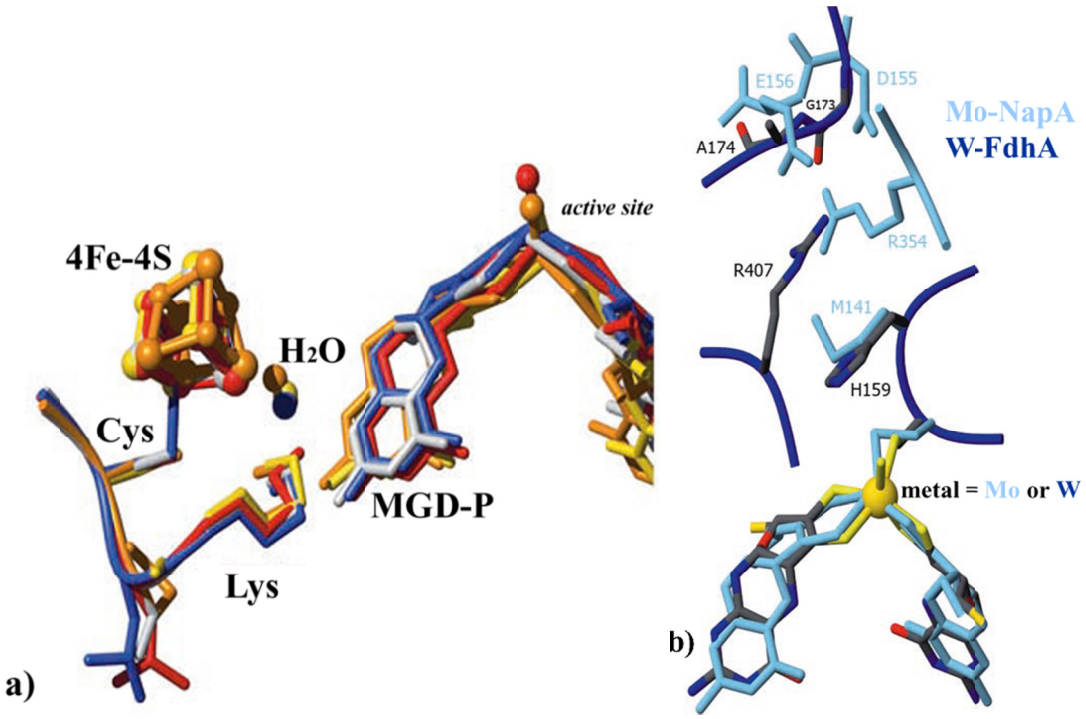

Figure 1.5: The structural superimposition of periplasmic nitrate reductase (Mo-NapA) and formate dehydrogenase (W-FdhA) illustrating the similarities in the vicinity of the iron sulfur cluster and differences in the residue composition surrounding the active site. **a)** Structural conservation of the electron transport pathway; the active site is linked to the [4Fe- 4S] cluster by the PGD-P ligand, a conserved water residue and a lysine residue, all are present is FdhA and NapA. Five structures were superimposed in this figure. **b)** The amino acid residues located in the active sites of NapA and FhdA differ. The residues line the substrate channel lending to substrate specificity, and can be involved in catalysis (for example, the histidine in Fdh deprotonates formate). The residues are represented as sticks, and labeled according to the respective residue number: Fdh (PDB 1HOH) with black labels and residues color-coded according to element; NapA has blue labels and structures (PDB_2Nap).This figure, published by José Moura *et al.*in the Journal of Biological Inorganic Chemistry (2004), [13] was modified and used with the publishers permission: License number 2661940798241.

The covalently bonded ligands, which are directly involved in reaction mechanism, also vary significantly (**Table 1.1**). It is important to note that the ligand composition surrounding the metal in the active site is not stagnant. The number of coordinating ligands is subject to the oxidation state of the metal [48] (molybdenum, or in select cases tungsten). For simplicity, the oxidized molybdenum, Mo^{VI}, will be discussed. Most enzyme isolates are oxidized a result of purification. Consequently, more structural data are available for the oxidized Mo^{VI} state. As previously described, molybdenum is ligated in the active site by four dithiolene sulfurs provided by the PPT cofactor (**Figure 1.3**). In addition to the four dithiolene sulfurs, one ligand is typically donated from an amino acid side chain: sulfur from cysteine, selenium from selenocysteine, and oxygen from aspartate or serine. Arsenate oxidase, which does not contain a coordinating amino acid,[35] is the exception to this generalization. The sixth ligand is typically an oxo- (=O), hydroxyl- (–OH), sulfido- (=S), or sulfanyl- (–SH), however the nature of this ligand is difficult to assess experimentally.

As mentioned previously the type of metal in the active site can also vary. The PPT can bind tungsten (W) or molybdenum (Mo). Mo-PPT enzymes are more common, presumably due to the relatively greater abundance of Mo on Earth. In general, organisms which utilize W-PPT enzymes exclusively are extremophiles, and grow at higher temperatures. Interestingly, some enzymes can retain activity with either W or Mo in the active site, such as dimethyl sulfoxide reductase isolated from *R. capsulatus*; [49] conversely, the replacement of Mo with W in the growth media can also abolish function, as observed in *E. coli* periplasmic nitrate reductase. [50]

Of the DMSOR family enzymes, formate dehydrogenase and nitrate reductase are the most extensively studied. [13] In fact, the numerous studies conducted on these enzymes have increased our knowledge of molybdopterin enzymes as a whole. Still, with each new isolate, variation in the active site and functionality is revealed. For example, the formate hydrogen lyase (Fdh_H) complex was isolated with W in the active site *Desulfovibrio gigas* and as a Mo-containing enzyme from *E. coli.* [24] The second type of formate dehydrogenase (Fdh_N), which is linked nitrate respiration, has only been isolated as a Mo enzyme. [44] Nitrate reductases, which have even more diverse physiological functionality, exhibit diverse active sites; the ligand composition in the metal coordination sphere varies among the three types of nitrate reductases. Nap and Nas contain coordinating cysteine sulfur. Nar utilizes oxygen from asparagine. A detailed discussion on the active site variability within nitrate reductase will be covered in a latter section (**section 1.2.1.**), as exploring the molecular basis for the catalytic diversity exhibited by bacterial nitrate reductases is a fundamental motivation for this dissertation.

1.2. Nitrate reductases

The enzymatic reduction of nitrate to nitrite via nitrate reductases (NRases) is ubiquitous in nature, as a result the environmental and physiological significance of NRases have been investigated for well over 50 years. This section will provide a summary on the importance of nitrate reduction in human health and the global nitrogen cycle.

1.2.1. The pathological significance of nitrate reductases in humans

Nitrogen is vital for all forms of life on Earth, as it is an indispensable component of peptides and nucleic acids. Humans typically obtain nitrogen in the form of nitrate.

Food, such as fruits, vegetables, grains, meat, and dairy products, is the main source of nitrogen. [51] Organic nitrogen (i.e. amino acids) is also an important nitrogen source. The natural concentration of nitrate in meats is low (~5 mg • kg^{-1}); however, nitrate (and nitrite) are added in higher concentrations (>10 mg • kg^{-1}) to "cure" mea*t.* [51] Plants can contain much larger concentrations of nitrate, from 13 mg • kg^{-1} in asparagus, to a high of 2500 mg • kg^{-1} in spinach.

In general, nitrate is considered to be inert. The only example of "nitrate toxicity" in humans, methemoglobia, is the result of nitrate reduction to nitrite by bacterial nitrate reductases (NRases) in the oral cavity [52-54] and gastrointestinal tract. [55-59] On the other hand, nitrite does manifest various pathological consequences. In methemoglobia, nitrite (or other oxidants) can react with the iron center of hemoglobin, oxidizing the Fe^{2+} to Fe^{3+}, producing methemoglobin. Methemoglobin cannot bind and transport oxygen, a condition which would quickly progress into deadly consequences. Methemoglobin reductases quickly transform methemoglobin back into hemoglobin. Unfortunately, infants do not have high levels of methemoglobin reductase at birth, and as a result methemoglobin levels can accumulate in the blood stream, leading to hypoxia. In the United States methemoglobia is associated with nitrate and/or nitrite contaminated well water, although congenital methemoglobia does exist.

Nitrate reductases have not been identified from any human (or vertebrae) tissue, although nitrate reduction occurs throughout the gastrointestinal tract by the microbial flora.[60] Many gastrointestinal pathogens, such as *E. coli*, *Campylobacter* species and *Helicobacter* species, can grow on nitrate and nitrite.[61] [62] For many years, nitrate reductases have been implicated in human carcinogenesis,[63] due to the generation of

multiple “toxic” nitrogenous compounds, such as nitrite, ammonia and nitrosamines.[64-67] As previously described, nitrite toxicity would be a significant risk for individuals which are prone to methemoglobia.[68] While nitrate reduction can produce toxic nitrogen compounds, recent studies describe the beneficial consequences of microbial nitrate reduction.[68] These studies focus on the influence of commensal bacteria nitrate reduction in human health. Lundberg *et al.* contend that nitrite aids in the human host’s defense mechanisms, mucus generation, and vasodilation; [69] as nitrite can be transformed to nitric oxide under acidic conditions. Nitric oxide (NO) is a pluripotent signaling molecule in the human body, and is very important in vasodilation.[70] The prospective benefits of nitrate or nitrite therapy in myocardial infarction, stroke, systemic and pulmonary hypertension, and gastric ulceration have been postulated.[71, 72] The involvement of microbes in organ function is a relatively new concept; however, evidence that microbial activity can affect organ function in mammals is increasing [73, 74]. Detailed biophysical studies conducted on the pathogenic or communalistic specific NRases can provide insight into the effects of bacterial nitrate reduction in the human gastrointestinal tract.

1.2.2. The environmental impact of nitrate reduction

Nitrate reductases play a key role in the global nitrogen cycle. Nitrogen is cycled through the environment and living organisms, shifting oxidation state and transforming through chemical reactions (**Figure 1.6**). The stable nitrogen species involved in the global nitrogen cycle are nitrate (NO_3^-), nitrite (NO_2^-), nitrogen dioxide (N_2O), nitric oxide (NO), nitrogen gas (N_2), ammonia (NH_3^+) and ammonium (NH_4^+). Nitrate and ammonium are important nitrogen sources for plants; the fixation of nitrogen in sediment prevents the loss of nitrogen into the atmosphere via volatile nitrogen species (e.g., N_2, NO) and run off into the water table. Disruption of the nitrogen cycle has consequences for plants and humans. Human activity, through the use of fossil fuels and nitrogen rich fertilizers, disrupts the environmental nitrogen balance. As a result, water supplies become contaminated with agricultural run-off (nitrates and ammonia), and nitrogen dioxide is released into the atmosphere through the burning of fossil fuels. Nitrogen dioxide is the 3rd most abundant greenhouse gas, although it possesses the greatest heating capacity, over carbon dioxide and methane.

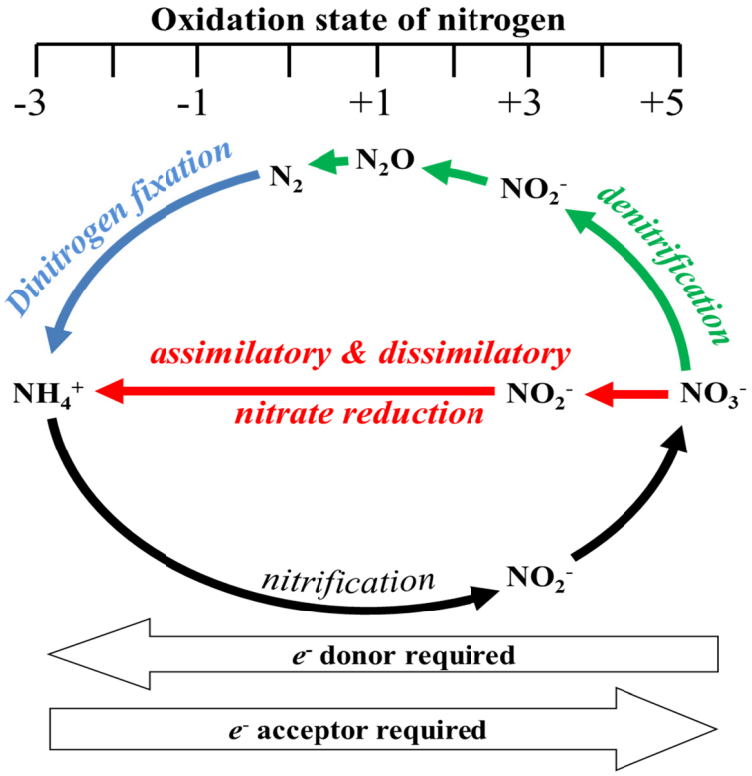

Figure 1.6: A schematic representation of the nitrogen cycle. Reproduced from Stolz and Basu (2002). [75] Copy right clearance was given by the publisher (license number 2707740565498)

1.2.3. Assimilatory vs. Dissimilatory nitrate reduction

Nitrate reduction is commonly designated as either an assimilatory or a dissimilatory metabolic process (**Figure 1.7**). Assimilatory nitrate reduction, a type of constructive metabolism, is the transfer of nitrogen from nitrate into the organism's biomass. Conversely, dissimilatory nitrate reduction, a type of deconstructive metabolism or catabolism, does not incorporate the products of nitrate reduction into the biomass, instead the products are excreted from the cell. In some cases, dissimilatory nitrate reduction is an energy yielding process; therefore, the term "nitrate respiration" is used to specify nitrate reduction coupled to ATP generation. Dissimilatory nitrate reduction can be further divided into two categories, denitrification and dissimilatory nitrate reduction to ammonia (DNRA) (**Figure 1.7**). DNRA is an important part of the global nitrogen

cycle, as the ammonia produced can be stored in the soil; whereas denitrification generates volatile compounds, which accumulate in the atmosphere.

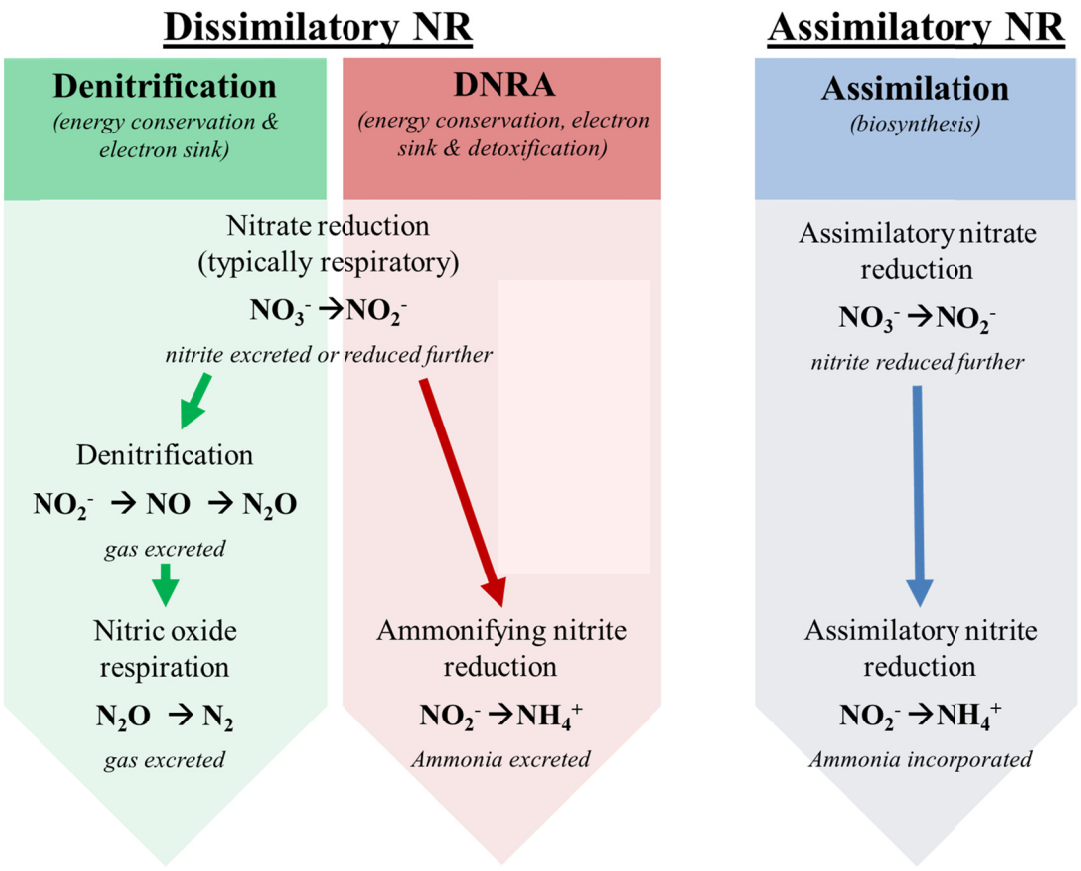

Figure 1.7: Diagram of dissimilatory and assimilatory nitrate reduction (NR). Modified from Zumft, 1997. [76]

1.2.4. Taxonomy of prokaryotic nitrate reductases

Nitrate reductases are classified into four groups, based on the catalytic site of the molybdopterin containing subunit, cellular location and the metabolic pathway in which it precipitates.[75] Animals do not encode a classical nitrate reductase; therefore, only the combined efforts of plant and microbial nitrate reduction contribute to the global nitrogen cycle. Plant eukaryotic assimilatory nitrate reductase (EukNR) will not be discussed in detail, as it is beyond the scope of this study.

Three prokaryote nitrate reductases have been identified: one assimilatory nitrate reductase (Nas) and two dissimilatory nitrate reductases Nar and Nap. [75] All nitrate

reductases contain two redox active cofactors, a Mo-PPT and an iron sulfur cluster. The catalytic subunits of both dissimilatory nitrate reductases, NapA and NarG, are members of the DMSOR family as they contain the *bis*PGD cofactor. The assimilatory nitrate reductases, EukNR and NasA, are predicted to be members of the SO family (**Figure 1.8**).Based on spectroscopic studies and amino acid composition the active site of NasA is predicted to be similar to NapA. Both NapA and NasA contain a conserved cysteine residue in the active site [19], however Nas is believed to only contain one PPT molecule and two oxo groups. NapA is coordinated by two sulfur ligands. One ligand is derived from a conserved cysteine residue. Nar is coordinated by two oxygen asparagine residue ligands.

The variability of nitrate reductase active site could provide insight into the evolution and relatedness of molybdopterin enzymes. **Chapter 4** provides detailed evidence of the hypothesized evolution of nitrate reductases and the divergence of Nap from assimilatory nitrate reductases, ultimately providing clues as to the importance of the *bis*PGD cofactor, which is only present in Nap, not Nas.

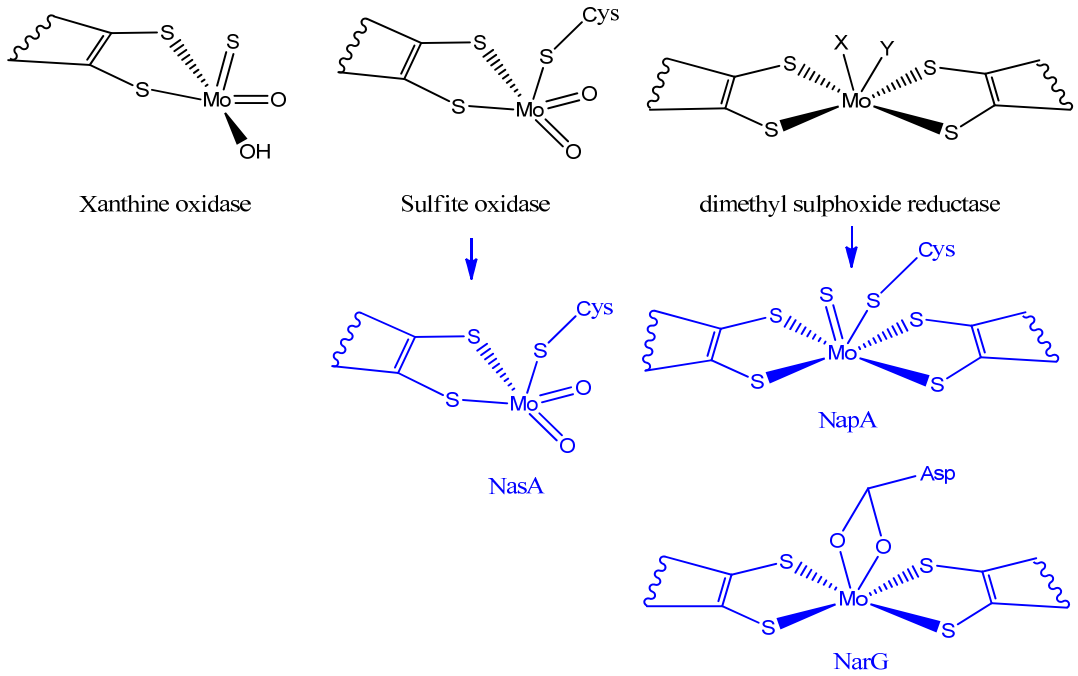

Figure 1.8: Classification of prokaryote nitrate reductases into molybdopterin enzyme families based on active site composition. The ligand composition differs among the molybdopterin enzyme families (black), xanthine oxidase, sulfite oxidase and dimethyl sulphoxide reductase, and among prokaryotic nitrate reductases (blue). The nitrate reductases, assimilatory nitrate reductase (NasA) and the dissimilatory nitrate reductases (NapA and NarG), are displayed under the classifying family.

The cellular compartment in which each NRase protein complex is localized also differs. The assimilatory NRases are soluble-cytoplasmic proteins. The dissimilatory NRases (i.e., Nap and Nar) are membrane associated. In bacteria, the Nar complex faces the cytoplasm, and, in archaea, the periplasm (pNar). [77] The Nap complex, which is only found in bacteria, faces the periplasm.

As a result of the cytoplasmic location, Nar couples nitrate respiration to proton translocation across the inner membrane of bacteria. The resulting electrochemical gradient can be used to fuel ATP generation via ATP synthase. Conversely, periplasmic-oriented complexes, Nap and pNar, would yield a zero net proton change in the periplasmic space from nitrate reduction to nitrite; indicating that Nap and pNar are not capable of producing a proton motive force by nitrate respiration, and that Nap and pNar

do not function in energy acquisition. However, this is not always the case, some organism, primarily the Epsilonproteobacteria, [78] do rely on Nap for anaerobic nitrate respiration. **Section 1.3.1** will discuss the function of periplasmic nitrate reductase in respiration.

1.3. Periplasmic nitrate reductase

The periplasmic nitrate reductase (Nap) was first isolated from *Paracoccus denitrificans* by Sears *et al.* [79] Initially it was differentiated from the well-known respiratory nitrate reductases (Nar) by its insensitivity to azide and its inability to reduce chlorate, in addition to the periplasmic location. As mentioned previously, the molybdenum containing catalytic site also differs. Since the discovery of Nap in 1993, multiple genetic and peptide level variations have been revealed among prokaryotes. The differences in the *nap* operon structure and organization, *nap* gene content, mechanisms of transcriptional regulation and amino acid composition of the catalytic subunit are the apparent sources for the functional diversity of the periplasmic nitrate reductase. The following sections will review each feature in detail.

1.3.1. Functional diversity of periplasmic nitrate reductase

While the specific roles of Nas and Nar remain consistent from species to species, Nap is functionally diverse. It has been implicated in dissimilatory nitrate reduction (both denitrification and nitrate reduction to ammonia), [80, 81] maintenance of cellular oxidation-reduction potential (i.e., redox poise) [82] and nitrate scavenging. [83] The functional diversity of Nap demonstrates that the presence of a *napA* homolog in an organism's genome does not confer homologous functionality.

As previously discussed, Nar is the prototypical respiratory nitrate reductase; however, the Nap system does have the ability to function in nitrate respiration when

coupled to quinone oxidation.[84] In some organisms, nitrate respiration is dependent on the *nap* operon,[85] most of these organism belong to the Epsilonproteobacteria class of gram negative bacteria.[78, 86] Nap has also been associated with pathogenecity in the gastrointestinal pathogens *Helicobacter* and *Campylobacter.* In *C. jejuni,* Nap is with colonization. In both organisms, Nap is up-regulated in response to oxidative stress.[62, 87-91] The role of Nap in pathogenesis is discussed in greater detail within **Chapter 3**.

The Epsilonproteobacteria are unique in their conserved ability to utilize the periplasmic nitrate reductase (Nap) in nitrate respiration. Raising the question, what is different about the Epsilonproteobacteria Nap? In order to explore the unique features of the Epsilonproteobacterial Nap, a review of the known Nap features will be presented. The mechanisms of transcriptional regulation, the diversity of the *nap* operon, and the biophysical features of the Nap protein will be discussed. The following sections aim to define the properties which make the Epsilonproteobacterial Nap unique.

1.3.2. Operon structure and organization

Genes which are co-transcribed and co-regulated, and located within close proximity to each other, are collectively referred to as an operon. The *nap* operon is typically located within the organism's genomic DNA. Although some organisms contain a plasmid borne *nap* operon (e.g., *Paracoccus denitrificans, R. metallidurans, Sinorhizobium meliloti, S. medicae Sulfuricurvum kujiense*, *Rhodobacter sphaeroides*, [92] *Ralstonia eutropha* [93] and *Cupriavidus necator*. [94]). Some organisms carry multiple copies of the *nap* operon. [95, 96]

The *nap* operon exhibits significant variability in the genes organization and composition (**Figure 1.9**). In addition to the *napA* gene, eleven *nap* genes have been identified to date. [47, 97, 98] The *nap* genes can be divided into redox active or

maturation based on the physiological functions of the translated proteins. Redox active genes (*napC, napG, napH, napB, napM*) encode proteins involved in electron transport to or from the terminal reductase, NapA. Maturation genes (*napD, napL and napF*) encode proteins which are involved in post-translational modification of NapA. Some less common *nap* genes (*napS, napK* and *napE*) have unclear functions.

The most commonplace *nap* operon is the *napEDABC*, which is found in some Alpha-, Beta-, and Gamma- proteobacteria, though multiple *nap* operons have been identified. Each *nap* operon differs in gene organization and content. **Table A.1** categorizes the operons on a basis of membrane quinone oxidase content, a noteworthy feature as Nap can be involved in nitrate respiration; the *nap* operon can encode two (*napC* & *napH*), one (*napC* or *napH*) membrane quinone oxidases, while others are devoid of a putative membrane quinone oxidase. The variability and diversity in the *nap* operon could suggest that the *nap* operon is diverging into different functional roles.

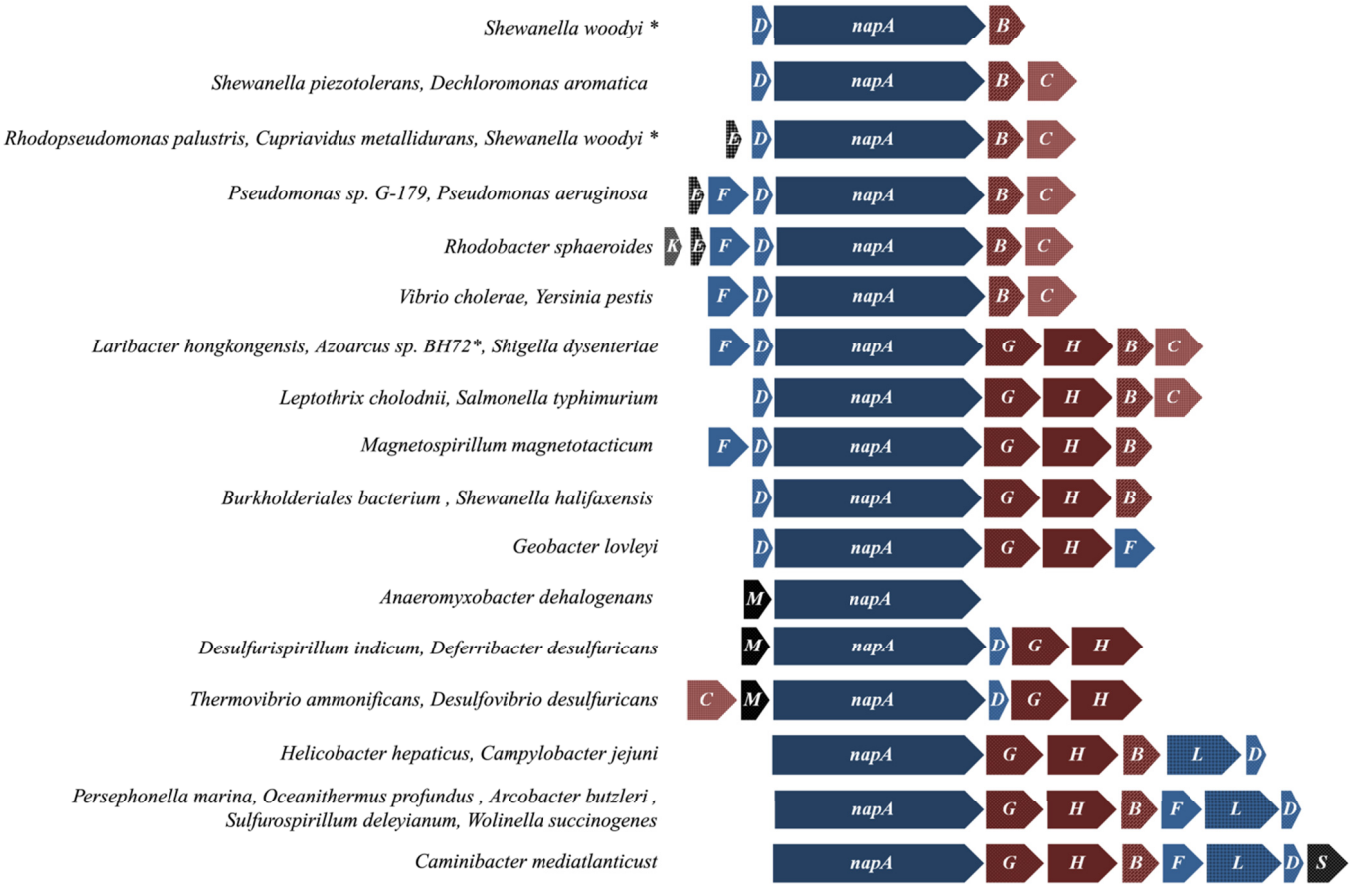

Figure 1.9: The *nap* operon gene content and organization in some bacteria. For a complete list see **Table A.1** in Appendix I. Each nap gene (Arrow) was identified by preforming a blast search with-in the NCBI database. The *nap* genes are listed by the order in which each is found. (*) indicates organisms which encode two nap operons.

1.3.3. Regulation of the nap operon

The functional diversity of Nap has a foundation in transcriptional regulation. The *nap* operon can be regulated in response to multiple environmental cues (i.e. the absence or presence of nitrate, oxygen, molybdenum and/ or iron, the type of as carbon source, or redox potential). The mechanisms of *nap* transcription regulation are not conserved. Thus, considerable variations in the regulatory mechanisms do exist from organism to organism.

Microbes utilize multiple terminal reductases during respiratory growth, regulating translation of each reductase, under the appropriate conditions, is a concerted endeavor. During aerobic growth, oxygen is typically the preferred terminal electron acceptor, a result of the high redox potential ($E^{o'}$ = +840 mV). Under anaerobic conditions, nitrate takes precedence to other anaerobic dehydrogenases ($E^{o'}$ = +420 mV). Not surprisingly, the presence and absence of both oxygen and nitrate can affect transcription of nitrate reductases.

Multiple global transcription regulators have been identified for nitrate reductases. Although no unique *nap* regulator has been identified. **Figure 1.10** provides a graphical overview of the transcriptional regulators which can affect the *nap* operon. Each regulatory protein binds to a DNA consensus sequence upstream from the regulated genes. In response to oxygen, the fumarate and nitrate reductase (FNR) protein can control transcription of the *nap* operon. [99, 100] Additionally, the NarPQ/ NarLX, dual interacting two-component regulatory system is employed to regulate transcription of *nap* in the presence of nitrate.[101] The dualistic constituents, a membrane bound sensor (i.e. NarX and NarQ) and a DNA binding response regulator (i.e. NarL and NarP), work together to fine tune expression of the controlled genes. *E. coli* uses both the Fnr and

NarPQ/NarLX transcriptional regulators to sense nitrate and oxygen levels in the environment and coordinate expression of nitrate reductases (*i.e.*, Nap and Nar) and nitrite reductases (*i.e.*, Nrf and Nir). [102] Nap is maximally expressed anaerobically in the presence of low nitrate concentrations, possibly providing a selective advantage over Nar during colonization of the human GI tract. [103-106]

The *Bradyrhizobium japonicum* NapEDABC expression is also up-regulated in response to micro-aerophillic growth and the presence of nitrate. In *B. japonicum* the FixLJ-FixK2-NnrR regulatory cascade controls *nap* expression in response to oxygen **[107, 108]**. FixLJ, a two-component regulatory system, down-regulates translation of the *nap* operon when elevated concentrations of oxygen are present. However translation of the *nap* operon is not always repressed in the presence of oxygen. In *Paracoccus pantotrophus* Nap expression occurs aerobically. The *P. pantotrophus nap* operon does not have a FNR-binding site upstream. [109] *Rhodobacter capsulatus* and *R. sphaeroides* express *nap* both in the presence and absence of oxygen. [110]

The cellular redox status can also regulate *nap* expression. *P. pantotrophus* utilizes the ferric uptake regulator (Fur) as a transcriptional regulator of NarP and NarL. Fur is a global regulator which controls iron (Fe^{+2}) uptake and detoxification. [111, 112] Fur controls *nap* expression response to oxygen and cellular redox status as it is dependent on free Fe^{+2}. Consequently oxidants (*i.e.*, O_2) can decrease Fur activity. [102]

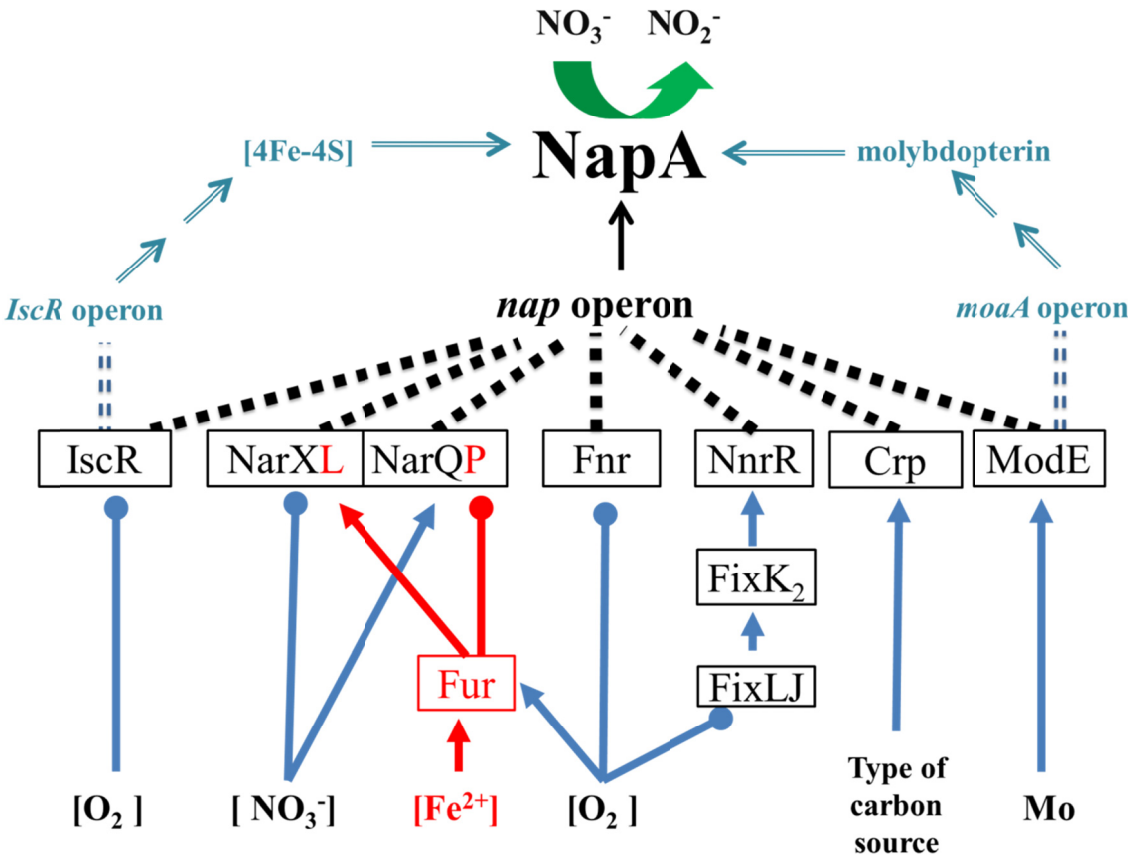

Figure 1.10: Transcriptional regulation of the *nap* operon and the pyranopterin and iron sulfur cofactor biogenesis operons. It is important to note that not all regulatory effects are present in the same organism. The acronyms of each regulatory protein are enclosed in boxes (see text for details). Proteins which directly regulate *nap* operon transcription are connected to "NapA" with a dashed line (▪▪▪), and those which affect cofactor biogenesis operons are connected to the specific operons via a double dashed line (**===**). The operons for *bis*PGD and [4Fe-4S] cofactor biogenesis (blue) are *moaABCDE* and *iscRSUA-hscBA-fdx*, respectively. Lines with arrow (➞) denote a positive regulatory effect, up-regulation, in the presence of the associated environmental signal; negative effects, down-regulation, is indicated with circles (━●). Concentration dependent regulation is indicated with brackets surrounding the chemical, for example $[O_2]$.This figure was partially reproduced, and updated, from Rabin and Stewart's publications [101, 113]

In *E. coli*, the cyclic AMP receptor protein (Crp) has also been demonstrated to up-regulate *nap* operon translation in response the type of carbon source. Less favorable sugars, such as mannose, increased *nap* translation compared to the typical fermentative sugars, such as glucose. [114]

The *nap* operon translation is also coordinated with the biosynthesis of the iron sulfur cluster and the PPT cofactors required in the active NapA. An iron-sulfur cluster-containing transcription factor, the iron-sulfur cluster regulator (IscR), represses *nap* transcription under aerobic conditions. [115] IscR also regulates iron-sulfur cluster biogenesis. [115] The IscR binding motif is typically located up-stream from the *nap* operon. The IscR binding region overlaps with an additional regulatory protein binding site, the molybdate-responsive (ModE) transcriptional regulator protein. In response to molybdenum, ModE up-regulates the *nap* operon translation. ModE also regulates transcription of the PPT biosynthesis genes (MoaABCDE) [116] and a high affinity molybdate transporter (ModABC).[117] The ModE and IcsR regulatory site are located further up-stream from the *nap* operon than the FnrR, NarP, NarL binding sites.[118] Thus ModE and IscR can supersede transcription of the *nap* operon if molybdate (MoO_4^{-2}) and iron are lacking,[119] even if FnrR, NarP, or NarL regulatory elements are up-regulating translation of the *nap* operon.

The Epsilonproteobacterium *C. jejuni* appears to employ analogous regulatory mechanisms for nitrate respiration. Unlike *E. coli*, which encodes three dissimilatory NRases (i.e. NapA, NarG and NarZ), *C. jejuni* only encodes NapA. In *C. jejuni* NapABGH are expressed in response to iron [120-122] and molybdenum. [91, 122] This suggests that the IscR and ModE regulatory proteins are involved in transcriptional

regulation of the *C. jejuni nap* operon. Additionally, *C. jejuni* preferably up-regulates Nap expression anaerobically. The *napABG* expression is up-regulated during chicken colonization [123] and *napABGH* in elevated growth temperatures, [124] possibly an indication of Fnr regulation. The alignment of the *C. jejuni* pre-*nap* operon DNA with the corresponding *E. coli* sequence indicates that all of the regulatory element binding sites are conserved.

1.3.4. The catalytic subunit, NapA

The catalytic subunit NapA contains a molybdenum active site (Mo- *bis*PGD) and an iron sulfur cluster [4Fe-4S] (**Figure 1.11**). The N-terminus of the translated protein also contains a twin arginine translocase (TAT) leader sequence which signals the protein for transportation to the periplasmic space. In most organisms NapA is isolated as a heterodimer accompanied by its physiological redox partner, NapB. The *Rhodobacter sphaeroides* and *Cupriavidus necator* NapAB heterodimer structure has been determined using X-ray crystallography.[125] Additionally, the crystal structures of two monomeric NapAs are available.[39, 42] While *E.coli* NapA does function as a heterodimer, NapB is not present in the crystal structure because the NapAB dimer dissociated during purification. *D. desulfuricans* does not contain a *napB* gene, thus NapB is absent in the NapA crystal structure. A strictly conserved lysine residue is proposed to transport electrons from the [4Fe-4S] to the molybdenum active site. A tyrosine residue in NapA is proposed to aid in electron transfer from the heme of NapB to the [4Fe-4S] cluster of NapA. This tyrosine residue is conserved in all heterodimeric NapA proteins and absent in monomeric NapA proteins such as *D. desulfuricans*. [126] Kinetics studies of the Alpha, Beta and Gamma- proteobacteria NapA indicated a high affinity for nitrate. The

properties of the Epsilonproteobacteria NapA must be established to determine if all NapA proteins exhibit the same affinity.

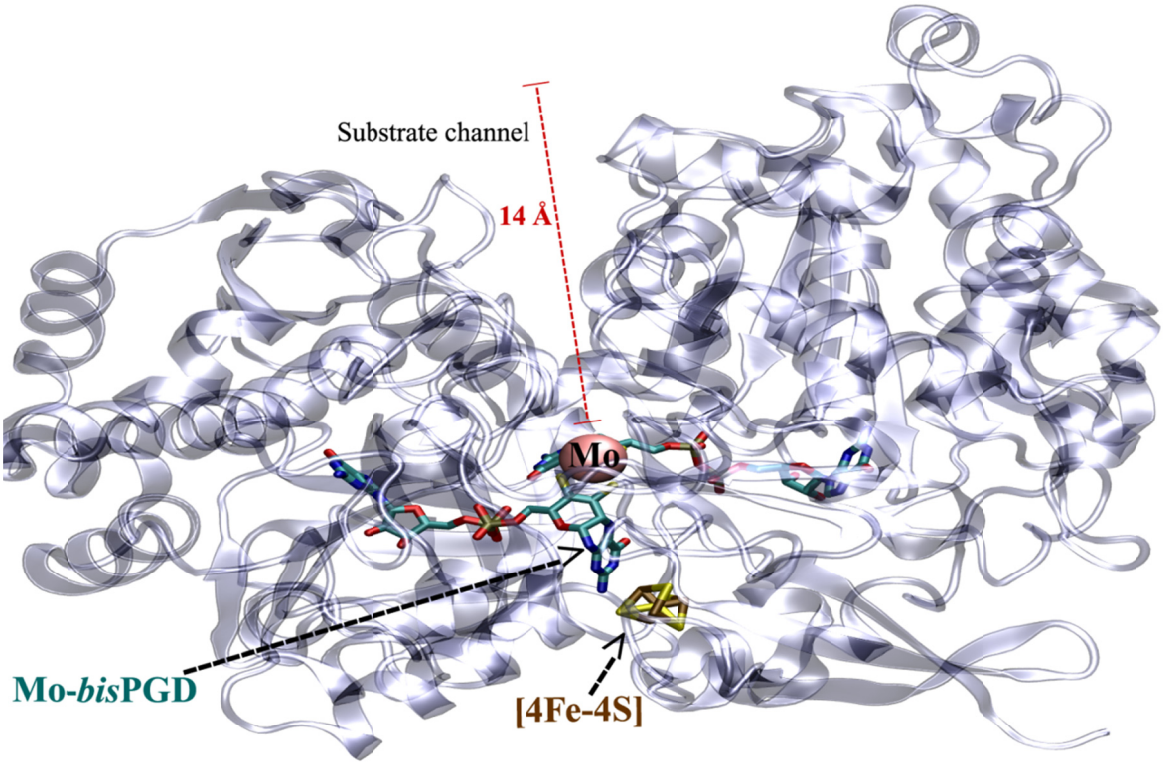

Figure 1.11: The structure of NapA illustrating the location of the iron sulfur cluster [4Fe-4S] and the Mo-*bis*PGD. The structure of *E. coli* NapA (2NYA) was downloaded from pbd.org; illustration was created using the Visual Molecular Dynamics software.

1.3.5. Auxiliary Nap proteins: the benefits of team work in nitrate reduction

While the monomeric NapA and dimeric NapAB isolates are capable of nitrate reduction, these proteins do not act alone during catalysis within the organism. Redox active Nap proteins transfer electrons to NapA. Maturation proteins aid in the posttranslational modification of NapA. The presence of the maturation or redox active *nap* genes varies among organisms. No solitary *nap* gene can be considered ubiquitous in all *napA* encoding organisms. Mutational studies conducted on *R. sphaeroides* [127], *E. coli* [83], and *Wolinella succinogenes* [86] have given insight into the significance of each auxiliary *nap* gene in nitrate reduction *via* Nap.

Of the auxiliary Nap proteins, the *napD* gene is the most common and appears to be the most vital. The *R. sphaeroides*, *E. coli,* and *W. succinogenes* mutational studies are in agreement, napD is an essential component of nitrate reduction. In all *napD* mutants nitrate reduction is inhibited. [127] [83] [86] Translated NapD is a dedicated chaperone protein as it has a defined role in NapA maturation. [46] NapD is a member of the well-studied TorD chaperone protein family.[128-130] NapD interacts with the TAT machinery and possibly other maturation proteins, such as NapF, in the biosynthesis of NapA.[131] NapD impedes the periplasmic export of NapA via the TAT machinery by binding to the N-terminal TAT leader sequence of NapA. Structural characterization of the *E. coli* NapD [131] indicates that the non-polar residues in the β-sheet of NapD bind, via protein-protein interactions, to the TAT leader-sequence of NapA (**Figure 1.12**). It is conceivable that NapD delays export of NapA until the protein is properly folded and the cofactors are inserted. [131] While the purpose of the NapA-D interaction is predicted to

be comparable in all organisms, the chemical basis of the interaction is species-specific. NapD lacks a conserved NapA binding motif.

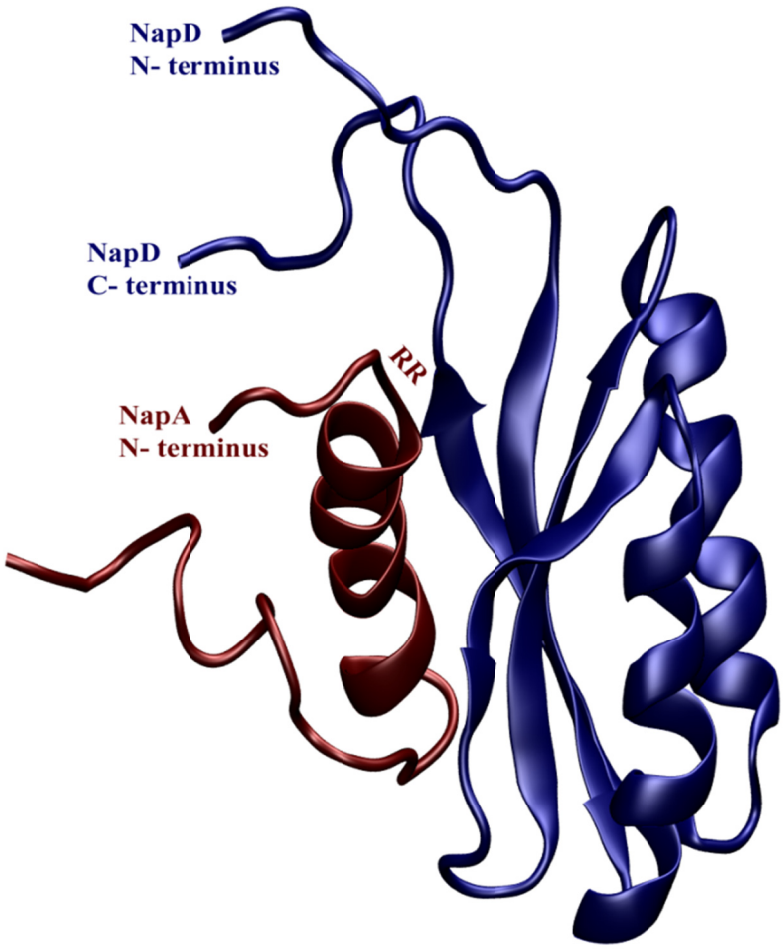

Figure 1.12: The protein structure of *E. coli* NapD in complex with the N- terminus of NapA. The protein backbone, of NapD (**blue**) and NapA (**red**), is displayed as a ribbon. The location of the two arginine residues (**RR**), for which the TAT leader sequence is named, is on the N-terminus of NapA. The NMR solution structure (PDB ID: 2PQ4) was downloaded from the pdb.org. VDM (version 1.8.7) was used to create this figure.

Despite the importance of NapD in NapA maturation some organisms do not encode a *napD* homologue (*i.e., Sorangium cellulosum, Photobacterium damselae*, *Rhodothermus marinus*, and *Anaeromyxobacter* species). In general, *nap* operons which lack *napD* have relatively few genes. The absence of *napD* may be an indication of reduced functionality as a result of the attenuated or incapacity to synthesize a functional

NapA. This may be the case in *P. damselae*, [132] and *R. marinus* [133] as these organisms cannot reduce nitrate despite the presence of a *napA* homologue. *S. cellulosum* and *Anaeromyxobacter* species can reduce nitrate, [134, 135] though this activity cannot be attributed to NapA without a more detailed investigation. These organisms encode multiple nitrate reductases (*i.e.*, Nar, Nap and Nas). Comprehensive assessment of the necessity for *napD* in NapA maturation may come from studies with nitrate reducing organisms which lack the *napD* gene, such as *S. cellulosum* and the *Anaeromyxobacter* species.

NapF, a cytoplasmic, non-heme iron sulfur protein also plays a role in NapA maturation. While mutation of the *napF* gene does not completely abolish nitrate reductase activity in *E. coi*, [83] a drastic decrease in activity is observed in *R. sphaeroides* and *W. succinogenes*. [127, 136] NapF is not considered to be essential for NapA maturation, although NapF does aid in [4Fe-4S] insertion. [136, 137][138] NapF contains four iron sulfur binding motifs (CX_n CX_n CX_n CP). Mutation of each motif demonstrated that one specific motif is responsible for transferring the [4Fe-4S] cluster into NapA. [139] Moreover mutation of the *W. succinogenes* NapF lead to the accumulation of the inactive precursor NapA in the cytoplasm. [139] The ability of NapF to reconstitute the 4Fe-4S cluster of the apo-NapA has also been demonstrated *in vitro*.[140] The association of NapF and NapA has also been confirmed.[138] Interestingly, the recombinant affinity-tagged NapF has been used to purify NapA from *E. coli*.[138] NapA maturation is more efficient in the presence of NapF. Mature NapA is able to accumulate in the periplasmic space with time, as indicated by nitrate reductase

acidity assays, growth curves and SDS/PAGE data. NapF is possibly an evolutionary advantage to organisms which encode the *napF* gene.

A third predicted maturation protein, NapL, is found primarily in the Epsilonproteobacteria. NapL is a periplasmic protein with no known metal binding motifs. [78] While the function of NapL is unknown, mutation of *napL* in *W. succinogenes* and *C. jejuni* delays growth on nitrate media. [136, 141] This suggests that NapL may be involved in maturation of NapA.

Of the redox active Nap proteins, NapB is the most extensively studied. The small *c*- type cytochrome is an essential component of electron transport to NapA.[86] NapB has been demonstrated to be an essential component of nitrate reduction via NapA in organisms which encode the *napB* gene.[83, 136] NapB is not essential for all NapA isolates. Organisms which lack the *napB* gene, such as *D. desulfuricans*, encode alternative iron cofactor redox partners, such as NapM or NapC. [97] Although NapM has not been studied directly, *D. desulfuricans* does translate the tetra heme containing NapM. [142]

The crystal structure of the recombinant *Haemophilus influenza* NapB revealed that two heme molecules are stacked parallel and hydrogen bonded to each other via propionated side chains.[143] In this structure, the conserved residues of NapB are located along the heme binding motifs ($HX_n CX_n CH$). Poorly conserved regions of NapB are located at the N- and C- termini and are not involved in electron transfer with NapA.[143] The N-terminus encodes a hydrophobic signal sequence, roughly 30 amino acids long, which targets the unfolded NapB for periplasmic export via the sec dependent pathway.[144] [145] [41] Arnoux *et al.* suggest that the N- and C-termini are involved in

NapA binding.[146] The latter crystal structures of NapAB heterodimers, from *C. necator* and *R. sphaeroides*, underscore this aspect.[40, 146] The poor conservation of the NapA binding sites on NapB proteins could be the source of the different binding affinities observed in NapAB dimers. *E.coli* and *R. sphaeroides* NapAB exhibit different dissociation constants, 32 μM [147] and 5 x 10^{-4} μM [146] respectively, and are reflective of the purified form. *E. coli* NapA was isolated as a monomer and the NapAB interaction is correspondingly weaker than that of the *R. sphaeroides* homologue, which was isolated as a heterodimer.

Similar to NapA, NapB has been reported to utilize maturation proteins. The cytochrome *c* maturation (Ccm) proteins are involved in NapB cofactor synthesis and insertion. In *E. coli* and select organisms the *ccmABCDEFGHI* operon is located directly adjacent to the *nap* operon. [105] The *ccm* operon is not adjacent to the *nap* operon in the majority of *nap* encoding organisms. The *ccm* operon is missing completely from the genomes of the Epsilonproteobacteria, suggesting that these organisms have alternative methods for iron uptake and heme synthesis. In fact *C. jejuni* encodes a large variety of genes associated with iron scavenging, uptake, and storage, one of which (*chu*) can transport intact heme into the cell.[148] The ability of *C. jejuni* to utilize intact heme could make the cytochrome *c* biogenesis redundant and consequently energetically unfavorable.

NapC, a tetra-heme transmembrane protein, is also considered to be an essential component of electron transport to NapA in some organisms.[83] NapC transports electrons via the heme cofactors from the membrane quinone pool to the periplasmic NapB[149] (**Figure 1.13**). In *E.coli*, electron transfer from ubiquinone and menaquinone

to NapAB is dependent on NapC. Ubiquinone electron transfer from NapGH to NapABC is more efficient than ubiquinol transfer directly from NapC to NapAB. [137] Like *napB*, *napC* is not encoded in the *nap* operon of all organisms. NapC belongs to a large group of tetra heme proteins, the NapC/ NirT family. [150] The possibility that other members of the NapC/ NirT family, NrfH and Cym, could fulfill the function of NapC (i.e., electron transport to NapA) in organisms which lack *napC* has been postulated, [151] [152] although supporting experimental evidence is not available.

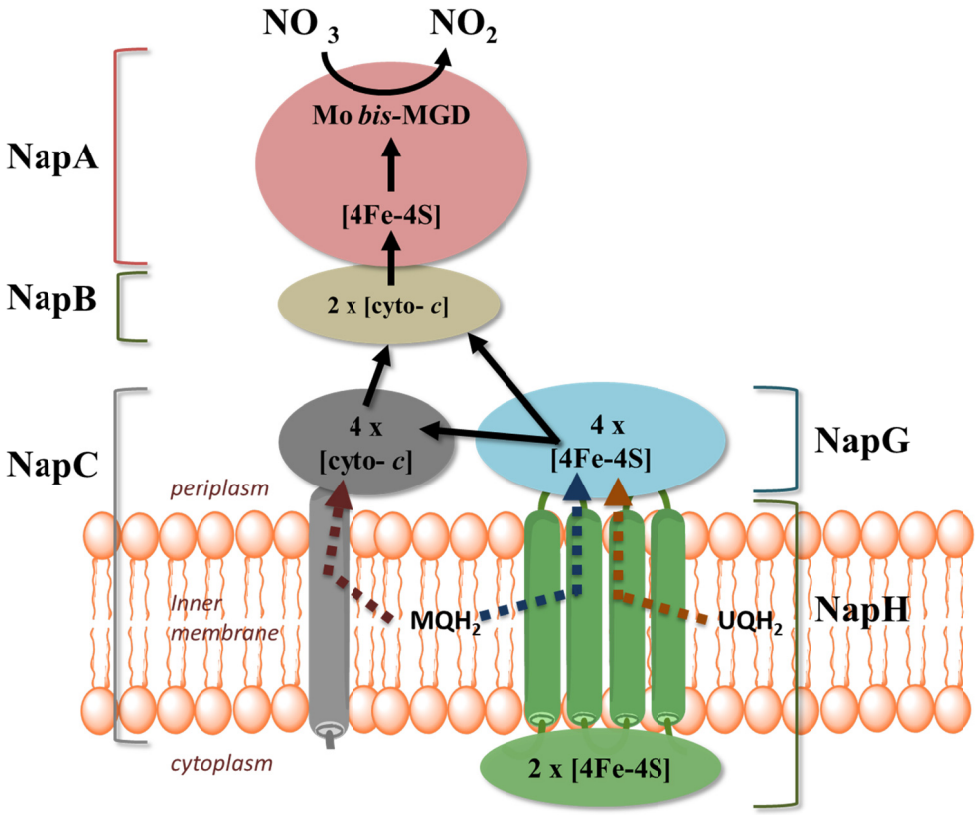

Figure 1.13: The proposed routes of electron transport to NapAB from quinone pool during nitrate reduction. Electrons can be transferred from menaquinone (MQH_2) or ubiquinone (UQ H_2) with in the inner membrane by a quinone oxidase (i.e., NapC or NapH). Electrons are transported to NapAB via NapC, NapGH or NapCGH.

The genes *napG* and *napH* encode the two putative ferredoxins. NapH is an integral membrane protein. The cytoplasmic portion of NapH contains two iron sulfur

binding motifs. NapG contains four iron sulfur binding motifs and is associated with the periplasmic face of the membrane. In organisms which do not encode a NapC homologue, NapG and NapH are predicted to transfer electrons from the quinone pool directly to NapAB. [153] *Campylobacter* only has menaquinone, but does not have a NapC homologue. In *Campylobacter*, NapGH are believed to transport electrons from the menaquinone pool to NapAB. [154] The MQH_2 couple has a lower midpoint redox potential than UQH_2, - 70 mV compared to + 90 mV, [153] indicating that MQH_2 would be a less efficient electron transport.

The variety of *nap* genes indicates that the *nap* operon evolved by gaining or losing genes in an effort to fit the functional needs of the organism. Chaperone proteins, such as NapF and NapL, while not essential for maturation, may help NapA mature quickly.

1.4. Conclusion

Molybdenum enzymes are essential for most organisms. Mononuclear molybdenum enzymes contain a pyranopterin cofactor, which coordinates molybdenum in the active site. These enzymes are assigned to four groups based on the molybdenum active site: sulfite oxidase, xanthine oxidase, dimethyl sulfoxide reductase and the mitochondrial amidoxime reducing component families. The DMSOR family is the most diverse and contains only prokaryotic enzymes.

Within the DMSOR family the two types of dissimilatory nitrate reductases, Nap and Nar, display diverse features. In the active site molybdenum is coordinated by cysteine in NapA and asparagine in NarG. NapA is a heterodimer and NarG is part of a stable membrane bound heterotrimer. Both are membrane associated, though Nap is

periplasmic and Nar is cytoplasmic. Nar is a dedicated respiratory enzyme and Nap is functionally diverse. Nap has been implemented in redox poise, nitrate scavenging, nitrate respiration and pathogenicity. In fact, human pathogens including *Haemophilus influenzae*, *Vibrio cholera*, *Yersinia pestis*, and *C. jejuni* have only Nap.

In addition to the functional diversity of Nap, genetic variability is common. The transcriptional level regulatory mechanisms and *nap* gene content and organization associated with the *nap* operon vary among organisms. As many as three promoters and seven regulatory-protein binding sites can precede the *nap* operon. The regulator proteins control the translation of the *nap* operon in respond to environmental conditions such as oxygen, iron, molybdenum, nitrate content and cellular redox potential. The *nap* operon contains genes which translate into dedicated chaperone proteins (i.e., NapD, NapL, and NapF) or redox active proteins (i.e., NapC, NapB, NapG, and NapH). The genetic diversity of *nap* could be a possible clue into the molecular basis of Nap's functional diversity. The presence (or absence) and type of membrane-bound quinone oxidase, NapC or NapH, used by each organism can provide clues into the respective physiological functions of Nap. In general, four *nap* genes are important for respiration: *napA, napB, napC* and *napD*. [83] However, NapC may not be essential as the Epsilonproteobacteria do not encode a *napC* homologue in the *nap* operon (**Figure 1.9**) but can perform nitrate respiration. [151]

The Epsilonproteobacteria, are an important group of pathogenic, (*i.e.*, *C. jejuni* and *H. pylori*) and free-living bacteria (i.e., *S. barnesii*). While nitrate reduction is a vital process for most Epsilonproteobacteria, the physiological function of Nap in these organisms is not well understood.

1.5. Specific aims of study

The global objective of this study was to elucidate the function of periplasmic nitrate reductase (Nap) in the Epsilonproteobacteria through isolation and characterization of the catalytic subunit, NapA. The goal of this research was to expand the current knowledge of the prokaryotic nitrate reductases, specifically Nap. NapA has been isolated from organisms belonging to other genre of proteobacteria, although the Epsilonproteobacteria NapA has not been fully characterized. The specific aims are: 1) isolate NapA from an Epsilonproteobacteria, 2) determine the kinetic parameters for nitrate reduction by NapA, and 3) determine if the Epsilonproteobacteria NapA is different than other NapA isolates.

The two organisms chosen to represent the Epsilonproteobacteria class were *Campylobacter jejuni* and *Sulfurospirillum barnesii*, thus providing insight into the function of NapA in both a human pathogen and a free living organism. The purification and characterization of NapA from *Sulfurospirillum barnesii* is presented in **Chapter 2**. The cloning and heterologous expression of *C. jejuni* and *S. barnesii* NapA, NapB, NapL & NapD, and the purification of the recombinant *C. jejuni* and *S. barnesii* NapA from *E. coli* are presented in **Chapter 3**. **Chapter 4** contains a bioinformatics investigation into the variability of the *nap* operon using computational approach and presents the theoretical structure of *C. jejuni* NapA. The unique molecular features of the Epsilonproteobacteria NapA are proposed by comparing the *C. jejuni* NapA structure to the experimentally determined NapA structures from *E. coli, Rhodobacter sphaeroides*, *C. necator* and *Desulfovibrio desulfuricans.* The physiological significance of the *nap*

operon organization and content is also discussed. **Chapter 5** will summarize the results from each study and consider the influence this study has on the current understanding of prokaryotic nitrate reduction. Also, preliminary research, conducted on the effect of chromate on dissimilatory nitrate reduction by *Geobacter metallireducens*, *D. desulfuricans,* and *S. barnesii* are placed in the Appendix.

CHAPTER 2: Purification of periplasmic nitrate reductase from *Sulfurospirillum barnesii* strain SES-3

2.1 Abstract

Sulfurospirillum barnesii strain SES-3, a free living soil microbe, is capable of using selenate, arsenate and nitrate as terminal electron acceptors during respiration *S. barnesii* uses this flexible respiratory chain to survive in response to changes in environmental conditions. While transformation of selenate and arsenate has obvious toxic repercussions on the environment, nitrate is ubiquitous in nature and can lead to the generation of toxic nitrogenous compounds (i.e., nitrite, nitrosamines and nitric oxide). In Epsilonproteobacteria, like *S. barnesii*, the periplasmic nitrate reductase (Nap) catalyzes the transformation of nitrate to nitrite. The catalytic subunit, NapA, was isolated from *S. barnesii*. The electronic spectrum of the purified sample indicates that a *c*-type cytochrome may also be present, possibly NapB. Although the yield of NapA was too low to perform kinetic experiments, the NapA enriched CHAPS soluble fraction indicates tight binding of nitrate (K_m =314 μM), in agreement with NapA activity from other organisms under similar conditions.

2.2. Introduction

Sulfurospirillum barnesii strain SES-3 is a gram negative Epsilonproteobacteria originally isolated from a selenate contaminated freshwater marsh in Nevada. [155, 156] The free-living, opportunistic organism has a diverse respiratory metabolism. *S. barnesii* can couple the oxidation of lactate to the reduction of multiple terminal electron acceptors such as selenate (SeO_4^{2-}), selenite (SeO_3^{2-}), nitrate (NO_3^-), nitrite (NO_2^-), iron (Fe^{III}), manganese (Mn^{IV}), fumarate, arsenate (As^V), elemental sulfur (S^o),

trimethylamine *N*-oxide (TMAO) and thiosulfate ($S_2O_3^{2}$). [155, 157],[158] Growth is supported by reduction of selenate to selenite, nitrate to nitrite, arsenate to arsenite, Fe^{III} to Fe^{II} and thiosulfate to sulfide. [4a,5] The thermodynamic estimations for nitrate reduction to ammonia via nitrite, selenate reduction to elemental selenium via selenite and arsenate reduction to arsenite (**Table 2. 1**) indicate that the organism would obtain the most energy by selanate reduction, however stoichiometric conversion of selenate to elemenatal selenium was not observed.[155]

Table 2. 1: Energy yields of arsenate, selenate, and nitrate respiration by *S. barnesii.*

***S. barnesii* respiratory reaction**	**Estimate of ΔG_f^o (kJ/mol of lactate)**
$Lactate^{-1} + 2HAs^{V}O_4^{2-} + H^+ \rightarrow Acetate^- + 2H_2As^{III}O_3^- + HCO_3$	-140.3[157]
$Lactate^- + 2SeO_4^{2-} + H^+ \rightarrow 3Acetate^- + Se^o + 3HCO_3^- + 2H_2O$	-467.4[155]
$4Lactate^- + 2NO_3^- + 2H_2O \rightarrow 4Acetate^- + 2NH_4^+ + 4HCO_3^-$	-245.0[155]

The transformation of arsenate, selenate, and nitrate are catalyzed by separate enzymes: arsenate reductase, selenate reductase, and nitrate reductase and nitrite reductase.[159, 160] Despite the relatively lower free energy yield, nitrate reduction is thought to be the preferred substrate.[161] Because nitrate is ubiquitous in nature,[155] the ability of *S. barnessi* to respire nitrate is important for the long term survival of this organsim.

S. barnesii's ablity to concurrently transform toxic compunds (i.e. arsenate and selenate) in the presence of nitrate is important to subsurface bioremediation,[155, 157, 161-163] as natural systems contain mixtures of metals, metalloids and inorganic oxyanions. [5] Furthermore, *S. barnesii* may serve the additional benefit as a non-pathogenic model for understanding nitrate reduction to ammonia in the Epsilonproteobacterial phylogenic class, which includes human pathogens such as

Campylobacter jejuni and *Helicobacter hepaticus*. As found in most Epsilonproteobacteria *S. barnesii* only encodes one nitrate reductase (NR), the periplasmic nitrate reductase (Nap), not the typical respiratory NR (Nar) or the assimilatory NR (Nas), underscoring the possibility for multiple functions of this enzyme in nitrogen metabolism.

The goal of this study was to isolate the catalytic subunit (NapA) from *S. barnesii,* in order to examine the kinetic properties of the enzyme. To date, wild type NapA has not been isolated from any Epsilonproteobacteria. Thus, the biochemical and structural properties are yet to be described. With the increasing volume of information available on nitrate reductase enzymes,[164],[165] it has become clear that significant variations exist among these proteins even within subclades of proteobacteria.

NapA has been isolated as a heterodimer with *c*-type cytochrome containing NapB from multiple organisms [41, 42, 93, 94, 166, 167] and as a monomer from *Desulfovibrio desulfuricans* [168]. Two general strategies have been employed for cultivating NapA, expression of the recombinant protein(s) in the native host cells (homologous over-expression), and isolation of naturally occurring proteins found in the native organism (native expression). Native purification has been the traditional method of NapA isolation. [93, 96, 166-168] Homologous over-expression has been employed in *Escherichia coli,* [42] *Rhodobacter sphaeroides*, [41] and *Cupriavidus necator* [94]. In *Rhodobacter sphaeroides* [41] and *Cupriavidus necator* [94] the *nap* operon is naturally located on a megaplasmid, not the organism's genomic DNA, making genetic manipulations more feasible. In this study, *S. barnesii* NapA was isolated *via* native

isolation. The objective was to develop a purification strategy and determine NapAs affinity for nitrate.

2.3. **Experimental**

2.3.1. Cultivation of S. barnesii

S. barnesii strain SES-3[156] was grown anaerobically on an enriched media (SES-3 nitrate medium, Appendix V) as originally described by Stolz et al,[169] with a final concentration 15 mM lactate and 20 mM sodium nitrate. The amount of yeast extract was raised to 2 g • L^{-1} to increase the cell mass. To provide a sterile environment, the growth media was autoclaved. Heat liable solutions (i.e. vitamins, minerals, sodium dithionite and sodium lactate) were sterilized using vacuum filtration (0.22 μm pore size filter), then amended at the time of inoculation. The inoculating culture (1L) was grown on nitrate media until log phase growth was reached, typically 2 days, before adding it to fresh 11 L of nitrate media. Sodium dithionite (1 %w/v) was added at the time of inoculation to ensure an anoxic environment. Under the specified growth conditions, *S.barnesii* reduces nitrate within the first 14 hours of incubation. [161] For that reason, *S. barnesii* was incubated at 30 ^{o}C with low agitation (30 rpm) in a 14 L fermenter (New Brunswick) for 12-14 hours. Cells were collected by centrifuging at 8000 g for 15 minutes, then frozen in liquid nitrogen and stored at -80^{o}C.

2.3.2. Purification of periplasmic nitrate reductase from S. barnesii

The *S.barnesii* cell paste (typically 10 g wet weight) was suspended in an anoxic buffer (SES-3 lysis buffer, Appendix V) using a dounce (Knotes). The homogenized cell slurry was passed through a French pressure cell press (Thermo Scientific) two times at ~14,000 psi before a protease inhibitor cocktail (Sigma- Aldrich) and deoxyribonuclease I (Sigma- Aldrich) were added. The lysate was then centrifuged at 8000 rpm for 10

minutes to remove unbroken cells and debris. The lysate was centrifuged at 300000 *g* (Beckman Coulter Ultracentrifuge, 50.2Ti rotor) for 1.5 hours to separate soluble (periplasm and cytoplasm) and insoluble particles (membrane and ribosomes). The insoluble pellet was homogenized with 10 mM Tris and incubated with 1% (w/v) of 3-[(3-cholamidopropyl) dimethylammonio]-1-propanesulfonate (CHAPS) overnight at 0 ^{o}C. The CHAPS insoluble fraction was removed by centrifuging the sample at 245000 *g* for 1 hour. The CHAPS soluble fraction was then subjected to stepwise ammonium sulfate (AS) precipitation at 30 %, 45 % and 60 % saturation (*S*). The weight (*X*) of solid ammonium sulfate required to reach the desired percent saturation (*S*) was calculated using **Equation 2.1**. [170]

$$X\ {}^{g}/_{L}\ (NH_4)_2\ SO_4 = \frac{533(S_2 - S_1)}{100 - 0.3(S_2)} \qquad \textbf{Equation 2.1}$$

The 60% fraction was dissolved (Buffer A, Appendix V) and the excess salt was removed with diafiltration, 30 KDa molecular weight cut off (Millipore), prior to chromatographic separation. The desalted fraction was loaded onto a macroprep® anion exchange resin (BioRad) pre-equilibrated with Buffer A (Appendix V) in a 2.5 cm diameter glass column using the BioLogic LP system (BioRad). A gradient of 0-100 % Buffer B was used to elute proteins over 4 column volumes at 0.5 mL• min^{-1}. Two columns, packed with macroprep resin (BioRad), were used to isolate NapA, and referred to as DEAE I (40 mL resin volume) and DEAE II (10 mL resin volume).

Two detergents were used in this study: the zwitterionic detergent, CHAPS, and the non-ionic detergent, 1% n-octyl-*b*-D-glucopyranoside (OBGP). *S. barnesii* was incubated with 1% (w/v) CHAPS or OBGP.

2.3.3. Characterization

2.3.3.1. Assays

Protein concentration was measured using the DC protein assay kit (Bio-Rad). The expected extinction coefficient of *S. barnesii* NapA (accession number 169104652), ϵ_{280nm} = 191,460 M^{-1} cm^{-1}, was used to estimate the protein concentration spectrophotometrically in purified NapA samples.

Fractions were routinely screened for nitrate reductase activity via the reduced methyl viologen linked nitrate reductase assay.[171, 172] Microscale assays were performed inside an inert atmosphere glove box (Vacuum Atmospheres) at 22 ^{o}C using the ELx808 absorbance microplate reader (BioTek). The oxidation of methylviologen was monitored at 630 nm using Gen5 Data Analysis Software (BioTek). The reaction buffer contained TrisHCl [100 mM] (pH 8), CHAPS [0.1mM], Na_2MoO_4 [1mM] and methylviologen [0.8mM]. All assay solutions were purged with nitrogen or argon gas for 20 minutes, and then sealed before transfer into the anaerobic chamber. The reduced methyl viologen was prepared by titrating with a sodium dithionite stock [60 mM] solution to yield a final absorbance of 1.2– 1.6 at 630 nm. The enzyme was incubated with the reduced methyl viologen for 10 minutes and the absorbance was monitored to ensure the rate of oxidation was insignificant, prior to addition of nitrate. The reaction was initiated by the addition of potassium nitrate and the absorbance was monitored until the reaction stopped (i.e. Abs =0). Under the given conditions, the rate of reduced methylviologen oxidation by the protein sample alone (i.e., no substrate) was found to be negligible.

The absorbance at 630 nm due to reduced methyl viologen (MVr) was used in obtaining concentration using the Beer-Lambert law ($A = \varepsilon bc$), given the reported extinction coefficient of MVr (13700 M^{-1}), [173] and the calculated path length (0.667 cm^{-1}). The rate of methyl viologen oxidation (i.e. decrease in [MV_r]) was determined by plotting the concentration of MV_r over time (seconds). Linear regression (GraphPad Prism) [174] of the initial data points (first 90 seconds after adding nitrate) was used to calculate the rate of methyl viologen oxidation. To estimate the rate of nitrate reduction, the rate of methylviologen oxidation was divided by 2 to correct for the stoichiometric ratio of methylviologen to nitrate (2:1). Each molecule of methylviologen is capable of donating a single electron to NapA for the two electron reduction of nitrate to nitrite (**Equation 2.2 and 2.3**). Non-linear regression using the Michaelis–Menten equation was performed on the data using GraphPad Prism (v 5.03, San Diego, CA, USA) to a 95% confidence limit. From the fitted equation, substrate affinity (K_m), maximum velocity (V_{max}) was determined.

$$[MV]^{2+} + e^- \rightarrow [MV]^{\bullet+} \qquad \textbf{Equation 2.2}$$

$$2\,[MV]^{\bullet+} + NO_3^- + 2\,H^+ \rightarrow 2\,[MV]^{2+} + NO_2^- + H_2O \qquad \textbf{Equation 2.3}$$

In addition to the methyl viologen assay, the concentration of nitrite produced was measured using the diazo coupling technique (Griess assay, Appendix V). [175] Potassium nitrite (Fluka) was used as a standard for nitrite estimation, within the range of 1.6 μM-100 μM.

2.3.3.2. Native gel electrophoresis and in-gel assays

Detergent soluble proteins were separated by electrophoresis under non denaturing conditions. Resolving and stacking gels contained 0.5% of CHAPS, a sample buffer contained 0.7% CHAPS and anode buffer 0.1% CHAPS (recipes in Appendix V). Electrophoresis was performed at 40 V. The in-gel assay was performed in 50 mM Tris-Cl (pH 7.9), with 10 mM methyl viologen as the electron donor, potassium nitrate [0.1M] as the electron acceptor, and sodium dithionite as the reductant. Images of the activity gels were documented using a densitometer (GS-800, Bio-Rad). After the activity assay was finished, gels were incubated for 15 minutes in 12.5% trichloroacetic acid (TCA) before staining with colloidal coomassie stain (Appendix V).

2.3.3.3. Denaturing protein gel electrophoresis

Discontinuous sodium dodecyl sulfate polyacrylamide gel electrophoresis (SDS/PAGE) was used to analyze fractions for purity and NapA content, using standard protocol (Appendix V). [176] After separation, the gel was incubated in 12% TCA for 30 minutes to precipitate proteins followed by a 10 minute wash in water. Proteins were stained with a colloidal coomassie blue G-250 solution (Appendix V) overnight, washed with methanol (25%) and scanned using a calibrated imaging densitometer (GS-800, BioRad). The relative density and molecular weight of the separated proteins were calculated with Quantity One software (BioRad). Molecular weight standards (Fermentas) were used to estimate the size of unknown proteins.

2.3.3.4. Metal analysis

Metal analyses of enzyme samples were conducted at the Chemical Analysis Laboratory at the University of Georgia (Athens, GA., USA) using a Thermo Jarrell-Ash

Enviro 36 Simultaneous Inductively Coupled Plasma-Optical Emission Spectrograph (ICP-OES).

2.4. Results and Discussion

2.4.1. Cultivation of S. barnesii

Growth of *S. barnesii* strain SES-3 on nitrate enriched media was unpredictable and cell yield was low. The typical cell yield was 0.8 g per liter (wet weight) when the culture reached a peak cell density within 12 hours incubation. When growth was not achieved within this time frame, NapA content was very low. Typically, ~100 ng of NapA was obtained from a 12 L culture. Ideally, the growth medium used for a protein purification procedure would yield maximum quantities of the target protein (NapA in this case) and cell mass. However this was difficult to achieve using a defined medium. *S. barnesii*, was originally isolated in 1994 from a selenate respiring and acetate oxidizing soil enrichment.[155] While defined mediums such as the SES-3 medium used in this study strive to mimic the natural growth conditions, reproducing an organism's natural environment is difficult. Additionally, using an acetate and selenate enriched environment for *S.barnesii* NapA purification would induce the production of selenate reductase (EC: 1.97.1.9), [155] an alternative respiratory enzyme. The presence of SerA, the selenate reductase catalytic subunit, could dilute the efforts to purify NapA. SerA and NapA are molybdopterin, iron sulfur containing enzymes of similar size (c.a. 100 kDa). [177] Moreover, assaying fractions containing both SerA and NapA for nitrate reductase activity could be complicated as *S.barnesii* SerA is capable of nitrate reduction,[178] and NapA has been reported to reduce selenate in *R. sphaeroides.*[179] To avoid potential complications during NapA purification, *S.barnesii* was grown anaerobically on the

nitrate medium. Selenate was provided in the media at low concentrations as it is an essential micronutrient.

A second obstacle to *S. barnesii* growth could be the presence of sulfur oxyanions. In an effort to maintain an anoxic environment, sodium dithionite was added to the *S.barnesii* culture at the time of inoculation. However, addition of dithionite can be problematic. Acidic hydrolysis of dithionite leads to formation of thiosulfate and bisulfite; sulfite and sulfide form under alkaline conditions. [180] Nitrate respiration could be inhibited in the presence of thiosulfate, which *S. barnesii* has been noted to respire. [157]

Also, the elimination of oxygen may have negatively impacted the growth of *S.barnesii*, as indicated by the low cell yield (less than 1g of cells per liter of growth media). The *C. jejuni,* a close relative to *S. barnesii*, contains an oxygen dependent ribonucleoside-diphosphate reductase (RNR), [181] and requires roughly 5% oxygen for optimal growth. [61] *S. barnesii* also encodes a RNR homologue. The translated *S. barnesii* protein shares 75 % sequence identity with C. *jejuni* RNR (NCBI accession number YP_002343496) and 93 % identity with the *S. delyanium* (YP_003303127). It is possible that the optimal levels of oxygen were not supplied during growth and as a result growth may have been hindered. The effect of oxygen on *S. barnesii* growth was not assessed experimentally in this study.

2.4.2. Purification of NapA

Prior to purification, the conditions for the methylviologen assay were established. Specifically, the effects of chemicals used in the purification process were investigated. S. *barnesii* lysate was incubated with CHAPS detergent, ammonium sulfate, EDTA, and a reductant (dithioteritol) (**Figure 2.1**). The samples were frozen at 0^{o}C

overnight. One aliquot was also stored in an inert atmosphere glove box at room temperature (30^{o}C) overnight. Buffer supplemented with ammonium sulfate [0.5 M], EDTA [25 mM], and CHAPS (1% w/v) doubles the nitrate reductase activity relative to incubating the lysate in Tris buffer alone (**Figure 2.1**). It is most likely that ammonium sulfate and CHAPS improve NapA solublization with-in the assay vessel, increasing the enzyme activity. EDTA increases the nitrate reductase activity, most likely by chelating inhibitory metals such as zinc. Zn^{2+} ions ($K_i^{'}$ =1 μM) can inhibit the nitrate reductase activity of NapA, EDTA chelates zinc and completely restores activity. [171] Dithioteritol tripled the nitrate reductase activity (**Figure 2.1 & Table 2. 2**). The aliquot incubated under anoxic conditions at room temperature overnight also displayed a higher (more than 2x) nitrate reductase activity than the lysate stored overnight at 0^{o}C. This may indicate that the air-oxidation of the NapA molybdenum center rendered the enzyme inactive, and that incubating the enzyme with reductants, such as dithiothreitol, can reduce the active site. Also, storing the enzyme under inert atmosphere is more important than freezing the sample. Freezing is used to slow enzyme proteolysis; however degradation does not appear to be a problem in these experiments.

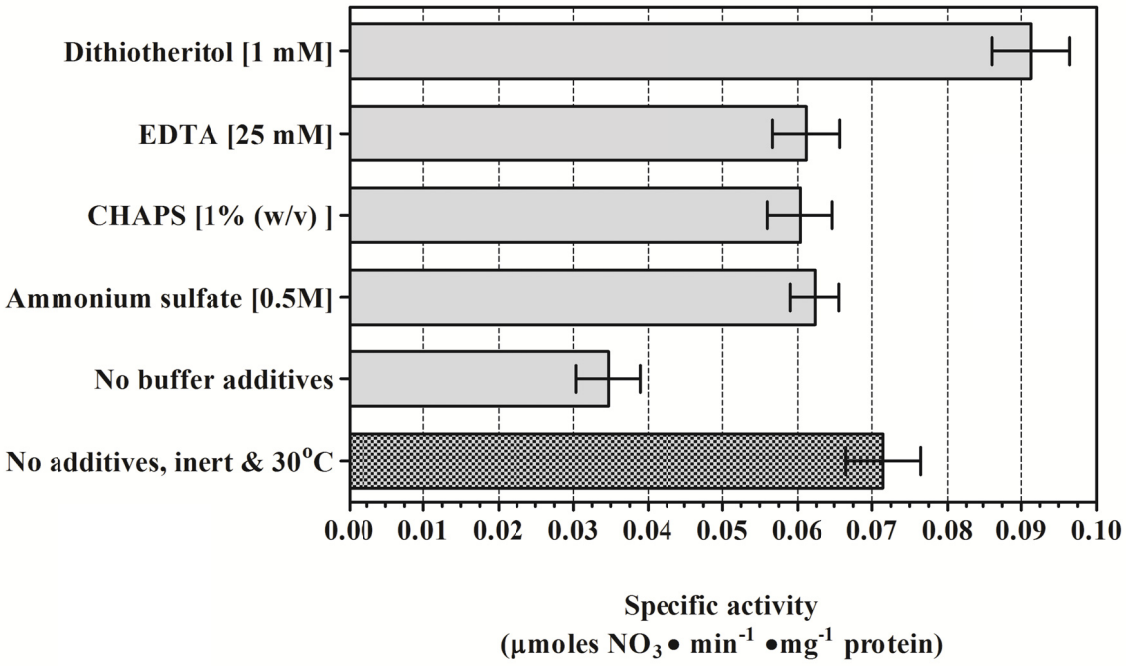

Figure 2.1: The effect of storage temperature, ammonium sulfate, CHAPS detergent, dithioteritol and EDTA on the specific activity of *S. barnesii* lysate. After overnight (16 hours) storage, the protein lysate was incubated in presence of 0.1 M Tris-HCl buffer, which was supplemented with ammonium sulfate, CHAPS, dithioteritol, EDTA or water, at room temperature, then the nitrate reductase activity was assayed using the methylviologen active assay. The values used to create this bar graph are presented in **Table 2.2**.

Table 2. 2: The effect of ammonium sulfate, CHAPS detergent, dithiothreitol and EDTA on the specific activity of *S. barnesii* lysate. After an overnight (16 hours) storage, the protein lysate was incubated in presence of 0.1 M Tris-HCl buffer, which was supplemented with ammonium sulfate, CHAPS, dithiothreitol, EDTA or water, at room temperature, then the nitrate reductase activity was assayed using the methylviologen active assay (n=5). This is a tabular format of the data graphed in Figure 2.1.

Storage temperature	Compound	Mean rate ± SD (μmoles NO_3^- • min^{-1} • mg^{-1} protein)
30 °C	No buffer additives	0.071 ± 0.005
0 °C	No buffer additives	0.035 ± 0.004
	Ammonium sulfate [0.5M]	0.062 ± 0.003
	CHAPS [1% (w/v)]	0.060 ± 0.004
	Dithiothreitol [1 mM]	0.091 ± 0.005
	EDTA [25 mM]	0.061 ± 0.005

The amphoteric detergent CHAPS was routinely used to solubilize NapA in this study. In addition to increasing the nitrate reductase activity in *S. barnesii* lysate, CHAPS detergent has properties which are beneficial in protein purification. Compared to the more common detergents, Triton X and Tween, CHAPS can be used at higher concentrations without the formation of micelles which can complicate chromatographic separations. The critical micelle concentration (CMC) of CHAPS is 0.49 % (w/v). The CMC of Tween and Triton are much lower, 0.002 and 0.021 respectively. CHAPS micelles are also smaller, typically 6 kDa, compared to the large micelles formed by Tween and Triton X (over 76kDa). Unfortunately CHAPS binds to the DEAE resin and is eluted with low NaCl concentration due to the amphoteric nature of the chemical. The elution of CHAPS was monitored by following the absorbance at 280 nm. For this reason the non-ionic detergent, 1% n-octyl-*b*-D-glucopyranoside (OBGP) was also investigated because it has similar micelle properties to CHAPS. In an effort to establish the effect of OBGP on nitrate reductase activity, the *S. barnesii* lysate was fractionated using CHAPS and OBGP with differential solublization techniques. The *S. barnesii* cells were lysed, and then the insoluble fraction was separated from the soluble supernatant using

ultracentrifugation. The insoluble fraction was aliquoted and then incubated with 1% (w/v) detergent, OBGP or CHAPS (**Figure 2.2**). The insoluble particulate was then removed from the soluble supernatant by ultracentrifugation.

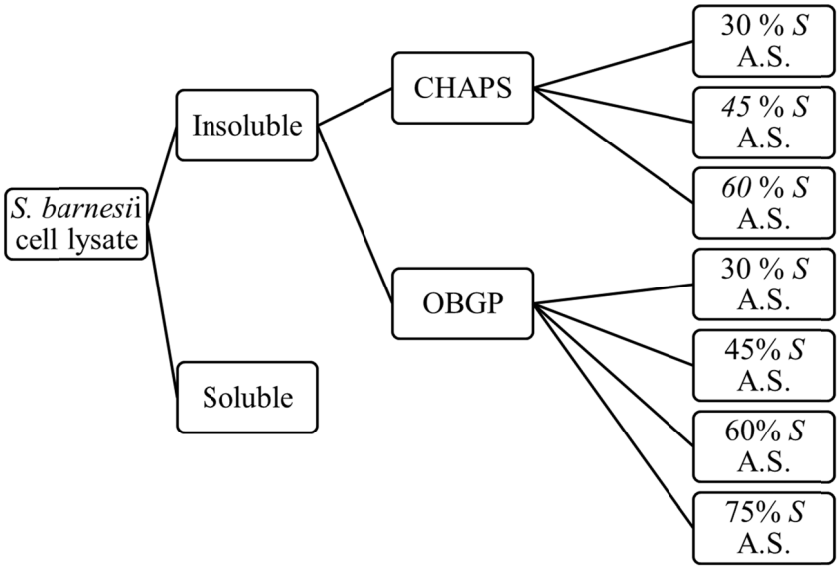

Figure 2.2: Scheme of the differential solublization of *S. barnesii* proteins using CHAPS and OBGP detergents. The insoluble pellet isolated by ultracentrifugation was suspended in 50 mM Tris-HCl buffer (pH= 7.7), then separated into 2 aliquots. Membrane protein aliquots were solubilized with 1% CHAPS or 1% OBGP at 0^{o}C overnight. The detergent soluble proteins were precipitated with subsequent saturation steps of ammonium sulfate (AS) in 10mM Tris-Cl (pH6.6) buffer + 0.1% detergent (OBGP or CHAPS). The saturated AS pellet were resuspended in 10 mM TrisHCl and dialyzed to lower the salt concentration.

The OBGP detergent solubilized more protein than CHAPS; 44 mg of protein was recovered with OBGP compared to 39 mg recovered with CHAPS. The SDS-PAGE gel of the CHAPS and OBGP solubilized fractions (**Figure 2.3**) indicates that a 51 kDa protein band is more intense in the OBGP fraction. A 31 kDa protein band is more intense in the CHAPS fraction. Each band was extracted from this gel and analyzed by MALDI-TOF MS. The OBGP enriched 51kDa protein was successfully identified as the metalloid reductase, RarA, from *S. barnesii* strain SES-3 (accession number 23394982) with 45% sequence coverage. The function of RarA is unknown function.

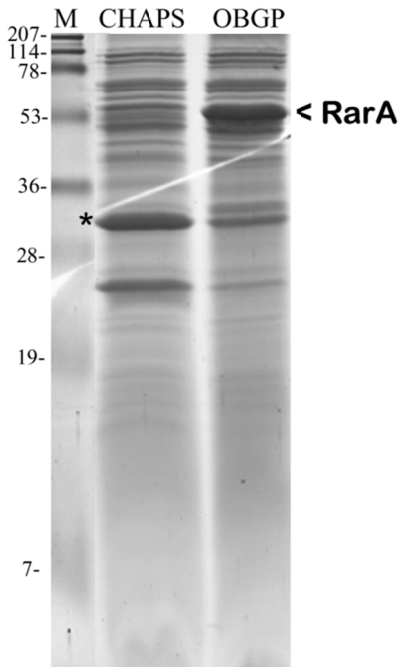

Figure 2.3: SDS/PAGE separation of proteins from the *S. barnesii* OBGP and CHAPS solubilized fractions illustrating the enrichment of RarA in the OBGP fraction. The ~48kDa protein band in the OBGP solubilized fraction was excised (<) , subjected to trypsin digestion, and then MALDI-TOF MS analysis (conducted by a fellow lab member). Using Mascot, the protein was identified as the metalloidreductase, RarA, from *S. barnesii* (MW= 48133) with 45% sequence coverage (accession number 23394982).

The nitrate reductase activity was measure in each fraction by quantifying the nitrite produced from nitrate via the Griess assay. The OBGP and CHAPS detergents solubilize comparable amounts of nitrate reductase activity. In-gel activity assays were also used to determine the effect of each CHAPS and OBGP detergent on nitrate reduction. The detergent solubilized proteins were first separated using native PAGE. Similar to SDS-PAGE, each detergent was used in the polyacrylamide gels and running buffer to maintain solubility. After electrophoresis, the gels were stained with methyl viologen, and then washed with nitrate to locate the protein complex responsible for nitrate reduction. The bleaching of methylviologen indicates an "active" protein band. The active band was excised from native gel, incubated with SDS to release the proteins,

and then concentrated with ultrafiltration. The isolated protein complex was then separated under denaturing conditions, SDS/ PAGE,

In contrast with the solution assay, the in-gel nitrate reductase activity assay reveals that only the CHAPS solubilized fraction has nitrate reductase activity (**Figure 2.4**), not the OBGP fraction (gel not shown). The nitrate reductase active band, from the CHAPS soluble fraction, was extracted from the gel and separated using denaturing electrophoresis (SDS-PAGE) to resolve all of the protein components (**Figure 2.4**). Only a 100 kDa band is visible, consistent with the predicted size of *S. barnesii* NapA.

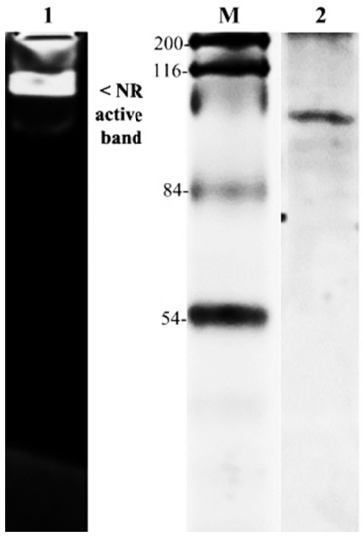

Figure 2.4: Native gel electrophoresis and in-gel nitrate reductase activity of CHAPS solubilized *S. barnesii* proteins. The active NapA from native PAGE and subsequent separation via SDS/PAGE (lane 2). CHAPS solubilized membrane proteins were first separated via native gel electrophoresis, and then the gel was stained with reduced methylviologen and incubated with a nitrate solution (lane 1). The nitrate reductase activity bleached the methylviologen, indicating the location of nitrate reducing proteins. The gel was scanned with a densitometer (Bio-Rad, GS 800) and then stained with colloidal coomassie blue. The coomassie and viologen stained gels were overlaid to determine the band responsible for NR activity. The band was then excised from a CHAPS native gel and incubated with SDS loading buffer at 90^{o}C for 10 minutes to denature. The sample was separated on a SDS/PAGE gel (Lane 2). The molecular weight of the protein in lane 2, 100 kDa, was calculated by comparison to a molecular weight standard (Lane M).

While this experiment indicated that the OBGP solubilized fraction had no nitrate reductase activity, the OBGP fraction did have high nitrite reductase activity in the in-gel assay. Comparison of the CHAPS and OBGP soluble in-gel nitrite reductase assays (**Figure 2.5**) illustrates the relatively more active nitrite reductase activity in the OBGP soluble fraction. As previously described, the active nitrite reductase band was extracted from the native gel and separated using SDS-PAGE. No proteins were detected in the SDS-PAGE separation of the CHAPS band. The CHAPS active band was not defined (**Figure 2.5**), possibly leading to low protein recovery prior to the SDS-PAGE. Multiple proteins were extracted from the OBGP active band. The sizes of the peptides are 98, 78, 68, and 55 kDa (**Figure 2.6**), conceivably the nitrite reductase (NrfA c.a. 55 kDa). Unfortunately we were not able to identify any of the proteins using MALDI-TOF MS. The spectra are saved and awaiting the completion of the *S. barnesii* genome.

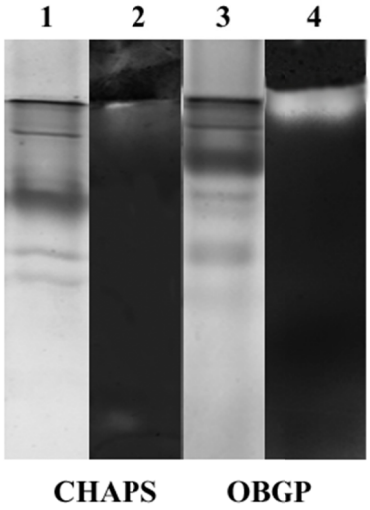

Figure 2.5: Native gel electrophoresis and in-gel nitrite reductase activity assay of the CHAPS and OBGP solubilized *S. barnesii* fractions. The coomassie stained native gels for the CHAPS (**lane 1**) and OBGP (**lane 3**) soluble fractions. The in-gel nitrite reductase activity assay was conducted by staining the gel with dithionite reduced benzylviologen after electrophoresis, and then incubated with nitrite. The nitrite reductase assay of the CHAPS (lane 2) and OBGP (lane 4) soluble fractions is presented; the bleached bands are indicative of nitrite reductase activity. The same bands display nitrate reductase activity also (data not shown).

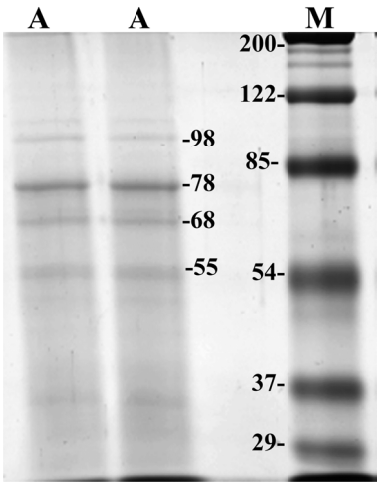

Figure 2.6: SDS/PAGE of nitrite and nitrate reductase active bands excised from the OBGP native gel. The active bands were excised from the OBGP native gel in **Figure 2.5**, incubated in 2% SDS to solubilize the proteins, and then the acrylamide was removed by microscale diafiltration (Pall). After colloidal coomassie blue staining, the gel was scanned with a densitometer (Bio-Rad, GS 800) and the molecular weights calculated (Quanity One, Bio-Rad). The active band (**A**) was extracted twice. A BioRad molecular weight marker (**M**) was used as a standard.

From the coomassie stained N-PAGE separation (**Figure 2.5**) it was apparent that most protein complexes do not travel far into the gel. To achieve better separation without lowering the acrylamide concentration and diffusing the active band the pH of the resolving gel was lowered from 8.8 to 6.8. While fewer protein bands are in the pH 6.8 gel, two nitrite reductase active bands were resolved (**Figure 2.7**). The top band is located between the stacking and resolving gels, most likely insoluble proteins which were not able to enter the higher percentage acrylamide matrix of the resolving gel. All of the active bands were extracted and separated using SDS-PAGE (**Figure 2.7**). A 65 kDa band is enriched in the nitrite reductase band which traveled into the N-PAGE resolving gel (the bottom band in F**igure 2.7**). The 65 kDa band was identified as RarA by MS.

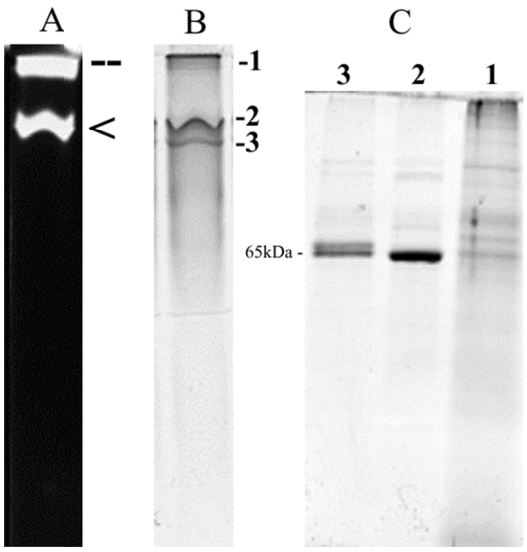

Figure 2.7: Native gel electrophoresis, in-gel nitrite reductases activity assay, and SDS/PAGE separation of RarA from OBGP soluble *S. barnesii* fraction. The same process, used to isolate the active bands from OBGP soluble fraction in Figure 2.6 and was repeated, but in this experiment the pH of the resolving gel was lowered to 6.8 from 8.8. The dark 65 kDa band was identified as RarA. **A**) Two nitrite reductase active bands were resolved (**--**) and (**<**). **B**) Staining the gel with coomassie blue indicated that three bands are present, numbered 1-3. Each was excised, incubated in 2% SDS to solubilize the proteins, and then the acrylamide was removed by microscale diafiltration (Pall), and then separated using SDS/PAGE. **C**) The three bands were loaded in lanes 1-3 respectively. The coomassie stained gel was scanned with a densitometer (Bio-Rad, GS 800) and the molecular weights calculated (Quanity One, Bio-Rad). The active band (**A**) was extracted twice. A BioRad molecular weight marker (**M**) was used as a standard.

The OBGP and CHAPS soluble fractions were further fractionated using ammonium sulfate precipitation. The OBGP solubilized proteins precipitated over a larger range of salt than the CHAPS soluble fraction. In the CHAPS solubilized fraction most proteins precipitated under 60 % *S*, and no protein was detected in the 60 % *S* supernatant. OBGP provided more separation, proteins precipitated from 30 % *S* to 75 % *S*, and the 75 % *S* supernatant also contained protein. In the OBGP fractions, nitrite reductase activity was highest in the 30 % *S* fraction and nitrate reductase activity was distributed over the 45 % *S*, 60 % *S*, and 75 % *S* fractions. The nitrate and nitrite reductase activity was highest in the 45 % *S* and 60 % *S* precipitated CHAPS proteins.

SDS-PAGE analysis indicates that a ~ 100 kDa protein is enriched in the CHAPS fractions precipitated with 45 % *S* and 60 % *S* AS, and in the OBGP fractions precipitated with 60 % *S* and 75 % *S* AS (**Figure 2.8**). Although, the nitrate reductase activity measured in the CHAPS fractions was higher (over 10 x) than the OBGP fractions. The ammonium sulfate precipitation and in-gel nitrate reductase activity assays indicate that CHAPS detergent was more successful at solubilizing active nitrate reductase. Therefore CHAPS was used for future purification experiments. The CHAPS solubilized proteins precipitated with 60% and 45 % *S* ammonium sulfate were desalted and then separated using liquid chromatography.

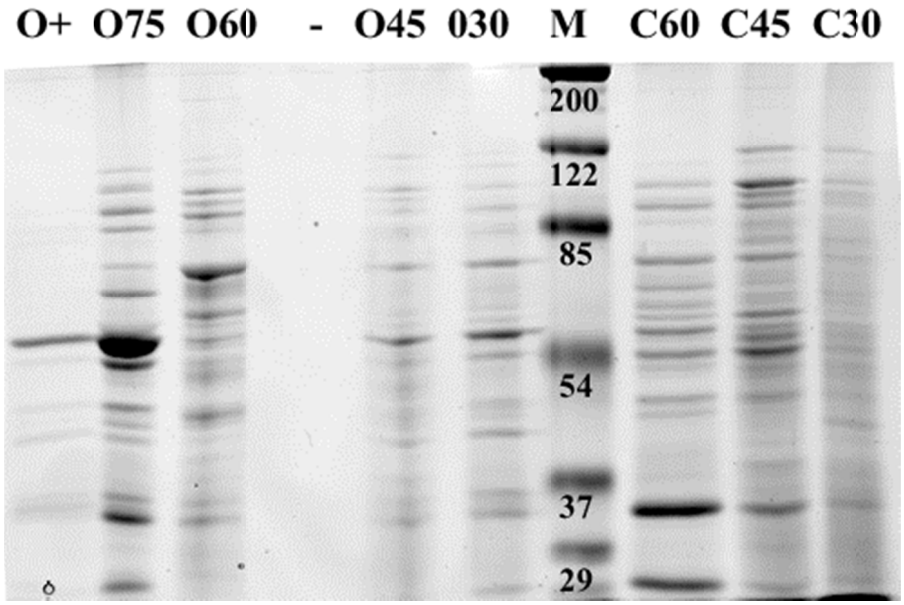

Figure 2.8: Stepwise ammonium sulfate precipitation of proteins from the *S. barnesii* OBGP and CHAPS solubilized fractions. Abbreviations: OBGP **(O)**, CHAPS **(C)**, molecular weight marker (BioRad) (**M**) with the molecular weight (kDa) provided under each band. The ammonium sulfate steps: 0% saturation (*S*) to 30% *S* **(30)**, 30% *S* to 45% *S* (**45**), 45% *S* to 60% *S* (**60**), 60% *S* to 75% *S* (**75**), and the supernatant (**+)**

NapA was isolated from *S.barnesii* by fractionation with CHAPS detergent, ammonium sulfate precipitation, and anion exchange chromatography (**Figure 2.9**).

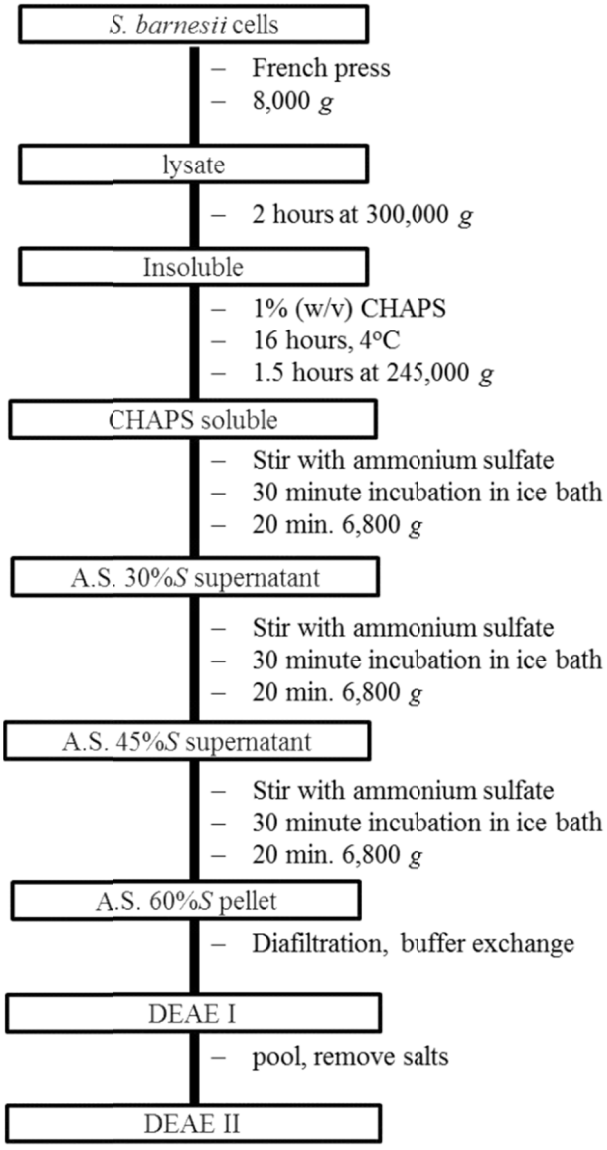

Figure 2.9: Overview, flow chart, of the *S. barnesii* NapA purification process. **A.S.** = ammonium sulfate precipitation; **DEAE**= anion exchange chromatography.

The purity of NapA was monitored using a combination of denaturing electrophoresis. The reduced methylviologen nitrate reductase activity assay was used to monitor nitrate reductase activity. A summary of the nitrate reductase assay results from a representative NapA preparation is presented in **Table 2. 2** and illustrated in **Figure 2.10**.

Figure 2.11 displays the corresponding SDS/PAGE separation of the proteins in each fraction. Briefly, the whole cell lysate was separated into an insoluble pellet and a soluble supernatant. While these fractions recovered comparable quantities of nitrate reductase activity, the in-gel native-PAGE assay suggested that most of the protein derived nitrate reductase activity is isolated in the insoluble pellet. No nitrate reductase band was observed in the in-gel assays using lysate. The soluble fraction may include redox active metabolites which are capable of nitrate reduction or methyl viologen oxidation. The CHAPS soluble extract was prepared by incubating the insoluble fraction overnight with CHAPS. Approximately 88% of the NR activity in the insoluble fraction was recovered in the CHAPS soluble fraction. The nitrate reductase activity was precipitated at 60 % ammonium sulfate saturation (*S*). Approximately 80 % of the NR activity measured in the 45 % *S* supernatant was recovered in the 60% saturated ammonium sulfate pellet (**Figure 2.10, Table 2.3**). Buffer exchange using diafiltration was efficient at removing salts, 60 % of the activity was recovered. Overall the yield of active NapA is low. Metal analysis indicates that molybdenum is lost during purification. In the presented preparation, the CHAPS soluble fraction contained ~ 90 % (mole Mo per mole protein). Molybdenum saturation shrunk to 30 % in the 60 %S ammonium sulfate pellet.

Table 2.3: Nitrate reductase activity in *S .barnesii* NapA purification.

Fraction	Total activity (µmoles NO_3^- • min^{-1})	± SD	% recovery	% yield
lysate	30.11	8.07	-	100
Insoluble	17.83	6.37	59	59
Soluble	20.49	6.16	68	68
Chaps Insoluble	9.64	2.4	54	32
Chaps Soluble	15.77	0.87	88	52
30%*S* A.S. pellet	0.01	0.13	0	0
30%*S* A.S. supernatant	12.89	4.33	82	43
45%*S* A.S. pellet	0.19	0.34	1	1
45%*S* A.S. supernatant	9.05	3.83	70	30
60%*S* A.S. pellet	6.77	2.47	75	22
desalted A.S. pellet	3.88	0.31	57	13
60%*S* A.S. supernatant	0.81	0.18	12	3

SD, The standard deviation. **A.S.**, Ammonium Sulfate, $(NH_4)_2SO_4$

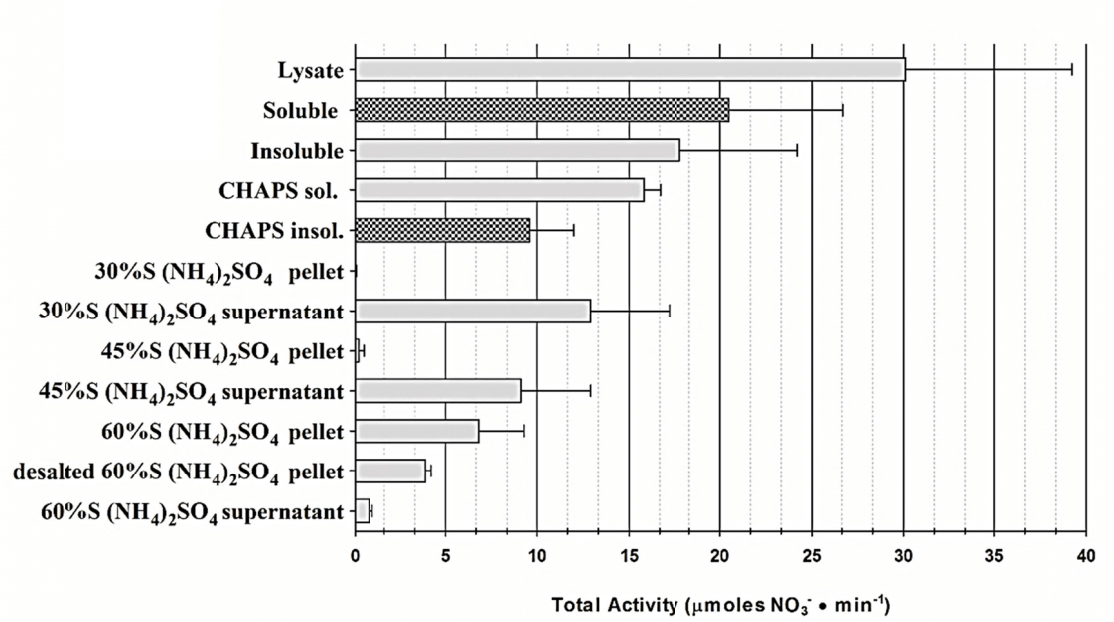

Figure 2.10: The total nitrate reductase activity measured in crude fractionation of *S. barnesii.* Shaded bars indicate fractions not used for subsequent fractionation. (N = 3) The data is also presented in **Table 2. 3**.

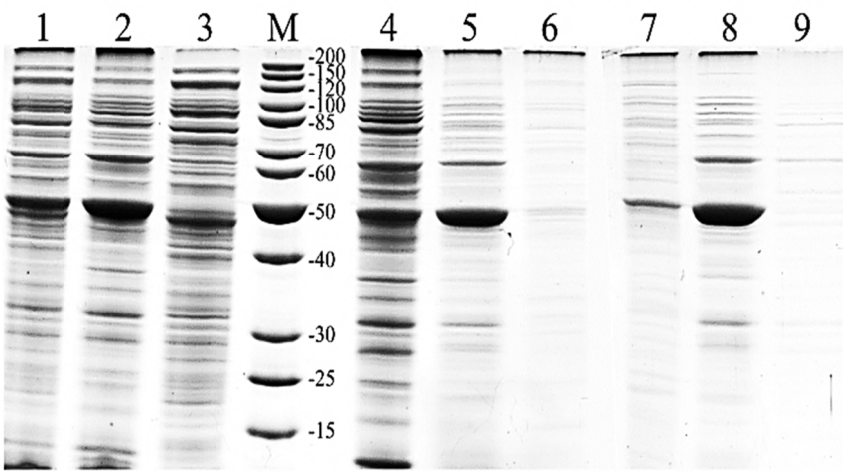

Figure 2.11: SDS-PAGE of the crude *S.barnesii* fractions. Lysate (0.6 µg, lane 1); insoluble (0.9 µg, lane 2); soluble (0.3 µg, lane 3); CHAPS insoluble (0.3 µg, lane 4); CHAPS soluble (0.9 µg, lane 5); pellet precipitated at 30 % *S* $(NH_4)_2SO_4$ (0.3 µg, lane 6); pellet precipitated at 45 % *S* $(NH_4)_2SO_4$ (0.8 µg, lane 7); pellet precipitated at 60 % *S* $(NH_4)_2SO_4$ (1.3 µg, lane 8), remaining supernatant at 60 % *S* $(NH_4)_2SO_4$ (0.2 µg, lane 9), Fermentas molecular weight marker (M).

The 60% saturated ammonium sulfate pellet was applied to a DEAE anion exchange resin (DEAE I), after desalting. The column was developed with a gradient of Buffer B, 0-100% (**Figure 2.12**), and NapA was eluted at ~ 0.2 mS • cm^{-1} conductivity and a smaller quantity at 0.6 mS • cm^{-1}. The specific activity was calculated to be 80,694 ± 212 µmoles NO_3^- • sec^{-1} • mg^{-1} protein, post DEAE I. The low salt NapA was loaded onto DEAE II, and NapA was then isolated from the high salt eluent (**Figure 2.13**). A summary of the mass spectroscopy results is provided in Appendix III. The purification procedure was repeated independently ten times, although the yield of NapA varied significantly. As mentioned previously, variation in *S. barnesii* cell yield less than consistent. It is possibly that this is the source of the NapA yield fluctuations.

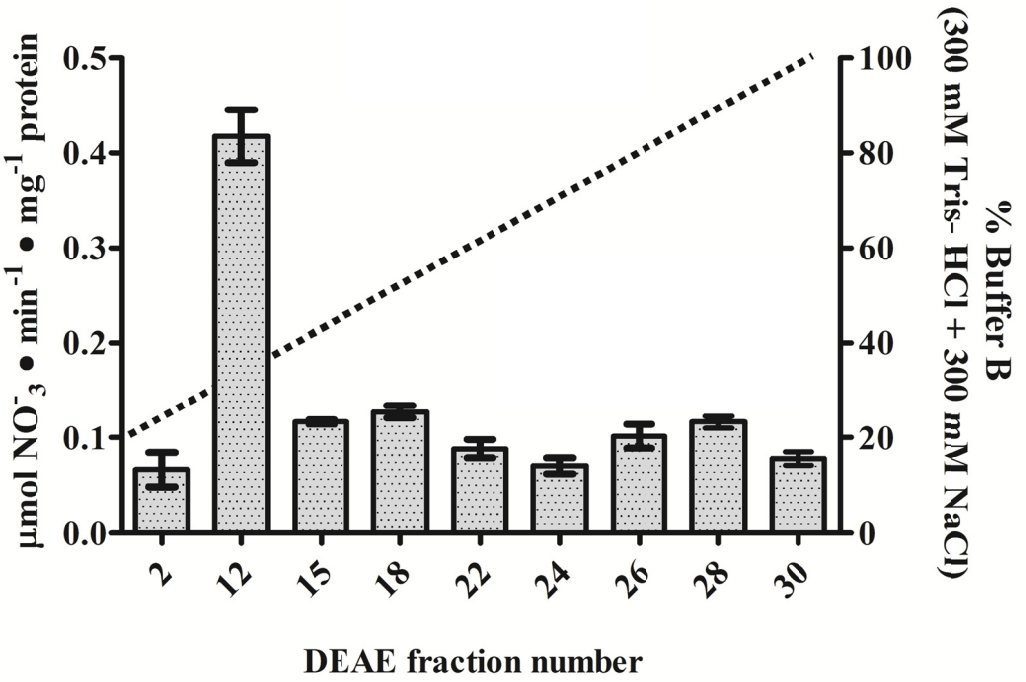

Figure 2.12: The nitrate reductase activity measured in protein fractions separated with anion exchange chromatography. The fractions were eluted from the first DEAE column (DEAE I) by applying a salt gradient (dotted line). Fraction #12 had the most nitrate reductase activity. Only fractions which contained protein were assayed.

The most common unwanted protein contaminant of NapA purification was the metalloid reductase, RarA (accession number AAN31662) by mass spectroscopy analysis. Separation of RarA and NapA was achieved by chromatography (**Figure 2.13**). First, the fractions eluted under low salt concentrations from DEAE I, which contained both NapA and RarA (**Figure 2.13**, fractions 5 - 24), were pooled together, desalted and applied to DEAE II. Next, the NapA was purified by collecting the high salt fractions from DEAE II, which did not include RarA (**Figure 2.13**, lanes A & B). Separation of NapA and RarA was difficult because both proteins elute from the DEAE resin at similar salt concentrations (0.2 mS • cm^{-1}). The strong electrostatic interactions between RarA and NapA made the proteins difficult to separate using ion exchange chromatography; RarA is electronegative (pI = 5.49) while NapA is electropositive (pI = 8.7). The

electrostatic interaction was interrupted at high salt concentrations, aiding in separation. However, the majority of NapA elutes under low salt concentration because the protein is overall cationic, and the binding affinity to an anion exchange resin would be poor, causing NapA to elute under low salt concentrations. Hydrophobic interaction chromatography and cation exchange chromatography were also investigated; however, they yielded insufficient separation.

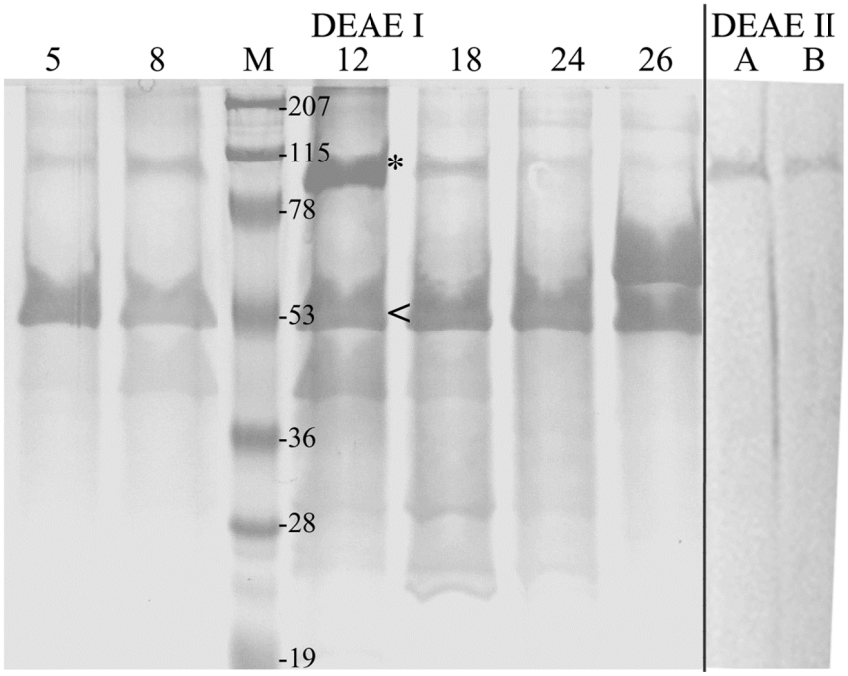

Figure 2.13: SDS/PAGE of select anion exchange chromatography fractions, including the purified NapA. The DEAE I fractions were eluted with low salt (fractions 5, 8, 12, 18, 24, 26). A major contaminate of NapA purification was identified as RarA (~50kDa) "<" by MS (see **Appendix III**). The protein band which was identified by MS as *S. barnesii* NapA is identified with an asterisk (*). Fractions isolated from DEAE II, lanes A and B, contain a 108 kDa band, also identified by MS as *S. barnesii* NapA.

NapB was not detected in the SDS-PAGE stained with colloidal coomassie blue, although the electronic spectrum of the purified NapA sample indicates that NapB is present (**Figure 2.14**). Like *Haemophilus influenzae* NapB, [144] the oxidized protein exhibits a 410 nm absorption peak, which upon reduction with dithionite shifts to 420 nm (Sorret peak). Additionally two peaks appear at 522 nm (α) and 550 nm (ß), indicative of

reduced *c*-type cytochromes [182] Sabaty *et al.* report that NapB does not stain with coomassie blue and requires silver staining for detection. [179]

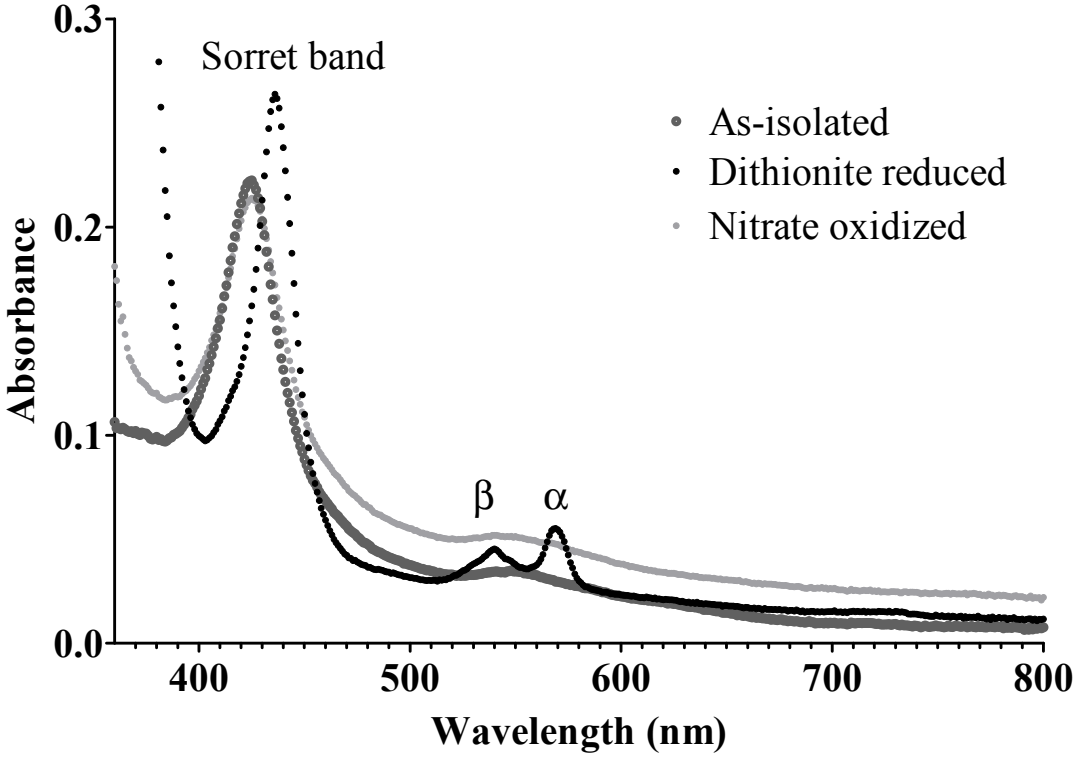

Figure 2.14: The electronic spectra of *S. barnesii* NapA: as- isolated, dithionite reduced and nitrate oxidized.

Given the low yield of purified NapA, the CHAPS soluble fraction was used to determine nitrate affinity. *S.barnesii* is predicted to only encode the Nap type nitrate reductase, as this is a characteristic of Epsilonproteobacteria such as *Campylobacter* species and *S. delyanium*. The velocity data was plotted as a function of nitrate concentration, and fit using the Michaelis-Menten non-linear regression (**Figure 2.15**). The measured affinity for nitrate (314 μM) was lower than that observed by Oremaland *et al.* with *S. barnesii* membranes (K_m = 0.7 μM & 63.4 μM). [161] However the double reciprocal plot used to estimate the nitrate affinity in these studies often miscalculates the

K_m values due to extrapolation far outside of the measured nitrate concentrations. The current study assayed nitrate reductase activity at a wide span of nitrate concentration, 1.6 µM- 14 mM, in triplicate. The R^2 value was 0.99, indicating that fitting the data using the Michaelis-Menten equation was appropriate.

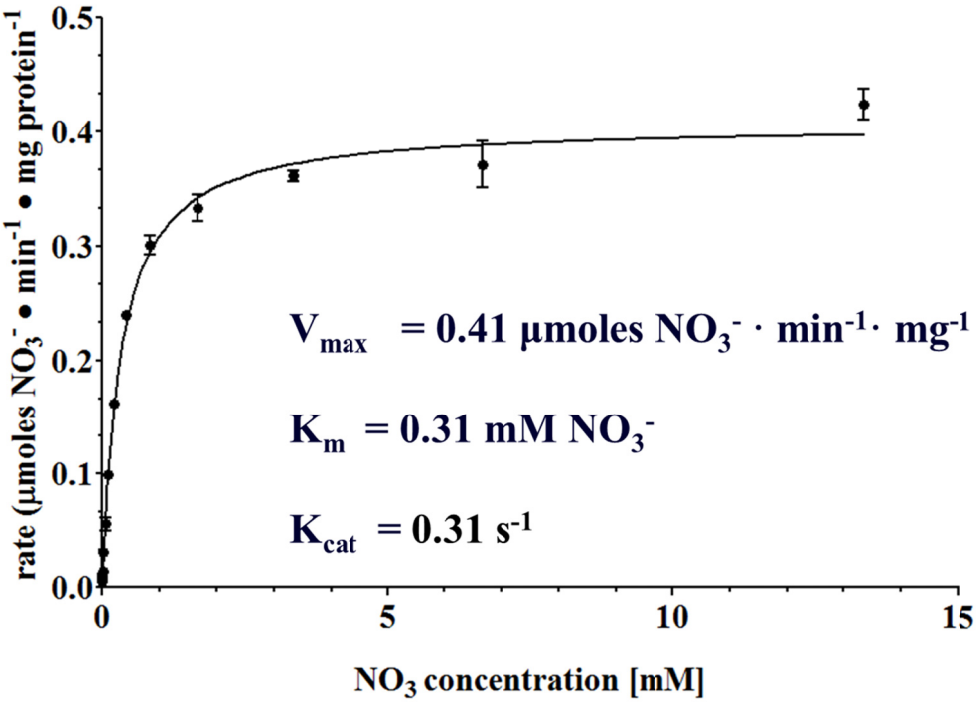

Figure 2.15: Michaelis–Menten kinetics of nitrate reduction in the NapA enriched CHAPS soluble fraction using the reduced methylviologen coupled nitrate reductases assay. Data analysis was performed using Prism v 5.03 (Graph Pad).

2.5. Conclusions

S. barnesii is an ecologically important soil bacterium, as it is capable of concurrently reducing selenate (to elemental selenium), and nitrate (to ammonia). The native isolation of *S. barnesii* NapA, although successful, yields undesirably low quantities of the active protein, too low to preform future studies. Under the specified growth conditions the amount of NapA expressed was low. The kinetic data, collected from the CHAPS soluble fraction, reveals that *S. barnesii's* NapA has a strong affinity for nitrate. This is consistent with values obtained from other NapA isolates.

CHAPTER 3: Cloning, expression and characterization of the *Campylobacter jejuni* strain RM1221 and *Sulfurospirillum barnesii* strain SES-3 periplasmic nitrate reductase (Nap) proteins.

3.1. Abstract

Prior to this work NapA has only been isolated from the native organism. Genetic manipulations have been employed to homologously overproduce recombinant NapA. In the present study, *Escherichia coli* was used as the host for expression of the recombinant *C. jejuni* and *S.barnesii* NapA. To our knowledge, this is the first successful heterologous expression and purification of a functional NapA. NapD, a well-characterized dedicated NapA-chaperone protein, and NapL, a proposed NapA chaperone, were co-expressed with NapA. *C. jejuni* and *S. barnesii* NapA display Michaelis-Menten type kinetics, with a calculated maximum velocity (V_{max}) of 0.042 ± 0.004 and 0.084 ± 0.009 μmoles [NO^-_3] • min^{-1} • mg $protein^{-1}$, respectively. The K_m for nitrate was calculated to be 2.3 ± 0.68 mM for *C. jejuni* and 7.2 ± 1.6 mM for *S. barnesii.*

3.2. Introduction

Periplasmic nitrate reductase (Nap) catalyzes the reduction of nitrate to nitrite in a variety of prokaryotes. The catalytic subunit, NapA, has three classifying features: 1) a molybdenum center, coordinated by a strictly conserved cysteine residue and two pyranopterin cofactors; 2) an iron sulfur cluster (4Fe-4S); 3) an N-terminal twin arginine translocase (TAT) leader sequence, which signals the protein for transportation to the periplasmic space. Although the residues involved in cofactor binding and periplasmic transportation are conserved, NapA is employed by bacteria for various physiological motives: dissimilatory nitrate reduction (both denitrification [80] and nitrate reduction to ammonia [81]), maintenance of cellular oxidation-reduction potential (i.e., redox poise) and nitrate scavenging. [82, 83] Moreover, many human pathogens encode Nap without the respiratory nitrate reductase (Nar) or assimilatory nitrate reductase (Nas). The physiological function of Nap in pathogen is not clear.

In *C. jejuni*, NapA is a vital metabolic enzyme; *C. jejuni* can readily generate energy from nitrate reduction via NapA[183], and its growth is dependent on the ability to reduce nitrate.[88] The *nap* genes (i.e., *napBGH*) are up-regulated by *C. jejuni* in response to oxidative stress.[184] NapA is up-regulated in *Helicobacter pylori*, a gastrointestinal pathogen and a close relative of *C. jejuni* in response to oxidative stress.[87] Additionally, *C. jejuni* induces expression of *napABG* genes during colonization in chickens.[123] Thus, nitrate reduction via NapA appears to relieve oxidative stress in pathogenic microbes and may be very important for the survival of gastrointestinal pathogens such as *C. jejuni* in the host.

NapA has been isolated as a heterodimer with *c*-type cytochrome containing NapB. To date, the Epsilonproteobacterial NapA is yet to be isolated, thus basic enzymatic properties of this protein remain unknown. In order to isolate *C. jejuni* and *Sulfurospirillum barnesii* NapA we have cloned and heterologously expressed the recombinant protein in *E. coli* Homologous expression of functional NapA and NapB has been reported from *R. sphaeroides*[41] and *Cupriavidus necator[94]*; however, heterologous expression of *Pseudomonas* strain G-179 NapA in *E. coli* resulted in non-functional protein was found in inclusion bodies.[185] To our knowledge this study represents the first successful method of heterologous expression of functional NapA. Herein, we report the details of molecular cloning and expression of NapA from *C. jejuni* and *S. barnesii*. Kinetics of nitrate reduction was also investigated to understand the function of the recombinant enzyme.

3.3. Experimental

3.3.1. Cloning of nap genes

The flow chart in **Figure 3.1** provides an overview of cloning procedure used to create the *nap* plasmids for this study.

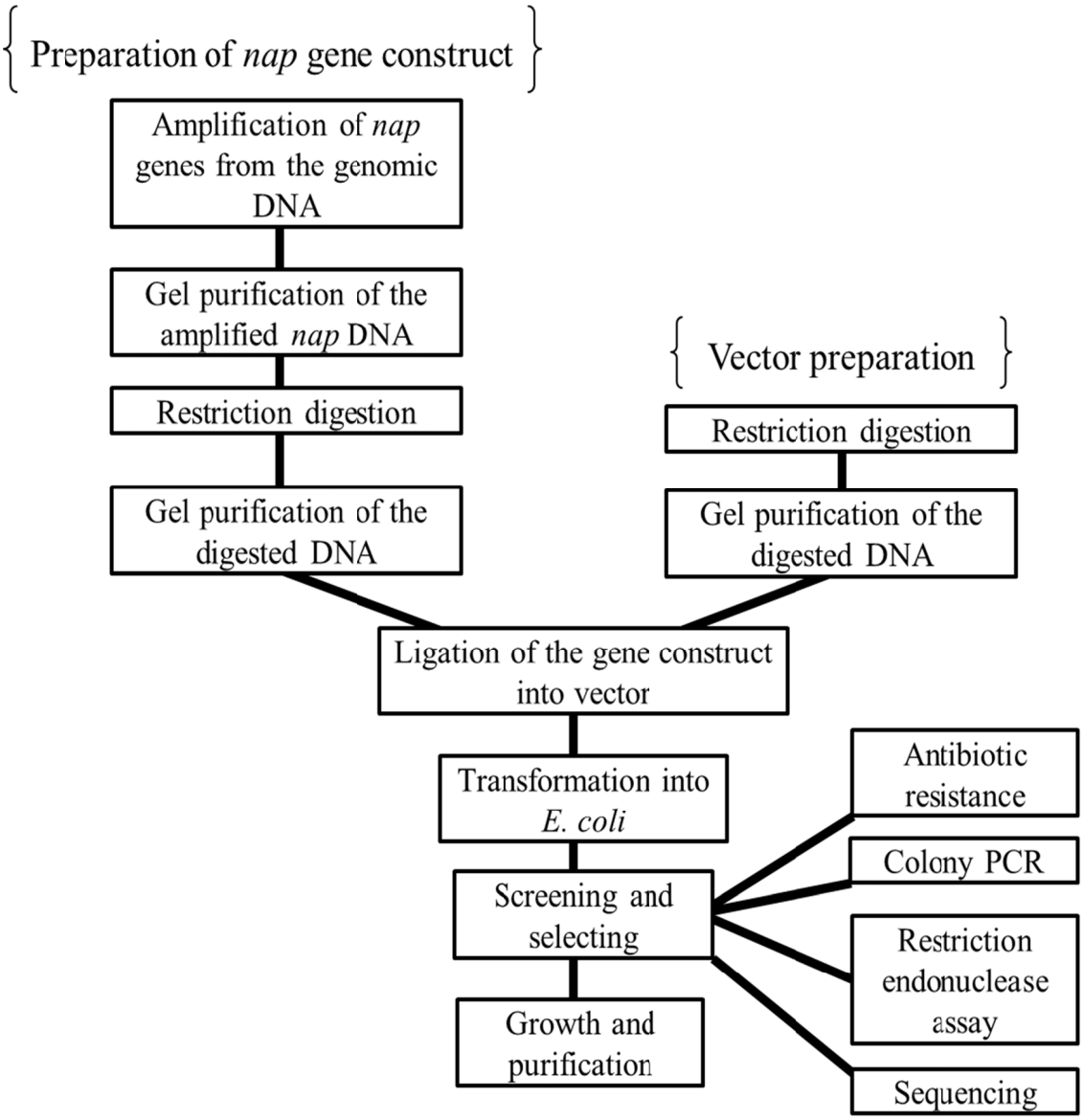

Figure 3.1: An overview of the cloning procedures used to create *nap* plasmids.

3.3.1.1. Bacterial strains and media

Escherichia coli strain DH5α (Invitrogen) was used for all standard plasmid manipulations. *E. coli* T7 express (New England Biolabs) and BL21 (DE3) cells (Stratagene) were investigated for protein expression. Lysogenic broth (LB), Lennox recipe (LB media, Appendix V) was used for growth of *E. coli* on liquid or solid media (with agar). The final concentration of ampicillin 100 μg • mL^{-1} and/or kanamycin 25 μg • mL^{-1} were used to grow bacteria transfected with a plasmid encoding the respective antibiotic resistant gene, Amp^R or Kan^R.

3.3.1.2. DNA Electrophoresis

Electrophoretic separation of DNA was conducted according to standard procedures in TAE buffer at 100V for 20-30 minutes. [186] DNA, stained with ethidium bromide (loading buffer or PCR mixture), was visualized using UV light and photographed. The size of the separated DNA fragments was estimated by comparison to a molecular weight standard (1Kbp DNA ladder, Fermentas). Two gel sizes are used in this study. Preparative gels, which had a 35 μL loading capacity and analytical gels, which had a 20 μL loading capacity.

3.3.1.3. Amplification *nap* genes from the genomic DNA

Genomic DNA of *C. jejuni* strain RM1221 [187] and *S. barnesii* strain SES-3[188] were provided by Dr. William Miller (United States Department of Agriculture, USDA), and Ms Rishu Bansal and Ms. Shrabani Basu (Duquesne University), respectively. The genome of *S. barnesii* strain SES-3 was not complete at the time of the primer design, although a preliminary, shot-gun, sequencing data was available. Unfortunately, the *napB* gene appeared to be truncated or incomplete so primers for *napB*

were designed for the flanking genes, *napH* and *napF,* to amplify the DNA with PCR and obtain a sequence of *napB.* Preparative polymerase chain reaction (PCR) was used to amplify the *napA* genes from the genomic DNA of *C. jejuni* (NCBI Accession No. YP_178873) and *S. barnesii* (AAM21158) and *C. jejuni napB* (YP_178876). The *C. jejuni napLD* maturation genes (YP_178877 and YP_178878) were also amplified.

The oligonucleotides listed in **Table 3.1** were used as primers to amplify the target *nap* genes by preparative polymerase chain reaction (PCR). For each gene restriction enzyme sites were introduced within the primer sequences. Two different restriction sites were used for the 3' and 5' ends of each gene to ensure the proper insertion of the genes, in the intended orientation and in the promoter reading frame. In order to preserve the N-terminal signal sequences in the NapA and NapB proteins the His_{6x} affinity tag was introduced at the C-terminus of each protein. To place the genes in the correct reading frame with the hexahistidine (His_{6x}) coding sequence the XhoI and BglII restriction sites were used in the reverse primers of *napA* and *napB* respectively. Plasmid maps for each construct are provided in Appendix I to illustrate the location of the relevant genetic features (i.e., promoters, restriction sites, and affinity tag coding regions.

A Taq DNA polymerase mixture (ReadyMix™, Sigma) was used as instructed, with the addition of Pwo DNA polymerase. The details on the PCR reaction mixture and thermocycler parameters are in **Appendix V**. Amplified constructs were purified by preparative electrophoresis. A DNA standard (Fermentas) was used to estimate the size of unknown DNA bands. The DNA was then extracted from the gel my manual excision and purified using the NucleoSpin® kit (Macherey-Nagel) according to manufacturer's

guidelines. [189] Briefly, agarose was melted at 50 ^{o}C in a buffer solution. DNA is bound to the membrane by centrifuging at 11,000 x g for 1 minute. The membrane was washed with a 60% ethanol solution (300 µL x 2) by centrifuging at 11,000 x g quickly. After removing the eluent, the membrane is dried at 11,000 x g for 3 minutes. The DNA is eluted by incubating the membrane with 20-50 µL of elution buffer and centrifuging the column in a sterile eppendorf tube at 11,000 x g. The DNA concentration of the eluent was measured in 2 µL volume using a nanodrop spectrophotometer by measuring the absorbance at 260 and 280 nm.

Table 3.1: Polymerase chain reaction (PCR) conditions and primers used to amplify *nap* genes.

Organism	Gene target (NCBI Accession number)	Size (bp)	RE/ direction	Primer nucleic acid sequence (5' to 3')	PCR conditions	
					Elongation time (sec)	Annealing Temp (^{o}C)
C. jejuni RM 12221	*napA* (YP_178873)	2800	NdeI/ forward	CAG ACC ATA TGA ATA GAA GGG ATT T	180	52
			XhoI/ reverse	GGT GCT CGA GAG CCT TAT AAA TTT TTA C		
			829-849*	CAT CCA GAG GCT ATG GAT ATG	NA	NA
	napLD (YP_17887, YP_178878)	1250	NcoI/ forward	GAC ACC ATG GAT GAA AAA ATT TCT TT	75	51
			EcoR1/ reverse	GAG CTC GAA TTC AGA AAA TTG ATT AAA TAC		
	napB (YP_178876)	522	NcoI/ forward	GAC ACC ATG GAT GAA GAA GAA ATT G	40	53
			Bgl11/ reverse	GTG ATG AGA TCT CTT TAC ACC CTC ATT		
S. barnesii SES-3	*napA* (AAM21158)	2800	NdeI/ forward	GCA CTG CAT ATG TCG CTT TCA AGA AG	180	58
			XhoI/ reverse	CTA GTC TCG AGG GCT TTA TAG AGC TTA ACA G		
			811-830*	GGA ACT ATA TCG CTC GTG AG	NA	NA
	napFLD	~1100	NcoI/ forward	CTA GCC ATG GAT GAG CCG GGT ACC GG	70!	60!
			PstI/ reverse	CGT ACT GCA GGG CAT TTT GGA GCT TTT C		
	napHBF	~1000	Blunt end	CAA ATG AAA ACA TGG ATT CG	70	46
				CCA AAT ACT TCA TGA CTC		
	napB	550	NcoI/ forward	GCA GAC CAT GGA TGA TGA GTA GAA AA	40	62
			Bgl11/ reverse	GTG ATG AGA TCT CTT CAC GCC CTC ATT		

* Internal binding primers used for sequencing of the *napA* genes
! Multiple elongation times and annealing temperatures were explored

3.3.1.4. Restriction digestion and purification of digested DNA

The amplified *nap* gene constructs were digested with two restriction endonucleases (RE), in order to create complementary and cohesive "sticky" ends. Restriction assays were performed according to a standard protocol (Appendix V, preparative restriction assay), as directed by the manufacturer (New England Biolabs). The expression vectors, pET-21α, pQE-60 and pRSF Duet-1 (**Table 3.2**) were also cleaved by this method in order to prepare the plasmid for *napA, napB* and *napLD* construct insertion, respectively. After digestion was complete, the enzymatically treated DNA was purified by gel electrophoresis, excised from the agarose and isolated via the NucleoSpin® kit (Macherey-Nagel) as previously described. [189]

3.3.1.5. Ligation of *nap* gene constructs and expression vectors

Ligation of the *nap* gene constructs and vector DNA was performed by incubating a 4:1 mixture, respectively, for 5 minutes at 45^{o}C. The mixture was then cooled using an ice bath. Ligation buffer was added, followed by T4 ligase. The mixture was incubated for 2 hours at 15 ^{o}C (ligation reaction, Appendix V). The entire mixture was used for transformation in *E. coli DH5α*.

3.3.1.6. Ligation of nap gene constructs and pJET 1.2 cloning vector

In tandem, the same *nap* gene constructs were ligated into the pJet2.1 vector. Ligation of genes directly into expression vectors, which have low copy numbers, is risky. So to ensure that the amplified *nap* genes were ligated into a plasmid the pJet 2.1 high copy cloning vector was used. The inserts are digested with a blunting enzyme (provided in kit) prior to ligation into the pJET 1.2 (Fermentas). The ligated *nap* gene pJET 1.2 constructs were used to transform *E. coli* DH5α cells.

Table 3.2: Summary of plasmids used in this study.

Plasmids	Pertinent information	Source
pET21α	5443 bp plasmid with Amp^R and a *lacI* gene	Novagen
pRSFDuet-1	3829 bp plasmid with Kan^R and a *lacI* gene	
pQE-60	3431 bp plasmid with Amp^R	Qiagen
pREP4	3740 bp plasmid with Kan^R. Constitutively expresses the *lacI* repressor gene, used in conjunction with pQE-60	
pJET 1.2	2974 bp blunt ended high copy cloning vector with Amp^R	Fermentas
pCnapA	The 2.8 kbp NdeI- XhoI *napA* gene construct amplified from *C. jejuni* , then cloned into pET-21α at the corresponding restriction sites (Amp^R)	This work
pJCnapA	The 2.8 kbp NdeI- XhoI *napA* gene construct amplified from *C. jejuni*, digested with blunting enzymes & cloned into pJET 1.2 using the blunt ended cloning site (Amp^R)	This work
pCnapB	The 522 bp NcoI- BglII *napB* gene construct amplified from *C. jejuni*, then cloned into pQE-60 at the corresponding restriction sites (Amp^R)	This work
pJCnapB	The 522 bp NcoI- BglII *napB* gene construct amplified from *C. jejuni*, digested with blunting enzymes & cloned into pJET 1.2 using the blunt ended cloning site (Amp^R)	This work
pCnapLD	The 1.25 kbp NcoI- EcoRI *napLD* gene construct amplified from *C. jejuni*, then cloned into pRSF Duet-1 at the corresponding restriction sites (Kan^R)	This work
pJCnapLD	The 1.25 kbp NcoI- EcoRI *napLD* gene construct amplified from *C. jejuni*, digested with blunting enzymes & cloned into pJET 1.2 using the blunt ended cloning site (Amp^R)	This work
pSnapA	The 2.8 kbp NdeI- XhoI *napA* gene construct amplified from *S. barnesii*, then cloned into pET-21α at the corresponding restriction sites (Amp^R)	This work
pSnapB	The 522 bp NcoI- BglII *napB* gene construct amplified from *S. barnesii*, then cloned into pQE-60 at the corresponding restriction sites (Amp^R)	This work
pJSnapHBF	The ~1 kbp *napHBF* gene construct amplified from *S. barnesii*, digested with blunting enzymes & cloned into pJET 1.2 using the blunt ended cloning site (Amp^R)	This work

Amp^R, resistance to ampicillin
Kan^R, resistance to kanamycin
bp, base pair

3.3.1.7. Amplifying genes from the pJET 1.2 cloning vector

For two genes, *C. jejuni napA* and *S. barnesii napB*, ligation of the construct directly into the expression vector was not successful, therefore the pJET 1.2 construct was used as a template for PCR amplification. The *C. jejuni napA* and *S. barnesii napB* genes were then digested, and ligated into expression vectors, pET21α and pQE-60, respectively, as previously in the previous section.

3.3.1.8. Transformation of *E. coli* DH5α

Chemically competent DH5α (Invitrogen) cells, were thawed and incubated with the plasmid DNA for 30 minutes on ice. After incubation, the cells are shocked by heating at 42^{o}C for 90 seconds. After cooling, the heat shocked cells were resuspended in

800 µl LB (liquid) medium (without antibiotic) and incubated with agitation at 37°C for 45-90 minutes. The culture was spread onto a LB (agar) plate with the appropriate antibiotic (ampicillin 100 µg • mL^{-1} or kanamycin 25 µg • mL^{-1}) and incubated overnight at 37°C. Only the colonies with the plasmid encoding the resistance to the antibiotics are able to grow; providing a method of screening. Colonies, which were able to grow on the antibiotic supplemented agar plates, were also analyzed for the presence of the full length *nap* genes by colony PCR.

3.3.1.9. Colony PCR

Colonies were scraped with a sterile pipette tip and mixed directly with 20 µl of the PCR mixture (Colony PCR, Appendix V) by swirling, and then the tip was ejected into 5 mL LB media (with antibiotic) and incubated overnight with shaking at 37°C. The PCR settings used to amplify the genes from organisms genomic DNA was repeated (**Table 3.1**), the entire reaction mixture loaded onto a 1% agarose gel and electrophoretically separated.

3.3.1.10. Plasmid extraction from *E.coli*

Cultures inoculated during colony PCR, were collected by centrifugation at 11,000 x g for 5-10 minutes. The resulting cell pellets were lysed and the plasmid DNA was purified with the NucleoSpin® kit for plasmid preparation according to the manufacturer's protocol. [189] The plasmid was eluted into ~50 µL of buffer. The concentration of DNA was determined spectrophotometrically and the sample was stored at -20°C.

3.3.1.11. Restriction enzyme assay

The plasmid constructs were subjected to a restriction digestion assay to confirm the sequence (Test restriction assay, Appendix V). DNA management software, GENtle [190], was used to predict which enzymes could cleave the constructed plasmids at two sites, one cleavage site within the *nap* gene sequence and a second cleavage site with in the corresponding plasmid sequence, producing two unequally sized fragments of DNA. The digestion buffer and ratio of enzyme the used for each assay differs according to the RE combination exploited (**Table 3.2**). The double digest™ tool, provided by Fermentas (http://www.fermentas.com/en/tools/doubledigest) was utilized to determine the recommended assay conditions such as type of buffer, ratio of RE, and incubation time and temperature. After completion the reaction was analyzed by gel electrophoresis. The entire assay mixture was loaded onto an agarose gel to purify the DNA and determine the size of the resulting DNA fractions.

Table 3.3: Restriction endonuclease (RE) assay conditions for the *nap* plasmids

Plasmid ID	Gene target	Vector	RE	Volume (µL)	Buffer	Expected sizes (bp)	
C. jejuni							
pJCnapA	*napA*	pJET 1.2	NcoI^{N}	0.5	#3^{N}	4527	1237
pJCnapB	*napB*	pJET 1.2	PstI^{N}	0.3	#3^{N}	3112	404
pCnapB	*napB*	pQE-60	NcoI^{N} & BglII^{F}	0.3	Tango^{F}	2959	985
pJCnapLD	*napLD*	pJET 1.2	HindIII^{F}	0.5	#3^{N}	2819	1420
pCnapLD	*napLD*	pRSFDuet	HindIII^{F}	0.5	#3^{N}	3848	1187
S. barnesii							
pSnapA	*napA*	pET21	AccI^{N}	0.2	# 4^{N}	4620	3534

Fermentas^{F} or New England Biolabs^{N} supplied the enzymes and buffers.

3.3.1.12. DNA Sequencing

DNA sequencing was performed by GATC Biotech (Konstanz, Germany). For *S.barnesii napA*, a T7 promoter-binding primer was used to confirm insertion of the gene construct into the reading frame of the promoter. An internal binding primer was also used to ensure complete coverage of the 2.8 kbp gene (**Table 3.1**). The Clone JET^{TM} (Fermentas) forward and reverse primers were used for sequencing genes cloned into the pJET 1.2 cloning vector (*C. jejuni napA*, *napB* and *napLD* and *S. barnesii napHBF*). The PCR primers used to amplify the *C. jejuni napLD* and *napB* were used to sequence the genes cloned into the pRSF and pQE-60 expression constructs (pCnapLD and pCnapB), correspondingly.

The DNA sequence data were compared to the target gene sequences by preforming a primary sequence alignment with the published sequences using GENtle [190]. Sequence data is included in the Appendix II. Only the *S. barnesii napA* gene sequence was published. Therefore, the DNA sequencing data obtained from the *napH, B, F, L* or *D* genes was analyzed by comparison to the *S. delyanium* genome. The *S. barnesii nap* genes should share high identity to those in *S. delyanium.*

3.3.2. Protein expression and purification

3.3.2.1. Co- transformation of the *E. coli* expression strains

Two *E. coli* expression strains, T7 express and BL21 were investigated. Cells were co-transformed with two plasmids: pCnapA and pCnapLD; pSNapA and pCnapLD; or pCNapB and pREP. Both of the plasmids (< 5 ng) were incubated with 100 µL of competent cells on ice for 30 minutes. The cells were subjected to a heat shock by placing the Eppendorf tubes in a 42 ^{o}C block heater for 90 seconds, and then cooling for

1-2 minutes on ice. LB media (200 µL) was added to the cells before the entire suspension was spread onto a LB agar plate with ampicillin and kanamycin, and then incubated overnight at 37 ^{o}C. Colonies were transferred with a pipette tip to a fresh 5 mL liquid culture of LB. The expression strain stocks were prepared by diluting the cultures using sterile glycerol to a final concentration of roughly 50% (v/v), then quickly freezing the culture by submerging the tube in liquid nitrogen. Expression cultures were stored in the -80^{o}C freezer.

3.3.2.2. Pilot expression studies

The expression strain and optimum growth conditions used for NapA and NapB expression was established by varying the temperature and time of incubation after inducing the cultures with 0.1 mM isopropyl-b-D-thiogalactopyranoside (IPTG). The induction conditions were established using a small scale liquid culture. *E. coli* expression cell strains T7 express and BL21 (DE3) were used for each expression study (i.e., Napa or NapB). For each strain a single inoculating culture was used. From the inoculating culture 3 mL was transferred into fresh media. Each expression culture contained 50 mL of LB media in a 300 mL Erlenmeyer flask. The expression cultures were grown to log phase (A_{600nm} = 1.2) at 37 ^{o}C with agitation (200 rpm). IPTG was added to induce expression. Cultures were then transferred to the one of the following three temperatures: 20, 30 and 37 ^{o}C and incubated for 24 hours. In addition, each strain was grown at 20 ^{o}C for 48 hours post induction. All liquid media was sterilized by autoclaving in the 300 mL Erlenmeyer flask used for growth. Ampicillin and kanamycin were added at the time of inoculation; sodium molybdate (1mM) was added to NapA

expression cultures. Cells were collected by centrifuging the culture at 6000 x g for 20 minutes and washed with buffer before freezing at -80^{o}C.

Cells were fractionated by creating spheroplasts, and collecting the periplasmic contents in a soluble fraction.[191] Salts and ethylenediaminetetraacetic acid (EDTA) introduced in the periplasmic isolation were removed by passing the periplasmic fraction through a PD10 desalting column (Amersham Biosciences) according to the manufacturer's guidelines. A phosphate lysis buffer (Ni-lysis buffer, Appendix V) was used to elute the protein fraction. The protein eluent was then incubated with 1 mL nickel-nitrilotriacetic acid (Ni-NTA) superflow resin (Qiagen) for 1 hour to bind the His_{6x} tagged protein. The Ni- lysis buffer was used to wash the resin using 4 column volumes. Using an imidazole - phosphate buffer (Ni-elution buffer, Appendix V) the bound protein was eluted into 0.5 mL fractions. Fractions which contained a detectable amount of protein, as determined via Bradford protein assay, were analyze for the presence of the NapA or NapB using SDS-PAGE, western blotting and mass spectrometry. The nitrate-coupled methyl viologen activity assay was also used to determine NapA content.

3.3.2.3. Large scale expression of NapA

The *napA* constructs (i.e., pCjnapA and pSbnapA) were co-expressed with pCjnapLD in the *E. coli* "T7 express" (New England Biolabs) cells. Expression cultures were maintained on LB Lennox media with ampicillin (100 µg/ mL) and kanamycin (25 µg/ mL). Inoculating cultures were generally grown overnight, 14-16 hours, at 37 ^{o}C. To isolate NapA, 1.5 L LB media was prepared in 6L Erlenmeyer flask. Following inoculation with 100 mL of an overnight culture, the expression culture was incubated at room temperature (20-23 ^{o}C) with vigorous shaking until the culture reached an

optimized cell density (Abs_{600nm} = 0.9). Sodium molybdate (1 mM) was then added and the cells were induced for 48 hours by adding IPTG to a final concentration of 0.75 mM. The cells were collected by centrifugation (8,000 x g for 20 minutes) and washed with a phosphate buffer (Ni-lysis buffer, Appendix V) prior to flash freezing the cell pellet in liquid nitrogen. Approximately 8 g wet weight per 1.6 L culture was obtained.

3.3.2.3. Purification of NapA

Purified NapA was obtained by resuspending the frozen cell pellet in the phosphate buffer (Ni-lysis buffer, Appendix V) buffer (pH 8.0) immediately prior to passage through a French pressure cell press (Thermo Fisher). Insoluble particles were pelleted by centrifuging the lysate (6,000 x g for 20 minutes) and the soluble supernatant was passed through a filter (0.44 μm pore size, Millipore) to reduce the viscosity of the sample. The supernatant was incubated with nickel-nitrilotriacetic acid (Ni-NTA) superflow resin (Qiagen) for one hour with agitation at 4^{o}C to bind the His_{6x} tagged NapA. Chromatographic separation of NapA was achieved with the LP BioLogic (Bio-Rad) system. To remove unbound proteins from the column, the resin was washed with the same loading buffer (Ni-lysis buffer, Appendix V) at 2.5 mL • min^{-1} until a stable baseline absorbance was obtained and protein elution minimized (*i.e.,* Abs_{280} = 0). A second wash step was performed, in the phosphate buffer the concentration of imidazole was elevated slightly, [30 mM], and the pH lowered to 7.0, (Appendix V, "Ni-wash buffer"). NapA was eluted by increasing the concentration of imidazole (400 mM) and raising the pH to 7.5, (Ni-elution buffer, Appendix V). The protein was immediately

concentrated using centrifugal filters with a 30 kDa MWCO (Millipore) and stored in 10% glycerol at -80^{o}C after flash freezing in liquid nitrogen.

3.3.3. Detection and characterization

3.3.3.1. Protein gel electrophoresis

Discontinuous sodium dodecyl sulfate polyacrylamide gel electrophoresis (SDS-PAGE, Appendix V) was used to analyze fractions using standard protocol. [176] After separation, the gel was incubated in 12% trichloroacetic acid for 30 minutes to precipitate proteins. Proteins were stained with a colloidal coomassie blue G-250 solution (0.1% coomassie G-250, 2% H_3PO_4, 5% methanol, 10% $(NH_4)_2SO_4$) overnight, then washed with methanol (25%) and scanned using a calibrated imaging densitometer GS-800 (Bio-Rad). The relative density and molecular weight of the separated proteins were calculated with Quantity One software (BioRad). Molecular weight standards (Fermentas) were used to estimate the size of unknown proteins.

3.3.3.2. Western blotting

Proteins were separated by SDS-PAGE as described earlier using a 6% acrylamide resolving gel for NapA and 10% acrylamide for NapB separation. Immunoblotting was conducted according to standard procedures [186] using a mouse anti- His_{6x} primary antibody (Dianova) and goat anti-mouse alkaline phosphatase conjugate secondary antibody (Sigma). Molecular weight standard was used to estimate molecular weight of the protein and a positive His_{6x} tag was included as a positive control.

3.3.3.3. Mass spectrometry

Protein bands were excised manually from the SDS-PAGE gel; further processing and analysis was conducted by an outside source (Bruker, Germany) or co- worker (refer to Appendix V for this supplementary protocol [192].

3.3.3.4. Metal analysis

Metal analyses of enzyme samples were conducted at the Chemical Analysis Laboratory at the University of Georgia (Athens, GA., USA) using a Thermo Jarrell-Ash Enviro 36 Simultaneous Inductively Coupled Plasma-Optical Emission Spectrograph (ICP-OES).

3.3.3.5. Molybdenum cofactor determination

To quantify molybdenum cofactor (Moco) content in the NapA protein, the molybdopterin molecule was oxidized (Moco oxidation, Appendix V). Detection of the dephosphorylated Moco, Form A, by it characteristic emission spectra [193] was performed by another lab member (refer to Appendix V for this supplementary protocol).

3.3.3.6. Protein assays

Protein concentrations were determined using the DC protein assay kit (Bio-Rad) with bovine serum albumin standard (Pierce). Additionally, purified NapA concentration was spectrophotometrically determined using the calculated extinction coefficients for NapA from *C. jejuni* and *S. barnesii*, 178,800 M^{-1} cm^{-1} and 191,460 M^{-1} cm^{-1}, respectively.

Nitrate reductase activity was measured by monitoring the oxidation of reduced methyl viologen (λ_{max}= 610 nm) [47-49] in an inert atmosphere glove box at 22 ^{o}C using an ELx808 absorbance microplate reader (BioTek). The buffer contained TrisHCl [100 mM]

(pH 8), CHAPS [0.1mM], Na_2MoO_4 [1mM] and methylviologen [0.8 mM]. Methylviologen was partially reduced with a sodium dithionite stock [60 mM] solution to yield a final absorbance of 1.2– 1.6 at 630 nm prior to incubation with 80-100 µg of protein. The rate of methyl viologen oxidation was probed by monitoring the absorbance at 630 nm using Gen5 Data Analysis Software (BioTek). The reaction was initiated by the addition of potassium nitrate and monitored until the reaction stopped (i.e., Abs =0). Under this condition, the rate of oxidation of the reduced methylviologen by the protein sample alone (i.e., no substrate) was found to be insignificant. In addition to monitoring the oxidation of reduced methyl viologen the production of nitrite was confirmed with the Griess assay (Appendix V) [175] using potassium nitrite (Fluka) as a standard.

3.3.3.7. Kinetic analysis and data treatment

The absorbance data were converted to concentration following the Beer-Lambert law ($A = \varepsilon bc$), (ε = 13,700 $M^{-1}cm^{-1}$[173] and path length, b= 0.667 cm) Linear regression of the initial rate data (first 90 seconds) were used in determining the rate of methylviologen oxidation. The data were analyzed with non-linear regression of the Michaelis–Menten equation using GraphPad Prism [174] (v5.03, San Diego, CA, USA) to a 95% confidence limit to determine the substrate affinity (K_m), maximum velocity (V_{max}), and catalytic efficiency (K_{cat}). The concentration of molybdenum, determined by ICP-OES (*see* section 3.3.3.4), was used to as an estimate of the total amount of enzyme active sites (E_t) in each assay. E_t was used to estimate the catalytic efficiency (K_{cat}).

3.4. Results and Discussion

3.4.1. Amplification, cloning and transformation of napA, napB and napLD

In *C. jejuni*, all gene targets, *napA, napB* and *napLD*, were successfully amplified. Only *napA* and *napB* were amplified from the genome of *S. barnesii* (**Figure 3.2**). Amplification of *S. barnesii* maturation proteins, *napFLD*, was not successful. At the time of this investigation, complete genome of *S. barnesii* was not available, which presumably led to the design of non-complimentary primers. Care was taken to preserve the TAT leader sequence in the NapA constructs. The *C. jejuni* NapA TAT leader sequence, SRRxFLK [194] has been demonstrated to be required for maturation of functional NapA. [195].

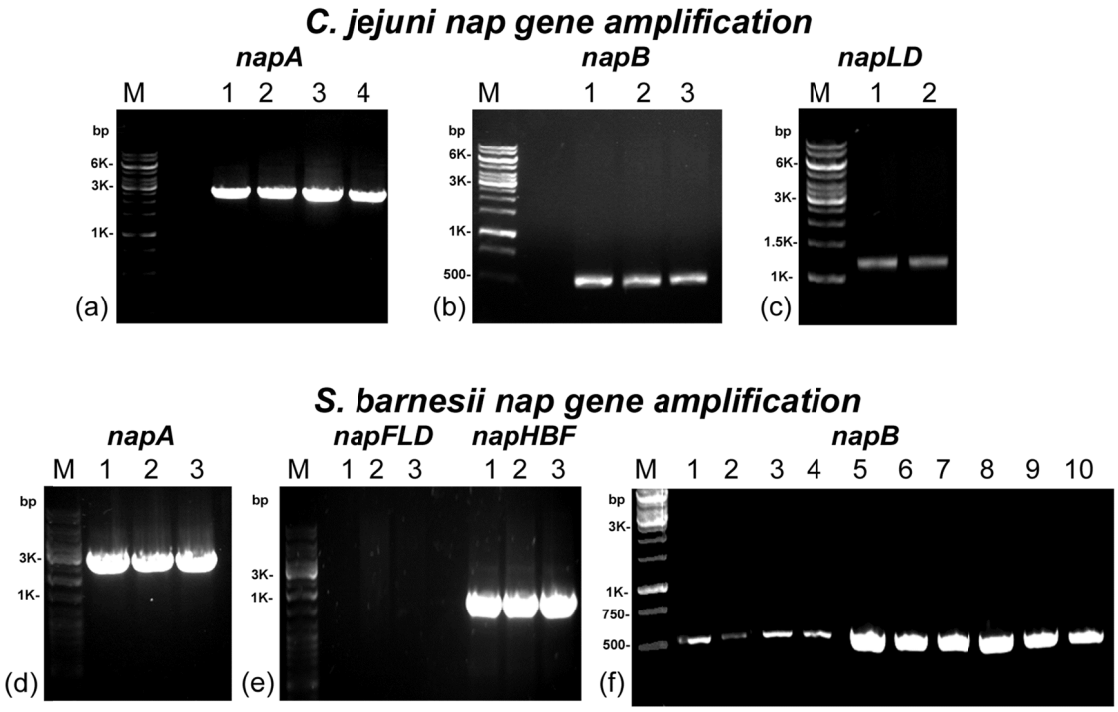

Figure 3.2: Preparative gel electrophoresis of the *nap* genes amplified from *S .barnesii* and *C. jejuni*. (**a**) *C. jejuni napA*, (**b**) *C. jejuni napB*, (**c**) *C. jejuni napLD*, (**d**) *S .barnesii napA*, (**e**) the attempted amplification of *S .barnesii napFLD* and the amplification of the *napHBF* fragment from *S .barnesii*, and (f) *S .barnesii napB*. Aliquots of the same PCR reaction, which were loaded into multiple wells on the agarose gel, are numbered (**lanes 1-3**) above the respective lane. *S .barnesii napB* (**f**) was amplified from the genomic DNA (**lanes 1-4**) and the *napHBF* construct pJSnapHBF (**lanes 5-10**). **M**= GeneRuler^{TM} 1kb DNA ladder, 250-10,000 bp (Fermentas). After PCR, the entire mixture was loaded onto a TAE 1% agarose gel. DNA was stained with ethidium bromide and the bands subsequently extracted from the gels to isolate the DNA. **Table 3.1** lists the expected sizes of the amplified *nap* gene constructs.

As a precautionary measure, *napA, napB and napLD* from *C. jejuni* and *napHBF* from *S. barnesii* were inserted into a cloning vector, pJET 1.2, creating pJCnapA, pJCnapB, pJCnapLD, pJSnapHBF, respectively. pJET 1.2 is a blunt ended high copy cloning vector, therefore, gene insertion is usually more successful than direct insertion into an expression vector which convey low copy number. This was the case with *C. jejuni napA*; therefore, pJCnapA plasmid was used as the template to amplify *C. jejuni*

napA with PCR. After PCR, preparative gel electrophoresis was use to purify the *napA* gene (**Figure 3.3**), which was subsequently digested with XhoI and NdelI, before insertion of the gene into the expression vector (pET21α).

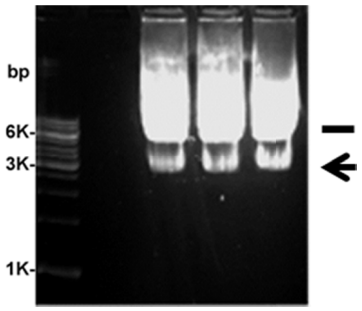

Figure 3.3: Agarose gel electrophoresis of the *C. jejuni napA* gene amplified from pJCnapA. The ~2.8 kbp *napA* band (←) was excised from the gel and ultimately inserted into pET21α. The pJCnapA plasmid band, ~ 6kbp is marked indicated (–).
Cloning of the amplified *napA* from *C. jejuni* and *S. barnesii* into the pET21α vector produced two constructs, pCnapA and pSnapA, respectively. The maturation genes, *napLD*, from *C. jejuni* were cloned into the pREP vector, creating pCnapLD for co-expression with NapA. The amplified *napB* genes from *C. jejuni* and *S. barnesii* were cloned into pQE-60, creating pCnapB and pSnapB.

Table 3.4: The predicted sizes of each *nap* gene amplified by colony PCR. **M,** GeneRuler^{TM} 1kb DNA ladder (Fermentas).

Plasmid ID	Expected size of *nap* gene construct amplified by PCR (kbp)
(a) pJCnapA	2.9
(b) pCnapLD	1.3
(c) pJCnapLD	1.4
(d) pCnapB	0.5
pJCnapB	0.6
(e) pSnapA	2.8
(f) pSnapB	0.5
(g) pJSnapHBF	2.0

Immediately after ligation, the plasmids were used for transformation of *E. coli* DH5α for screening and selection. Antibiotic resistant colonies were selected and analyzed for the presence of the *nap* gene construct by colony PCR (**Figure 3.4**). Colonies positive for *nap* gene insertions were proliferated and the plasmid was purified.

Test restriction assays confirmed the insertion of the genes into the respective plasmids. The sizes of the DNA fragments resolved using gel electrophoresis (**Figure 3.5**) were in agreement the predicted sizes of the digestion fragments (**Table 3.2**). Sequence data was aligned with the expected *nap* sequences and checked for mutations (**Appendix II)**. Colonies with the most similar DNA sequence to the targeted gene were selected. The sequence of *S. barnesii napB* was derived from the sequencing of the pSnapHBF (pJET 1.2 plasmid with the inserted *S. barnesii napHBF* genes). The *S. barnesii napHBF* gene construct was also compared to *S. delyanium napHBF*. The sequence of *S. barnesii napB* is provided in **Figure 3.6a** (see Appendix II for *napHBF* sequence data). The *S. barnesii napB* shares 87% sequence identity with the *S. deleyianum* NapB protein **(Figure 3.6b).**

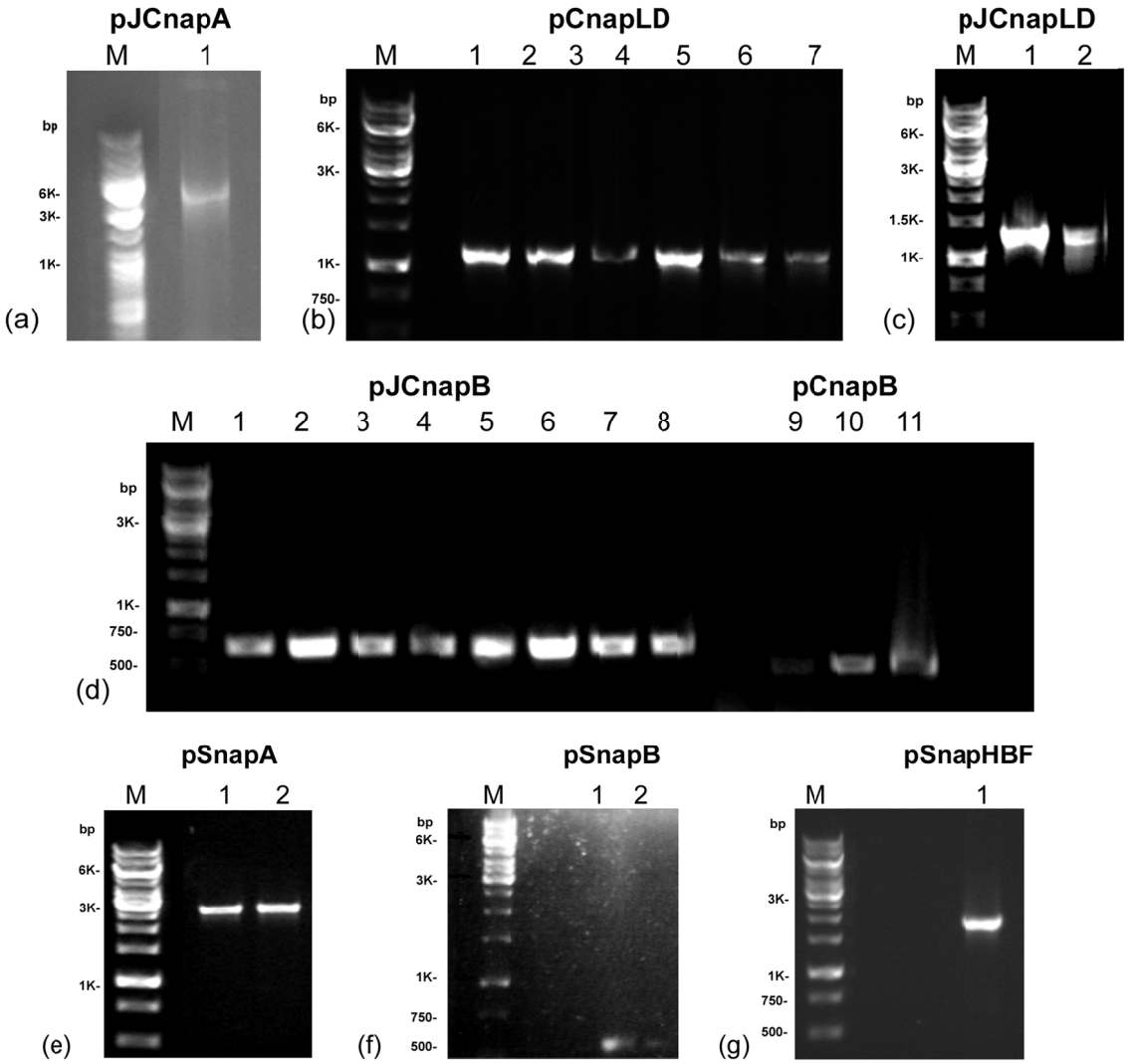

Figure 3.4: DNA gel electrophoresis of colony PCR. The *nap* genes were amplified from antibiotic resistant *E. coli* DH5α colonies containing (a) pJCnapA, (b) pCnapLD, (c) pJCnapLD, (d) pJCnapB, lanes 1-8 and pCnapB, lanes 9-11; (e) pSnapA, (f) pSnapB, and (g) pJSnapHBF. Each lane number represents a separate colony**.** The sizes of the amplified gene vary according to primer position in the plasmid. Specifically, the pJET1.2 primers are further away from the *napB* gene than the primers used for pQE-60 amplification, resulting in a larger sized DNA fragment in pJET colonies.

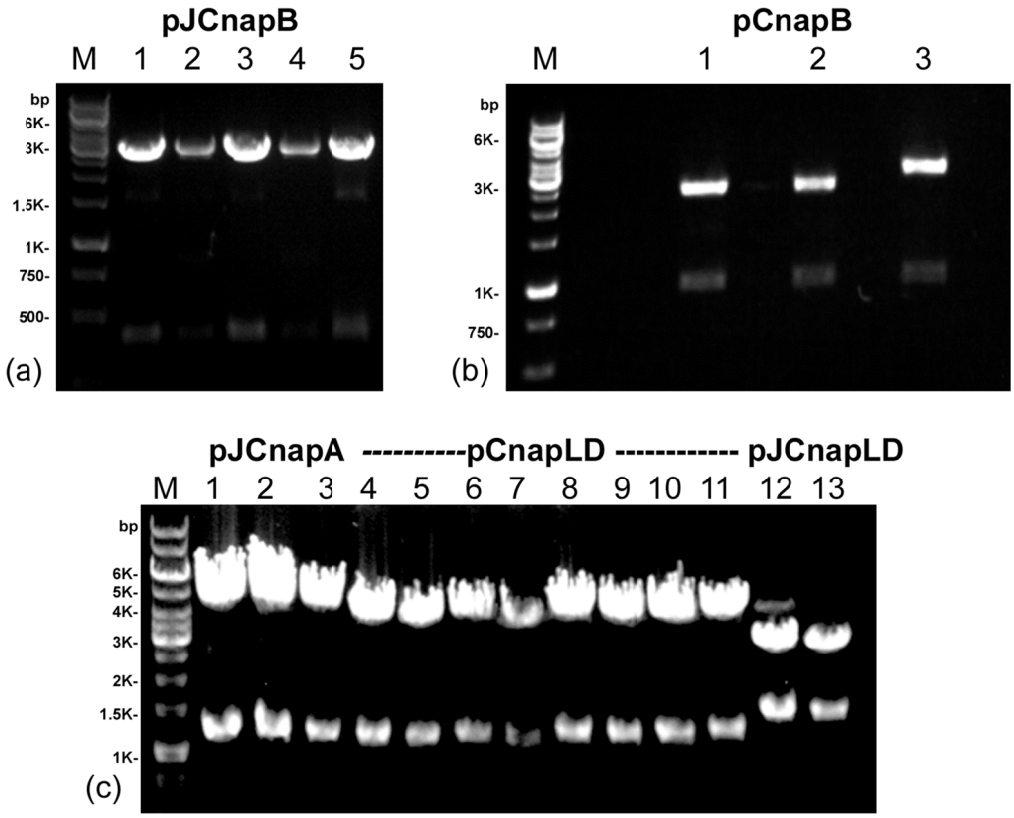

Figure 3.5: Gel electrophoresis of restriction digest assays preformed on *C. jejuni nap* plasmids. Each lane represents a separate plasmid preparation, originating from a single colony (a) pJCnapB digested with PstI, five colonies (lanes 1-5). (b) pCnapB digested with PstI and BamHI, three colonies (lanes 1-3). (c) pJCnapA digested with NcoI, three colonies (lanes 1-3); pCnapLD digested with HindIII, eight colonies (lanes 4-11); and pJCnapLD, two colonies digested with HindIII (lanes 12-13). The DNA was stained with ethidium bromide and separated on 1% agarose gel. M= GeneRuler^{TM} 1kb DNA ladder (Fermentas).

(a)

>*S.barnesii napB*

atgatgagtagaaaaacattaatattagcctctttattaggtattttagttgcntcaggatgtgccgtgtcacaatcgtataa
agaggaagagttagggcttagaaaggtggacctatacagtgaaaaaacagtagtagctgaatcaacagcctactcaa
gtgtcgctgcaggtgagtctaaagtatttgagcgctcttttgaaaatgctcctccaatgattcctcatgatgttgagggtat
gttggatatgacaaaagagagtaatgcgtgtacagggtgtcaccttccagaagtggcagaagcagtgaatgctacac
cgattccaaaatcgcatttctttgatatgcgtacacaaaaagttttaacagagatgagtcaagctcgttataactgtaatgc
atgccatgcaccgcaatcgaacaatcagcctttggtcaaaaatgagtttgaaccagagtatcgttccaaagagggtgtg
gcacgctcaaaccttcttgataccttaatgagggcgtgaagtag

(b)

>ref|YP_003303796.1| Nitrate reductase cytochrome c-type subunit (NapB) [Sulfurospirillum deleyianum DSM 6946]
gb|ACZ11761.1| Nitrate reductase cytochrome c-type subunit (NapB) [Sulfurospirillum deleyianum DSM 6946]
Length=173

Score = 323 bits (829), Expect = 4e-87, Method: Compositional matrix adjust.
Identities = 151/173 (88%), Positives = 164/173 (95%), Gaps = 0/173 (0%)

```
Query  2    MSRKTLILASLLGILVXSGCAVSQSYKEEELGLRKVDLYSEKTVVAESTAYSSVAAGESK  61
            MSRKTLIL SLLG+LV SGCA SQSY EEELGLRKVDLYSEKTVVAESTAYS+VAAGESK
Sbjct  1    MSRKTLILVSLLGVLVASGCAASQSYTEEELGLRKVDLYSEKTVVAESTAYSTVAAGESK  60

Query  62   VFERSFENAPPMIPHDVEGMLDMTKESNACTGCHLPEVAEAVNATPIPKSHFFDMRTQKV  121
            V+ER+FENAPPMIPHDVEGML+++KE+NAC GCHLPEVAEAV ATPIPKSHF+DMRT+K+
Sbjct  61   VYERAFENAPPMIPHDVEGMLEISKENNACIGCHLPEVAEAVKATPIPKSHFYDMRTKKM  120

Query  122  LTEMSQARYNCNACHAPQSNNQPLVKNEFEPEYRSKEGVARSNLLDTLNEGVK  174
            L E+SQAR+NCNACHAPQSNNQPLVKNEF PEYRSKEG ARSNLLDTLNEGVK
Sbjct  121  LGELSQARFNCNACHAPQSNNQPLVKNEFSPEYRSKEGTARSNLLDTLNEGVK  173
```

Figure 3.6: *S. barnesii napB* sequence. (**a**) The gene sequence of *S. barnesii napB* determined by sequencing of pJSnapHBF. The DNA sequence was determined to be 525 bp long, similar to *S. deleyianum* DSM 6946 *napB*. (**b**) Using the NCBI database, a blast search with the translated NapB sequence (**Query**) identified *S. delyanium* DSM 6946 NapB as the closest match (**Subject**).

3.4.2. Expression and growth conditions

For NapA expression, pCnapA and pCnapLD, the maturation gene-containing plasmid, were co-transformed into *E. coli* strains T7 express and Bl21 (DE3). Due to the absence of the *S. barnesii* maturation proteins, the *C. jejuni* construct, pCnapLD was co transformed with pSnapA into *E.coli* strain T7 express and BL21 (DE3). For NapB expression, pSnapB and pCnapB were co-transformed with pREP4 into *E. coli* strains T7 express and Bl21 (DE3).

The pilot expression experiment established that only the *E. coli* T7 express strain was able to express detectable amounts of NapA. The expression of NapA from *S. barnesii* was monitored by SDS-PAGE (**Figure 3.7**), nitrate reductase activity assays, and Western blot (**Figure A.1**). The identity of *S. barnesii* NapA was confirmed by mass spectroscopy (MS) (Bruker Corporation, Germany). A detailed report of the MS analysis is located in **Appendix III**. The cofactor content of the protein samples in **Figure 3.7** were estimated using florescence spectroscopy. The protein was approximately 11% saturated with the molybdopterin cofactor. Of the conditions tested in the pilot expression, optimal NapA was isolated from the periplasmic fraction when incubated at 20^{o}C for 44 hours with shaking, although, NapA was also detected in of cells grown at 30 ^{o}C for 19 hours (**Table 3.5** and **Figure 3.7**). All cultures were induced with 0.1 mM IPTG, and the inoculating culture was the same for each strain.

Table 3.5: Summary of results from the *S. barnesii* NapA pilot expression. Temperature during incubation, Temp). Incubation time (Time). NapA detectable in the Ni-NTA eluent was determined by protein assay, SDS-PAGE and Western blot.

Wet weight of cells (g)	*E. coli* strain	Time (hours)	Temp (°C)	NapA detectable in Ni-NTA eluent
0.3	BL 21	19	37	No
0.3	BL 21	19	30	No
0.3	BL 21	19	20	No
0.6	BL 21	44	20	No
0.4	T7 express	19	37	No
0.4	T7 express	19	30	**Yes**
0.4	T7 express	19	20	No
0.3	T7 express	44	20	**Yes**

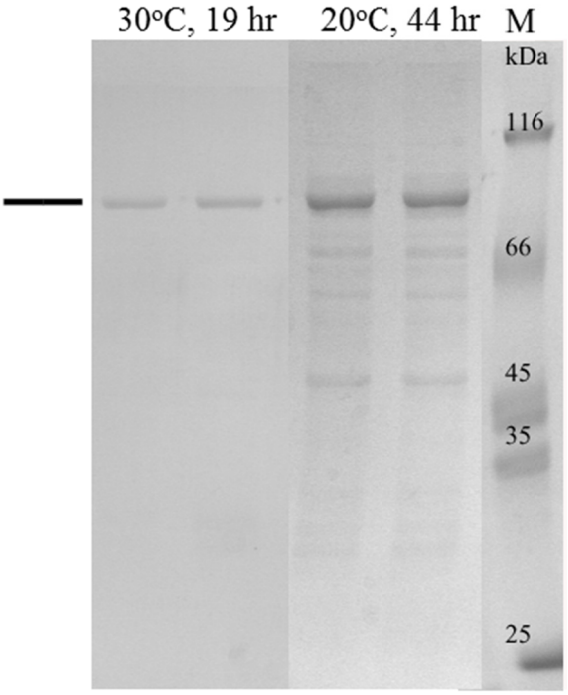

Figure 3.7: SDS-PAGE of *S. barnesii* NapA purified from *E. coli* strain T7 express during the pilot expression experiment. NapA was only isolated from T7 express cells which were incubated at (a) 30 ^{o}C for 19 hours and (b) 20 ^{o}C for 44 hours, following induction with 0.1 mM IPTG. NapA is indicated by a black line (**–**), the photographed bands were excised and identified, by mass spectrometry, as NapA.

The pilot expression of *C. jejuni* NapB indicated that NapB was expressed at all tested temperatures, 20, 30 and 37 ^{o}C, as indicated by Western blot (**Figure A.2**) and SDS-PAGE (**Figure 3.8**) of the periplasmic fraction. Purification of NapB using IMAC was not successful. It is possible that the protein degraded during purification; however this experiment must be repeated to confirm.

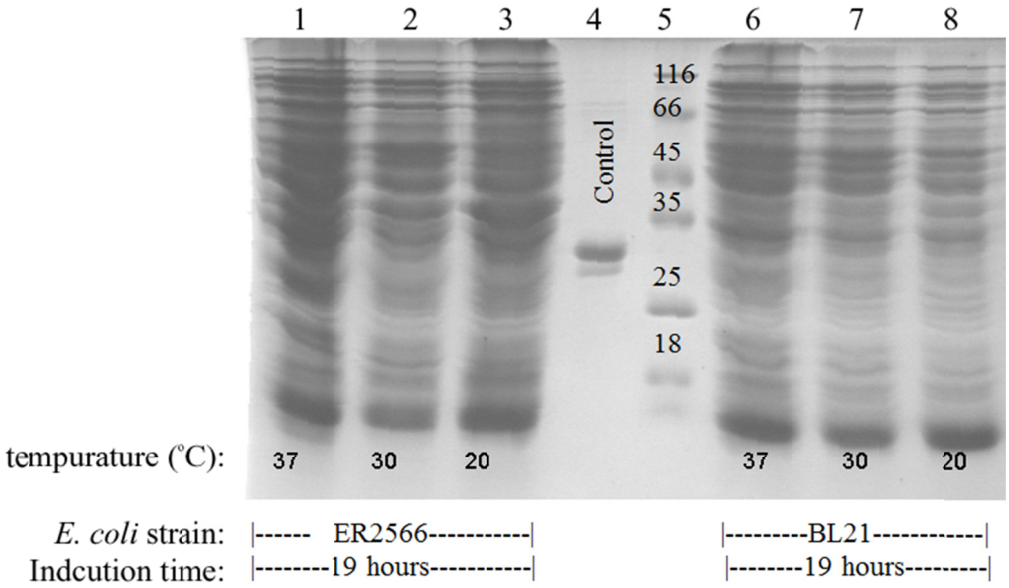

Figure 3.8: SDS/PAGE of the periplasmic extract from the *C. jejuni* NapB pilot expression experiment. Lane 1, T7 express cells incubated for 19 at 37 °C; lane 2, T7 express cells incubated for 19 at 30 °C; lane 3, T7 express cells incubated for 19 at 20 °C; lane 4 is 29 kDa western blot control; lane 5 is the molecular weight marker; lane 6, BL21 star cells incubated for 19 at 37 °C; lane 7, BL21 star cells incubated for 19 at 30 °C; lane 8, BL21 star cells incubated for 19 at 20 °C.

Table 3.6: Summary of results from the *C. jejuni* NapB pilot expression. WB, western blot; Temp, temperature during incubation; Time, duration of incubation.

Wet weight of cells (g)	*E. coli* strain	Time (hours)	Temp (°C)	WB
0.3	BL 21	19	37	+
0.5	BL 21	19	30	+
0.6	BL 21	19	20	+
0.4	T7 express	19	37	+
0.4	T7 express	19	30	+
0.4	T7 express	19	20	+

C. jejuni and *S. barnesii* NapA were expressed by incubating the cells for 48 hours at 23 ^{o}C after IPTG induction (**Figure 3.9**). Because molybdenum salts are required in the growth media to express Moco proteins, [196, 197] LB media was supplemented with 1mM sodium molybdate at the time of induction. Induction of *S. barnesii* NapA and *C. jejuni* NapA expression cultures with IPTG provided inducible expression of a 106 kDa proteins, the predicted size of the recombinant NapA protein with the TAT leader sequence and polyhistidine tag. The presence of the His_{6x}-Tag epitope in the 106 kDa protein was confirmed by western blotting, indicating the production of the full length protein (**Figure A.1**). Relative to *S. barnesii* NapA, expression of *C. jejuni* NapA was greater under the given conditions. In SDS-PAGE gel 18% of total protein density is attributed to the 106 kDa band in *C. jejuni* while that accounts for 11% in *S. barnesii*. Overexpression of *C. jejuni* NapL and *C. jejuni* NapD in response to IPTG was not detected by SDS-PAGE (**Figure 3.9**). Expression at higher temperatures (over 30^{o}C) and shorter induction times (less than 24 hours) did not produce detectable quantities of NapA. Slow growth at relatively low temperatures is favorable for expression of large proteins which have a high propensity to accumulate in inclusion bodies.

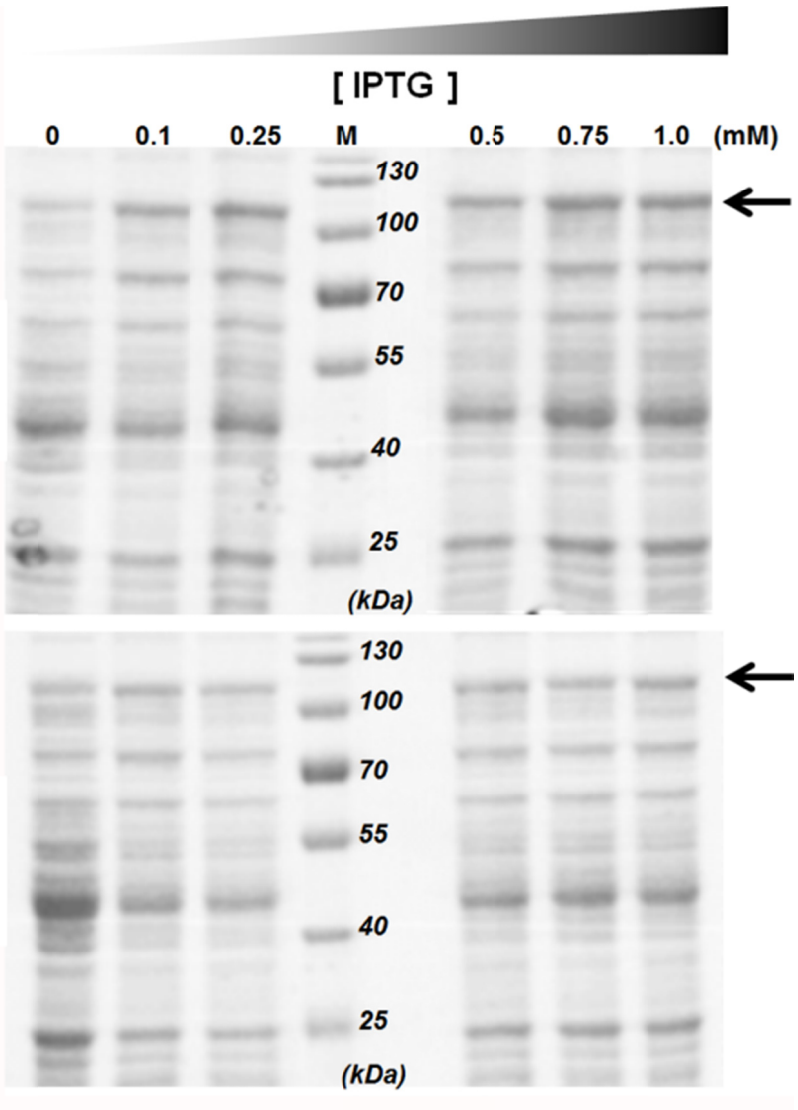

Figure 3.9: SDS-PAGE illustrating the IPTG concentration-dependent expression of *S. barnesii* and *C. jejuni* NapA in *E. coli*. The density of a 106 kDa NapA band (**arrow**) is clearly more intense in lanes exposed to IPTG when compared to uninduced cultures (0mM). Expression *C. jejuni* NapA (**top**) increases 18%, while *S. barnesii* NapA (**bottom**) intensity is only 11 % greater in cells induced with IPTG. Whole cell lysate was separated by SDS-PAGE and stained with Colloidal Coomassie Blue G-250. All cells were incubated at 23 ^{o}C for 48 hours post induction. Fermentas pre-stained molecular weight marker (M) contains bands at the following molecular weights: 170, 130, 100, 70, 55, 40 and 25 kDa.

3.4.3. Purification of NapA

The flow chart in **Figure 3.10** provides an overview of protein expression and purification procedures conducted to independently isolate the polyhistidine tagged NapA and NapB using the *C. jejuni* and *S.barnesii nap* plasmids created previously.

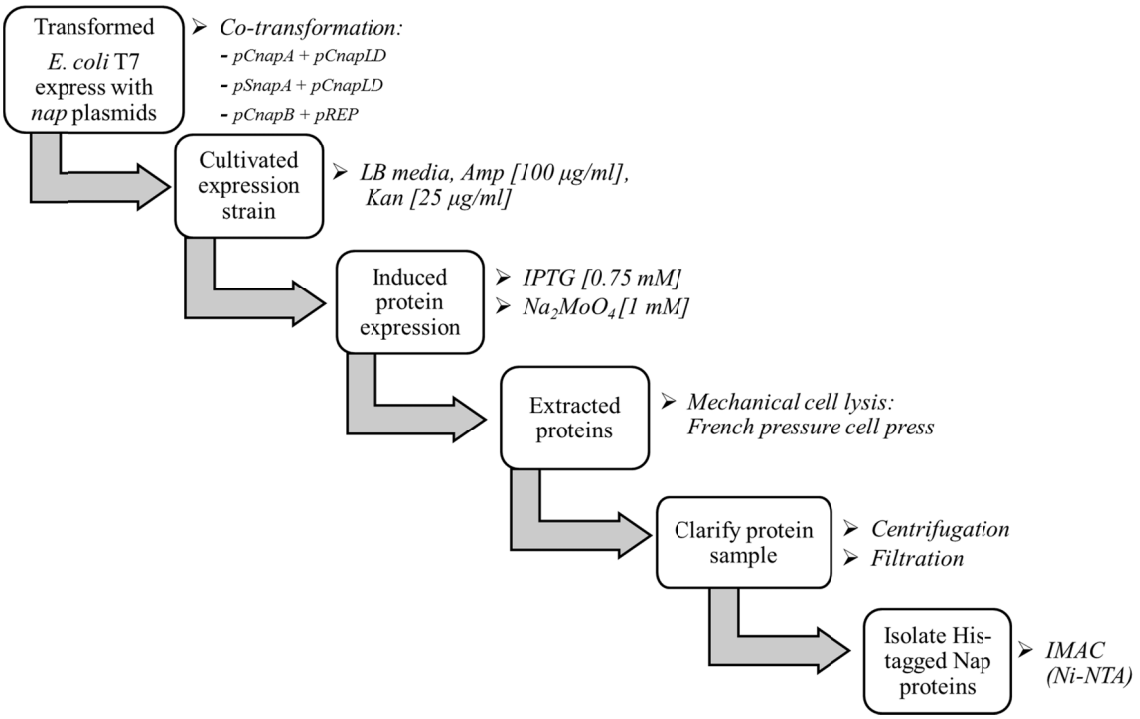

Figure 3.10: An overview of the expression and purification of affinity tagged NapA and NapB.

Purification of the recombinant NapA via immobilized metal affinity chromatography (IMAC) from cell cultures induced with 0.75 mM IPTG had a significantly larger yield (12-14 mg per 1.5 liter of culture) of NapA relative to cultures induced with 0.1 mM IPTG (5 - 7 mg per 1.5 liter of culture), therefore large scale production was conducted at 0.75 mM IPTG. Purified NapA from *C. jejuni* and *S. barnesii* was electrophoretically pure, as evidenced by protein band densitometry (analyzed gel is in **Figure 3.11**). The identities of the 106 kDa proteins as the target

proteins, periplasmic nitrate reductase from *C. jejuni* (gi 57237625) and *S. barnesii* (gi 169104652) were confirmed by mass spectrometry.

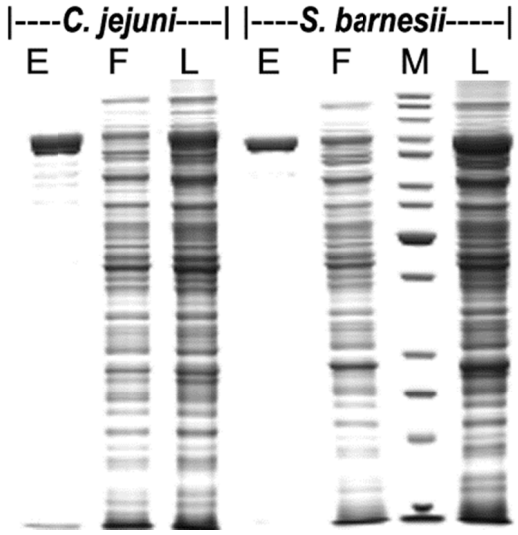

Figure 3.11: SDS-PAGE of fractions obtained during the purification of *C. jejuni* and *S. barnesii* NapA from *E. coli* using immobilized metal affinity chromatography. Separation of E. coli protein fractions, Ni- NTA eluent (E), flow through (F) and Lysate (L) of, via SDS-PAGE and proteins were stained with CCB. The Fermentas protein standard (M) has the following protein sizes; 200, 150, 120, 100, 85, 70, 60, 50, 40, 30, 25, 20, 10 kDa.

During the optimization of NapA expression, two interesting differences between *C. jejuni* NapA and *S. barnesii* NapA were observed. First, the *C. jejuni* NapA appears on the SDS-PAGE as a single band, while *S. barnesii* NapA appears as a doublet. Second, *C. jejuni* NapA is co-purified with *Cj*NapD whereas no NapD could be detected in *S. barnesii* NapA expression (**Figure 3.12**). The two protein bands (106 kDa and a 98 kDa), resolved in the SDS-PAGE gel of *S. barnesii* NapA (**Figure 3.12**), were both identified as NapA from *S. barnesii*. We suggest that the 106 kDa *Sb*NapA in the precursor state with the TAT leader sequence. The 103 kDa band is most likely the protein (**Figure 3.12**) without the TAT leader sequence (3 kDa), which is cleaved after NapA is exported to periplasm.[198]

The small 13 kDa protein, shown in **Figure 3.12,** was identified as NapD (YP_178878) from *C. jejuni* RM1221. Mass spectroscopy results are included in Appendix III. The presence of *C. jejuni* NapD in the eluent indicates that the protein was expressed and is able to bind to NapA. The *Cj*NapD protein does not have any histidine residues, so it is not expected to assocate with the Ni-NTA resin.

A similar experiment performed by Nilavongse *et al.* used an nickel immobilized His_{6x}-tagged NapF to purify NapA.[138] The interaction between NapA and the NapF chaperone protein was confirmed using the bacterial two hybrid system. Their experiments suggest that NapF and NapD interact strongly with NapA, not NapG, NapH or NapC. [138]

The presence of *C. jejuni* NapD in the *S. barnesii* NapA eluent could not be positively confirmed by mass spectrometry. The lack of *C. jejuni* NapD in the *S. barnesii* NapA eluent may be due to poor interactions between *C. jejuni* NapD and *S. barnesii NapA*. The homology of NapD between *C. jejuni* and *Sulfurospirillum* species (*S. barnesii* and *S. delyanium*) exhibits less than 30% sequence identity. Lanciano *et al* have suggested the catalytic subunit that harbors the molybdenum cofactor (NapA in this case) requires species-specific maturation proteins for proper folding and cofactor insertion. [199, 200]

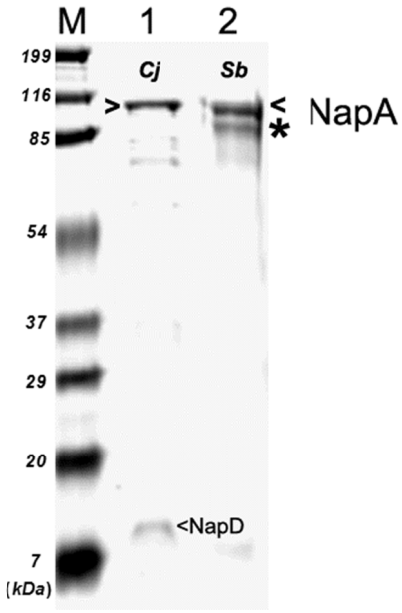

Figure 3.12: SDS-PAGE of the purified *C. jejuni* NapA and NapD complex, and the purified *S. barnesii* NapA. **Lane 1**, *C. jejuni* (***Cj***) NapA(106 kDa) and *C. jejuni* NapD (13kDa) isolated by nickel affinity chromatography; only NapA contained the His_{6x}- tag. **Lane 2**, NapA from *S. barnesii* (***Sb***) separates into 2 bands on denaturing electrophoresis, the premature "<" (106 kDa), mature "*" (98 kDa). Bands were excized from this gel and identifed by mass spectrometry. Molecular weight marker (Fermentas) indicated by M.

In addition to the presence of NapD, the size of *C. jejuni* NapA (~106 kDa) on the SDS-PAGE gel (**Figure 3.12**) suggests that the TAT leader sequence had not been cleaved. Taken together, suggesting that the *C. jejuni* NapD inhibited the export of NapA, as a result *C. jejuni* NapA is not fully mature. NapD, a cytoplasmic protein, [127, 145] is a dedicated NapA maturation protein [201] that impedes the periplasmic export of NapA via the TAT pathway, possibly attenuating export until NapA is properly folded and the molybdenum cofactor inserted. [131] The *S. barnesii* NapA expression did not have the appropriate chaperone, *S. barnesii* NapD, therefore NapA was able to be exported and the TAT leader sequence cleaved faster than the *C. jejuni* NapA expression.

3.4.4. Spectral Characterization

The electronic absorption spectra of *C. jejuni* NapA (**Figure 3.13**) shows a band at 400 nm, indicating the presence of iron-sulfur cluster. No such band was resolved in the spectrum of *S.barnesii* NapA. The electronic spectrum of *C. jejuni* NapA appears similar to that reported for the *D. desulfuricans* NapA [168] that exhibits bands at 400 nm, 340 nm, and low intensity band at 510 nm. The 510 nm band was not observed in the *C. jejuni* NapA, possibly due to low concentrations. The A_{400}/ A_{280} ratio for *C. jejuni* NapA and *S. barnesii* NapA are calculated to be 0.22 and 0.19, respectively. This value is comparable to the monomeric NapA from *D. desulfuricans* (0.17) [168] and *Shewanella gelidimarina* (0.19) [96].

The purified enzymes were subjected to molybdenum and iron analyses by ICP-OES. The molybdenum concentration in the NapA isolates was found to be 2.53 μM and 1.88 μM, for the *C. jejuni* and *S. barnesii*, respectively. From these data, molybdenum incorporation into NapA was determined to be 30 % in *C. jejuni* NapA and 43% in *S. barnesii* NapA. The iron concentration was determined to be 6.68 uM and 6.08 μM for *C. jejuni* and *S. barnesii*, respectively. The Fe: Mo ratio was 2.6 in *C. jejuni* NapA and 3.2 in *S. barnesii* NapA. Thus the ratio of iron to molybdenum was less than the theoretical value (4:1) in each isolate. This indicates that iron-sulfur cluster incorporation is low. Sodium molybdate was provided in the growth media, iron was not.

NapA cofactor insertion is predicted to occur in the cytoplasm. When present, the cytoplasmic NapF is the predicted insert the iron-sulfur cluster into NapA.[139] While no *napF* homolog could be found in the *C. jejuni* genome, the spectroscopic data on *C. jejuni* NapA indicates the presence of iron-sulfur cluster in the purified protein (*vide infra*). Thus, mechanism of iron-sulfur insertion in *C. jejuni* NapA maturation remains an

open question. As found in the majority of the Epsilonproteobacteria, *S. barnesii* and S. delyanium are predicted to encode the *napF* gene in the *nap* operon (*napAGHBFLD*) Interestingly, deletion of *napF* in the Epsilonproteobacterium *W. succinogenes* resulted in a higher quantity of the precursor NapA. [136, 139] This is consistent with our findings, *S. barnesii* NapA can exist in both precursor and mature state.

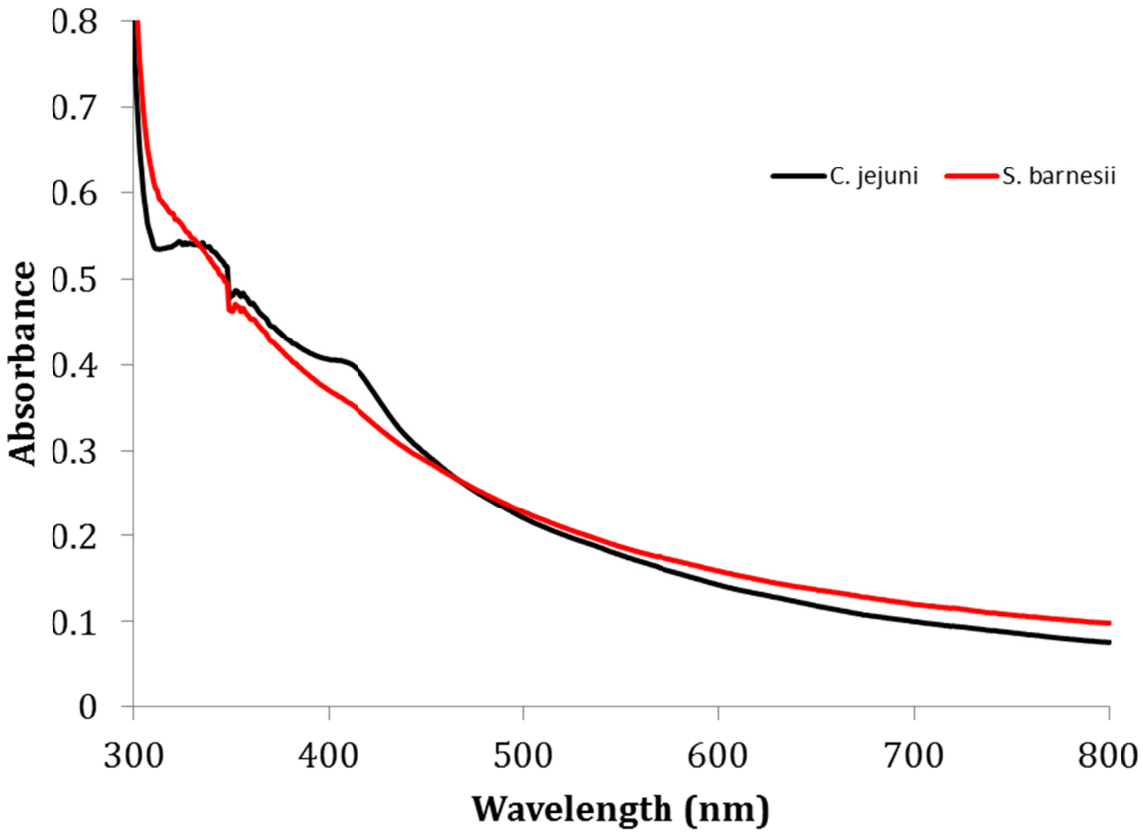

Figure 3.13: The electronic spectra of the purified NapA proteins. *S. barnesii* NapA (black line), *C. jejuni* NapA (red line). The as-isolated fractions were analyzed using a Carry 500 spectrophotometer.

3.4.5. Kinetic analysis of recombinant NapA

Both *C. jejuni* NapA and *S. barnesii* NapA display Michaelis-Menten type kinetics (**Figure 3.14**), with a calculated maximum velocity (V_{max}) of 0.042 ± 0.004 and 0.084 ± 0.009 μmoles • min^{-1} • mg $protein^{-1}$, respectively. The K_m for nitrate was calculated to be 2.3 ± 0.68 mM for *C. jejuni* and 7.2 ± 1.6 mM for *S. barnesii*. The k_{cat}

was calculated to be 0.09 ± 0.01 s^{-1} and 0.23 ± 0.03 s^{-1} for *C. jejuni* and *S. barnesii*, respectively. The production of nitrite was confirmed via the Griess assay (data not shown), and confirmed that *S. barnesii* NapA produced a larger amount of nitrite than *C. jejuni* NapA in the allotted time, a consequence of the different velocities.

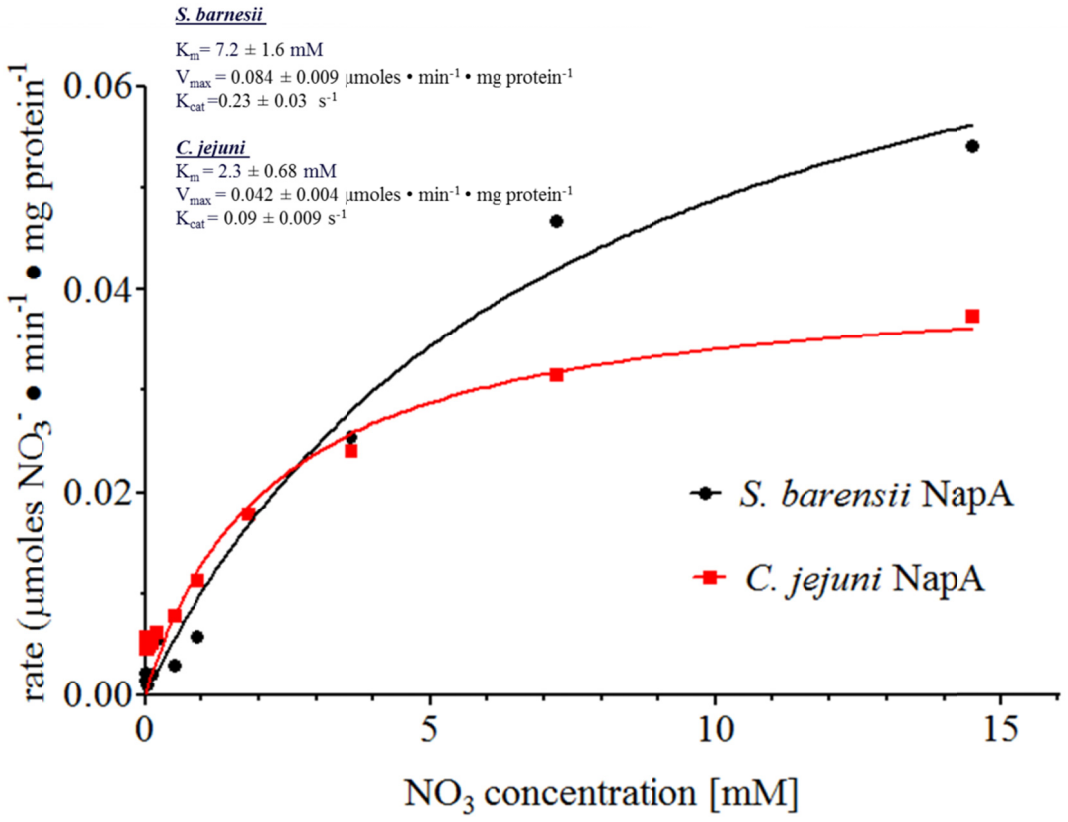

Figure 3.14: Michaelis-Menten, non-linear, plot of the enzyme rate versus substrate concentration for *C. jejuni* and *S. barnesii* NapA. Analyses were performed using the Prism v 5.01 (Graph Pad).

Comparison of the K_m and V_{max} of *C. jejuni* NapA and *S. barnesii* NapA, with values previously reported for NapA isolates (**Table 3.7**), reveals dramatic differences in the kinetic properties. The velocity and affinity for nitrate is lower. The K_m value for NapA isolates is typically in the micro molar range (3.2-240 µM), while in the present study the values are in the millimolar range.

The possibility that the kinetics behavior of *C. jejuni* and *S. barnesii* NapA is not physiologically relevant has been considered. Mutational studies on the *W. succinogenes* and *C. jejuni nap* operon provide insight into the nitrate reductase activity of premature NapA. In In both organisms mutating the maturation genes (i.e., *napF*, *napL* and *napD*) decreases the rate of nitrate reductase activity in lysates, [141] [139] [136] as measured by the methylviologen coupled nitrate reductase assay. In *Wolinella*, *napL* and *napD* mutants exhibited less than half the nitrate activity of the wild type strain, *napF* mutants also had attenuated activity. [139] [136] Similarly, *C. jejuni napL* mutants exhibited half nitrate reductase activity compared to the wild type cells.[141] To summarize, the absence of maturation proteins (NapF, NapL and NapD) does not completely inactivate NapA, it only decreases the velocity of nitrate reduction. This appears to be the case in the current study. Both NapA isolates have low velocities. In *C. jejuni* both maturation proteins were cloned, however the expression of NapL was not confirmed. As mentioned above, the *S. barnesii* NapF, NapL and NapD were not expressed as the gene amplification was not successful. Therefore it is possibly that NapA may have low activity due to the absence of maturation proteins.

Table 3.7: A summary of kinetic properties from NapA enzymes. All data was obtained using the methylviologen coupled nitrate reductase assay. Organisms are organized according to proteobacteria class: Alpha-(α), Beta-(β), Gamma-(γ), Delta-(δ) and Epsilon-(ε). *note: The presence of NapB was not confirmed in the NapA enriched *S. barnesii* fraction studied in Chapter 2 (CH 2). Data not available (-NA-)

Class	Organism	Subunit(s)	K_m (μM)	V_{max} (μmol . min^{-1} mg^{-1})	Ref
α	*Magnetospirillum magnetotacticum*	NapAB	3.2	-NA-	[202]
	Rhodobacter sphaeroides	NapAB	120	39	[179]
		NapAB	170	25	[41]
		NapA	45	5.9	
	Paracoccus pantotrophus	NapAB	240 [3μM Mo]	3.4	[50]
		NapAB	3910 [100μM W]	0.05	
	Paracoccus denitrificans	NapAB	280	50	[203]
	Thiosphaera pantotropha	NapAB	--	95	[167]
β	*Achromobacter fischeri*	NapAB	65	*1.5*	[166]
	Alcaligenes eutrophus	NapAB	120	-NA-	[93]
γ	*Escherichia coli*	NapAB	--	70	[50]
δ	*Desulfovibrio desulfuricans*	NapA	116	-NA-	[204]
		NapA	32	18.6	[205]
		NapA	12	-NA-	
ε	***C. jejuni***	**NapA**	**2300**	0.04	**This work**
	S. barnesii		**7290**	**0.08**	
		NapAB *	**314**	**0.41**	CH 2

The possibility that the kinetics behavior of *C. jejuni* and *S. barnesii* NapA is not physiologically relevant has been considered. Mutational studies on the *W. succinogenes* and *C. jejuni nap* operon provide insight into the nitrate reductase activity of premature NapA. In In both organisms mutating the maturation genes (i.e., *napF*, *napL* and *napD*) decreases the rate of nitrate reductase activity in lysates, [141] [139] [136] as measured by the methylviologen coupled nitrate reductase assay. In *Wolinella*, *napL* and *napD* mutants exhibited less than half the nitrate activity of the wild type strain, *napF* mutants

also had attenuated activity. [139] [136] Similarly, *C. jejuni napL* mutants exhibited half nitrate reductase activity compared to the wild type cells.[141] To summarize, the absence of maturation proteins (NapF, NapL and NapD) does not completely inactivate NapA, it only decreases the velocity of nitrate reduction. This appears to be the case in the current study. Both NapA isolates have low velocities. In *C. jejuni* both maturation proteins were cloned, however the expression of NapL was not confirmed. As mentioned above, the *S. barnesii* NapF, NapL and NapD were not expressed as the gene amplification was not successful. Therefore it is possibly that NapA may have low activity due to the absence of maturation proteins.

A kinetic study with *Paracoccus pantotrophus* NapA can also give some insight into the effect of inproper NapA cofactor incorporation on K_m. In the study, Gates *et al.* were interested in determining the effect of tungsten on the nitrate reductase activity, as replacing tungsten for molybdenum in the active site can deactivate molybdopterin enzymes. *P. pantotrophus* was gorwn on media supplimented with 100 μM tungsten or 3 μM molybdenum, presumably yeilding "W-NapA" and "Mo-NapA". The reduced methyl viologen coupled nitrate reductase assay was used to study the functionality of NapA. The W-NapA had a lower rate (Vmax = 0.058 μmole $[NO_3^-]$ • min^{-1} • mg^{-1}) and nitrate affinity (Km=3.9 mM) than the Mo-NapA (Vmax= 3.418 μmole $[NO_3^-]$ • min^{-1} • mg^{-1}, and Km= 0.24 mM).[50] While the actual incorporation of tungsten into the active site of NapA was not confirmed, this study does demonstrate the effect of improper cofactor insertion on the affinity for nitrate in NapA. As in the *P. pantotrophus* W-NapA, the from has a similar dissociation constant and velocity to the *C. jejuni* and *S. barnesii* NapA isolates presented in this study (**Table 3.7**). Thus, the relatively high K_m values of *C.*

jejuni and *S. barnesii* NapA isolates presented in this study are most likely due to improper cofactor insertion and maturation of NapA.

The kinetic analysis of *S. barnesii* fractions (see Chapter 2) supports this theory. In the native isolate the affinity for nitrate is consistent with published data (**Table 3.7**) **Table 3.8** summarizes the kinetic data from the native and recombinant NapA enzymes. While the Kcat values are similar in the both enzymes, the recombinant enzymes are clearly not active as the native isolates.

Table 3.8: Summary of the kinetic data from the recombinant and native NapA isolates.

	Recombinant NapA		Native NapA
	C. jejuni	***S. barnesii***	***S. barnesii***
V_{max} (μmoles • min^{-1} • mg $protein^{-1}$)	0.042 ± 0.004	0.084 ± 0.009	0.41 ± 0.006
K_{cat} (s^{-1})	0.09 ± 0.009	0.23 ± 0.03	0.31 ± 0.004
K_M (mM)	2.3 ± 0.68	7.2 ± 1.6	0.31 ± 0.02
K_{cat}/K_m (mM^{-1} • s^{-1})	0.04	0.03	0.98

3.5. Conclusions

The native isolation of *S. barnesii* NapA (*see* chapter 2) yielded low quantities of the active protein. Because the yield was low to preform future studies, heterologous expression of NapA was re-investigated. Previous attempts to heterologously express *S. barnesii* NapA in an *E.coli* host were unsuccessful. [206] In the current study the molecular cloning approach was adjusted to encourage the natural post-translational modification of NapA. The twin-arginine translocase signal peptide was included in the *napA* gene constructs to ensure periplasmic translocation of the protein. The *C. jejuni napLD* genes were also cloned. NapD, a well-characterized dedicated NapA-chaperone protein, and NapL, a proposed NapA chaperone, were co-expressed with NapA in *Escherichia coli* strain T7 express. With this approach we were able to isolate the full

length NapA; however kinetic analyses indicate that the recombinant enzymes have attenuated activity. Typically NapA isolates have a strong affinity for nitrate, while the recombinant enzymes display a low affinity for nitrate. The NapA enriched *S. barnesii* fractions display a high affinity for nitrate (*see* Chapter 2). Characterization of the NapA proteins indicate that the enzymes may be in a precursor state (*i.e.,* TAT leader sequence attached and low cofactor incorporation). Thus the attenuated activity is most likely the result of low quantities of mature NapA, underscoring the importance of proper NapA maturation.

CHAPTER 4: Characteristics of the Epsilonproteobacteria periplasmic nitrate reductase: theoretical modeling of *Campylobacter jejuni* NapA

4.1. Abstract

The Epsilonproteobacteria are a diverse group of prokaryotes that includes both free-living (e.g., *Sulfurospirillum, Wolinella, Nautilia*) and pathogenic (e.g., *Campylobacter, Helicobacter, Arcobacter*) species. Many are capable of using nitrate as a terminal electron acceptor during respiration using the periplasmic nitrate reductase (Nap). Sequence analysis of the catalytic subunit, NapA, indicates that the Epsilonproteobacteria NapA the largest (102 kDa) and forms a unique clade, distinct from other Proteobacteria NapA. To investigate possible structural differences, the *C. jejuni* NapA protein sequence was used to generate a three dimensional structural NapA model. The crystal structures of NapA from *Escherichia coli, Rhodobacter sphaeroides*, *Desulfovibrio desulfuricans* and *Cupriavidus necator* were used to create the *C. jejuni* NapA. Using the Molecular Operating Environment (MOE) software, the structure of *C. necator* NapA was used as the templates for building the folded protein structure. The electrostatic surface potentials were calculated for the *C. jejuni* NapA and structurally characterized NapA proteins. The most notable structural aspect of the *C. jejuni* NapA is the location of a large sequence insertion above the active site cavity. The close proximity of the loops to the active site cavity raises the possibility that the insertions could, in principle, affect the function of the protein. Furthermore, the unique genes (e.g., *napL*) and insertion sequences in NapA may be useful for design of diagnostic tools for *C. jejuni* identification.

4.2. Introduction

The Epsilonproteobacteria class of gram negative proteobacteria includes both free-living and host-associated species. Currently, the Epsilonproteobacteria are grouped into two orders, the *Nautiliales* and the *Campylobacterales*. Some species remain unclassified (i.e. *Sulfurovum*, *Nitratiruptor*, and *Thioreductor*). Nautiliales is comprised of marine species, some thermophiles (e.g., *Caminibacter, Nautilia, Lebetimonas*). The larger of the two orders, *Campylobacterales* contains both free-living (e.g., *Sulfurospirillum*) and host-associated species (e.g., *Campylobacter*, *Helicobacter*, and *Wolinella*). Two of the most prominent Epsilonproteobacteria, *Campylobacter jejuni* and *Helicobacter pylori*, are human gastrointestinal pathogens. *C. jejuni* is one of the leading causes of food-borne bacterial gastroenteritis in the United States; infection can also develop into chronic conditions, such as Guillian-Barré syndrome and reactive arthritis. [207] Studies with *H. pylori*, conducted by Marshall and Warren, established that *Helicobacter* infection can produce stomach ulcers and predispose the carrier for stomach cancer, [208] introducing the relationship between chronic infection, inflammation and cancer. Consequently, the researchers received the 2005 Nobel Prize in medicine and physiology.

Many of the Epsilonproteobacteria are capable of respiratory nitrate reduction. During nitrate respiration, nitrate is reduced to nitrite via a periplasmic nitrate reductase (Nap). Nitrite can then be transformed by nitrite reductases, Nrf or Nir, producing ammonia or dinitrogen, respectively. [78] In most organisms, multiple nitrate reductases are present. The Epsilonproteobacteria only encode Nap. Interestingly, Nap was found to be a crucial component of *H. pylori*'s defense mechanism against oxidative stress. [87]

Sequence analysis of the catalytic subunit, NapA, indicates that the Epsilonproteobacteria NapA forms a distinct clade. [164] This is somewhat unusual as the NapA phylogeny typically diverges from the phylogenic classification, especially in the Alpha-, Beta-, and Gamma- proteobacteria.

Furthermore, the Epsilonproteobacterial *nap* operon exhibits unusual continuity. Typically Epsilonproteobacterial *nap* operon take one of the following forms: *napAGHBFLD, napAGHBLD,* or *napAGHBFSLD* (collectively referred to as the *napA* operon). The Alpha-, Beta-, Gamma-, and Delta- proteobacteria do not exhibit similar conservation of gene content and organization (see **Table A.1** for a complete list of all available *nap* operons). The well-studied *nap* operons are *napEDABC* (*Paracoccus pantotrophus,* formerly *Thiosphaera pantotropha*), [145] *napFDAGHBC* (*Escherichia coli*), [118] and *napKEFDABC* (*Rhodobacter sphaeroides*). [209] in these operons, *napA* is preceded by the chaperone genes, *napD* and *napF*, which encode proteins involved in NapA maturation. Conversely, *napA* is the initial gene in the Epsilonproteobacteria *napA* operon, a possible indication of transcriptional or translational differences. It is pertinent to mention that a few organisms outside of the Epsilonproteobacteria contain the *napA* operon, they are: Aquificae species, *Sulfurihydrogenibium* sp. YO3AOP1, *Persephonella marina* EX-H1, and *Hydrogenivirga* sp. 128-5-R1-1, and one Deinococcus species, *Oceanithermus profundus*.

Two unique *nap* genes are exclusive to the *napA* operon, *napL*, which encode a 35 kDa periplasmic chaperone protein, [78, 86] and, *napS*, which is predicted to encode a 17 kDa signal peptide. While the functions of *napL* and *napS* are unclear, studies with *Wolinella succinogenes* suggest that NapL is involved in NapA maturation. [86] No

experimental evidence is available to confirm if NapS is translated, and if so, what the function may be. The *napS* gene, found in *Arcobacter butzleri* (YP_001489295.1 or ZP_07891038.1), *Sulfurovum* sp. (YP_004049825.1), Nitratiruptor sp. SB155-2 (YP_001357263.1) and *Sulfurimonas denitrificans (YP_003892305.1),* is annotated as a methyl-accepting chemotaxis sensor protein, part of the PAS (Per-ARNT-Sim) superfamily. The putative NapS proteins exhibits significant homology with the structurally characterized region of *Azotobacter vinelandii* NifL (**Figure 4.1**). NifL is the redox sensor domain of the NifLF two-component regulatory system, which, along with NifA, regulates nitrogen fixation genes in response to oxygen.[3] NapS may be involved in regulation of the *nap* operon; however, this is yet to be experimentally determined.

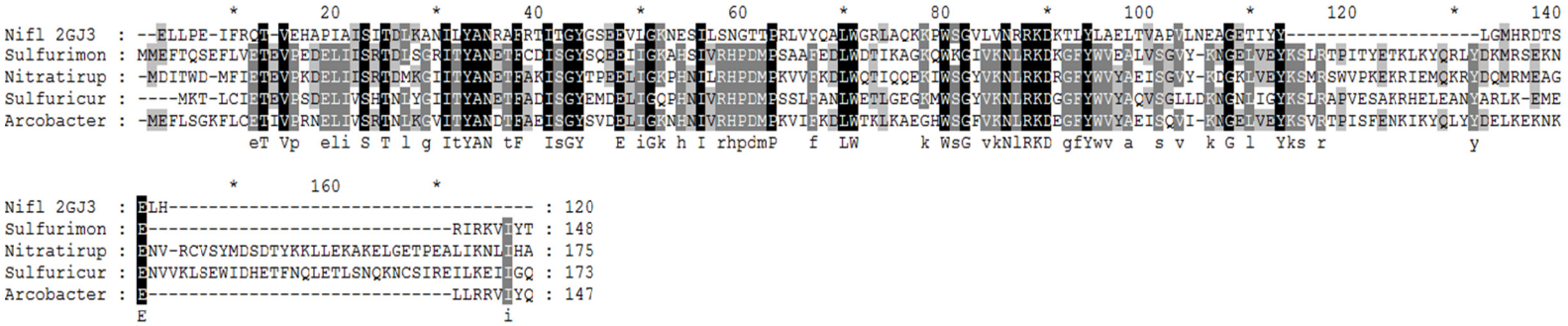

Figure 4.1: The sequence alignment of *Azotobacter vinelandii* NifL with the putative NapS proteins from Epsilonproteobacteria. NifL is a crystalographically characterized (PDB IA: 2GJ3) redox sensor protein and transcriptional regulator of nitrogen fixation. [3] The NapS protein sequences used in the alignment are: *Arcobacter butzleri* (YP_001489295.1), *Sulfurovum* sp. (YP_004049825.1), *Nitratiruptor* sp. SB155-2 (YP_001357263.1) and *Sulfurimonas denitrificans* (YP_003892305.1). The alignment was performed using ClustalX alignment software with the BLOSUM 62 matrix. GeneDoc was used to display the alignment and shade identical residues (Black) and similar residues (Grey).

In addition to the unique *napA* operon organization and gene content the catalytic subunit, NapA, exhibits distinguishing physiochemical features, such as a relatively larger size and more basic isoelectric point (**Table 4.1**). Typically, the unprocessed NapA is roughly 90 kDa. The Epsilonproteobacteria NapA is larger, approximately 105 kDa. The isoelectric point of the Epsilonproteobacteria NapA is typically in the basic range (for example, *C. jejuni* NapA pI = 9), as a result of differences in the amino acid composition (i.e. more charged residues, specifically lysine and arginine, and less non-polar). Conversely *R. sphaeroides* (pI = 6) is more acidic. While differences in the amino acid content and size have the potential to effect protein function, these differences may not have any effect on catalysis in the folded protein. Therefore the objective of this study was to examine the possible location of the Epsilonproteobacterial NapA sequence inserts on the three dimensional protein structures, and compare the structure to experimentally characterized homologues from other bacterial classes.

Table 4.1: Comparison of the NapA physical properties among each class of proteobacteria: Alpha (α), Beta (β), Gamma (γ), Delta (δ), and Epsilon (ε). One representative species is presented; however, multiple organisms were evaluated from each class. The values presented were estimated using the Protein calculator v3.3 from the Scripps Research Institute (scripps.edu)

Proteobacteria class	γ	α	β	δ	ε	
Organism name	*E. coli*	*R. Sphaeroides*	*V. fischeri*	*D. desulfuricans*	*C. jejuni*	*S. barnesii*
MW (kDa)	93	93	93	83	105	104
pI	8	6	8	8	9	9
Charge at pH7	+ 8	- 9	+ 12	+ 7	+ 16	+ 19

At the time of this study, the Epsilonproteobacteria NapA had not been structurally characterized, thus theoretical modeling was used to create a three

dimensional structural model of the Epsilonproteobacteria NapA. Using molecular modeling approaches it is possible to predict the three dimensional structure of a protein if a suitable three dimensional template structure has been determined experimentally (e.g. X- ray crystallography). Ideally, the template protein sequence should share a high degree of sequence identity (greater than 40%) when aligned with the structurally uncharacterized protein sequence.[210-212] Although significant structural models have been created with lower sequence identity.[213] Creating a theoretical model of the Epsilonproteobacteria NapA should be straightforward, as the structure of several pterin-containing molybdenum enzymes are available (*see* Chapter 1) including four functional homologues of NapA.[39, 40, 146, 147] Thus, sufficient structural data is available to facilitate the selection of a trustworthy NapA template structure. Of the Epsilonproteobacteria, *Campylobacter jejuni* has the most sequence data available. Sixteen strains of *C. jejuni* have been sequenced completely. In addition to the significance of *C. jejuni* as a human pathogen, the purification and kinetic analysis *C. jejuni* NapA is presented in Chapter 4; therefore we selected the structure of *C. jejuni* NapA as a target.

4.3. Experimental

4.3.1. Bioinformatics investigation of the nap operon

All gene and protein searches were performed using the National Center for Biotechnology Information (NCBI) database (http://www.ncbi.nlm.nih.gov). The *nap* operon composition was investigated using the NCBI Gene database, which provides chromosomal and plasmid gene maps. Although the genes can be annotated, in some organisms, the identity of each potential *nap* gene was confirmed individually, whether

annotated or not, by preforming a blast search. The Molecular Evolutionary Genetics Analysis (MEGA) Software [214] Version 5.03 was used to align proteins sequences and create phylogenetic trees.

4.3.2. Theoretical modeling of the C. jejuni NapA enzyme structure

Molecular modeling experiments were performed entirely with the Molecular Operating Environment (MOE) 20010.10 [1] using a Windows 7 operating system. As expected, the best candidates for the *C. jejuni* NapA structural template were NapA homologues, isolated from *Cupriavidus necator* (PDB ID: 3ML1),[40] *E. coli* (PDB ID: 2NYA),[42] *R. sphaeroides* (PDB ID:1OGY),[215] and *D. desulfuricans* (PDB ID: 2NAP).[39] Templates were selected by a preforming a blast search on NCBI website using the *C. jejuni* NapA sequence as the query and limiting the search to only structurally characterized proteins with-in the PDB database.

The structural coordinates (.pdb files) for all four structures (PDB IDs: 3ML1, 2NYA, 1OGY, and 2NAP) were downloaded from the research collaboratory for structural bioinformatics protein data bank (RCSB-PDB) at pdb.org. All files were opened using MOE. To isolate a single NapA molecule and the associated cofactors, all additional protein chains (i.e., NapB or additional NapA molecules) were deleted. The NapA structures were superimposed and aligned using the default settings. The RSMD of all aligned atoms was 1.09 Å. The NapA protein sequence from *C. jejuni* strain RM1221 (NCBI accession number YP_178873), which was derived from the organisms complete genome sequencing, was downloaded from the NCBI database. Next the *C. jejuni* NapA sequence was aligned with the four template structures using the alignment feature within MOE 2010.10 (**Figure A.3**).[1] A BLOck SUbstution Matrix[216] (BLOSUM62) matrix

was used with the following default settings: for the sequence alignment (gap start = 7, gap extend =1, a tree-based build-up, iteration limit = 100, failure limit = 10, and secondary structure = actual), and for the structural alignment (gap start = 1, and Gap extent = 0.1). Based on this alignment, *C. jejuni* NapA had the highest percentage of identical residues in common with *C. necator* NapA (57.9 %), thus *C. necator* NapA was chosen to act as a template to build *C. jejuni* NapA. Finally, the *E. coli*, *R. sphaeroides*, and *D. desulfuricans* NapA structures were removed from MOE.

The pairwise alignment of the *C. jejuni* and *C. necator* NapA (3ML1) sequences, used to generate the three dimensional *C. jejuni* NapA structure, is presented in **Figure 4.2.** Features, such as the iron-sulfur (4Fe-4S) binding motif (C-X_2-C-X_3-C-X_{24-26}-C), located at the N-terminus, the conserved cysteine residue, which has been crystallographically demonstrated to coordinate the molybdenum atom,[39, 146] and a conserved lysine residue, proposed to transport electrons from the 4Fe-4S cluster to the PGD, were used to evaluate the alignment of *C. jejuni* NapA with the template sequence. After alignment, the twin arginine translocase (TAT) leader sequence (MNRRDFIKNTAIASAASVAGLSVPSS) was removed from the N- terminus of the putative *C. jejuni* NapA sequence. The post translational cleavage of the TAT leader sequence occurs naturally after periplasmic export.

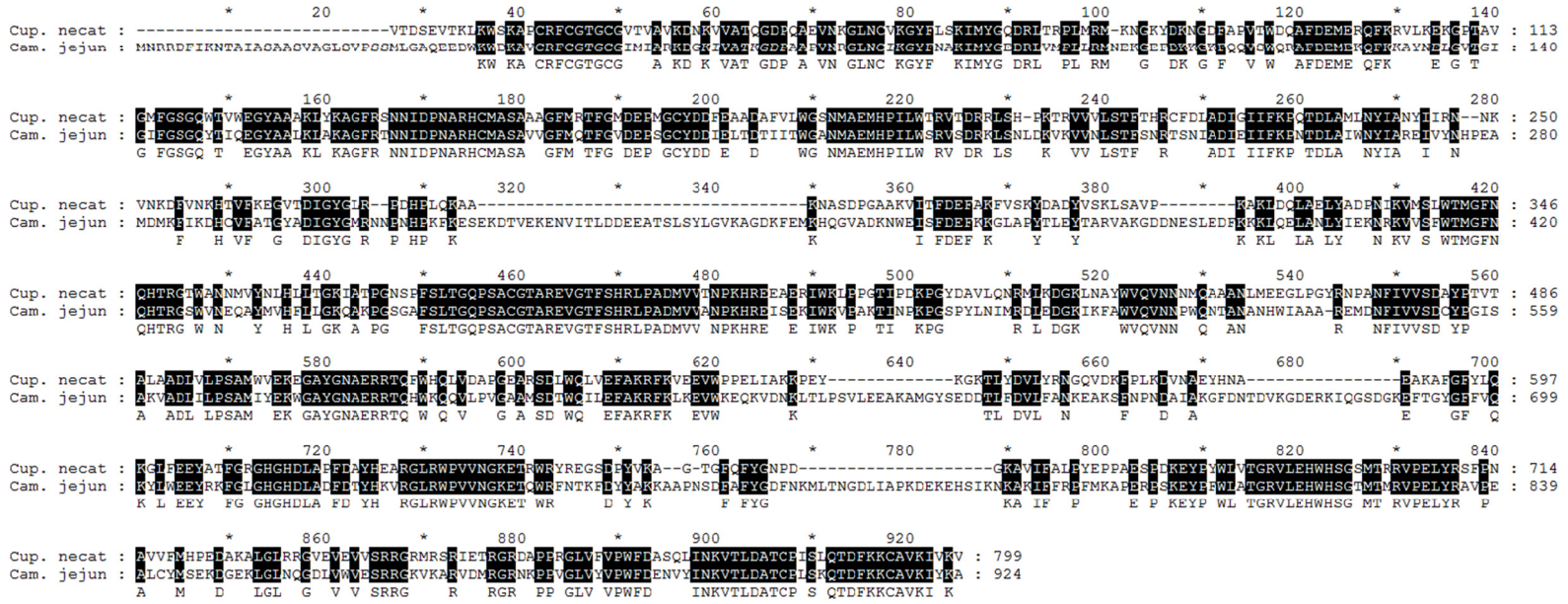

Figure 4.2: The protein sequence alignment of *C. jejuni* and *C. necator* NapA used to create the *C. jejuni* NapA structure. The alignment, which was performed using MOE[1], is displayed using GeneDoc software.[2] Identical residues are shaded black, and a consensus sequence, of all identical residues, is provided below the sequences.

The *C. jejuni* NapA homology model was created by folding the peptide in the presence of the stationary prosthetic groups, one molybdenum- *bis*pyranopterin guanine dinucleotide (Mo-*bis*PGD) cofactor and one 4Fe-4S cluster, the coordinates for which were provided by the *C. necator* structure. In general, the default homology modeling settings were used: ten independent models were created and minimized using the medium minimization. The final model generated had the lowest potential energy. The AMBER 99 force field was selected.

4.3.3. Determining the surface charge of NapA proteins: electrostatic potential calculations

The potential energy for each NapA protein was calculated using MOE2010.10. For each isolated NapA molecule, hydrogen's were added, then the partial charges calculated using an Amber99 force field and default settings. Next the surface was determined and the electrostatic surface potential, which is calculated using the Poisson-Boltzmann equation, was mapped onto Gauss-Connolly surfaces of the protein.

4.4. Results and Discussion

A three dimensional model of the *C. jejuni* NapA structure was created. The structure of *C. necator* NapA was used as a template due to the close sequence homology (58 % amino acid identity), well above the threshold for creating a reliable homology model. When superimposed, the *C. jejuni* and *C. necator* NapA structures have a low root mean square deviation (RMSD) between the carbon backbones of the two structures, 0.89 Å. The large sequence inserts, characteristic the Epsilonproteobacteria NapA, were the principal obstacle to creating the 3D structure of *C. jejuni* NapA. The regions flanking the sequence inserts exhibit poor sequence homology with the template, which complicated

the precise placement of the inserts onto the template structure; moreover, determining the confirmation of the sequence inserts from the know structures is not possible, as no template is available from a structurally characterized protein. To address these challenges the following approach was taken: first, a consensus sequence alignment, using the sequences from the four structurally characterized NapAs, was used to generate the sequence alignment between *C. jejuni* and *C. necator* NapA (**Figure 4.2**). Next, after the *C. jejuni* NapA model was created, the three dimensional confirmation of the sequence inserts was determined using the LowModeMD feature in MOE 2010.10. The inserts range in size from 2 to 30 amino acids long. The five, significantly large sequence inserts, were then isolated and relaxed, while the coordinates of the remaining atoms in the *C. jejuni* NapA structure were the fixed. Inserts which were smaller than 5 residues, were disregarded. All inserts are located on the surface of the protein.

Interestingly, the two larger inserts in the Epsilonproteobacteria NapA expand upon the same polypeptide inserts found in heterodimeric NapAs like *R. sphaeroides* and *E. coli* (insets 1 and 3 in **Figure 4.4**).[42] Jepson *et al.* described the two inserts as an evolutionary feature, which can be used to distinguish the smaller monomeric NapAs (i.e. *D. desulfuricans*) from larger heterodimer NapAs (i.e., *R. sphaeroides* and *E. coli)*.[126] In accordance with Jepson's prediction, the Epsilonproteobacteria NapA is predicted to function as heterodimer, based on the presence of a *napB* gene.

In the *C. jejuni* NapA structure, the insertion sequences are not directly involved in the binding of the cofactors (i.e. molybdenum center, iron sulfur cluster) or intermolecular electron transport. Based on the structure, the insertion sequences present in Epsilonproteobacterial NapA, are predicted to lie on the outer surface of the protein

(**Figure 4.3**). This would be expected as molybdopterin proteins which share a high degree of sequence similarity and are relatively larger distribute the extra residues, sequence inserts, over the molecular surface. [13]

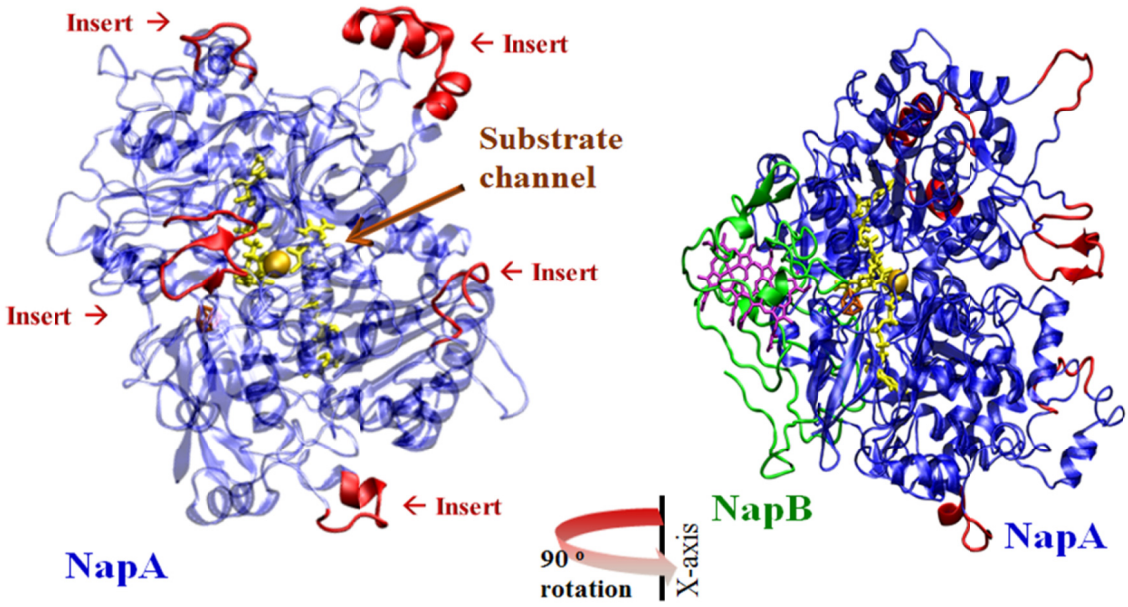

Figure 4.3: The theoretical three-dimensional model of *C. jejuni* NapA. The sequence inserts (red) are located on the outside of the NapA structure, and do not appear to affect NapB binding. The structure of NapB is represented with a green ribbon diagram, and the two inclusive cytochrome-*c* ligands are purple. NapA is displayed as a blue ribbon diagram, the Mo-*bis*PGD cofactor is displayed as a yellow stick model, molybdenum is a yellow circle, and the 4Fe-4S cluster is a brown stick model. This figure was created in VMD version 1.8.7. [217]

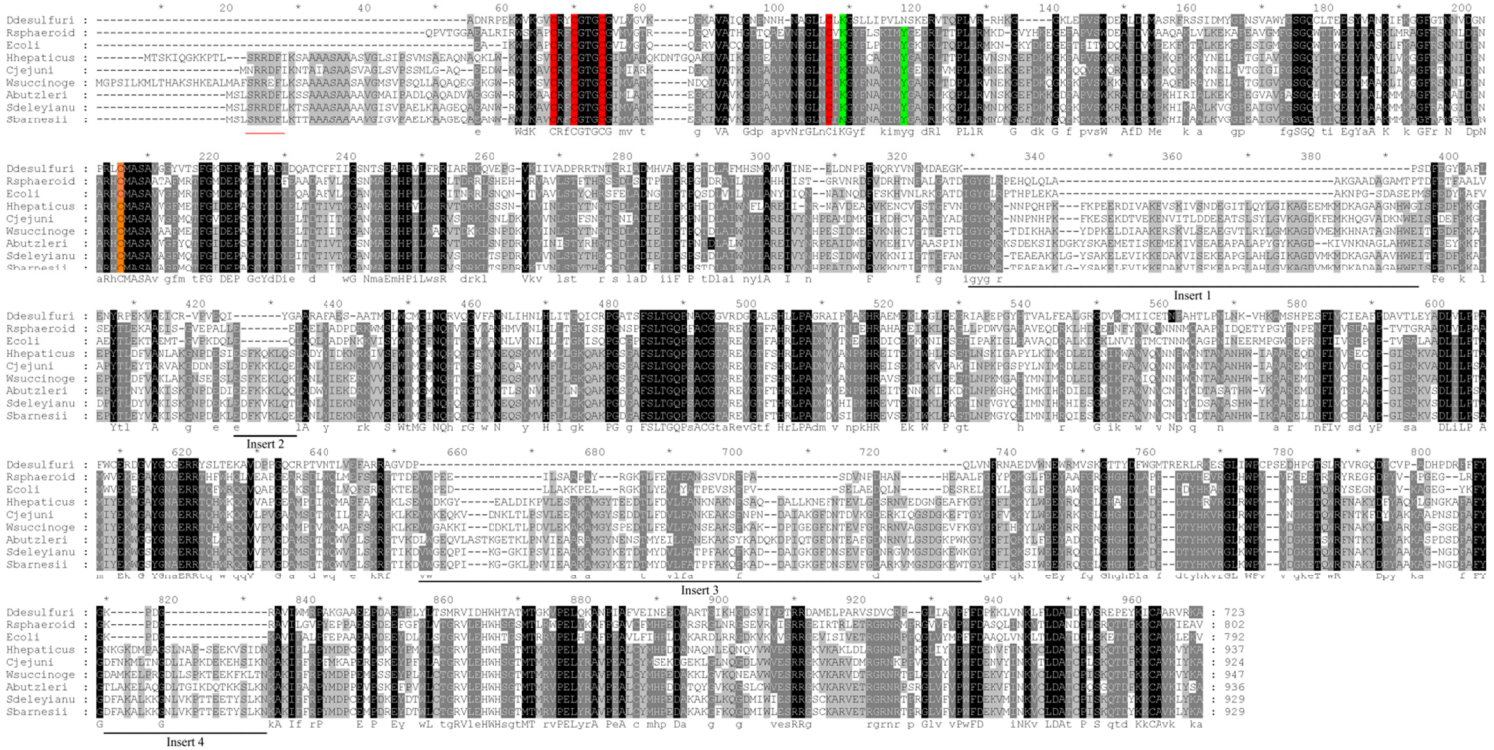

Figure 4.4: A global sequence alignment of the relatively larger Epsilonproteobacteria NapA from *C. jejuni*, *W. succinogenes*, *A. butzleri*, *S. deleyianum*, and *S. barnesii* with the smaller NapA sequences from crystalographically studied organisms, *R. sphaeroides, E. coli* and *D. desulfuricans*. This figure illustrates sequence inserts, located in the middle of the proteins, in all Epsilonproteobacteria. The sequence inserts are not located close to important regions of the peptide; such as the iron-sulfur cluster (4Fe-4S) binding motif (**red**), the conserved cysteine residue which is covalently bound to molybdenum in the active site (**orange**), and residues which are involved in electron transport (**green**): the lysine residue that is involved in electron transfer from the 4Fe-4S cluster to the Mo active site, and the tyrosine residue implicated in electron transfer from the heme in NapB to the 4Fe-4S cluster in NapA. The Epsilonproteobacteria twin arginine translocase (TAT) signal

Because of the superficial location of the sequence inserts on the *C. jejuni* NapA structure, we can theorize that the sequence inserts could, in principle, effect external interactions. The known NapA protein-protein interactions are between NapA and NapB (heterodimer formation), between NapA (homodimer formation) and between maturation proteins (i.e. NapD and NapF), and NapA.[138] To address the significance of the inserts in each of the listed external interactions, the *C. jejuni* NapA structure will be compared to crystallographically determined structures of NapA.

The ability of NapA to homodimerize has been demonstrated in vitro, [138] although the location for the NapA-NapA interaction on the three dimensional protein structure is not clear. Conceivably, the interaction may be similar to that of the *R. sphaeroides* NapA structure (PDB ID: 1OGY), which includes eight NapAB molecules in the asymmetric unit; however, crystalized proteins sometime become immobilized in unnatural confirmations during the crystallization process. This could be determined experimentally by comparing the homodimerization properties of the native *C. jejuni* NapA with that of insert mutants. In any case, the structure of *C. jejuni* NapA was superimposed onto one monomer in *R. sphaeroides* NapAB octomer (**Figure 4.5**). From this representation, it appears as though the inserts do not disturb the interaction between adjacent NapA molecules. Also, the *C. jejuni* NapA sequence inserts are clearly not located in the proximity of the NapB binding site of *R. sphaeroides* NapA (**Figure 4.3**), suggesting the insertion loops are not involved in heterodimer formation. The superimposition of *C. jejuni* NapA and the heterodimeric NapAB from *R. sphaeroides* suggests that the sequence inserts are located on the opposite side of NapAs' NapB docking site, and are closer to the active site cavity.

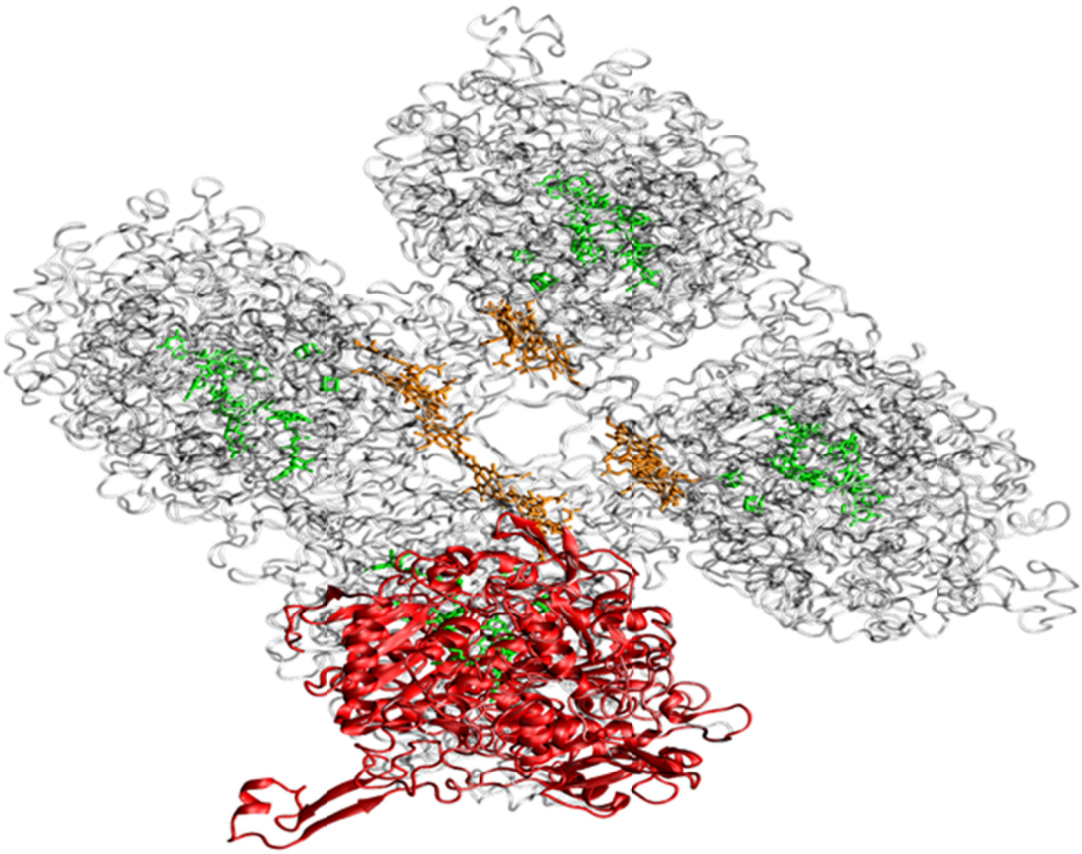

Figure 4.5: Superimposition of the *C. jejuni* NapA model onto the *R. sphaeroides* NapAB octomer. *R. sphaeroides* NapA and NapB are grey ribbons, the From this representation, it appears as though the inserts do not disturb the interaction between adjacent NapA molecules. The insert in the photograph was not subjected to lengthy molecular dynamics simulations; therefore, the presented fold is not intended to represent the actual structure, but provide a location of the sequence inserts on the surface of NapA.

The active site of NapA is buried roughly 14 Å below the surface of the protein; a large funnel shaped cavity directs nitrate to the molybdenum active site. The most prominent sequence insert in *C. jejuni* NapA structure, approximately 30 amino acids long (insert # 1 in **Figure 4.4**) are located particularly close to the entrance of the active site funnel. The close proximity to the active site cavity raises the possibility that the insertions could, in principle, affect the catalytic function of the protein; in the event the loops fold over the cavity and modulate the substrate entrance, or product release. Still, the *C. jejuni* NapA active site appears to be the same as structurally characterized NapA; the residues involved in the construction of the catalytic pocket, directly above the molybdenum active site, are conserved (**Figure 4.6**).

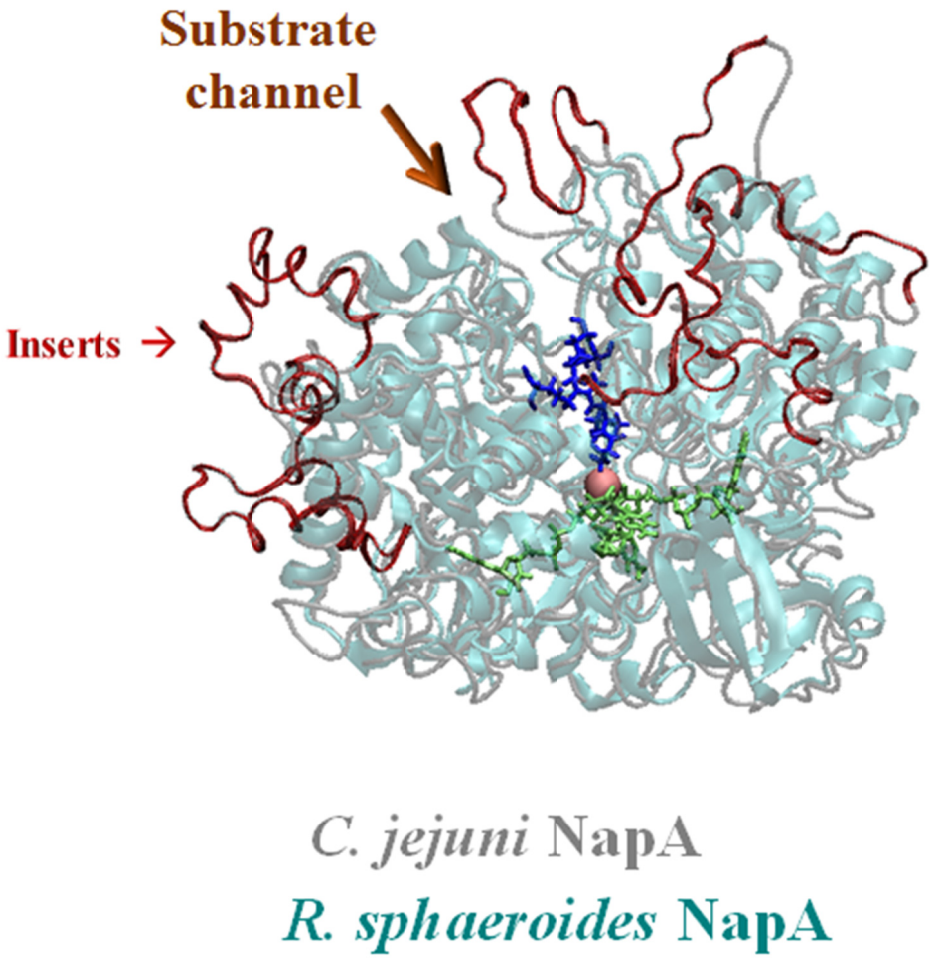

Figure 4.6: Superimposition of the *C. jejuni* and *R. sphaeroides* NapA structures. The protein backbones of each NapA structures are displayed. *R. sphaeroides* NapA is represented a teal ribbon. The *C. jejuni* NapA as grey lines with the sequence inserts highlighted in red. In the *R. sphaeroides* NapA structure, molybdenum is displayed as a pink circle, the *bis*PDG cofactor as green stick figure, and the residues which line the active site funnel, directly above the active site, are displayed as blue stick figures. The lower panel, in which the *R. sphaeroides* NapA backbone has been removed, shows the superimposition of the active site residues from *C. jejuni* NapA, represented as grey stick figures, with the active site residues from *R. sphaeroides* NapA. The active site residues are conserved in both NapA sequences and the superimposition the two NapA structures illustrates the almost indistinguishable location of the active site residues in each structure. VMD was used to create this illustration.

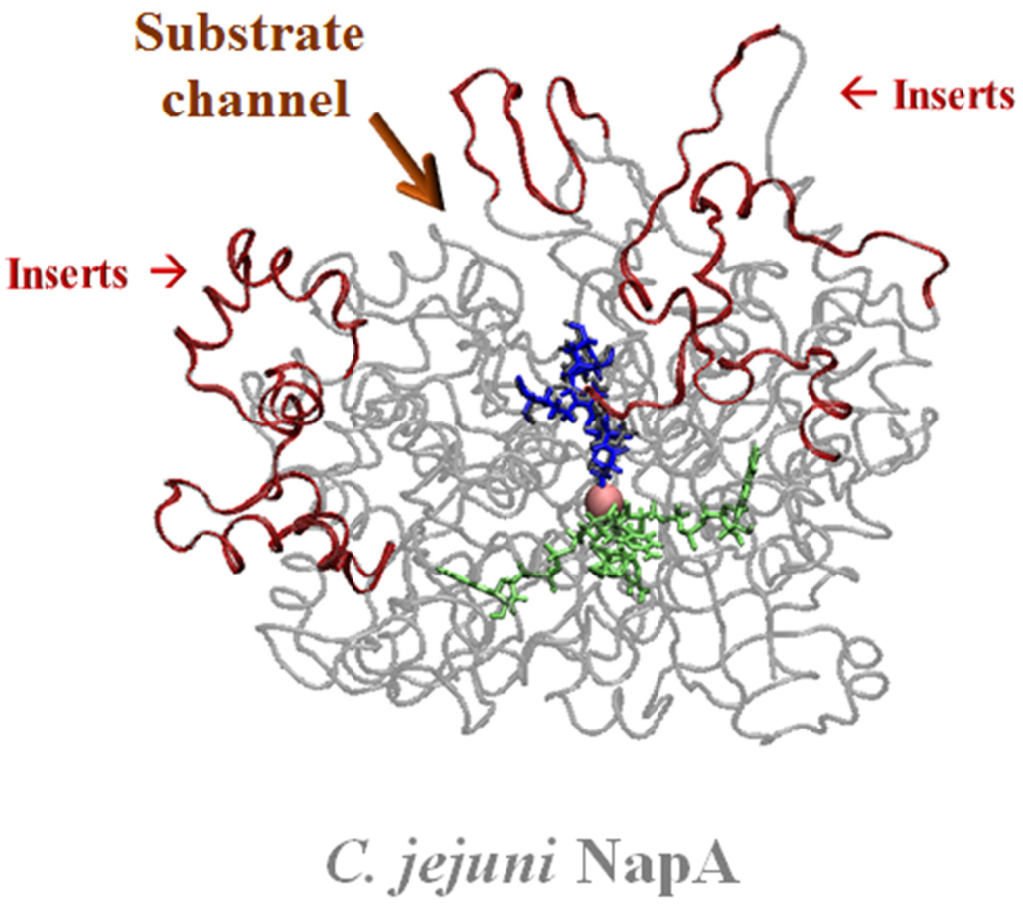

Figure 4.6 (continued): The C. *jejuni* and *R. sphaeroides* NapA structures.

A second possibility, is that the sequence inserts could affect maturation of NapA; however, the mechanism of cofactor insertion (i.e., *bis*PGD and 4Fe-4S), and post translational modification (i.e., N-terminus TAT leader sequence cleavage) is not completely understood. The currently accepted theory is that NapD inhibits transport of NapA to the periplasmic space by binding to the N-terminus TAT leader sequence of NapA; [131] the NapD-NapA interaction has been structurally confirmed (see PDB ID: 2PQ4). NapD, a cytoplasmic protein, is believed to retain NapA in the cytoplasm until

the cofactors are inserted, as the TAT export system transports the folded NapA into the periplasm. Currently, the mechanism of *bis*PGD cofactor insertion is not known. NapF is believed to insert the 4Fe-4S cluster into NapA; however, *C. jejuni* does not encode a NapF homologue. Also, the possibility that NapL interacts with the sequence inserts cannot be overlooked; NapL is proposed to be NapA chaperone protein which is only found in organisms with large NapA proteins, such a *C. jejuni*. Future experiments with *C. jejuni* NapA should explore the significance of the sequence inserts in catalysis and maturation.

The polarity and hydrophobicity of amino acids located on the protein surface play a fundamental role in chemistry of proteins, especially protein-protein interactions. [218] The electrostatic potential was calculated for *C. jejuni* NapA, and, for comparison, the *C. necator, R. sphaeroides*, *D. desulfuricans*, and *E. coli* NapA structures. In all structures, a dense region of positive charge is localized in the active site funnel,[40] possibly used to attract and facilitate the transport of nitrate into the cavity for catalytic transformation; however, *C. jejuni* NapA is relatively more basic, a characteristic that may influence the product binding and substrate release. Of the four NapA structures investigated in this current study, *C. jejuni* was found to have the most basic global charge; *R. sphaeroides* was the most acidic. The acidic nature of *R. sphaeroides* is consistent with an earlier description by Jepsen *et al.*, [147, 219] in which they suggest that monomeric NapA proteins (i.e. *D. desulfuricans*) have a relatively more basic surface charge than heterodimeric NapA's (i.e. *R. sphaeroides* and *E. coli*). Contradictory, our calculations indicate that NapA from *C. jejuni*, which is expected to be a heterodimeric protein, is the most basic of the four structures. Thus, Epsilonproteobacterial NapA is unique in this

regard; models of *S. barnesii* NapA proteins supported this observation (data not included).

Richardson *et al.* demonstrate that an evolutionary link, between the assimilatory nitrate reductase NarB and the monomeric NapA from *D. desulfuricans*, is evident in the biophysical properties of the active subunit.[126] Specifically, they found that the monomeric NapA, found in the delta proteobacteria *Desulfovibrio desulfuricans*, is more similar in size and electrostatic surface charge to the monomeric NarB, than the dimeric NapAs, which are relatively larger and exhibit a more negative surface charge.[126] However that study neglected to include the Epsilonproteobacteria NapA, which is also a close relative to assimilatory nitrate reductases.[75] We have found that the Epsilonproteobacteria NapA is relatively more negative than the monomeric NapA from *D. desulfuricans* (**Figure 4.7**) in disagreement with the generalization that heterodimeric NapAs are more positive.

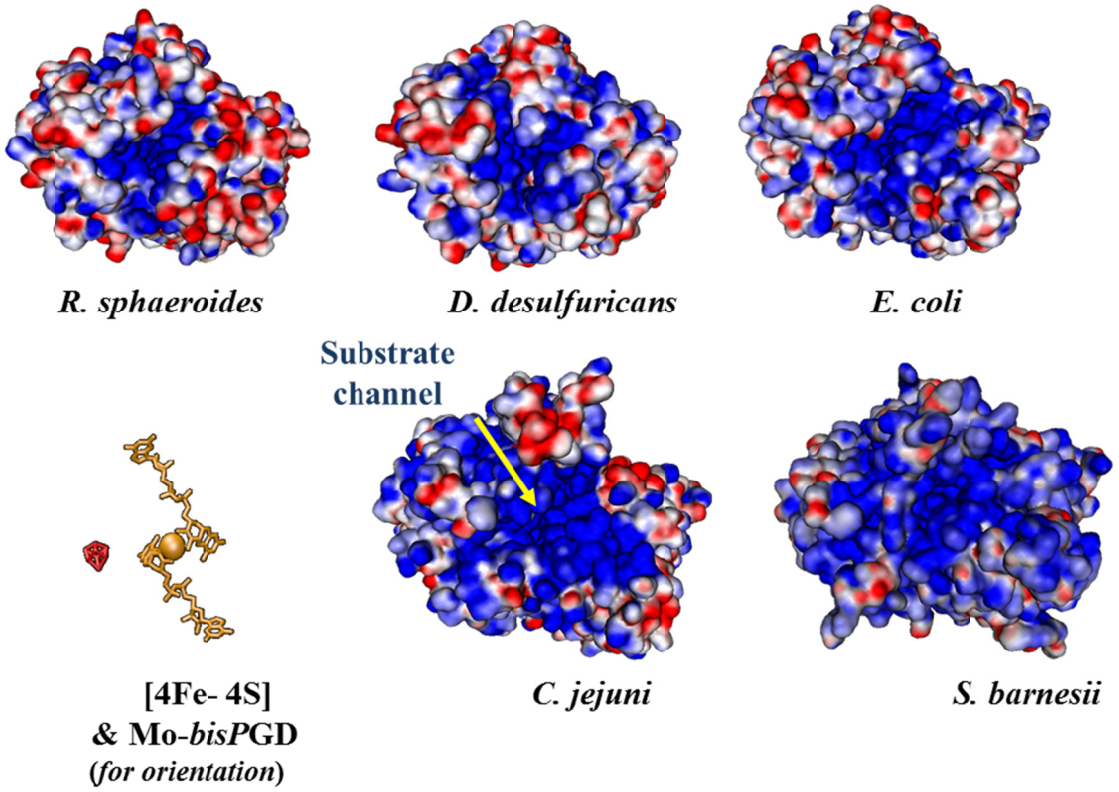

Figure 4.7: The electrostatic surface potential of NapA proteins. The structures of *R. sphaeroides* (1OGY), *D. desulfuricans* (2NAP), and *E. coli* (2NYA) were downloaded from the RSCB PDB (pbd.org). The structures of *C. jejuni* and *S. barnesii* (data not included) NapA were created using the same methods. Surface potential was calculated and plotted to the protein surface for each NapA protein separately using MOE. All proteins were superimposed to assume the same orientation for this figure; the *bis*PGD cofactor was included to illustrate the orientation of the proteins. The active site funnel is perpendicular to the plane of this page, leading to the Mo atom

As mentioned, NapA has a close phylogenic relationship with the catalytic subunit of the assimilatory nitrate reductases. [75, 126] Three types of bacterial assimilatory nitrate reductase have been identified; the active subunits, NasA, NasC and NarB, [47] have different biochemical properties. NarB is the closest phylogenetic relative of NapA.[126] The active site of NarB and NapA is predicted to be similar; molybdenum is coordinated by conserved cysteinyl sulfur and dithiolene sulfurs provided

by a pterin (one in NarB and two in NapA); however, many differences exist. The cellular location differs, NarB is cytoplasmic and NapA is found primarily in the periplasm, a result of an N-terminal TAT leader sequence of NapA. The source of electrons, required for the reduction of nitrate to nitrite, also differs; NarB accepts electrons from a reduced ferrodoxin, and NapA typically collects electrons indirectly from a membrane quinone pool. The operon content also varies, *narB* is the only nitrate reductase gene in the *nar* operon, while, the *nap* operon has recruited several additional genes, typically more than four additional genes. Despite the differences between the two enzyme systems, NarB is the closest phylogenic relative of NapA. Interestingly, the *nap* operon is associated with transposase genes in some organisms; therefore it is conceivable that NapA has evolved from assimilatory nitrate reductases, via horizontal gene transfer, and, in the process, NapA acquired more genes which aid in catalytic efficiency and maturation.

Computational phylogenetics was used to determine the relatedness of NapA sequences. A neighbor joining tree was constructed from the multiple sequence alignment of over 288 NapA sequences and, as outliers, three assimilatory nitrate reductases and formate dehydrogenase (**Figure 4.8**). The monomeric NapA, typified by *D. desulfuricans* NapA, is clearly the most similar to the assimilatory nitrate reductase. The deepest branch in the NapA tree (most similar to assimilatory nitrate reductases) is comprised mainly of Deltaproteobacteria, along with some non-proteobacteria (*i.e.*, Firmicutes, Deferribacteres, Bacteroidetes and Chrysiogenetes). A second, deep branch in the NapA tree is comprised of mainly Epsilonproteobacteria, Aquificae and one Deinococcus also cluster into this branch. NapA from the Alpha-, Beta- and Gamma- proteobacteria are

located in one large branch, indicating a relatively less similar sequence to the assimilatory nitrate reductases than the delta branch.

Interestingly, the phylogeny of NapA correlates with the *nap* operon structure (**Figure 4.8**). Examining the presence, or absence, of *nap* genes, which encode proteins involved in post-translational modification of NapA (i.e. NapD, NapF and NapL) and electron transport to NapA (i.e. NapB, NapC, NapG, NapH), can provide fundamental information on how the mechanism of NapA maturation and electron transport differs in each organism. While the presence of dedicated *nap* chaperone proteins and electron transport proteins would increase the overall efficiency of nitrate reduction via NapA, it is possible that, in the absence of these dedicated genes, the organism can uses more undefined proteins to fulfill the same role. For example, in *Shewanella oneidensis* uses CymA, a *c* - type cytochrome containing membrane protein similar to NapC, to transfer electrons from the quinone pool to NapA [220] The interaction between NapAB and membrane-bound Nap proteins (i.e. NapGH or NapC), has been described as "transient", [46] compared to molybdopterin containing enzymes which have stable interactions with membrane-bound complexes (i.e. formate dehydrogenase (FdhGHI) and respiratory nitrate reductase (NarGHI)). The correlation between *nap* operon gene content and organization, and NapA phylogeny suggests an evolutionary progression of the *nap* operon, possibly away from the monomeric assimilatory nitrate reductase operon of NarB, into more complex operons, such as found in the Epsilonproteobacteria (*napAGHBFLD*).

Figure 4.8 (next page): Phylogenic tree of NapA. The Neighbor-Joining method was used to infer the evolutionary relationship among the 292 protein sequences analyzed. Positions containing gaps were eliminated, yielding a total of 600 amino acid positions in the final dataset. The Poisson correction method was used to calculate the number of amino acid substitutions per site. The tree branches are drawn to scale (lower left corner) and the branch lengths correspond to the number of amino acid substitutions per site, values greater > 0.05 are listed above each respective branch). The bootstrap consensus tree (inferred from 100 replicates) is presented. The percentage of replicate trees in which the associated taxa clustered together in the bootstrap test is provided above each node. MEGA5 software was used for alignments and phylogenetic analyses. Formate dehydrogenase was included in the analysis as an outlier. Three assimilatory nitrate reductases were also included for reference. NapA sequences were collected from the NCBI database. Branches corresponding to similar species (**sp.**) or subspecies (**ssp.**) are collapsed. The colored circles indicate the type quinone oxidase (NapH or NapC) found with NapA in the *nap* operon (*see* **Table A.1** for details). NapC (green circle) and if NapC + NapF (blue circle). NapC and NapH (pink circle). NapH (brown circle) and if NapH + NapL (red circle). No quinone oxidase (grey circle).

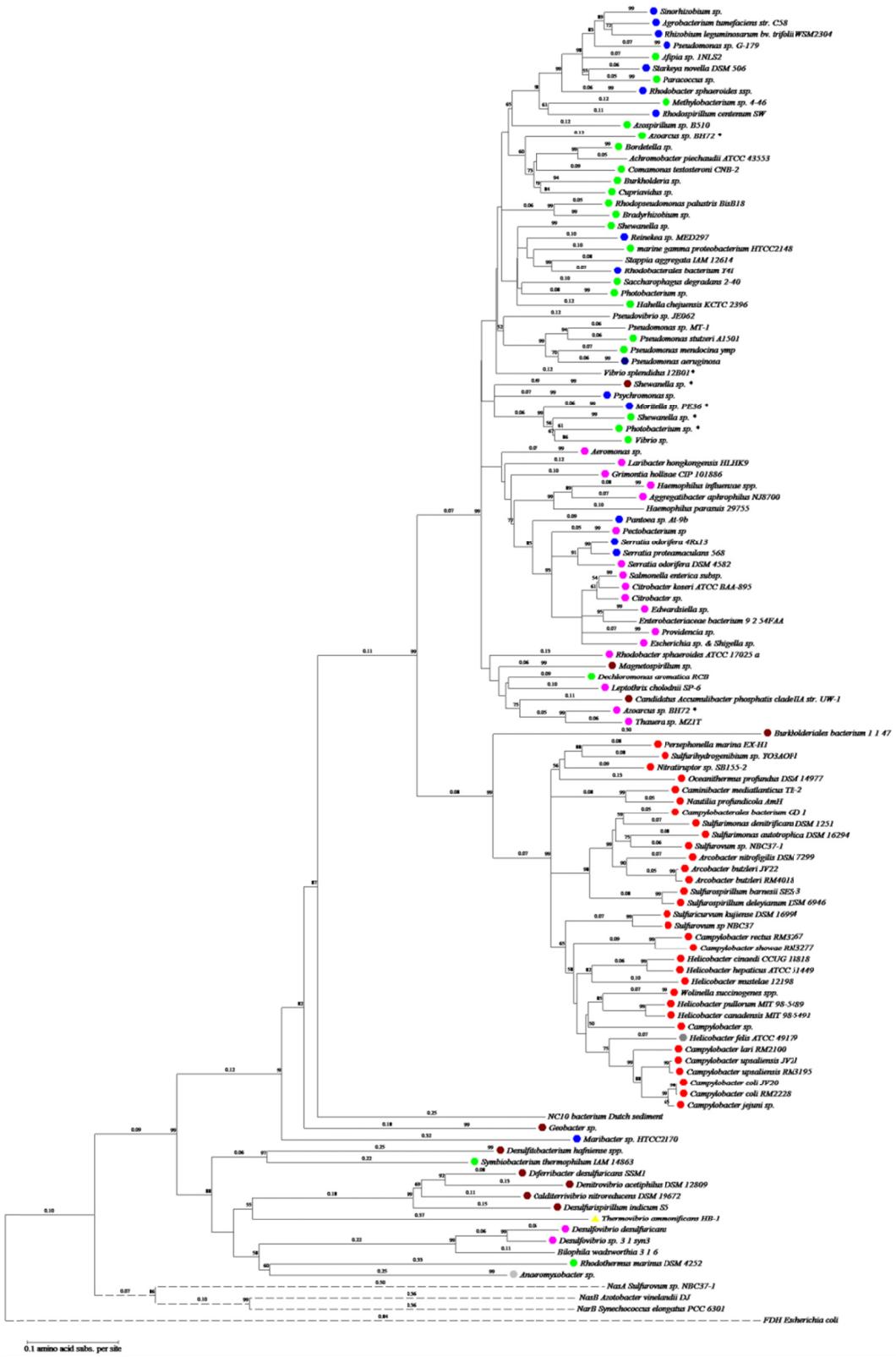
Sinorhizobium sp.
Agrobacterium tumefaciens str. C58
Rhizobium leguminosarum bv. trifolii WSM2304
Pseudomonas sp. G-179
Alfipia sp. 1NLS2
Starkeya novella DSM 506
Paracoccus sp.
Rhodobacter sphaeroides ssp.
Methylobacterium sp. 4-46
Rhodospirillum centenum SW
Azospirillum sp. B510
Azoarcus sp. BH72 *
Bordetella sp.
Achromobacter piechaudii ATCC 43553
Comamonas testosteroni CNB-2
Burkholderia sp.
Cupriavidus sp.
Rhodopseudomonas palustris BisB18
Bradyrhizobium sp.
Shewanella sp.
Reinekea sp. MED297
marine gamma proteobacterium HTCC2148
Stappia aggregata IAM 12614
Rhodobacterales bacterium Y4I
Saccharophagus degradans 2-40
Photobacterium sp.
Hahella chejuensis KCTC 2396
Pseudovibrio sp. JE062
Pseudomonas sp. MT-1
Pseudomonas stutzeri A1501
Pseudomonas mendocina ymp
Pseudomonas aeruginosa
Vibrio splendidus 12B01*
Shewanella sp. *
Psychromonas sp.
Moritella sp. PE36 *
Shewanella sp. *
Photobacterium sp. *
Vibrio sp.
Aeromonas sp.
Laribacter hongkongensis HLHK9
Grimontia hollisae CIP 101886
Haemophilus influenzae spp.
Aggregatibacter aphrophilus NJ8700
Haemophilus parasuis 29755
Pantoea sp. At-9b
Pectobacterium sp
Serratia odorifera 4Rx13
Serratia proteamaculans 568
Serratia odorifera DSM 4582
Salmonella enterica subsp.
Citrobacter koseri ATCC BAA-895
Citrobacter sp.
Edwardsiella sp.
Enterobacteriaceae bacterium 9 2 54FAA
Providencia sp.
Escherichia sp. & Shigella sp.
Rhodobacter sphaeroides ATCC 17025 a
Magnetospirillum sp.
Dechloromonas aromatica RCB
Leptothrix cholodnii SP-6
Candidatus Accumulibacter phosphatis clade IIA str. UW-1
Azoarcus sp. BH72 *
Thauera sp. MZ1T
Burkholderiales bacterium 1 1 47
Persephonella marina EX-H1
Sulfurihydrogenibium sp. YO3AOP1
Nitratiruptor sp. SB155-2
Oceanithermus profundus DSM 14977
Caminibacter mediatlanticus TE-2
Nautilia profundicola AmH
Campylobacterales bacterium GD 1
Sulfurimonas denitrificans DSM 1251
Sulfurimonas autotrophica DSM 16294
Sulfurovum sp. NBC37-1
Arcobacter nitrofigilis DSM 7299
Arcobacter butzleri JV22
Arcobacter butzleri RM4018
Sulfurospirillum barnesii SES-3
Sulfurospirillum deleyianum DSM 6946
Sulfuricurvum kujiense DSM 16994
Sulfurovum sp NBC37
Campylobacter rectus RM3267
Campylobacter showae RM3277
Helicobacter cinaedi CCUG 18818
Helicobacter hepaticus ATCC 51449
Helicobacter mustelae 12198
Wolinella succinogens spp.
Helicobacter pullorum MIT 98-5489
Helicobacter canadensis MIT 98-5491
Campylobacter sp.
Helicobacter felis ATCC 49179
Campylobacter lari RM2100
Campylobacter upsaliensis JV21
Campylobacter upsaliensis RM3195
Campylobacter coli JV20
Campylobacter coli RM2228
Campylobacter jejuni sp.
NC10 bacterium Dutch sediment
Geobacter sp.
Maribacter sp. HTCC2170
Desulfitobacterium hafniense spp.
Symbiobacterium thermophilum IAM 14863
Dferribacter desulfuricans SSM1
Denitrovibrio acetiphilus DSM 12809
Calditerrivibrio nitroreducens DSM 19672
Desulfurispirillum indicum S5
Thermovibrio ammonificans HB-1
Desulfovibrio desulfuricans
Desulfovibrio sp. 3 1 syn3
Bilophila wadsworthia 3 1 6
Rhodothermus marinus DSM 4252
Anaeromyxobacter sp.
NasA Sulfurovum sp. NBC37-1
NasB Azotobacter vinelandii DJ
NarB Synechococcus elongatus PCC 6301
FDH Escherichia coli
0.1 amino acid subs. per site

4.5. Conclusions

Periplasmic nitrate reductase has been proposed to carry out a variety of physiological functions. While operon composition may play a role in the functionally diverse nature of Nap, differences in the structure and the electrostatic potential of the NapA could also influence the catalytic function of NapA. [221] The results presented here provide evidence that the periplasmic nitrate reductase from the Epsilonproteobacteria has differentiating features. The Epsilonproteobacterial NapA is the largest of all known NapA proteins; the primary amino acid sequence contains several insertion sequences which are predicted to lie on the protein surface. Because these inserts are found exclusively in Epsilonproteobacterial NapA, they could be exploited to target pathogens (i.e. *C. jejuni* or *H. pylori*) in diagnostics or therapeutic approaches.

The *napA* operon has unique gene organization, typically taking the form of *napAGHBFD*, and can include the *napL* and *napS* genes (i.e. *napAGHBFLDS*). The *napS* gene, which is predicted to be a regulatory protein, is only found in four Epsilonproteobacteria, and the *napL* gene, which is predicted to encode a NapA chaperone protein, are exclusive to the *napA* operon. Phylogenic analysis of all known NapA proteins confirms that the Epsilonproteobacteria NapA form a defined phylogenetic clade, along with species of Aquifae and interestingly the presence of the *napA*-type operon is segregated to this clade.

CHAPTER 5: Conclusions

NapA is a molybdopterin and iron sulfur protein that typically has a high affinity for nitrate, K_m < 300 uM. Even though NapA is one of the most extensively studied molybdopterin proteins, more experimental evidence is needed to fully understand the catalytic mechanism of nitrate reduction.[19] A proposed mechanism of nitrate reduction by NapA is shown in **Figure 5.1**.[38] From this mechanism it is clear that the many aspects require additional information. Thus the global aim of our research is to elucidate the mechanism of nitrate reduction in the molybdenum center of NapA.

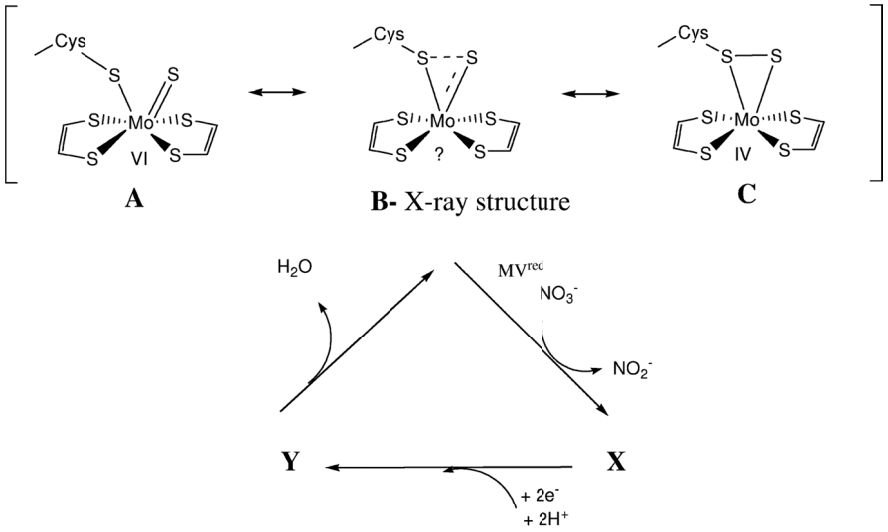

Figure 5.1: The proposed mechanism of nitrate reduction by NapA. [38] The possible species (X) are provided at the bottom of the figure. Y was not provided. This figure was used with permission from the Royal Society of Chemistry. [17]

The main objective of this study was to isolate and characterize NapA from the Epsilonproteobacteria, *Campylobacter jejuni* and *Sulfurospirillum barnesii*. We explored two methods of NapA purification: native expression and purification of NapA from the non-pathogenic Epsilonproteobacteria *S. barnesii* (**Chapter 2**), and the cloning, heterologous expression and purification of *C. jejuni* and *S. barnesii* NapA from *E. coli* (**Chapter 3**).

The heterologous expression of molybdenum enzymes is not straightforward, partially due to the complex nature of the pyranopterin cofactor and insertion of iron-sulfur cluster. Over the last decade, the involvement of dedicated chaperone proteins in the maturation of periplasmic molybdopterin proteins has been discovered. In NapA, two dedicated chaperone proteins have been identified, NapD and NapF. A third predicted NapA chaperone, NapL, is found primarily in the Epsilonproteobacteria. In all chaperone proteins the association with NapA is believed to be species-specific. To promote NapA maturation we integrated chaperone proteins into the molecular cloning approach. A NapLD construct was created for co-expression with NapA. The active *C. jejuni* NapA and *S. barnesii* NapA were isolated with metal affinity chromatography. From the characterization and kinetic analysis is clear that the recombinant enzyme has attenuated activity.

The experiments with *S. barnesii* cells indicate that NapA also has a tight affinity for nitrate, consistent with reports from other NapA isolates. In *C. jejuni* and *S. barnesii* NapA is predicted to be involved in respiratory nitrate reduction. [78] NapA's tight affinity for nitrate should not hinder the efficiency of nitrate respiration.

The Epsilonproteobacterial NapA is the largest NapA isolate to date, approximately 100 kDa. The extra amino acid residues (over 10 kDa) are distributed in the middle of the protein sequence. Sequence analysis of NapA proteins indicates that the Epsilonproteobacteria NapA form a unique clade, distinct from other bacterial NapA. In this clade, the *napAGHBFLD* operon is predominant. The *napA* operon contains a few unique features. NapC is not present in any Epsilonproteobacterial *nap* operons. NapC transfer electrons to NapA during nitrate respiration, although NapGH can fulfill this role. Also NapL is only found in this NapA clade. The unique *napL* gene and the NapA insertion sequences may be useful for design of diagnostic tools for *C. jejuni* identification.

In lieu of crystallographic data, the structure of *C. jejuni* NapA was investigated using theoretical modeling (**Chapter 4**). The amino acid residues in the active site of *C. jejuni* NapA are conserved. The large sequence inserts, which are characteristic of the Epsilonproteobacteria, are located close to the active site cavity and do not appear to be involved in NapB docking. The close proximity of the insertion sequence to the active site cavity raises the possibility that the extra residues in the *C. jejuni* NapA could, in principle, affect the function of the protein. A better understanding of how the additional residues may affect the structure and function of NapA is the first step towards revealing the chemistry of nitrate reductase.

5.1. Future directions

NapA was isolated from *S. barnesii* (*see* Chapter 2) with limited yield of the active protein. We isolated the NapA from a membrane enriched fraction; an alternative approach would be to focus on the periplasmic fractionation. This would reduce the

complexity of the sample prior to chromatographic separations. To determine the selectivity of the *S. barnesii* NapA for nitrate, the protein can be assayed for selenate, arsenate, tellurite, TMAO and DMSO reductase activity. NapA has been reported to reduce selenate and tellurite in *Rhodobacter sphaeroides*. [222] This is of particular significance to *S. barnesii*, which would encounter these oxyanions in the environment.

The cloning, expression and purification of *C. jejuni* and *S. barnesii* NapA, is the most promising avenue for future experiments. A method for cultivating and purifying *C. jejuni* and *S. barnesii* NapA in *E. coli* was established. The recombinant enzymes displayed a lower affinity for nitrate, decreased velocity, and less than ideal metal content, consistent with incomplete cofactor content. Future work should optimize the purification procedure to increase the recovery of active NapA. In the large scale expression and purification of NapA, NapA was isolated in complex with NapD. This indicates that NapA is cytoplasmic, as NapD acts as a NapA anti-porter in the cytoplasm and should not be translocated to the periplasmic space. Cytoplasmic NapA presumably has low cofactor content, therefore lower activity. One possible avenue to increasing the recovery of active NapA would be to isolate the NapA from the periplasm. The periplasmic isolation of NapA was successful in the small scale expression experiments (**Figure 3.7**). We were not able to successfully scale-up the periplasmic isolation procure.

The catalytic properties of *C. jejuni* and *S. barnesii* NapA can also be investigated. Other NapA isolates are capable of reducing tellurite and selenate, although with poor affinity and rates. [222] Non-competitive inhibition by Zinc has also been reported to be specific for NapA, not other DMSO reductases.[171] In high

concentrations (> 0.25M), potassium and sodium have an activating effect on NapA in *D. desulfuricans*. Calcium and magnesium are reported to decrease NR activity. [205]

Ultimately, future work should focus on determining the mechanism of nitrate reduction by periplasmic nitrate reductase (NapA). This could include crystallographic studies and more detailed spectroscopic studies which require larger quantities of enriched NapA. Protein film cyclic voltammetry can provide a more physiologically relevant measure of electron transfer. Furthermore, probing the redox chemistry of the molybdenum active site in is typically monitored by electron paramagnetic resonance spectroscopy in other molybdopterin enzymes, as the transformation of Mo^{VI} to the Mo^{IV} state involves the paramagnetic Mo^{V}.

We have created multiple *nap* plasmids in this study. The *C. jejuni napA*, *napLD*, and *napB* genes and *S. barnesii napA* and *napB* genes have been inserted into expression vectors and in some cases the pET 1.2 cloning vector. The *S. barnesii napFLD* genes were not amplified successfully. This was most likely the result of uncomplimentary primer design. The *S. barnesii* genome has been completed during the preparation of this dissertation. The primers can now be redesigned to amplify the *S. barnesii* maturation genes. This would provide a more direct comparison to the *C. jejuni* NapA-NapD interaction.

The *napL* and *napD* genes were amplified directly from *C. jejuni* as a single construct (i.e., *napLD*). Later review of the sequence data revealed that the two genes are out of frame from one another and overlap, *napL* and *napD* are transcriptionally coupled. The NapD protein was identified in the purified NapA fractions from *C. jejuni*. NapL was never detected. The sequencing data collected from the pCnapLD plasmid does not

include the sequence of the pRSF promoter (**Figure A.21**); therefore we could not confirm that this region was free of mutations. The sequence of the T7 promoter region in the pCnapLD plasmid should be confirmed by DNA sequencing. A conserved -10 region (TATAAT) was identified upstream from *napD*, with-in the *napL* sequence (**Figure A.14**). This indicated that NapD expression may have occurred using the natural transcriptional regulators of *E. coli*, as IPTG induced expression of NapD was not observed. To improve the maturation of NapA, one could address these potential problems and create separate *napL* and *napD* expression plasmid. Furthermore, the *napL* gene would have to be cloning and expressed separately from NapD to elucidate the function of NapL in NapA maturation. The co-expression of NapA with NapD or NapL can then be compared to determine the effect of maturation proteins on NapA cofactor content and the catalytic function.

Mutation of NapA, NapD, and NapL or NapB can be investigated to determine the mechanisms of protein- proteins interaction. Plasmids containing these *nap* genes were created in this study, making mutational studies easy. To determine the significance of the NapA insert sequences, which were predicted to be located in the vicinity of the *C. jejuni* active site (see Chapter 4), these regions of the *C. jejuni* NapA protein should be mutated.

S. barnesii and *C. jejuni napB* were cloned in to a pQE-60 expression vector. The preliminary NapB expression studies suggest that napB was expressed; however, NapB was never identified by mass spectroscopy. Future work on NapB will have to optimize the expression conditions, before the purification of the recombinant protein is possible. Cytochrome *c* maturation proteins (ccm) have been found to be important in the

maturation of the recombinant *H. influenzae* NapB. [144] We have obtained a plasmid which includes the *ccm* operon, pEC86. The expression of NapB may benefit from the inclusion of pEC86. Once NapB is isolated, binding studies between NapA and NapB can be conducted.

Appendix I: Supplemental Tables and Figures

Table A.1: The *nap* operon gene content and organization in bacteria. The *nap* operons categorized into four groups based on the presence or absence of a membrane quinone oxidase (*napC* or *napH*). The gene order in each organisms *nap* operon was provided by the NCBI gene and phenotype mapping database (http://www.ncbi.nlm.nih.gov/gene), and in a few cases the JGI database (http://img.jgi.doe.gov). The identity of each translated Nap protein was confirmed by preforming a blast search with-in the NCBI database. In each operon the *nap* genes are listed by the order in which they are found. Organisms which encode two separate *nap* operons are in bold **(*)**. **Abbreviations:** Class, refers to the bacterial phylogenic class; the alpha-, beta-, gamma-, and epsilon-proteobacteria are abbreviated with using the corresponding Greek letters (α, β, γ, δ, ε); clostridia (Clos.); Deferribacteres (Defer.); Chrysiogenetes (Chry.); Sphingobacteria (Sphin.); Aquificae (Aquif.); Deinococci (Dein.); Flavobacteria (Flav.); Ubiquinone oxidase (U ox.).

Quinone oxidase	***nap* Operon**	**Class**	**Organism**
H	AGHBF_LD	ε	*Sulfurovum* sp. Autotrophic
	AGHBFLD	Aquif.	*Hydrogenivirga* sp. 128-5-R1-1, *Persephonella marina* EX-H1, *Sulfurihydrogenibium* sp. YO3AOP1
		Dein.	*Oceanithermus profundus* DSM 14977
		ε	*Arcobacter butzleri* RM4018, *Ar. Nitrofigilis, Campylobacter concisis, C. curvis, C. hominis, C. fetus, Helicobacter mustelae* 1219*, Nautilla profundicola, Sulfuricurvum kujiensedum, Sulfurospirillum barnesii, S. deleyianum, Wolinella succinogenes*
	AGHBFLDS	ε	*Nitratiruptor* sp. SB155-2, *Caminibacter mediatlanticust*
	AGHBFLSD	ε	*Thiomicrospira* (formerly *Sulfurimonas*) *denitrificans* DSM 125
	AGHBLD	ε	*Campylobacter lari*, *C. coli, C. jejuni (8 strains), C. upsalensis, Helicobacter hepaticus*
	DAGHB	β	*Burkholderiales* bacterium 1_1_47
		γ	***Shewanella amazonensis* SB2B*,** *Sh. halifaxensis* HAW-EB4, ***Sh. loihica* PV-4*,** *Sh. oneidensis* MR-1, ***Sh. pealeana* ATCC 700345***, ***Sh. sediminis* HAW-EB3*, *Sh.*sp. ANA-3*, *Sh.* sp. MR-4*,** *Sh.*sp. MR-7, ***Sh.*sp. W3-18-1***
	DAGHB_F<	β	*Candidatus accumulibacter phophatis*
	DAGHF	δ	*Geobacter lovleyi*
	DGBAH:G	Clos.	*Desulfitobacterium hafniense* strains (2 DCB-2 & 2 DCB-1)
	FDAGHB	α	*Magnetospirillum magnetotacticum* AMB-1
	GBAH:G	Clos.	*Desulfitobacterium hafniense* Y51
	MADGH	Chry.	*Desulfurispirillum indicum*
		Defer.	*Calditerrivibrio nitroreducens, Deferribacter desulfuricans*, *Denitrovibrio acetiphilus*

Table A.1 (continued): The *nap* operon gene content and organization in bacteria.

Quinone oxidase	*nap* Operon	Class	Organism
C	ABC	γ	*Photobacterium damselae* CIP 102761, ***Ph. profundum* SS9***
	AC	Sphin.	*Rhodothermus marinus*
	CDAG	Clos.	*Symbiobacterium thermophilum*
	DABC	β	*Dechloromonas aromatica* RCB
		γ	*Hahella chejuensis* KCTC 2396, ***Photobacterium sp.* SKA34*, *Shewanella piezotolerans* WP3*, *Sh.sediminis* HAW-EB3*,** *Sh.violacea* DSS12, *Vibrio vulnificus* CMCP6
	DABCF	Flav.	*Maribacter* Sp. HTCC2170
	EABC	γ	***Photobacterium profundum* 3TCK***
	EDABC	α	*Afipia sp.* 1NLS, *Azospirillum sp.* B510,*Bradyrhizobium japonicum* USDA 110, *Bradyrhizobium sp.* BTAi1, *Bradyrhizobium sp.* ORS278, *Methylobacterium* sp. 4-46, *Paracoccus denitrificans* PD1222, *Pa. pantatrophus*, *Rhodopseudomonas palustris* BisB18
		β	*Achromobacter xylosoxidans* A8, ***Azoarcus sp. BH72****, *Burkholderia xenovorans* LB400, *Comamonas testosteroni* CNB-2, *Cupriavidus metallidurans* CH34, *Cu. taiwanensis* LMG 19424, *Ralstonia eutropha* H16, *Ra. eutropha* JMP134, *Ra. pickettii strains* (12D & 12J)
		γ	*Marine γ proteobacterium* HTCC2148, *Pseudomonas mendocina* ymp, *Pseudomonas stutzeri* A1501, *Saccharophagus degradans* 2-40, ***Shewanella amazonensis* SB2B***, *Sh. baltica* OS155, ***Sh. baltica* OS185***, ***Sh. baltica* OS195*,** *Sh. baltica* OS223, *Sh. denitrificans* OS217, *Sh. frigidimarina* NCIMB 40, ***Sh. loihica* PV-4*, *Sh. pealeana* ATCC 700345***, ***Sh.* sp. ANA-3*, *Sh.* sp. MR-4*, *Sh.* sp. W3-18-1*, *Sh. woodyi* ATCC 51908***
	EFDABC	α	*Agrobacterium tumefaciens* str. C58, *Pseudomonas* sp. G-179, *Rhizobium leguminosarum* bv. trifolii WSM2304, *Rhodobacterales bacterium* Y4I, *Rhodospirillum centenum* SW, *Sinorhizobium fredii* NGR234, *Si. medicae* WSM419, *Si meliloti* 1021, *Starkeya novella*
		γ	*Colwellia psychrerythraea* 34H, *Pseudomonas aeruginosa* (strains LESB58, UCBPP-PA14, PAO1 & PA7), *Reinekea* sp. MED297
	FDABC	γ	*Pantoea sp. At-9b, Photobacterium angustum S14,* ***Ph. profundum strains (3TCK* & SS9*),*** *Psychromonas ingrahamii 37, Serratia odorifera 4Rx13, Ser. proteamaculans 568, Vibrio cholerae str. N16961, V. harveyi ATCC BAA-1116, V. fischeri strains (ES114, MJ11), V. parahemeolyticus RIMD 2210633, V. vulnificus YJ016, Yersinia pestis (5 strains), Y. enterocolitica*
	FDABC_ABC	γ	*Moritella* sp. PE36
	KEFDABC	α	*Rhodobacter sphaeroides* strains (2.4.1 & **ATCC 17025***)

Table A.1 (continued): The *nap* operon gene content and organization in bacteria.

Quinone oxidase	*nap* Operon	Class	Organism
HC	CMADGH	Aquif.	*Thermovibrio ammonificans*
		δ	*Desulfovibrio desulfuricans*, *Desulfovibrio* sp. 3 1 syn3
	DAGHBC	β	*Leptothrix cholodnii*
		γ	*Aggregatibacter aphrophilus, Citrobacter koseri, Cit. rodentium, Escherichia coli* IAI3, *Salmonella typhimurium, Shigella flexneri* (2 strains)
	FDABGHBC	α	*Rhodobacter sphaeroides* ATCC 17025
	FDAGHBC	α	*Dinoroseobacter shibae* DFL 12, *Laribacter hongkongensis*
		β	***Azoarcus sp. BH72****, *Thauera* sp. MZ1T
		γ	*Aeromonas hydrophila, Edwardsiella ictaluri, Ed. tarda, Escherichia coli* (16 strains)*, Grimontia hollisae* CIP 101886, *Haemophilus influenza, Pectobacterium atrosepticum, P. carotovorum* (2 strains), *P. wasabiae, Providencia alcalifaciens, Pro. Rettgeri, Pro. rustigiianii, Pro. Stuartii, Salmonella enterica, Serratia odorifera* DSM 4582*, Shigella boydii* (2 strains), *Sh. dysenteriae*
NA	A	γ	***Photobacterium* sp. SKA34***
		ε	*Helicobacter felis*
	AB	δ	*Sorangium cellulosum*
	DAB	γ	***Shewanella baltica* OS185*, *Sh.baltica* OS195*, *Sh. Piezotolerans* WP3*, *Sh. woodyi* ATCC 51908***
	MA	δ	*Anaeromyxobacter* sp. K, *An. dehalogenans* strains (2CP-1 & 2CP-C)

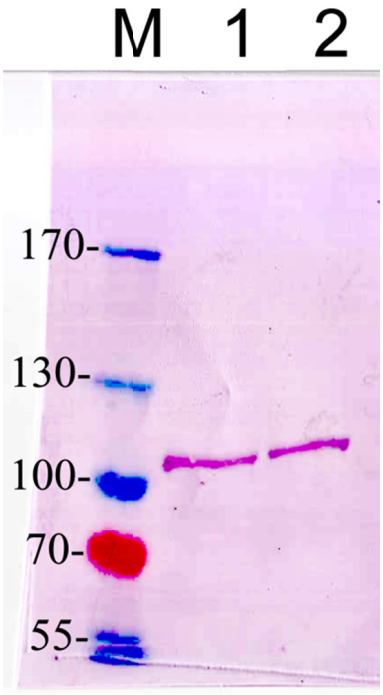

Figure A.1: A western blot of the purified *S. barnesii* NapA protein isolated from *E. coli* strain T7 express during the pilot expression experiments. (*see* **Chapter 3**) Molecular weight marker (**M**), the size (kDa) of each protein band is given in the figure. The purple protein bands are positive for the His_{6x} –tagged proteins. **Lane 1**, the protein purified from T7 express cells incubated for 19 at 30 ^{o}C; **lane 2**, the protein purified from T7 express cells incubated for 44 at 20 ^{o}C A coomassie stained SDS/PAGE fractions of the same samples are shown in **Figure 4.9**. A 10% polyacrylamide gel was used for separation. This western blot was prepared by Katrin Schrader. The ~110 kDa band in lanes 1 and 2 is the His_{6x} –tagged NapA.

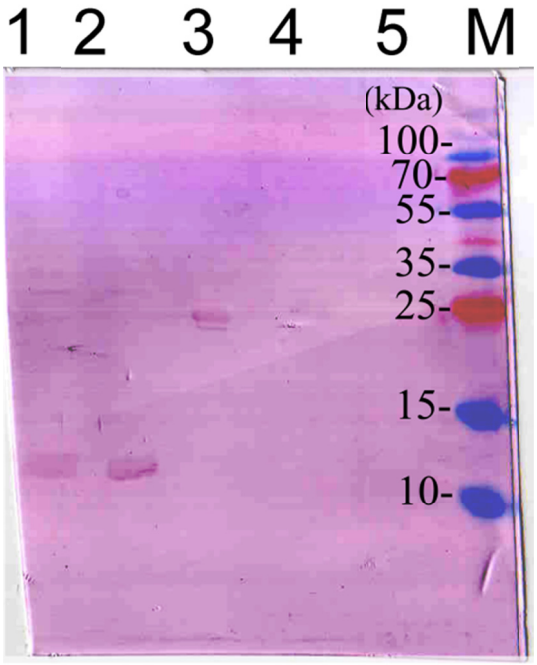

Figure A.2: A western blot of the periplasmic extract from the *C. jejuni* NapB pilot expression experiment. (*see* **Chapter 3**) Molecular weight marker (**M**), the size (kDa) of each protein band is given in the figure. The purple protein bands are positive for the His_{6x} –tagged proteins. **Lane 1**, BL21 star cells incubated for 19 at 30 ^{o}C; **lane 2**, BL21 star cells incubated for 19 at 20 ^{o}C; **lane 3**, a 29 kDa His_{6x} –tagged western blot control ; **lane 4**, BL21 star cells incubated for 44 at 20 ^{o}C; **lane 5**, T7 express cells incubated for 44 at 20 ^{o}C. A coomassie stained SDS/PAGE fractions of the same samples are shown in Figure 6.3.2.2. This western blot was prepared by Katrin Schrader. A 15% polyacrylamide gel was used for separation. The 14 kDa band in lanes 1 and 2 may be the His_{6x} –tagged NapB which is predicted to be ~16.

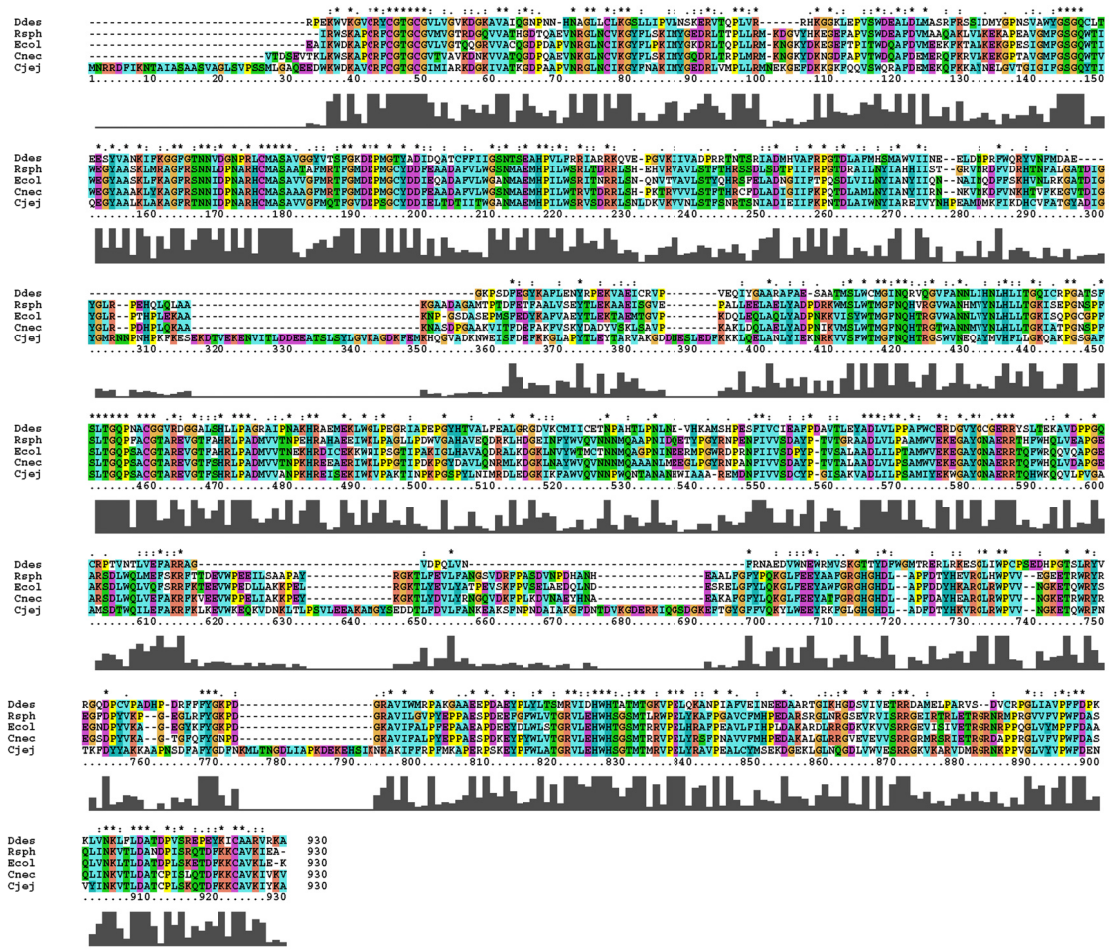

Figure A.3: The multiple sequence alignment of *C. jejuni* NapA (Cjej) with the sequences of the four structurally characterized NapA proteins from *D. desulfuricans* (Ddes), *R. sphaeroides* (Rsph), *E.coli* (Ecol) and *C. necator* (Cnec). This alignment was used to select the best template structure for the *C. jejuni* NapA, and, by providing multiple sequences that have associated structures, strengthening the alignment of the *C. jejuni* sequence inserts. The figure was created using clustal 2.0.11. Identical residues are marked above with an asterisk (*), and similar residues with a period (.) or semicolon (:). The bar graph, below the sequence alignment, illustrates the degree of sequence conservation as a function of residue number.

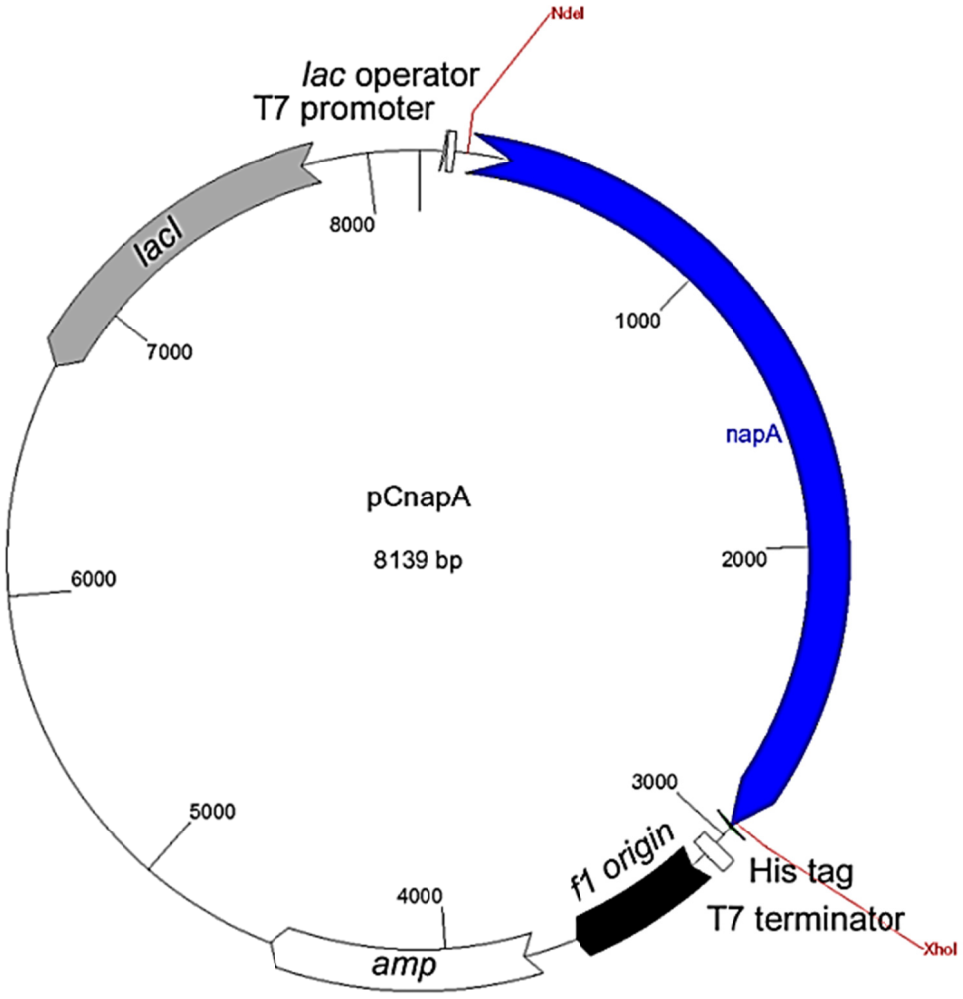

Figure A.4: A plasmid map of the pCnapA vector. The amplified *C. jejuni napA* construct (blue arrow) was digested with the NdeI and XhoI restriction endonucleases and inserted into the pET21α plasmid using the corresponding RE sites (red). The DNA sequence of the *napA* construct and translated protein are in **Figure A.5**. The vector features which are relevant to this study are illustrated: the *lacI* gene (grey arrow), the ampicillin resistance gene (white arrow), the f1 origin (black arrow) hexa-histidine tag (His tag), the T7 terminator, the T7 promoter, and the *lac* operator. The DNA sequences of the plasmid, primers, and *nap* gene were downloaded into the GENtle software program.[190] The *in silico* cloning was conducted to reproduce the experimental procedure used in this study.

.

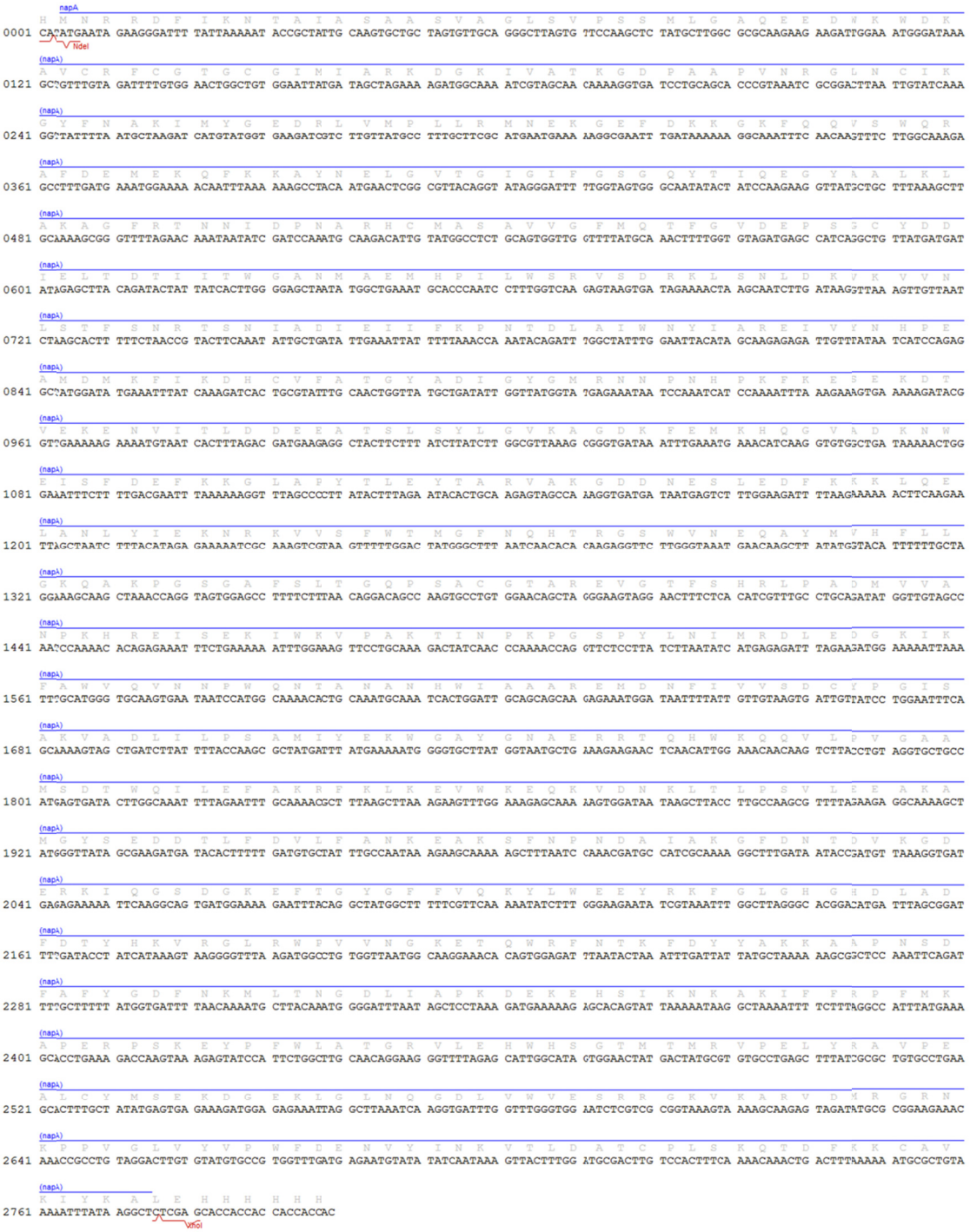

Figure A.5: The DNA and protein sequences of the recombinant *C. jejuni* NapA. The translated protein sequence is provided above the *napA* gene DNA sequence (blue line). The restriction endonuclease sites are indicated in red. GENtle was used to create this illustration.[190]

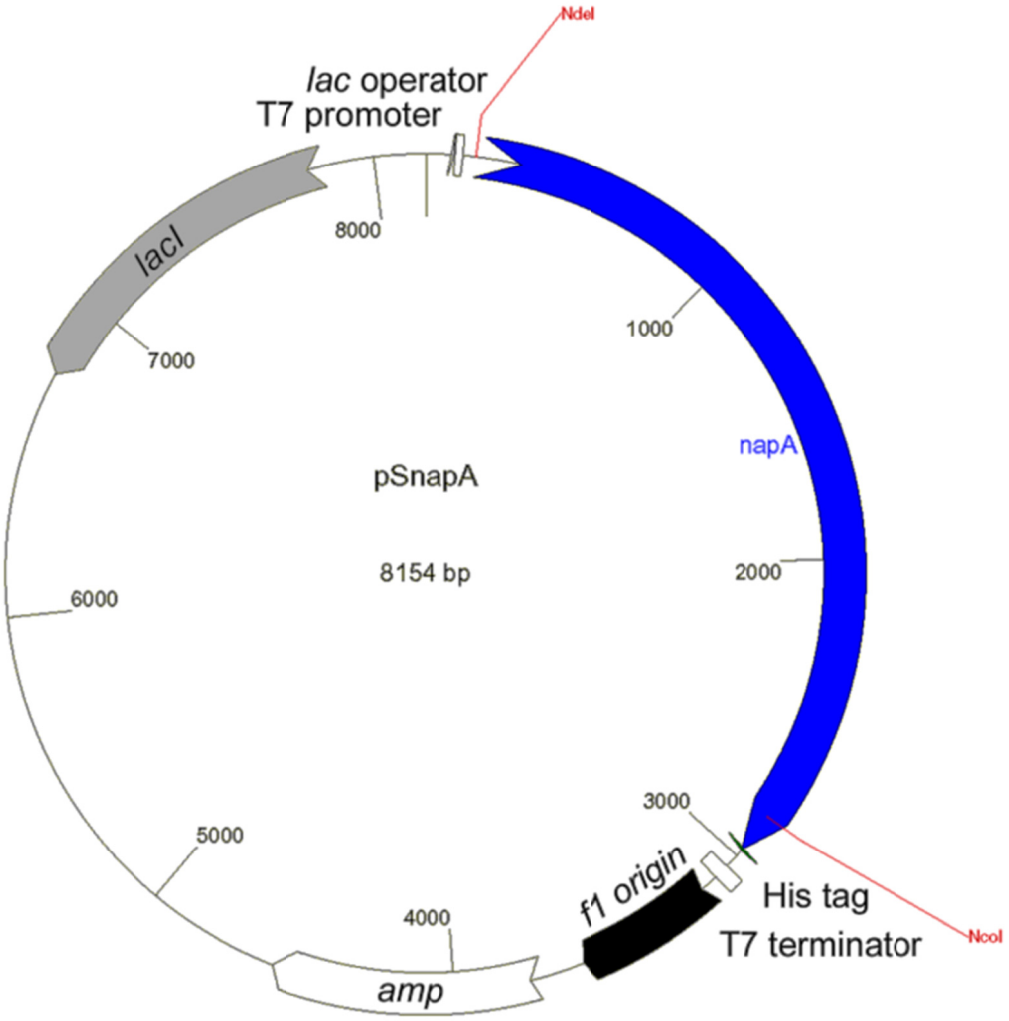

Figure A.6: A plasmid map of the pSnapA vector. The amplified *S. barnesii napA* construct (blue arrow) was digested with the NdeI and XhoI restriction endonucleases and inserted into the pET21α plasmid using the corresponding RE sites (red). The DNA sequence of the *napA* construct and translated protein are in **Figure A.7**. The vector features which are relevant to this study are illustrated: the *lacI* gene (grey arrow), the ampicillin resistance gene (white arrow), the f1 origin (black arrow) hexa-histidine tag (His tag), the T7 terminator, the T7 promoter, and the *lac* operator. The DNA sequences of the plasmid, primers, and *nap* gene were downloaded into the GENtle software program. [190] The *in silico* cloning was conducted to reproduce the experimental procedure used in this study.

Figure A.7: The DNA and protein sequences of the **r**ecombinant *S. barnesii* NapA. The translated protein sequence is provided above the *napA* gene DNA sequence (blue line). The restriction endonuclease sites are indicated in red. GENtle was used to create this illustration. [190] GENtle was used to create this illustration. [190]

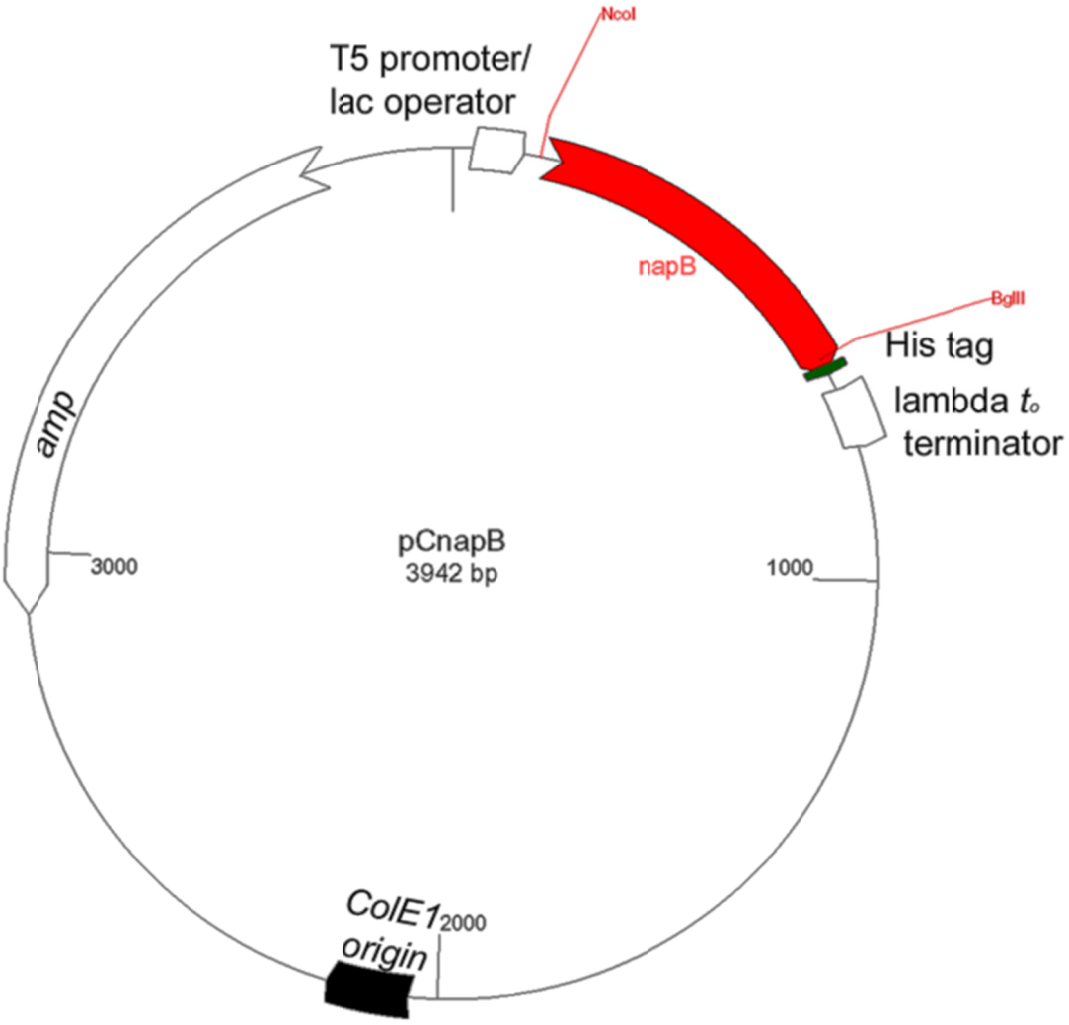

Figure A.8: A plasmid map of the pCnapB vector. The amplified *C. jejuni napB* construct (red arrow) was digested with the NcoI and BglII restriction endonucleases and inserted into the pQE-60 plasmid using the corresponding RE sites (red). The sequence of the *napB* insert is in **Figure A.9**. The vector features which are relevant to this study are illustrated: the ColEI origin (black arrow), the ampicillin resistance gene (white arrow), the T5 promoter/ *lac* operator (white box), hexa-histidine tag (green box), and the lambda t_o terminator. The DNA sequences of the plasmid, primers, and *nap* gene were downloaded into the GENtle software program. [190] The *in silico* cloning was conducted to reproduce the experimental procedure used in this study.

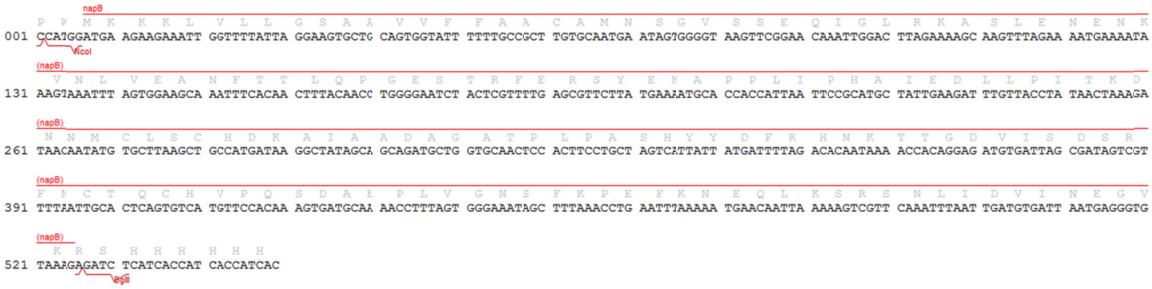

Figure A.9: The DNA and protein sequences of the recombinant *C. jejuni* NapB. The translated protein sequence is provided above the *napB* gene DNA sequence (red line). The restriction endonuclease sites are indicated in red. GENtle was used to create this illustration. [190]

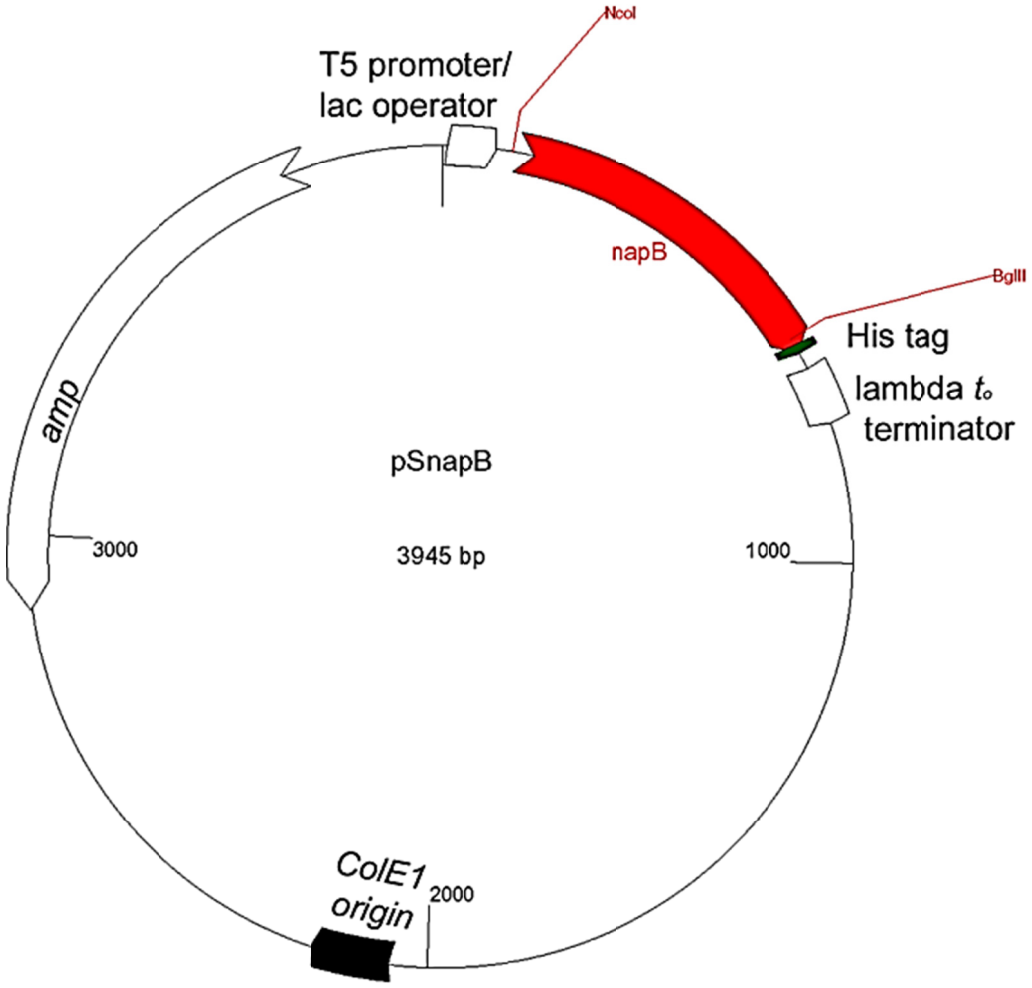

Figure A.10: A plasmid map of the pSnapB vector. The amplified *S. barnesii napB* construct (red arrow) was digested with the NcoI and BglII restriction endonucleases and inserted into the pQE-60 plasmid using the corresponding RE sites (red). The sequence of the *napB* insert is in **Figure A.11**. The vector features which are relevant to this study are illustrated: the ColEI origin (black arrow), the ampicillin resistance gene (white arrow), the T5 promoter/ *lac* operator (white box), hexa-histidine tag (green box), and the lambda t_o terminator. The DNA sequences of the plasmid, primers, and *nap* gene were downloaded into the GENtle software program. [190] The *in silico* cloning was conducted to reproduce the experimental procedure used in this study.

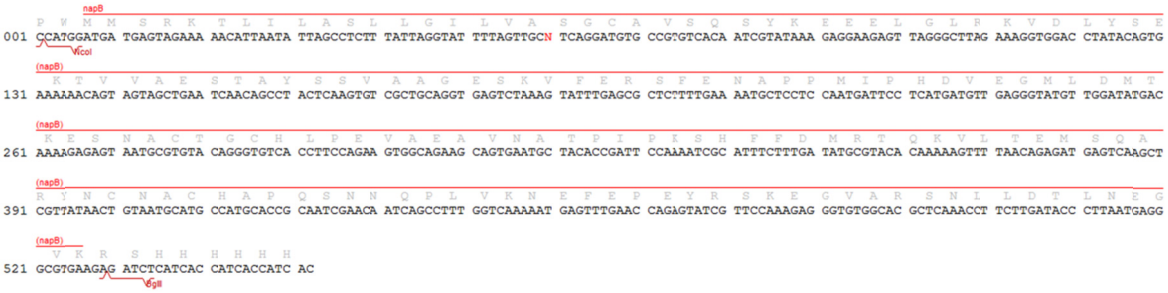

Figure A.11: The DNA and protein sequences of the recombinant *S. barnesii* NapB. The translated protein sequence is provided above the *napB* gene DNA sequence (red line). The restriction endonuclease sites are indicated in red. GENtle was used to create this illustration. [190]

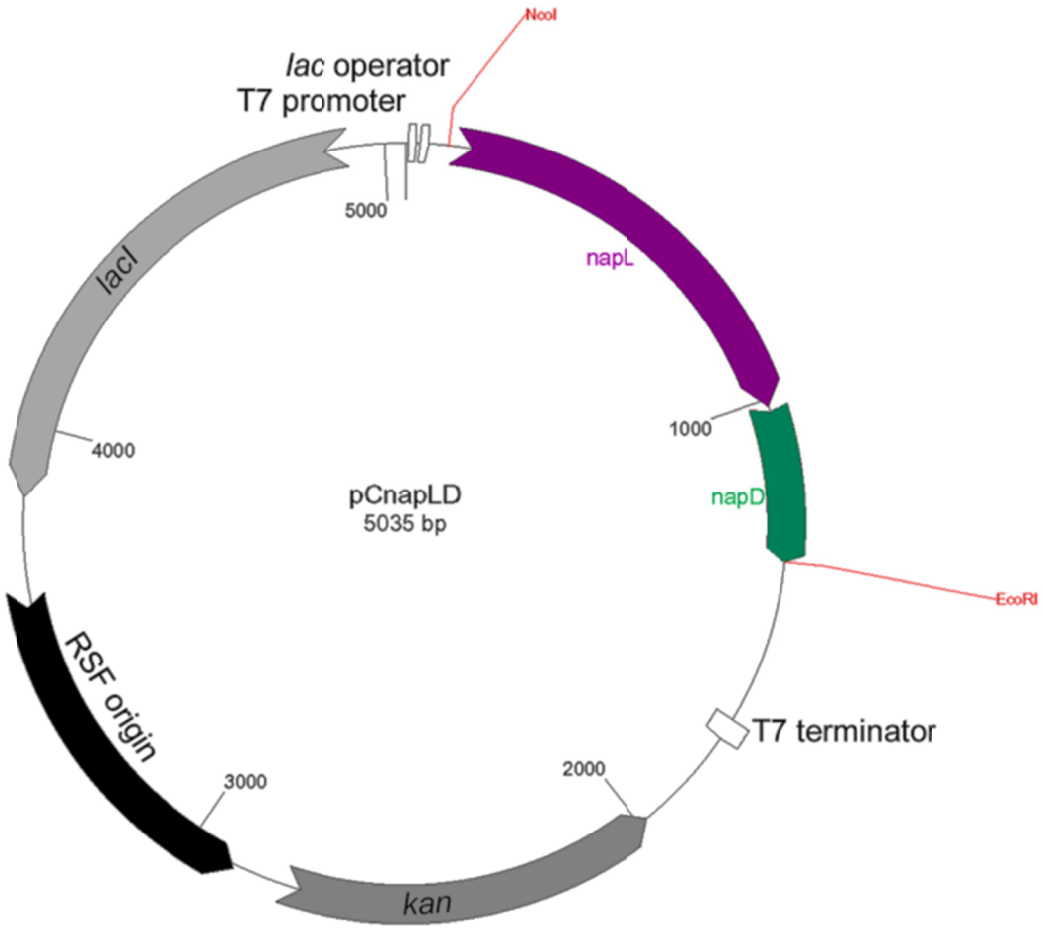

Figure A.12: A plasmid map of pCnapLD. The amplified *C. jejuni napLD* construct (*napL*, purple arrow and *napD*, green arrow) was digested with the NcoI and EcoRI restriction endonucleases and inserted into the RSF-duet plasmid using the corresponding RE sites (red). The sequence of the *napLD* insert is in **Figures A.13 and A.14**. The vector features which are relevant to this study are illustrated: the RSF origin (black arrow), the *lacI* gene (light grey arrow), the kanamycin resistance gene (grey arrow), the T7 promoter/ *lac* operator (white boxes), and the T7 terminator (white rectangle). The DNA sequences of the plasmid, primers, and *nap* gene were downloaded into the GENtle software program. [190] The *in silico* cloning was conducted to reproduce the experimental procedure used in this study.

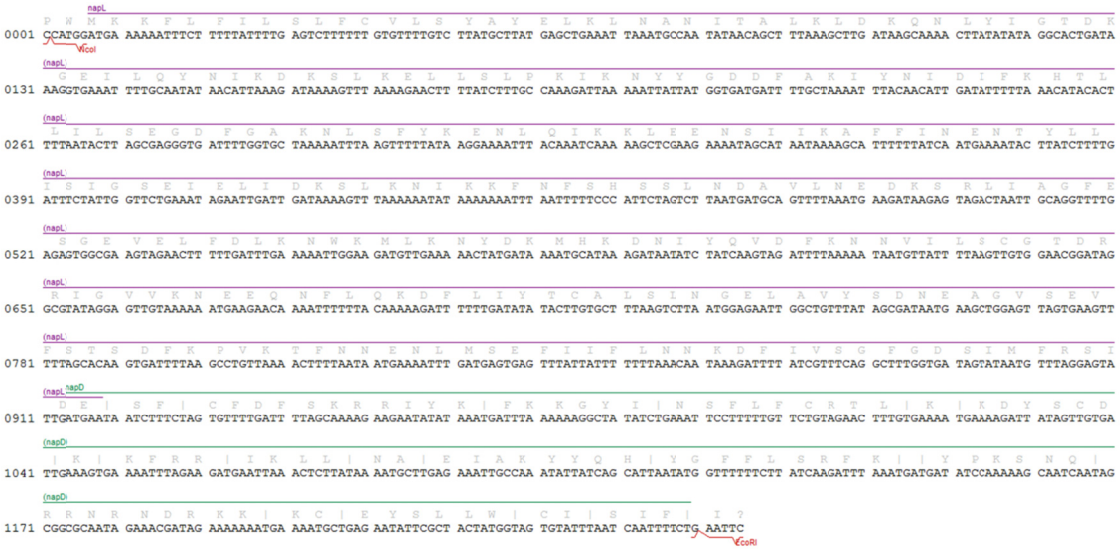

Figure A.13: The DNA sequence of the *C. jejuni napLD* construct and protein sequence of the recombinant *C. jejuni* NapL. The translated protein sequence is provided above the *napL* gene DNA sequence (Purple line). The *napD* gene is indicated also (green line). The restriction endonuclease sites are indicated in red. GENtle was used to create this figure. [190]

Figure A.14: The DNA sequence of the *C. jejuni napLD* construct and protein sequence of the recombinant *C. jejuni* NapD. The translated protein sequence is provided above the *napD* gene DNA sequence (green line). A conserved -10 region (TATAAT) upstream of the *napD* gene (blue line). The *napL* gene is indicated also (purple line). The restriction endonuclease sites are indicated in red. GENtle was used to create this figure. [190]

Appendix II: DNA sequencing data

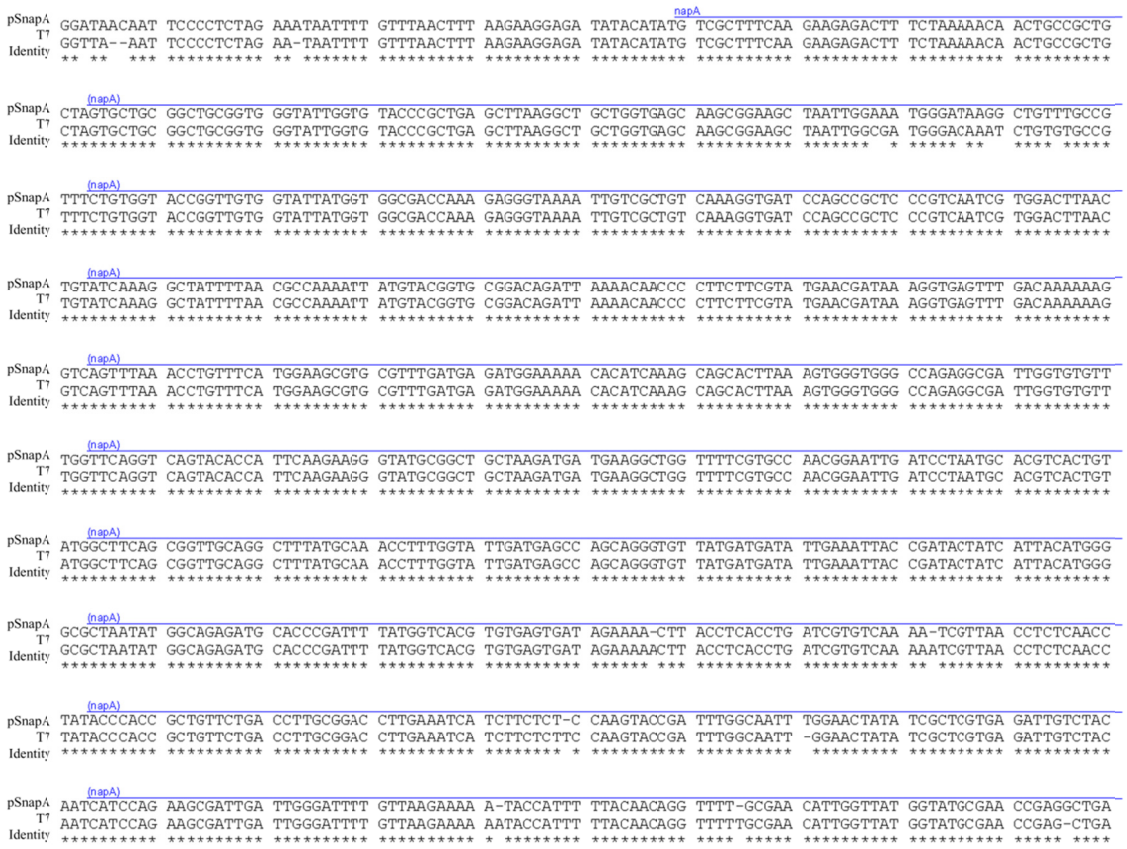

Figure A.15: Alignment of the *S.barnesii napA* gene with the sequencing data obtained from the pSnapA plasmid using the T7 promoter-binding primer. The pET21α T7 promoter-binding primer from Novagen was used for sequencing (**T7**). The sequence of *S.barnesii napA* (blue line) was inserted into the pET21α plasmid (**pSnapA**). Identical residues are indicated below the alignment (*). Gentle was used to align the sequences.

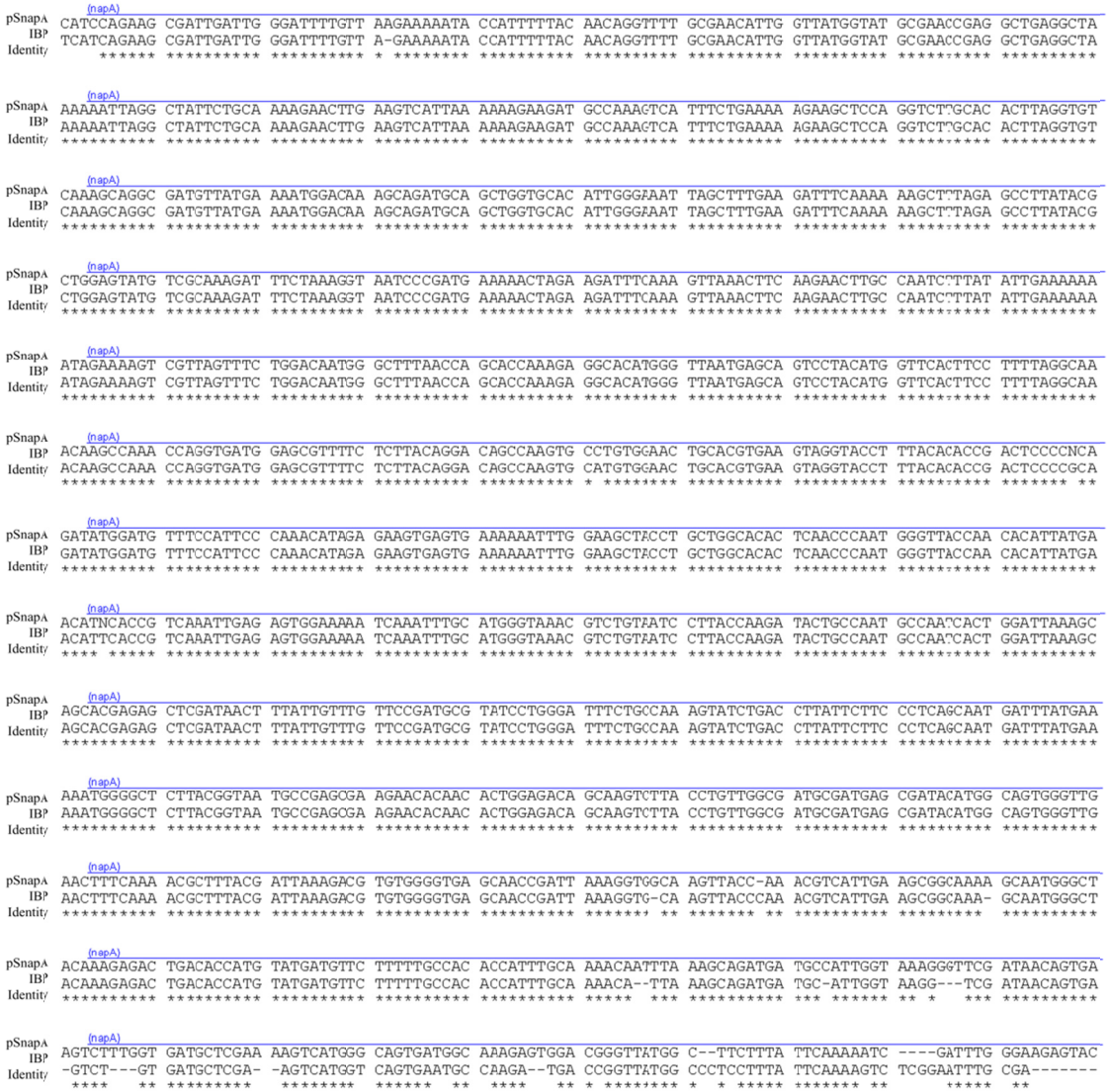

Figure A.16: Alignment of the *S.barnesii napA* gene with the sequencing data obtained from the pSnapA plasmid using the *S. barnesii napA* internal binding primer. The *S. barnesii napA* internal binding primer (**IBP**) was used for sequencing (*see* **Table 3.1** for sequence). The sequence of *S.barnesii napA* (blue line) was inserted into the pET21α plasmid (**pSnapA**). Identical residues are indicated below the alignment (*). Gentle was used to align the sequences.

Figure A.17: Alignment of the *C. jejuni napA* gene with the sequencing data obtained from the pJCnapA plasmid using the pJET 1.2 forward primer. Two colonies were examined (FPa and FPb) the later was used for expression. The pJET 1.2 forward primer from Fermentas was used for sequencing, the data collected is labeled (**FP**).The sequence of *C. jejuni napA* (**pJCnapA**). Identical residues are indicated below the alignment (*). Gentle was used to align the sequences.

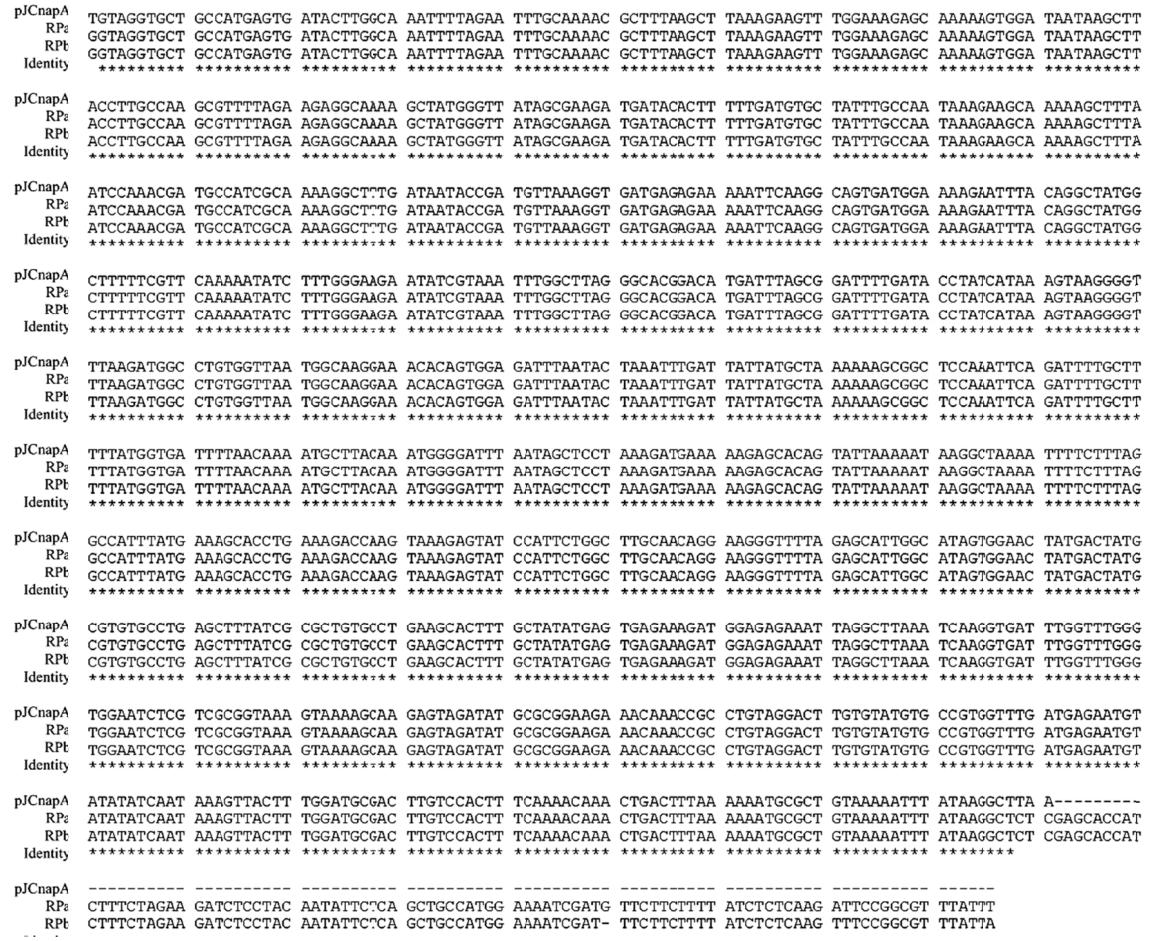

Figure A.18: Alignment of the *C. jejuni napA* gene with the sequencing data obtained from the pJCnapA plasmid using the pJET 1.2 reverse primer. Two colonies were examined (RPa and RPb) the later was used for expression. The pJET 1.2 reverse primer from Fermentas was used for sequencing, the data collected is labeled (**FP**).The sequence of *C. jejuni napA* (**pJCnapA**). Identical residues are indicated below the alignment (*). Gentle was used to align the sequences

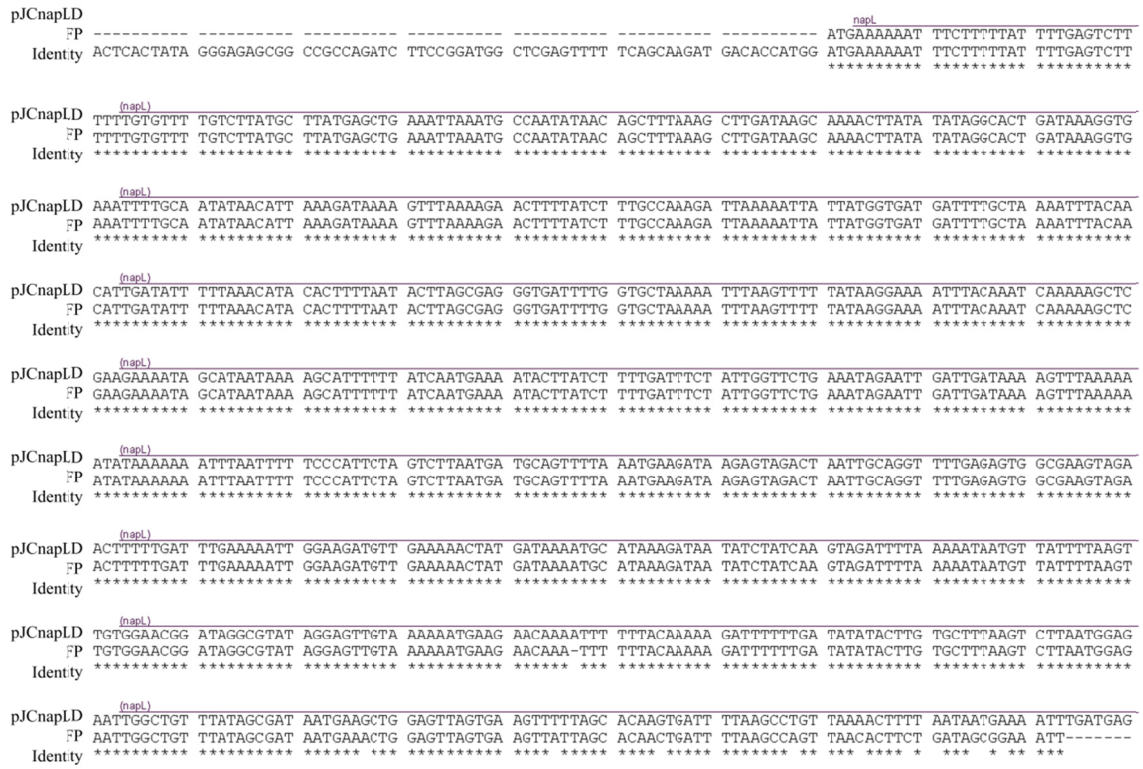

Figure A.19: Alignment of the *C. jejuni napL* gene with the sequencing data from the pJCnapLD plasmid using the pJET 1.2 forward primer. The pJET 1.2 forward primer from Fermentas was used for sequencing, the data collected is labeled (**FP**).The sequence of *C. jejuni napL* (purple line) is labeled (**pJCnapLD**). Identical residues are indicated below the alignment (*). Gentle was used to align the sequences.

Figure A.20: Alignment of the *C. jejuni napB* gene with the sequencing data from the pCnapB plasmid using a pQE-60 sequencing primer. The pQE-60 reverse primer from Qiagen was used for sequencing; the data collected is labeled (**RP**).The sequence of *C. jejuni napB* gene inserted into pQE-60 was used (**pCnapB**). Identical residues are indicated below the alignment (*). Gentle was used to align the sequences.

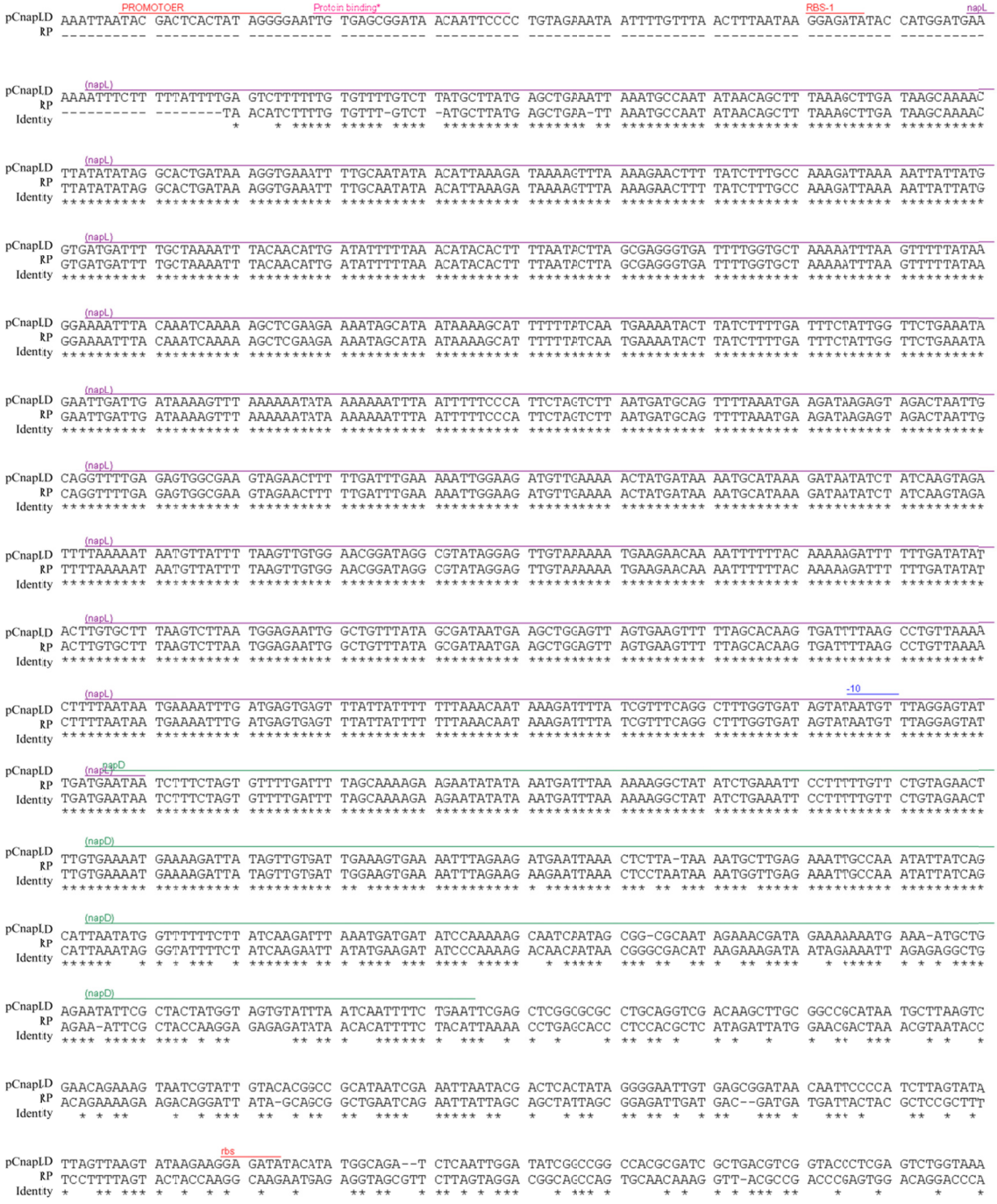

Figure A.21: Alignment of the *C. jejuni napLD* genes with the sequencing data from the pCnapLD plasmid using a pRSF reverse primer. A pRSF reverse primer from Novagen was used for sequencing; the data collected is labeled (**RP**).The sequence of the *C. jejuni napLD* inserted into the pRSF vector (**pCnapLD**). Identical residues are indicated below the alignment (*). Gentle was used to align the sequences.

Figure A.22: Alignment of the *S. barnesii napH* gene with the sequencing data from the pJSnapHBF plasmid using the pJET 1.2 forward primer. The pJET 1.2 forward primer from Fermentas was used for sequencing; the data collected is labeled (**FP**). The sequence of the *S. barnesii napGH* gene was obtained from the primary shotgun sequencing of *S. barnesii's* genome therefore may be error prone. To confirm the sequences, the data was aligned with *S. delyanium* genes in Figure A.24. The sequence data which is not aligned corresponds to a portion of *napB*. Identical residues are indicated below the alignment (*). Gentle was used to align the sequences.

Figure A.23: Alignment of the *S. barnesii napF* gene with the sequencing data from the pJSnapHBF plasmid using the pJET 1.2 reverse primer. The pJET 1.2 reverse primer from Fermentas was used for sequencing; the data collected is labeled (**RP**). The sequence of the *S. barnesii napF* gene was obtained from the primary shotgun sequencing of *S. barnesii's* genome therefore may be error prone. To confirm the sequences, the data was aligned with *S. delyanium* genes in Figure A.25. The sequence data which is not aligned (top) corresponds to *napB*. Identical residues are indicated below the alignment (*). Gentle was used to align the sequences.

Figure A.24: Alignment of the *S. delyanium napHBF* genes with the sequencing data from the pJSnapHBF plasmid using the pJET 1.2 forward primer. The pJET 1.2 forward primer from Fermentas was used for sequencing; the data collected is labeled (**FP**). Identical residues are indicated below the alignment (*). Gentle was used to align the sequences.

```
                     (napH)
S. delyanium napHBF  TTTCAAAAAG CAGTGGAACG ATTGTTTCAG GAGAGTGTAC CAACTGTGGC AGATGTGTTG AGGTGTGTGA GAGTCATGCG CTCTTTTTTG GTGTAAGAAA
                 RP  ---------- ---------- ---------- ---------- ---------- ---------- -GGTGTGTGA GAGTCATGCG CTCTTTTTTG NTGTAAGAAA
           Indentity                                                                    ********* ********** **********  *********

                     (napH)                                     NapB
S. delyanium napHBF  TTACATTAAC ACAAATGTAG GAGAAAAGAA TGATGAGTAG AAAAACATTA ATATTGGTCT CTTTATTAGG TGTCTTGGTG GCTTCAGGAT GTGCGGCGTC
                 RP  TTACNTTAAC ACAAATGTAG GAGAAAAGAA TGATGAGTAG AAAAACATTA ATATTAGCCT CTTTATTAGG TATTTTAGTT GCNTCAGGAT GTGCCGTGTC
           Indentity **** ***** ********** ********** ********** ********** ***** * ** ********** * * ** **  ** ******* **** * ***

                     (NapB)
S. delyanium napHBF  TCAGTCGTAC ACAGAGGAAG AATTAGGGCT TAGAAAAGTG GATCTTTACA GTGAAAAAAC AGTGGTAGCT GAATCAACAG CTTATTCAAC CGTCGCAGCG
                 RP  ACAATCGTAT AAAGAGGAAG AGTTAGGGCT TAGAAAGGTG GACCTATACA GTGAAAAAAC AGTAGTAGCT GAATCAACAG CCTACTCAAG TGTCGCTGCA
           Indentity  ** *****  * ******** * ******** ****** *** ** ** **** ********** *** ****** ********** * ** ****   ***** **

                     (NapB)
S. delyanium napHBF  GGTGAGTCAA AAGTATATGA GCGTGCTTTT GAGAATGCTC CTCCGATGAT TCCTCATGAT GTTGAGGGAA TGCTTGAAAT TAGTAAAGAA AATAACGCAT
                 RP  GGTGAGTCTA AAGTATTTGA GCGCTCTTTT GAAAATGCTC CTCCAATGAT TCCTCATGAT GTTGAGGGTA TGTTGGATAT GACAAAAGAG AGTAATGCGT
           Indentity ******** * ****** *** ***  ***** ** ******* **** ***** ********** ******** * ** * ** **  *  *****  * *** ** *

                     (NapB)
S. delyanium napHBF  GTATCGGTTG TCACCTTCCT GAAGTGGCGG AAGCCGTTAA AGCAACGCCA ATTCCAAAAT CGCATTTTTA TGATATGCGA ACTAAAAAAA TGCTAGGCGA
                 RP  GTACAGGGTG TCACCTTCCA GAAGTGGCAG AAGCAGTGAA TGCTACACCG ATTCCAAAAT CGCATTTCTT TGATATGCGT ACACAAAAAG TTTTAACAGA
           Indentity ***  ** ** *********  ******** * **** ** **  ** ** **  ********** ******* *  *********  **  *****  *  **   **

                     (NapB)
S. delyanium napHBF  ACTAAGTCAA GCACGTTTTA ATTGTAACGC ATGTCATGCG CCACAATCAA ACAACCAGCC ATTGGTTAAA AATGAGTTTT CACCAGAGTA TCGCTCAAAA
                 RP  GATGAGTCAA GCTCGTTATA ACTGTAATGC ATGCCATGCA CCGCAATCGA ACAATCAGCC TTTGGTCAAA AATGAGTTTG AACCAGAGTA TCGTTCCAAA
           Indentity   * ****** ** **** ** * ***** ** *** *****  ** ***** * **** *****  ***** *** *********   ********* *** ** ***

                     (NapB)                                                 napF
S. delyanium napHBF  GAGGGTACTG CACGTTCTAA CCTTCTTGAT ACCCTCAATG AAGGCGTGAA GTAGTCATGC AAACTCGTGG CAGAAGAGAG GTTTTTACCT CTCTTTTTGG
                 RP  GAGGGTGTGG CACGCTCAAA CCTTCTTGAT ACCCTTAATG AGGGCGTGAA GTAGTCATGC AAGAGCGTGG CAGAAGAGAG GTCTTTACCT CTCTTTTTGG
           Indentity ******   * **** ** ** ********** ***** **** * ******** ********** **   ***** ********** ** ******* **********

                     (napF)
S. delyanium napHBF  TAAGAAGGAC GCAGAAAAAA ATCAAGATAA GTTGTGTGTG CGTCCTCCTT ACCACAAAGA GGGGGTTGAT TTTTCAAAGG CATGTCTCTC GTGTCAAGGC
                 RP  TAAGAAGGAC GCAGAAAAAC ATCGTGCAAC ATCTTCTTT- --TACATGTA AGGATTCAGA GGG--CTTAC ATGTAAAAGC TAAAATTGAT ATATTAG---
           Indentity ********** *********  ***  *  *   *  * * *    * *   *  *  *   *** ***   * *   * * ****   *    *     * * *

                     (napF)
S. delyanium napHBF  AATCCGTGTG TAGGAGCCTG TGAAGAGGAG ATTATGGT-C TTAGATGCCA CGAATGTTCC --TTATCTTG ATTTTAGTAA AGGGGGCTGT AC-CTTTTGC
                 RP  --CCTGTATG GCATGGCACC ATAATATGTG TCAGAGTTGT TTGGATGCAT GTGATGTAAG AGCTATTTCG TTTTTAGGGC TGTTTCGTCC ACACATCAAT
           Indentity    * ** **      **      ** * * *      * *   ** *****      ****       *** * *  ******     *     *    ** * *

                     (napF)
S. delyanium napHBF  GAAGCG-TGT GCAAATG-CG TGTGAAGAGA ACGTGCTTAC TCTTACATGT AACGAGACAA AAGCGTTAGA TGTAAAAGTA ACCATTGACG TGTTAGCCTG
                 RP  GAGGCACTGT GCAATGGATG CGATAGGTGC ACAAAGCTGT GTCCTAGTAA TGCAATACAC TTGTATCAAA AGGAGGAGTC ATGA--AGTA TTTGGATCTT
           Indentity ** **  *** ****  *  *  *  * * *  **     *          *        * * ***    *  * * *  * *  ***  *  *       * *    **

                     (napF)
S. delyanium napHBF  CATGGCATGG CATCAAAGTT TGTGTCAAAG TTGCCTAGAT GCGTGTGACG TACGTGCCAT TACGTTTTTA GGACTTTTTC GTCCTCAAAT AAATGCTACA
                 RP  TCTAGAAGAT CTCCTACAAT ATTCTCA--G CTGCCATGGA AAAT-CGATG TTCTT-CTTT TNTTCTCTCA A--------- ---------- ----------
           Indentity   * * *    *  * *   *   * ***  *  ****  *      *  ** * * * * *  * *    * * *
```

Figure A.25: Alignment of the *S. delyanium napHBF* genes with the sequencing data from the pJSnapHBF plasmid using the pJET 1.2 reverse primer. The pJET 1.2 reverse primer from Fermentas was used for sequencing; the data collected is labeled (**RP**). Identical residues are indicated below the alignment (*). Gentle was used to align the sequences.

Appendix III: Protein mass spectroscopy data

Chapter 2 Mass spectroscopy data: Bands were excised from the gel is in **Figure 2.6.** Mass spectroscopy analysis performed by Peter Chovanec. The results are presented below.

SDS-PAGE SAMPLE CES_01

Search title : **CES01**
Database : **NCBInr 20080314 (6307426 sequences; 2155784383 residues)**
Timestamp : **17 Mar 2008 at 16:36:56 GMT**
Top Score : **84 for gi|169104652, periplasmic nitrate reductase[Sulfurospirillum barnesii]**

Probability Based Mowse Score
Protein score is -10*Log(P), where P is the probability that the observed match is a random event. Protein scores greater than 81 are significant (p<0.05).

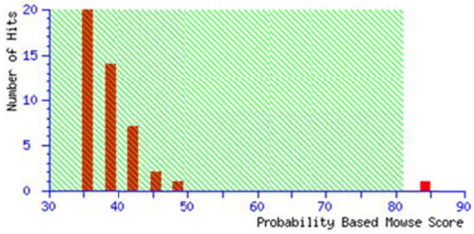

gi|169104652 **Mass:** 105393 **Score:** 84 **Expect:** 0.024 **Queries matched:** 31
periplasmic nitrate reductase [Sulfurospirillum barnesii]

Nominal mass (M_r): **105393**; Calculated pI value: **8.77**
Fixed modifications: Carbamidomethyl (C)
Variable modifications: Oxidation (M)
Cleavage by Trypsin: cuts C-term side of KR unless next residue is P
Number of mass values searched: **134**
Number of mass values matched: **31**
Sequence Coverage: **34%**
Matched peptides shown in **Bold Red**

```
   1 MSLSRRDFLK TTAAASAAAA VGIGVPAELK AAGEQAEANW KWDKAVCRFC
  51 GTGCGIMVAT KEGKIVAVKG DPAAPVNRGL NCIKGYFNAK IMYGADRLKQ
 101 PLLRMNDKGE FDKKGQFKPV SWKRAFDEME KHIKAALKVG GPEAIGVFGS
 151 GQYTIQEGYA AAKMMKAGFR ANGIDPNARH CMASAVAGFM QTFGIDEPAG
 201 CYDDIEITDT IITWGANMAE MHPILWSRVS DRKLTSPDRV KIVNLSTYTH
 251 RCSDLADLEI IFSPSTDLAI WNYIAREIVY NHPEAIDWDF VKKNTIFTTG
 301 FANIGYGMRT EAEAKKLGYS AKELEVIKKE DAKVISEKEA PGLAHLGVKA
 351 GDVMKMDKAD AAGAHWEISF EDFKKALEPY TLEYVAKISK GNPDEKLEDF
 401 KVKLQELANL YIEKNRKVVS FWTMGFNQHQ RGTWVNEQSY MVHFLLGKQA
 451 KPGDGAFSLT GQPSACGTAR EVGTFTHRLP XDMDVSIPKH REVSEKIWKL
 501 PAGTLNPMGY QHIMNXHRQI ESGKIKFAWV NVCNPYQDTA NANHWIKAAR
 551 ELDNFIVCSD AYPGISAKVS DLILPSAMIY EKWGSYGNAE RRTQHWRQQV
 601 LPVGDAMSDT WQWVELSKRF TIKDVWGEQP IKGGKLPNVI EAAKAMGYKE
 651 TDTMYDVLFA TPFAKQFKAD DAIGKGFDNS EVFGDARKVM GSDGKEWTGY
 701 GFFIQKSIWE EYRQFGLGHG HDLADFDTYH KVRGLKWPVV DGKETQWRFN
 751 AKYDPYAAKA GNGDFAFYGD FAKALKKGNL VKFTTEETYS LKNKAKIFFR
 801 PYMDPCEMPD REYDTWLCTG RVLEHWHSGT MTMRVPELYR AVPEALCYMH
 851 PEDAKAKGFK QGDMIWLESR RGSCKARVET RGRNRTPRGL VFVPWFDEKV
 901 MINKVCLDAT CPISKQTDYK KCAVKLYKA
```

SDS-PAGE SAMPLE CES_02

Search title : **CES02**
Database : **NCBInr 20080314 (6307426 sequences; 2155784383 residues)**
Taxonomy : **Proteobacteria (purple bacteria) (1856845 sequences)**
Timestamp : **17 Mar 2008 at 16:43:11 GMT**
Top Score : **79 for gi|23394982, metalloid reductase RarA [Sulfurospirillum barnesii]**

Probability Based Mowse Score
Protein score is -10*Log(P), where P is the probability that the observed match is a random event. Protein scores greater than 75 are significant (p<0.05).

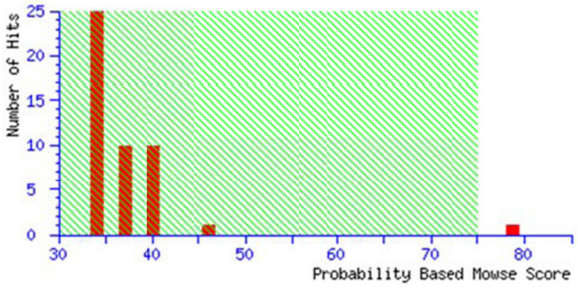

gi|23394982 **Mass:** 48133 **Score:** 79 **Expect:** 0.024 **Queries matched:** 12
metalloid reductase RarA [Sulfurospirillum barnesii]

Nominal mass (M_r): **48133**; Calculated pI value: **5.49**
Fixed modifications: Carbamidomethyl (C)
Variable modifications: Oxidation (M)
Cleavage by Trypsin: cuts C-term side of KR unless next residue is P
Number of mass values searched: **63**
Number of mass values matched: **12**
Sequence Coverage: **34%**

Matched peptides shown in **Bold Red**

```
    1 MKLAKLSLAA MIVAGLASSS FAADTLADAF KNGKVSGEIK AWYFDKTVEN
   51 TDAAKDKENN ANIANFGLTL GFVTDSLYGF YAGATFQGSA TPFIDNDAEG
  101 KNTAKDGKAD TANFGTTNAA SGAVLSEAYL GYKLGKTDVK VGRQFISTPL
  151 VNGSGSRFFK ESFEGAVLVN TDLPQTTVFA GYAGKFQGRT SAVSGDGLGD
  201 APSFHKKAVY AGLKNALTGK SATDYTSRDG GYTAGAINKS ISNLTLTGQY
  251 LFVDNAHDTD GVDVYYTEAN YVLPMSGFKL GFDATFRGSH TRDDLDALNA
  301 SGHMFSGRVS LSGLAGFGAS FAAATTSSDH VLLGAGNGPT TYTATMIAGA
  351 ATPTAAANTD SYLFQVTYDF SKVGVAGLTA VAQYGWTEQG TQPKLDLETG
  401 NSSKVKGTDR TTYAAGVTYA VPALKGLTTS LQYEVQEADS KTAGTKTVDT
  451 DEMWFKASYK F
```

SAMPLE CS_02

Search title : sample_CS1
Database : NCBInr 20080221 (6122577 sequences; 2096230148 residues)
Timestamp : 29 Feb 2008 at 19:21:29 GMT
Top Score : 92 for gi|22651592, periplasmic nitrate reductase [Sulfurospirillum barnesii]

Probability Based Mowse Score

Protein score is -10*Log(P), where P is the probability that the observed match is a random event.
Protein scores greater than 80 are significant (p<0.05).

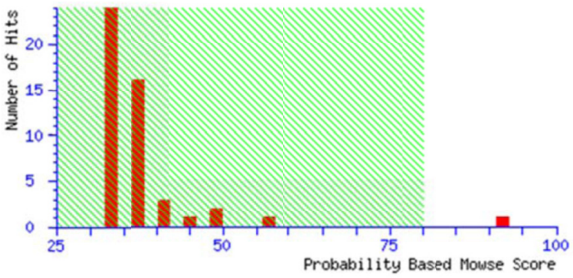

gi|22651592 Mass: **99749** Score: 92 Expect: **0.0039** Queries matched: **34**

periplasmic nitrate reductase [*Sulfurospirillum barnesii*]

Nominal mass (M_r): **99749**; Calculated pI value: **8.67**
NCBI BLAST search of gi|22651592 against nr
Unformatted sequence string for pasting into other applications
Taxonomy: Sulfurospirillum barnesii
Fixed modifications: Carbamidomethyl (C)
Variable modifications: Oxidation (M)
Cleavage by Trypsin: cuts C-term side of KR unless next residue is P
Number of mass values searched: **137**
Number of mass values matched: **34**
Sequence Coverage: **36%**

Matched peptides shown in **Bold Red**

```
   1 WKWDKAVCRF CGTGCGIMVA TKEGKIVAVK GDPAAPVNRG LNCIKGYFNA
  51 KIMYGADRLK QPLLRMNDKG EFDKKGQFKP VSWKRAFDEM EKHIKAALKV
 101 GGPEAIGVFG SGQYTIQEGY AAAKMMKAGF RANGIDPNAR HCMASAVAGF
 151 MQTFGIDEPA GCYDDIEITD TIITWGANMA EMHPILWSRV SDRKLTSPDR
 201 VKIVNLSTYT HRCSDLADLE IIFSPSTDLA IWNYIAREIV YNHPEAIDWD
 251 FVKKNTIFTT GFANIGYGMR TEAEAKKLGY SAKEIEVIKK EDAKVISEKE
 301 APGLAHLGVK AGDVMKMDKA DAAGAHWEIS FEDFKKALEP YTLEYVAKIS
 351 KGNPDEKLED FKVKLQELAN LYIEKNRKVV SFWTMGFNQH QRGTWVNEQS
 401 YMVHFLLGKQ AKPGDGAFSL TGQPSACGTA REVGTFTHRL PXDMDVSIPK
 451 HREVSEKIWK LPAGTLNPMG YQHIMNXHRQ IESGKIKFAW VNVCNPYQDT
 501 ANANHWIKAA RELDNFIVCS DAYPGISAKV SDLILPSAMI YEKWGSYGNA
 551 ERRTQHWRQQ VLPVGDAMSD TWQWVELSKR FTIKLVWGEQ PIKGGKLPNV
 601 IEAAKAMGYK ETDTMYDVLF ATPFAKQFKA DDAICKGFDN SEVFGDARKV
 651 MGSDGKEWTG YGFFIQKSIW EEYRQFGLGH GHDLADFDTY HKVRGLKWPV
 701 VDGKETQWRF NAKYDPYAAK AGNGDFAFYG DFAKALKKGN LVKPTTEETY
 751 SLKNKAKIFF RFYMDPCEMP DREYDTWLCT GRVLEHWHSG TMTMRVPELY
 801 RAVPEALCYM HPEDAKAKGF KQGDMIWLES RRGSCKARVE TRGRNRTPRG
 851 LVFVPWFDEK VMINKVCLDA TCRF
```

Chapter 3 Mass spectroscopy data:

Bruker MS analysis of the protein isolated in the *S. barnesii* NapA pilot expression and purification study.

Detailed Protein Report

Project Info

Name:	ZBA LCMS 2009	**Date:**	Thursday, February 5, 2009
Note:			

Search Result Info

Name: HCT_bacteria_Mascot_2009-09-08 15:54:09

Protein 1: **periplasmic nitrate reductase [Sulfurospirillum barnesii]**

Accession:	gi|169104652	**Score:**	2627.58
Database:	NCBInr(NCBInr_20090531.fasta)	**MW:**	104.43 kDa
Database Date:	2009-06-10	**pI:**	9.45
Modification(s):	Carbamidomethyl, Oxidation	**Sequence Coverage:**	58.88 %
		No. of unique Peptides:	68

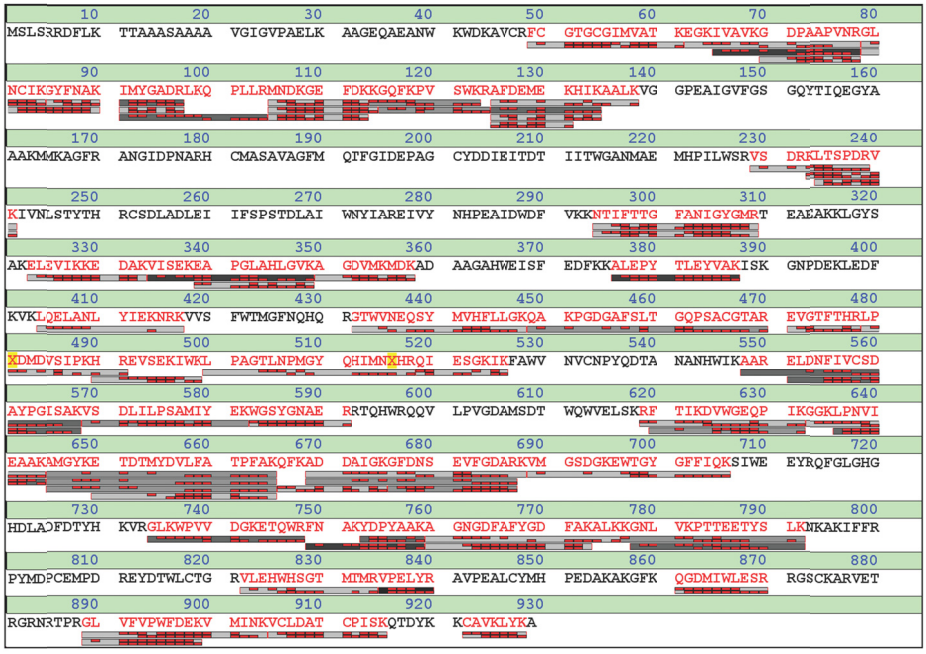

Detailed Protein Report

Cmpd.	No. of Cmpds.	m/z meas.	Δ m/z [ppm]	z	Rt [min]	Score	P	Range	Sequence	Modification
313	1	701.2300	-128.056	2	13.60	73.90	0	49-61	R.PCGTGCGIMVATK.E	Carbamidomethyl: 2, 6
219	1	574.2400	-153.801	3	10.20	21.60	2	62-78	K.EGKIVAVKGDPAAPVNR.G	
226	1	469.5400	-146.205	3	10.70	32.33	1	65-78	K.IVAVKGDPAAPVNR.G	
165	1	448.6800	-117.812	2	8.00	40.09	0	70-78	K.GDPAAPVNR.G	
187	1	352.6500	-118.018	2	9.00	28.42	0	79-84	R.GLNCIK.G	Carbamidomethyl: 4
334	1	692.7600	-138.166	2	14.40	42.53	1	79-90	R.GLNCIKGYFNAK.I	Carbamidomethyl: 4
227	1	350.1500	-76.144	2	10.60	24.60	0	85-90	K.GYFNAK.I	
181	1	421.1400	-135.971	2	8.70	29.01	0	91-97	K.IMYGADR.L	Oxidation: 2
210	1	413.1600	-96.353	2	9.90	23.11	0	91-97	K.IMYGADR.L	
323	1	558.6000	-99.352	3	13.90	30.34	2	91-104	K.IMYGADRLKQPLLR.M	
169	1	542.1700	-133.531	2	8.20	49.06	1	105-113	R.MNDKGEFDK.K	
110	1	550.1900	-90.622	2	5.80	33.80	1	105-113	R.MNDKGEFDK.K	Oxidation: 1
122	1	606.2200	-115.271	2	6.40	41.56	2	105-114	R.MNDKGEFDKK.G	
239	1	402.1800	-131.149	3	10.90	30.91	2	114-123	K.KGQFKPVSWK.R	
245	1	411.5300	-92.658	3	11.20	22.09	2	115-124	K.GQFKPVSWKR.A	
161	1	443.1700	-37.385	2	7.80	22.76	0	125-131	R.AFDEMEK.H	Oxidation: 5
243	1	416.5000	-98.78	3	11.00	31.18	1	125-134	R.AFDEMEKHIK.A	
171	1	632.2200	-135.28	2	8.20	21.99	1	125-134	R.AFDEMEKHIK.A	Oxidation: 5
344	1	544.2500	-77.588	3	14.90	24.17	2	125-138	R.AFDEMEKHIKAALK.V	
138	1	425.1900	-102.251	3	6.90	34.35	2	229-239	R.VSDRKLTSPDR.V	
2	1	522.2300	-160.867	2	0.00	44.05	2	233-241	R.KLTSPDRVK.I	
141	1	458.2100	-123.382	2	7.00	29.34	1	234-241	K.LTSPDRVK.I	
476	1	881.8100	-139.122	2	19.40	82.14	0	294-309	K.NTIFTTGFANGYGMR.T	
440	1	889.8400	-101.304	2	18.10	64.77	0	294-309	K.NTIFTTGFANGYGMR.T	Oxidation: 15
197	1	651.2700	-152.283	2	9.50	32.63	2	323-333	K.ELEVIKKEDAK.V	
292	1	549.9200	-119.53	3	12.80	50.29	1	334-349	K.VISEKEAPGLAHLGVK.A	
280	1	546.2600	-98.887	2	12.30	56.44	0	339-349	K.EAPGLAHLGVK.A	
185	1	497.6700	-137.512	2	8.90	68.00	1	350-358	K.AGDVMKMDK.A	
386	1	698.8000	-102.405	2	16.20	67.51	0	376-387	K.ALEPYTLEYAK.I	
316	1	433.7100	-90.504	4	13.60	20.70	2	404-417	K.LQELANLYIEKNRK.V	
529	1	1004.9100	-90.657	2	21.20	65.37	0	432-448	R.GTWVNEQSYMVHFLLGK.Q	
293	1	726.2700	-112.408	3	12.90	55.51	1	449-470	K.QAKPGDGAFSLTGQPSACGTAR.E	Carbamidomethyl: 18
178	1	473.6600	-170.327	2	8.50	48.12	0	471-478	R.EWGTFTHR.L	
291	1	493.5500	-96.544	3	12.80	34.37	1	479-491	R.LPADMDVSIPKHR.E	
191	1	437.8500	-138.041	3	9.20	30.41	2	490-499	K.HREVSEKMVK.L	
377	1	721.6300	-101.409	3	16.00	42.95	0	500-518	K.LPAGTLNPMGYQHIMNIHR.Q	
104	1	451.7100	-130.414	2	5.40	23.67	1	519-526	R.QIESGKIK.F	
399	1	766.2900	-116.396	3	16.60	53.38	1	548-568	K.AARELDNFMCSDAYPGISAK.V	Carbamidomethyl: 11
433	1	999.8700	-107.5	2	17.90	54.59	0	551-568	R.ELDNFMCSDAYPGISAK.V	Carbamidomethyl: 8
456	1	789.8500	-96.233	2	18.60	61.29	0	569-582	K.VSDLLPSAMYEK.W	
242	1	520.1600	-140.764	2	11.00	53.77	0	583-591	K.WGSYGNAER.R	
367	1	572.9100	-132.475	3	15.60	33.33	2	619-632	K.RFTIKDVWGEQPIK.G	
408	1	520.8900	-119.402	3	17.00	25.81	1	620-632	R.FTIKDVWGEQPIK.G	
284	1	399.5300	-103.696	3	12.50	30.41	1	633-644	K.GGKLPNVIEAAK.A	
308	1	477.7400	-93.279	2	13.40	53.07	0	636-644	K.LPNVIEAAK.A	
514	1	800.2900	-114.252	3	20.70	21.99	1	645-665	K.AMGYKETDTMYDVLFATPFAK.Q	

Cmpd.	No. of Cmpds.	m/z meas.	Δ m/z [ppm]	z	Rt [min]	Score	P	Range	Sequence	Modification
457	1	805.6200	-115.529	3	18.60	23.91	1	645-665	K.AMGYKETDTMYDVLFATPFAK.Q	Oxidation: 10
442	1	810.9500	-116.79	3	18.20	34.31	1	645-665	K.AMGYKETDTMYDVLFATPFAK.Q	Oxidation: 2, 10
557	1	924.8300	-118.767	2	22.00	60.47	0	650-665	K.ETDTMYDVLFATPFAK.Q	
217	1	546.7200	-124.067	2	10.10	43.87	1	666-675	K.QFKADDAIGK.G	
354	1	661.8800	-140.402	3	15.20	28.31	1	669-687	K.ADDAIGKGFDNSEVFGDAR.K	
329	1	704.5900	-115.321	3	14.20	33.99	2	669-688	K.ADDAIGKGFDNSEVFGDARK.V	
337	1	657.1800	-169.595	2	14.50	71.67	0	676-687	K.GFDNSEVFGDAR.K	
426	1	683.9400	-82.08	3	17.80	30.91	1	689-706	K.VMGSDGKEWTGYGFFIQKS	
355	1	600.2700	-91.302	3	15.20	30.33	2	734-748	R.GLKWPVVDGKETQWR.F	
255	1	429.8300	-125.124	3	11.60	42.18	1	749-759	R.FNAKYDPYAAK.A	
196	1	414.1700	-73.24	2	9.40	22.52	0	753-759	K.YDPYAAK.A	
419	2	740.2400	-122.376	2	17.30	95.67	0	760-773	K.AGNGDFAFYGDFAK.A	
451	1	597.8900	-119.637	3	18.40	30.61	1	760-776	K.AGNGDFAFYGDFAKALK.K	
260	1	603.2500	-135.116	3	11.40	26.86	2	777-792	K.KGNLVKPTTEETYSLK.N	
285	1	560.5500	-148.401	3	12.50	37.79	1	778-792	K.GNLVKPTTEETYSLK.N	
275	1	528.8500	-129.529	3	12.20	26.28	0	822-834	R.VLEHWHSGTMTMR.V	
264	1	388.6700	-125.273	2	11.90	38.35	0	835-840	R.VPELYR.A	
398	1	617.7100	-142.247	2	16.60	63.89	0	861-870	K.QGDMWLESR.R	
534	1	668.7600	-135.215	2	21.30	56.53	0	889-899	R.GLVPVPWFDEK.V	
510	1	961.4000	-120.502	2	20.60	46.06	1	889-904	R.GLVPVPWFDEKVMINK.V	
290	1	632.2300	-122.13	2	12.70	62.21	0	905-915	K.VCLDATCPISK.Q	Carbamidomethyl: 2,7
201	1	441.2000	-111.742	2	9.60	38.53	1	922-928	K.CAVKLYK.A	Carbamidomethyl: 1

Mass spectrometry analysis report identifying *S. barnesii* NapA, which isolated from *E. coli* T7 express. A) Coverage map, B) peptide list. See the recombinant *S. barnesii* NapA pilot expression and purification protocol in Chapter 3. After SDS-PAGE separation, the NapA band was extracted from the gel, and then sent for analysis (Bruker Corporation, Germany). The only significant hit was periplasmic nitrate reductase (NapA) from *S. barnesii* with 59% sequence coverage

Mass spectroscopy analysis and identification of NapA and NapD. Four samples were extracted from the SDS/PAGE gel below (*see* **Figure 3.12**) numbered 1-4. The MS data collected for these samples is provided below. Mass spectroscopy analysis performed by Peter Chovanec.

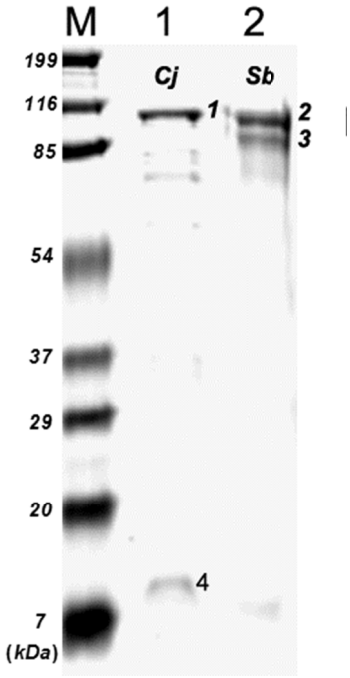

Sample 1

Match to: **gi|57237625** Score: **1217**
nitrate reductase [Campylobacter jejuni RM1221]
Found in search of C:\Documents and Settings\Administrator\Desktop\CS11269.mgf

Nominal mass (M_r): **105561;** Calculated pI value: **8.76**
NCBI BLAST search of gi|57237625 against nr
Unformatted sequence string for pasting into other applications

Taxonomy: Campylobacter jejuni RM1221
Fixed modifications: Carbamidomethyl (C)
Variable modifications: Oxidation (M)
Cleavage by Trypsin: cuts C-term side of KR unless next residue is P
Sequence Coverage: **45%**

Matched peptides shown in **Bold Red**

```
   1 MNRRDFIKNT AIASAASVAG LSVPSSMLGA QEEDWKWDKA VCRFCGTGCG
  51 IMIARKDGKI VATKGDPAAP VNRGLNCIKG YFNAKIMYGE DRLVMPLLRM
 101 NEKGEFDKKG KFQQVSWQRA FDEMEKQFKK AYNELGVTGI GIFGSGQYTI
 151 QEGYAALKLA KAGFRTNNID PNARHCMASA VVGFMQTFGV DEPSGCYDDI
 201 ELTDTIITWG ANMAEMHPIL WSRVSDRKLS NLDKVKVVNL STFSNRTSNI
 251 ADIEIIFKPN TDLAIWNYIA REIVYNHPEA MDMKFIKDHC VFATGYADIG
 301 YGMRNNPNHP KFKESEKDTV EKENVITLDD EEATSLSYLG VKAGDKFEMK
 351 HQGVADKNWE ISFDEFKKGL APYTLEYTAR VAKGDDNESL EDFKKKLQEL
 401 ANLYIEKNRK VVSFWTMGFN QHTRGSWVNE QAYMVHFLLG KQAKPGSGAF
 451 SLTGQPSACG TAREVGTFSH RLPADMVVAN PKHREISEKI WKVPAKTINP
 501 KPGSPYLNIM RDLEDGKIKF AWVQVNNPWQ NTANANHWIA AAREMDNFIV
 551 VSDCYPGISA KVADLILPSA MIYEKWGAYG NAERRTQHWK QQVLPVGAAM
 601 SDTWQILEFA KRFKLKEVWK EQKVDNKLTL PSVLEEAKAM GYSEDDTLFD
 651 VLFANKEAKS FNPNDAIAKG FDNTDVKGDE RKIQGSDGKE FTGYGFFVQK
 701 YLWEEYRKFG LGHGHDLADF DTYHKVRGLR WPVVNGKETQ WRFNTKFDYY
 751 AKKAAPNSDF AFYGDFNKML TNGDLIAPKD EKEHSIKNKA KIFFRPFMKA
 801 PERPSKEYPF WLATGRVLEH WHSGTMTMRV PELYRAVPEA LCYMSEKDGE
 851 KLGLNQGDLV WVESRRGKVK ARVDMRGRNK PPVGLVYVPW FDENVYINKV
 901 TLDATCPLSK QTDFKKCAVK IYKA
```

Sample 2

Match to: **gi|169104652** Score: **1367**
periplasmic nitrate reductase [Sulfurospirillum barnesii]
Found in search of C:\Documents and
Settings\Administrator\Desktop\CS21269.mgf

Nominal mass (M_r): **105393;** Calculated pI value: **8.77**
NCBI BLAST search of gi|169104652 against nr
Unformatted sequence string for pasting into other applications

Taxonomy: Sulfurospirillum barnesii

Fixed modifications: Carbanidomethyl (C)
Variable modifications: Oxidation (M)
Cleavage by Trypsin: cuts C-term side of KR unless next residue is P
Sequence Coverage: **49%**

Matched peptides shown in **Bold Red**

```
   1 MSLSRRDFLK TTAAASAAAA VGIGVPAELK AAGEQAEANW KWDKAVCRFC
  51 GTGCGIMVAT KEGKIVAVKG DPAAPVNRGL NCIKGYFNAK IMYGADRLKQ
 101 PLLRMNDKGE FDKKGQFKPV SWKRAFDEME KHIKAALKVG GPEAIGVFGS
 151 GQYTIQEGYA AAKMMKAGFR ANGIDPNARH CMASAVAGFM QTFGIDEPAG
 201 CYDDIEITDT IITWGANMAE MHPILWSRVS DRKLTSPDRV KIVNLSTYTH
 251 RCSDLADLEI IFSPSTDLAI WNYIAREIVY NHPEAIDWDF VKKNTIFTTG
 301 FANIGYGMRT EAEAKKLGYS AKELEVIKKE DAKVISEKEA PGLAHLGVKA
 351 GDVMKMDKAD AAGAHWEISF EDFKKALEPY TLEYVAKISK GNPDEKLEDF
 401 KVKLQELANL YIEKNRKVVS FWTMGFNQHQ RGTWVNEQSY MVHFLLGKQA
 451 KPGDGAFSLT GQPSACGTAR EVGTFTHRLP XDMDVSIPKH REVSEKIWKL
 501 PAGTLNPMGY QHIMNXHRQI ESGKIKFAWV NVCNPYQDTA NANHWIKAAR
 551 ELDNFIVCSD AYPGISAKVS DLILPSAMIY EKWGSYGNAE RRTQHWRQQV
 601 LPVGDAMSDT WQWVELSKRF TIKDVWGEQP IKGGKLPNVI EAAKAMGYKE
 651 TDTMYDVLFA TPFAKQFKAD DAIGKGFDNS EVFGDARKVM GSDGKEWTGY
 701 GFFIQKSIWE EYRQFGLGHG HDLADFDTYH KVRGLKWPVV DGKETQWRFN
 751 AKYDPYAAKA GNGDFAFYGD FAKALKKGNL VKPTTEETYS LKNKAKIFFR
 801 PYMDPCEMPD REYDTWLCTG RVLEHWHSGT MTMRVPELYR AVPEALCYMH
 851 PEDAKAKGFK QGDMIWLESR RGSCKARVET RGRNRTPRGL VFVPWFDEKV
 901 MINKVCLDAT CPISKQTDYK KCAVKLYKA
```

Sample 3

Match to: **gi|169104652** Score: **1154**
periplasmic nitrate reductase [Sulfurospirillum barnesii]
Found in search of C:\Documents and
Settings\Administrator\Desktop\CS31269.mgf

Nominal mass (M_r): **105393**; Calculated pI value: **8.77**
NCBI BLAST search of gi|169104652 against nr
Unformatted sequence string for pasting into other applications

Taxonomy: Sulfurospirillum barnesii

Fixed modifications: Carbamidomethyl (C)
Variable modifications: Oxidation (M)
Cleavage by Trypsin: cuts C-term side of KR unless next residue is P
Sequence Coverage: **43%**

Matched peptides shown in **Bold Red**

1 MSLSRRDFLK **TTAAASAAAA VGIGVPAELK** AAGEQAEANW KWDKAVCR**FC**
51 **GTGCGIMVAT KEGKIVAVKG DPAAPVNRGL** NCIKGYFNAK IMYGADRLKQ
101 PLLRMNDKGE FDKK**GQFKPV SWKRAFDEME** KHIKAALK**VG GPEAIGVFGS**
151 **GQYTIQEGYA AAKMMKAGFR** ANGIDPNARH CMASAVAGFM QTFGIDEPAG
201 CYDDIEITDT IITWGANMAE MHPILWSRVS DRKLTSPDRV K**IVNLSTYTH**
251 **RCSDLADLEI** IFSPSTDLAI WNYIAR**EIVY NHPEAIDWDF VKKNTIFTTG**
301 **FANIGYGMRT** FAEAKKLGYS AKELEVIKKE DAKVISFK**EA PGLAHLGVKA**
351 GDVMKMDKAD AAGAHWEISF EDFKK**ALEPY TLEYVAKISK** GNPDEKLEDF
401 KVK**LQELANL YIEKNRKVVS FWTMGFNQHQ RGTWVNEQSY** MVHFLLGKQA
451 KPGDGAFSLT GQPSACGTAR **EVGTFTHRLP XDMDVSIPKH** REVSEKIWK**L**
501 **PAGTLNPMGY QHIMNXHRQI** ESGKIK**FAWV NVCNPYQDTA NANHWIKAAR**
551 **ELDNFIVCSD AYPGISAKVS DLILPSAMIY EKWGSYGNAE** RRTQHWR**QQV**
601 **LPVGDAMSDT WQWVELSKRF** TIK**DVWGEQP IKGGKLPNVI EAAKAMGYKE**
651 **TDTMYDVLFA TPFAKQFKAD** DAIGK**GFDNS EVFGDARKVM** GSDGK**EWTGY**
701 **GFFIQKSIWE EYRQFGLGHG** HDLADFDTYH KVRGLK**WPVV DGKETQWRFN**
751 AK**YDPYAAKA GNGDFAFYGD FAKALKKGNL VKPTTEETYS LKNKAKIFFR**
801 PYMDPCEMPD R**EYDTWLCTG RVLEHWHSGT** MTMRVPELYR AVPEALCYMH
851 PEDAKAKGFK QGDMIWLESR RGSCKARVET RGRNRTPRGL VFVPWFDEKV
901 MINK**VCLDAT CPISKQTDYK** KCAVKLYKA

Sample4

Match to: **gi|57237630** Score: **193**
NapD [Campylobacter jejuni RM1221]
Found in search of C:\Documents and
Settings\Administrator\Desktop\CS41269.mgf

Nominal mass (M_r): **12950**; Calculated pI value: **4.28**
NCBI BLAST search of gi|57237630 against nr
Unformatted sequence string for pasting into other applications

Taxonomy: Campylobacter jejuni RM1221
Links to retrieve other entries containing this sequence from NCBI
Entrez:
gi|57166434 from Campylobacter jejuni RM1221

Fixed modifications: Carbamidomethyl (C)
Variable modifications: Oxidation (M)
Cleavage by Trypsin: cuts C-term side of KR unless next residue is P
Sequence Coverage: **52%**

Matched peptides shown in **Bold Red**

1 **MNNLSSVLIL AKEEYINDLK KAISEIPFCS VELCENEKII VVIESENLED**
51 **ELNSYK**MLEK LPNIISINMV FSYQDLNDDI QK**AINSGAIE TIEK**NENAEN
101 IRYYGSVFNQ FS

Appendix IV: The effect of hexavalent chromium on dissimulatory nitrate reduction to ammonia by the soil bacteria: *Sulfurospirillum barnesii*, *Geobacter metallireducens* and *Desulfovibrio desulfuricans*.

6.1. Introduction

Chromium has been considered to be both a toxin and an essential micronutrient to humans; [223] however, the benefits of chromium are still under debate. High valence states of chromium are notoriously toxic; Cr^{VI} is a known mutagen and carcinogen. [224] Chromium deficiency has been associated with metabolic disturbances, such as diabetes, [225-227] and many studies suggest that Cr^{III} is essential for lipid and carbohydrate metabolism. However, unlike other essential transition metals (i.e., Co, Cu, Fe, Mo, Mn, W, or V), no Cr-containing biomolecule has been identified in any organism, [228-230] if such as molecule does exist, the explicit function and mode of action is not known. Conversely, elevated levels of Cr^{III} also cause adverse health effects, [225, 231, 232]as Cr^{III} can damage DNA. Regardless, chromium has the demonstrated ability to be hazardous to human health, and the toxicity of chromium depends on the oxidation state, Cr^{VI} is the most toxic.

Chromium is found extensively in the earth's crust; Cr^{III}, the most common oxidation state, is naturally found in rocks, plants, soil, and animals. [233] Cr^{VI}, which is more water-soluble, is also prevalent in the environment, primarily as a result of human activities.[233] Chromium has many industrial uses, such as metallurgy, paint, dye and pigments, tanning, refractory materials, and chemical manufacturing. Chromium contamination has become more prevalent in the past 30 years as a result of improper

disposable practices and leaching; as a result, both Cr^{III} and Cr^{VI} have become more prevalent in the environment. In 1980, the comprehensive environmental response, compensation and liability Act, known as "Superfund", was enacted to identify and clean-up hazardous waste sites throughout the United States. Currently, over 200 chromium containing superfund sites are active.[234] Unfortunately, removing the Cr^{VI} contamination is not straightforward, as the chemical can leach deep into groundwater and subsurface sediment.

Ideally, bioremediation of chromium contaminated sediment would utilize naturally occurring soil organisms to transform Cr^{VI}, which is more mobile in the environment and more toxic, into Cr^{III}, the less mobile and the more inert chromium species. A similar strategy is employed for selenate contamination. Bioreactors, which were lined with immobilized *S. barnesii* cells, utilize the organism selenate reductase activity to transform selenate contaminate waste water into elemental selenium, which was essentially insoluble and less toxic.[163] Nitrate was also present in the waste water, *S. barnesii* was able to remove excess nitrate concurrently.[163] The success of this project pivoted on the fact that the enzymatic reduction of selenate and nitrate did not affect each other, as transformation selenate and nitrate utilize different enzymes, selenate reductase and nitrate reductase respectively. The direct application of this approach to chromate and nitrate reduction is hindered by one obstacle; elevated concentrations of chromate can completely inhibit nitrate reduction.[235, 236] The mechanism for this inhibition is not known; however, studying the enzyme activity may elucidate the molecular basis for the inhibitory effect of chromate on nitrate reduction .

Several “chromate reductase” enzymes have been investigated. While chromate reduction was once believed to be a secondary activity,[237] many NADH or NADPH dependent enzymes display a tight binding affinity for chromate. [238-244] In fact, the elected chromate reductases (ChrR) are flavin dependent. Nitroreductases,[245] *c*-type cytochromes[246] and hydrogenases [247] can also reduce chromate. The somewhat unspecific nature of chromate reduction by oxidoreductases enzymes[239] may be an indication that chromate can oxidize the enzymes responsible for nitrate reduction.

Therefore, in an effort to understand the mechanism of chromium reduction by *Sulfurospirillum barnesii,* we chose to examine the effect of Cr^{VI} reduction on nitrate reduction. In *S. barnesii*, nitrate is enzymatically reduced to ammonia, via nitrite, using two enzymes, the periplasmic nitrate reductase (Nap) and the membrane bound formate-linked nitrite reductase (Nrf). The catalytic subunit, NrfA is a cytochrome *c* containing enzyme, chromate may interact with NrfA similar to the *Desulfovibrio vulgaris* cytochrome *c*.[246] For comparison, *Geobacter metallireducens* and *Desulfovibrio desulfuricans* were investigated, as the closely related *Geobacter* and *Desulfovibrio* species can reduce Cr^{VI}. [246, 248, 249] The goal of this study was to: 1) establish the assay conditions for monitoring the enzymatic reduction of nitrate, nitrite, and chromium; and 2) study the effect of chromate (Cr^{VI}) on the enzymatic reduction of nitrate and nitrite

6.2. Experimental

6.2.1. Cultivation of bacteria

G. metallireducens was grown on freshwater acetate medium with nitrate as previously described.[248] *S. barnesii* and *D. desulfuricans* were grown on freshwater medium with lactate and nitrate as previously described[169]. Chromate was filter sterilized and amended after autoclaving.

6.2.2. Crude fractionation of bacteria cells

The cell paste was suspended in an anoxic buffer (SES-3 lysis buffer, Appendix V) using a dounce (Knotes). The homogenized cell slurry was passed through a French pressure cell press (Thermo Scientific) two times at ~14,000 psi (900 mPa gauge pressure) before a protease inhibitor cocktail (Sigma- Aldrich) and Deoxyribonuclease I (Sigma- Aldrich) were added. The lysate was then centrifuged at 8000 rpm for 10 minutes to remove unbroken cells and debris. The clarified lysate was centrifuged at 300000 *g* (Beckman Coulter Ultracentrifuge, 50.2Ti rotor) for 1.5 hours to separate soluble (periplasm and cytoplasm) and insoluble particles (membrane and ribosomes).

6.2.3. Detergent solublization of membrane proteins

The insoluble pellet was homogenized with 50 mM Tris HCl (pH7.6), and then the insoluble proteins were suspended by adding detergent and stirring overnight at 4^{o}C. Finally, the insoluble fraction was removed by centrifuging the sample at 245000 *g* for 1 hour, and then suspended in 3-[(3-cholamidopropyl) dimethylammonio]-1-propanesulfonate (CHAPS). *S. barnesii* was incubated with 1% (w/v) CHAPS, *D. desulfuricans* and *G. metallireducens* were incubated 5% (w/v) of CHAPS.

6.2.4. Preparative CHAPS native- polyacrylamide gel electrophoresis

Preparative CHAPS native- polyacrylamide gel electrophoresis (CN-PAGE) was used to separate proteins in the CHAPS soluble fraction. A solid cylindrical (tube) gel, 2.5 inch diameter, was created by casting the CN- PAGE inside a modified[250] Model 491 PrepCell (BioRad). The protocol for the CN- PAGE buffers is in Appendix V. Briefly, the resolving and stacking gels contained 0.5% of CHAPS, the sample buffer contained 0.7% CHAPS and the anode buffer 0.1% CHAPS. Electrophoresis was performed using cold buffer and separation was performed using 100 V for at least 3 hours. The entire tube gel was removed, washed with water, and then separated into small disk shaped sections, which were diced prior to electroelution. Electroelution was conducted using the Elutrap™ System (Whatman) according to the manufacturer's guidelines. The diced gel samples were immersed in the CHAPS anode buffer. Electrophoresis was conducted at 100 V for 1 hour. Each fraction was collected, and stored at -20 ^{o}C.

6.2.5. In-gel activity assays and native polyacrylamide gel electrophoresis

Detergent soluble proteins were separated by electrophoresis under non-denaturing conditions. Both the resolving and stacking gels contained 0.5% of detergent (CHAPS or OBGP), sample buffer contained 0.7% detergent and anode buffer 0.1% detergent (**Appendix V**). Electrophoresis was performed at 40 V.

The in-gel assay was performed in 50 mM Tris-Cl (pH 7.9) with 10 mM methyl viologen or benzyl viologen as the electron donor and potassium nitrate [0.1M], potassium nitrite [10 mM], or potassium chromate [0.7 mM] as the electron acceptors in presence of sodium dithionite. Images of the activity gels were collected with the Bio-

Rad densitometer GS-800. After the activity assay was finished gels were washed in de-ionized water, and then incubated for 15 minutes in 12.5 % (w/v) trichloroaceticacid solution prior to staining with colloidal coomassie stain (**Appendix V**). Proteins were stained with a colloidal coomassie blue G-250 solution (**Appendix V**) overnight, washed with methanol (25%) and scanned using a calibrated imaging densitometer (GS-800, BioRad). The relative density and molecular weight of the separated proteins were calculated with Quantity One software (BioRad).

6.2.6. Sodium dodecyl sulfate polyacrylamide gel electrophoresis

Discontinuous SDS/PAGE was used to analyze fractions for purity, using standard protocol[176] (**Appendix V**). A 12 % acrylamide resolving gel and a 5% stacker were used. After separation the gel was incubated in 12% trichloroacetic acid for 30 minutes to precipitate proteins followed by a 10 minute wash in water. The recipes can be found in (**Appendix V**). Electrophoresis was conducted using a constant voltage (60 V) for 2 hours and then at 120 V for 1 hour.

Unless noted otherwise, proteins were stained with a colloidal coomassie blue G-250 solution (**Appendix V**) overnight and washed with methanol (25%). Alternatively, the presence of covalently bound heme was determined as previously described.[251] Gels were scanned using a calibrated imaging densitometer (GS-800, BioRad). The relative density and molecular weight of the separated proteins were calculated with Quantity One software (BioRad). Molecular weight standards (Fermentas) were used to estimate the size of unknown proteins.

After SDS-PAGE, proteins were excised from the gel, digested with trypsin and analyzed with MALDI-TOF (trypsin digestion and MALDI-TOF were performed by a fellow lab member, a brief description of techniques used is located in Appendix V.

6.2.7. Assays

Protein concentration was measured using the DC protein assay kit (Bio-Rad). Bovine serum albumin (Pierce) was used as a standard.

Protein fractions were routinely screened for nitrate, nitrite, and chromate reductase activity via the reduced methyl viologen linked nitrate reductase assay.[171, 172] Microscale assays were performed inside an inert atmosphere glove box (Vacuum Atmospheres) at 22 ^{o}C using the ELx808 absorbance microplate reader (BioTek). The oxidation of methylviologen was monitored at 630 nm using Gen5 Data Analysis Software (BioTek).

The reaction buffer contained TrisHCl [100 mM] (pH 7.6). All stock solutions were prepared in the reaction buffer. The final concentrations of reactants were 3 mM methyl viologen or benzyl viologen. The substrate concentration is provided in the figure legends. All assay solutions were purged with nitrogen or argon gas for 20 minutes, and then sealed before transfer into the anaerobic chamber. Methylviologen was partially reduced by titrating with a sodium dithionite stock [60 mM] solution to yield a final absorbance of 1.2– 1.6 at 630 nm. The enzyme was incubated with the reduced methyl viologen for 10 minutes and the absorbance was monitored to ensure the rate of oxidation was insignificant, prior to addition of nitrate. The reaction was initiated by the addition of potassium nitrate and the absorbance was monitored until the reaction stopped (i.e. Abs

=0). Under the given conditions, the rate of reduced methylviologen oxidation by the protein sample alone (i.e., no substrate) was found to be negligible.

The absorbance of electromagnetic radiation (630 nm) by reduced methyl viologen (MV_r) was converted to a unit of concentration using the Beer-Lambert law ($A = \varepsilon bc$), given the reported extinction coefficient of MV_r ($\varepsilon = 13700\ M^{-1} \cdot cm^{-1}$) [173] or BV_r ($\varepsilon = 7400\ M^{-1} \cdot cm^{-1}$)[252] and the calculated path length ($b = 0.667\ cm^{-1}$). The rate of methyl viologen oxidation (i.e. decrease in $[MV_r]$) was determined by plotting the concentration of MV_r over time (seconds). Linear regression (GraphPad Prism)[174] of the initial data points (first 90 seconds after adding nitrate) was used to calculate the rate of methyl viologen oxidation.

In addition to the methyl viologen assay, the concentration of nitrite produced was measured using the diazo coupling technique (Griess assay, Appendix V).[175] Potassium nitrite (Fluka) was used as a standard for nitrite estimation, within the range of 1.6 μM-100 μM.

6.2.8. Spectroscopy and redox cycling of cytochromes

A Carry-500 spectrophotometer was used to collect the electronic spectra of protein samples. The cytochrome protein (400 μL) was reduced after the addition of 60 μL sodium dithionite [0.1 M], and then re-oxidized by adding 20 μL potassium chromate [0.1M].

6.3. Results and Discussion

6.3.1. The effect of chromate on Sulfurospirillum barnesii strain SES-3 nitrate and nitrite reductase activity.

While the main object of this study was to determine the effect of chromate on nitrite reductase, the technical aspects of simultaneously assaying chromate, nitrate and nitrite activity will be briefly discussed. In this study, the enzymatic reduction of chromate, nitrate, and nitrite (**Equations 1-3**) was monitored using multiple colorimetric assays. Methyl or benzyl viologen, are routinely used to estimate nitrate and nitrite reduction,[253-256] especially during protein purification. Reduced viologen is a deep purple to blue color, while the oxidized viologen is colorless;[252] therefore, the rate of viologen reduction can be easily monitored spectrophotometrically. However the reduced viologen assay has a more practical purpose, providing electrons to the enzyme during catalysis. The viologen, which is in the oxidized state, is typically reduced with a sodium dithionite solution (see **Table 6.2** for redox potentials), after the oxygen levels were minimized. Because this assay is using powerful reductants; the abiotic chromate reductase activity was carefully monitored using multiple control experiments. Figure 6.7 illustrates that the blank, dithionite reduced benzyl viologen is not oxidized, at any detectable rate, by chromate. Only the sample which contains enzyme and chromate can oxidize reduced benzyl viologen.

Equation 1: $NO_3^- + 2e^- + 2H^+ \rightarrow NO_2 + H_2O$ ($E° = 0.42$ V)

Equation 2: $NO_2^- + 6e^- + 8H^+ \rightarrow NH_4^+ + 2H_2O$ ($E° = 0.34$ V)

Equation 3: $Cr_2O_7^- + 6e^- + 14H^+ \rightarrow 2Cr^{+3} + 7H_2O$ ($E° = 1.33$ V)

Table 6.1: Redox potentials of compounds used in this study

Compound	# e^-	Redox potential, E_o (V)	reference
Dithionite	1	-0.660	[180]
Methyl Viologen	1	-0.440	[257]
Benzyl Viologen	1	-0.360	[257]
NAD^+/ NADH	2	-0.320	[257]
NO_2^- / NH_4^+	6	+ 0.340	[257]
NO_3^-/ NO_2^-	2	+ 0.421	[257]
½ O_2 / H_2O	2	+ 0.816	[257]
Cr^{VI}/ Cr^{III}	6	+1.33	[258]

For a more direct approach, nitrite was quantified after the nitrate and nitrite reductase assays completed. The diazo coupling technique,[259] referred to as the Griess assay, was used to measure nitrite concentration. Briefly, nitrite reacts with sulfanilamide creating a diazonium complex, and then napthylethylene-diamine dihydrochloride (NEDD) creates a red "azo dye". Unfortunately, the Griess assay denatures the enzyme, due to the acidic reagents. Thus only quantification of the quenched reaction is possible. The diphenylcarbohydrazide (DPC) assay, which can quantify the hexavalent chromium concentrations, was investigated. However the presence of dithionite inhibited the assay, as indicated by the false negative measurements potassium chromate standards (data not shown). Therefore, the DPC assay was not used to monitor chromate reduction,

First, the effect of chromate on the Griess assay was investigated. We have established that using the reduced methyl viologen assay under the specified conditions: 1) mixing chromate and nitrate does not affect the Griess assay (Figure 6.1), as the estimated nitrite concentration is comparable in both nitrate and nitrate mixed with chromate controls (i.e., with-out protein); 2) chromate does not affect the Griess assay by providing false

positives or negatives (**Figure 6.2**); 3) chromate may affect nitrite concentration (**Figure 6.2**), approximately 8 % less nitrite was measured in the nitrite plus chromate stock compared to the nitrite stock. This indicates that chromate may reduce nitrite or inhibit the formation of the azo dye in the griess assay. All reagents were prepared using the same nitrate or nitrite stock solution, chromate was amended where indicated; solutions were prepared using analytical glassware.

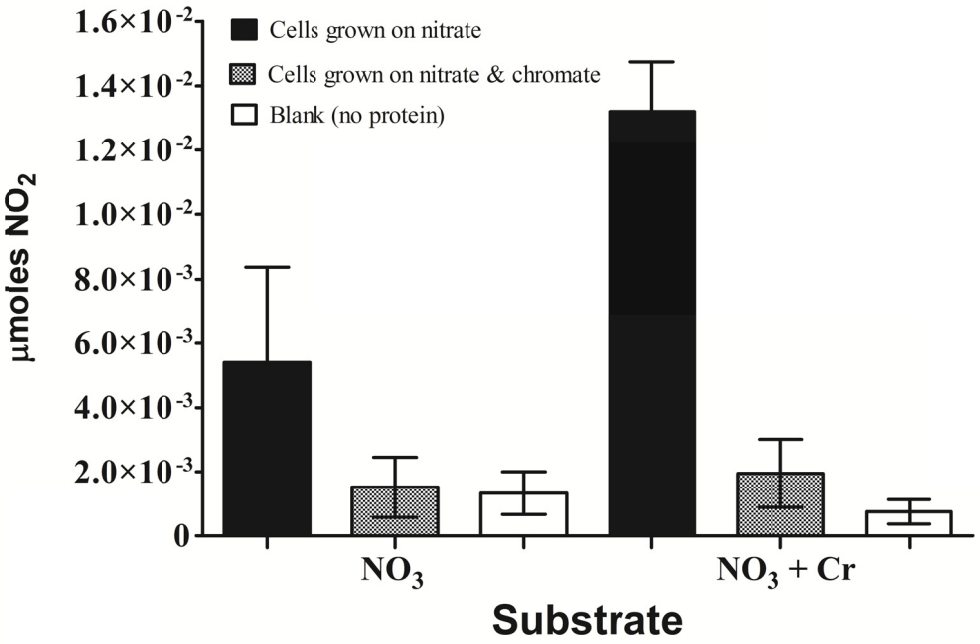

Figure 6.1: The effect of chromate on nitrate reductase activity in the *S. barnesii* lysate. Two protein samples were assayed, the lysate prepared from *S. barnesii* cells grown on nitrate media supplemented with 1 mM chromate (grey bars) or un-amended nitrate media (black bars). The blank, no protein, samples (white bars) indicated the initial concentration of nitrite in each. Cr = 0.7 mM potassium chromate.

Nitrate reductase activity appears to increase in the presence of chromate (**Figure 6.1**). However the data must be interpreted with care, as nitrite can be converted to ammonia via nitrite reductases. In other words nitrite concentrations may be higher when chromate is introduced because nitrite reductases are inhibited. The nitrite reductase activity assay confirms this concept (**Figure 6.2**). Nitrite reduction is inhibited by the

presence of chromate in *S. barnesii*. Assays conducted with nitrite and chromate decrease the conversion of nitrite from 65 % to 45 % in cell lysate of cultures grown on nitrate media and decreases from 91 % to 44 % in cell lysate of cultures grown on nitrate and chromate (**Table 6.2**). Surprisingly, *S. barnesii* cells exposed to chromate during growth reduced the most nitrite, 91 % of the initial nitrite was reduced. The lysate extracted from *S. barnesii* cell which were not exposed to chromate reduced 65 % of the initial nitrite. However, the *S. barnesii* growth conditions had no effect on nitrite conversion when chromate was present in the assay compared to the nitrite only assay, 44% and 45 % conversion.

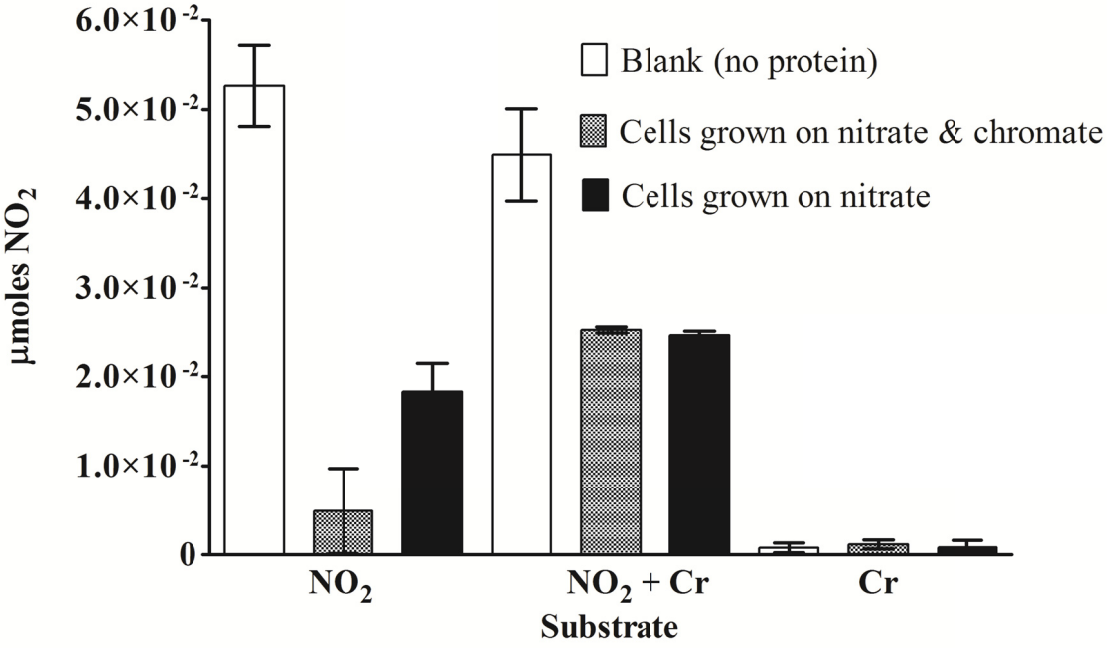

Figure 6.2: The effect of chromate on the nitrite reductase activity of *S. barnesii* lysate. Two protein samples were assayed, the lysate prepared from *S. barnesii* cells grown on nitrate media supplemented with 1 mM chromate (grey bars) or un-amended nitrate media (black bars). The blank, no protein, samples (white bars) indicated the initial concentration of nitrite in each. The final concentration of substrates was the same in each assay, potassium chromate [0.7 mM] and potassium nitrite [1.0 mM].

Table 6.2: The effect of chromate on the nitrite reductase activity of *S. barnesii* lysate. Cells were grown on nitrate enriched media in the presence or absence of 1 mM chromate. To assay nitrite reductase activity, the methylviologen assay was used to nitrite reductase activity was calculated by he values presented are percent difference.

Substrate	**NO_2**	**NO_2 + Cr**
Cells grown on nitrate	65 %	45 %
Cells grown on nitrate + chromate	91 %	44 %

S. barnesii lysate, obtained from cells grown under nitrate respiratory conditions, can reduce Cr^{VI} (**Figure 6.3**). When the protein sample was incubated with chromate, benzylviologen is quickly oxidized; the solution was completely oxidized in under 200 seconds (i.e., Abs = 0). The data suggests that chromate can be enzymatically reduced by *S. barnesii*. Methyl viologen was not used as an electron donor because the background rate of oxidation in the presence of chromate was larger, possible due to the different redox potentials of methyl and benzyl viologen, - 0.47 V and – 0.35 V respectively (**Table 6.1**).[252]

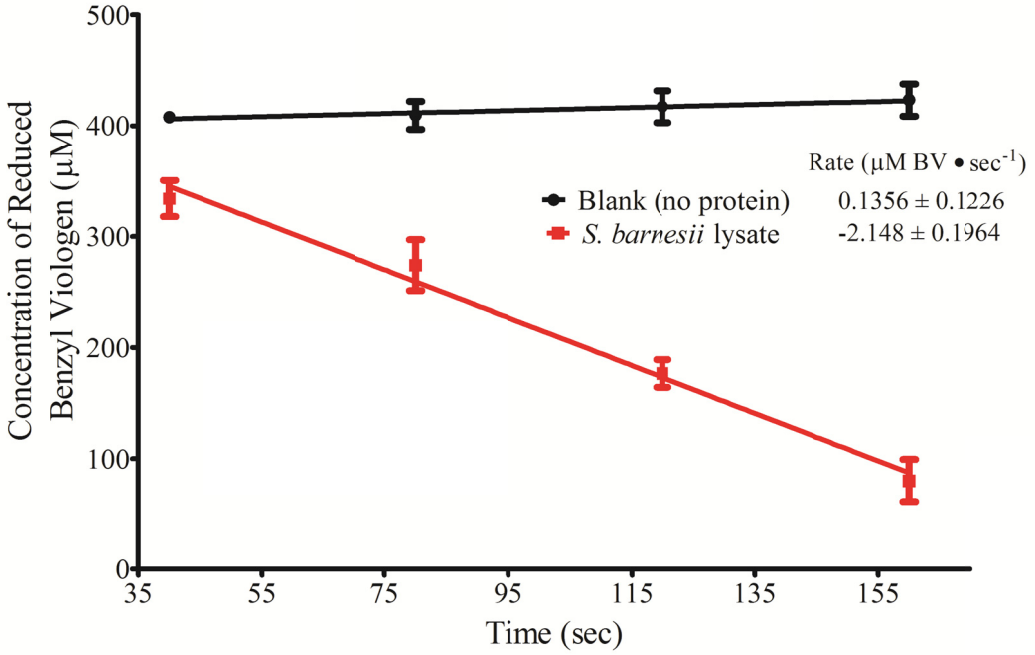

Figure 6.3: The oxidation of reduced benzyl viologen by *S. barnesii* lysate in the presence of chromate. The concentration of benzyl viologen was estimated by monitoring the assay solution spectrophotometrically. The BioTek ELx808 multichannel plate reader was used to measure the absorbance at 630 nm inside an inert atmosphere glove box. In the presence of 100 uM potassium chromate, the dithionite reduced benzyl viologen (-●-) had an absorbance of ~1.3 at 630 nm, which was stable in the anaerobic atmosphere. *S. barnesii* lysate (200 µg of protein) quickly oxidizes benzylviologen in the presence of chromate (-■-). Analyses were performed using Prism (GraphPad). The rate of benzyl viologen oxidation was determined to be 2.148 µM per second (R^2=0.92). Three replicates were used, N=3. The rate of benzyl viologen oxidation by the enzyme was determined to insignificant.

To confirm if the viologen-coupled reduction of chromate is performed by a protein, native gel electrophoresis and in-gel activity assays were conducted. The CHAPS soluble fraction was chosen to remove interference from small redox active proteins in the whole cell lysate. The in-gel chromate reductase assay suggests that a *S. barnesii* protein is reducing chromate (**Figure 6.4**). A chromate reductase active band was observed in the in-gel assay preformed with cells exposed to chromate during growth but not in the un exposed cells (grown only on nitrate media). The chromate reductase band appears to be the same band as the nitrite reductase active band (**Figure 6.4**). The nitrite

reductase active band was present in fractions isolated from cells grown in the presence and absence of chromate. The fraction which was not able to oxidize benzyl viologen in the presence of chromate was isolated from cells which were not exposed to chromate during growth. This indicates that the *S. barnesii* protein expression may have changed by the presence of chromate. In any case the presence of a chromate reducing protein was established therefore, the focus of the future experiments moved to isolate the chromate reducing protein using preparative native gel electrophoresis. Because, the same protein complex exhibited chromate and nitrite reductases activity, both activities were monitored during purification.

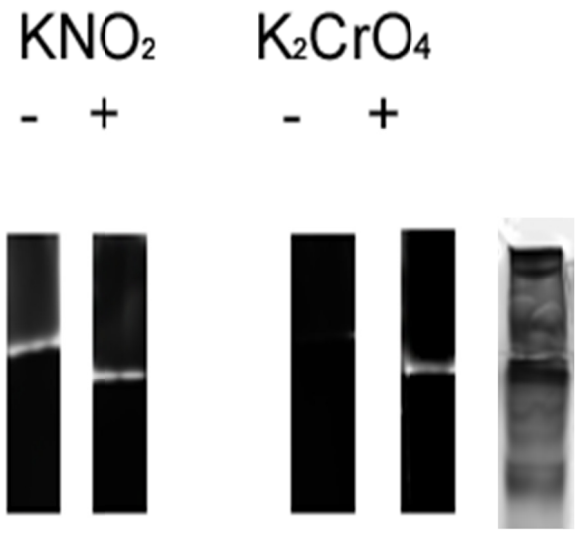

Figure 6.4: *S. barnesii* native gel electrophoresis and in-gel nitrate and chromate activity assay. The membrane proteins, collected in the insoluble fraction, were solubilized with 1% CHAPS, then separated via CN-PAGE. The gel was stained with a reduced methyl viologen solution, and then incubated for ~ one minute with substrate, either 0.1mM potassium nitrite (KNO_2) or 0.1 mM potassium chromate (K_2CrO_4), before transferring to the densitometer to capture this image. The local oxidation of methylviologen is indicative of "active" protein bands; the oxidation of reduced methylviologen in this assay appears as bleaching (white bands). Oxidation occurred in less than 10 minutes, in the case of chromate, and with-in 5 minutes with nitrate. The plus sign (+) indicates the bacteria were grown in the presence of 100 μM potassium chromate, (-) indicates the bacteria were not grown in the presence of chromate. For reference, the coomassie stained gel is provided.

The large scale purification of the nitrite-chromate reductase was conducted by simply scaling up the reagents used in the mini-scale CN-PAGE. Instead of casting a flat gel, a tube gel was utilized. Also, bromophenel blue was omitted from the loading buffer so that the cytochromes could be visualized easily. A photograph of the tube gel after electrophoretic separation is provided to illustrate the presence of colored protein bands (**Figure 6.5**). After the proteins were electroeluted, the electronic absorption spectrum was collected for each sample. Because nitrite reductase (Nrf) contains four *c*- type cytochromes [151, 260] the presence of cytochromes was monitored spectrophotometrically. The ratio of A_{280}/ A_{400} provides an indication of the iron sulfur

content, relative to protein concentration, in each fraction (**Table 6.3**), as iron-sulfur containing proteins characteristically exhibit an absorbance at 400 nm. Fractions four and five, which were yellow (**Figure 6.5**), have the highest iron-sulfur content. The fraction, which displays nitrate, nitrite and chromate reduction using the in-gel assays (fraction 1) contained low iron sulfur content. The SDS-PAGE gel of select fractions is in **Figure 6.6**.

Table 6.3: The electronic absorption data of *S. barnesii* fractions isolated with preparative CN-PAGE. The ration of A_{280}/ A_{408} provides an indication of the iron sulfur content in each fraction; as A_{408} is indicative of iron-sulfur proteins. Fractions four and five, the yellow samples (see **Figure 6.5**), have the highest iron sulfur content.

S. barnesii Fraction #	A_{280}/ A_{408}
1	0.06
2	0.11
3	0.17
4	0.44
5	0.60
6	0.39
7	0.12
8	0.01

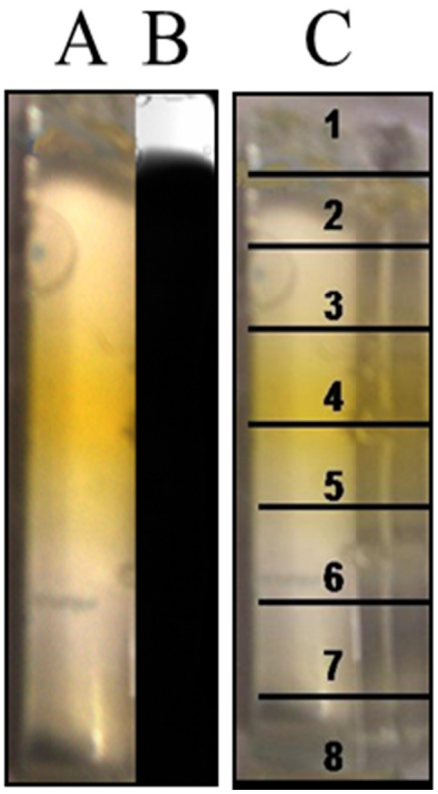

Figure 6.5: The preparative fractionation of the *S. barnesii* CHAPS soluble fraction using electrophoresis. The 1% CHAPS soluble fraction was separated using preparative CN-PAGE using a *modified* Model 491 Prep Cell (BioRad). A) A photograph of the resulting gel, B) the in-gel nitrite reductase activity assay preformed on a horizontal slice from the tube gel C) a diagram of the tube gel sectioning. The eight segments were isolated from the acrylamide gel matrix by electroelution.

To further probe for the presence of *c*-type cytochromes, the electronic absorption spectra were collected for the as-isolated protein sample and the reduced protein, in the presence of dithionite. The sorret band shift from 408 to 420 nm is indicative of cytochromes, and the appearance of α and β bands (520 & 550 nm), c- type cytochromes. Fractions four and five, the yellow protein, had the highest protein and iron sulfur content. The electronic spectrum indicates that this protein does not include a c-type cytochrome (**Figure 6.7**).

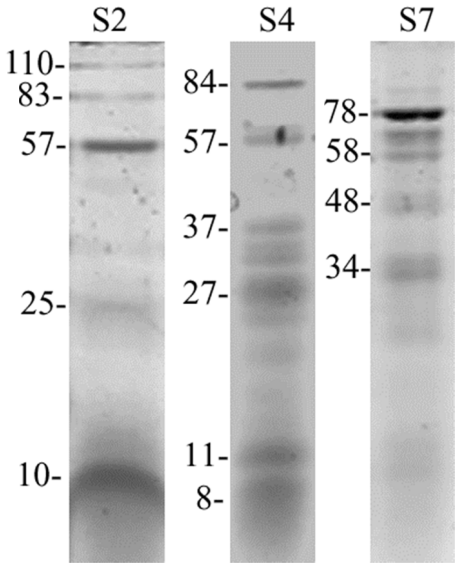

Figure 6.6: SDS-PAGE of *S. barnesii* protein fractions isolated with preparative CN-PAGE. A 12 % acrylamide gel was used. After colloidal coomassie blue staining, the gel was scanned with a densitometer (Bio-Rad, GS 800) and the molecular weights calculated (Quanity One, Bio-Rad). S2, fraction 2; S4, fraction 4; and S7, fraction 7

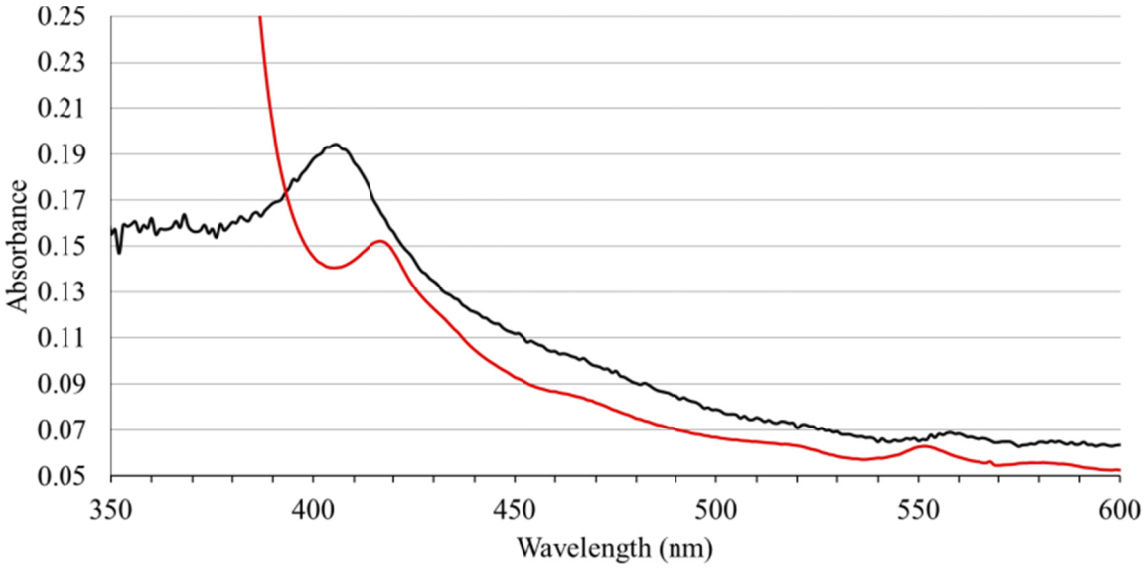

Figure 6.7: The electronic absorption spectra of the yellow protein fraction isolated from *S. barnesii.* The as- isolated protein (black line), and the dithionite reduced (red line).

6.3.2. The effect of chromate on D. desulfuricans nitrate and nitrite reductase activity.

The preparative CHAPS native polyacrylamide gel electrophoresis (CN-PAGE) procedure used to in the purification of *S. barnesii* proteins was repeated for *D.*

desulfuricans. Like *S. barnesii*, the in-gel nitrite and chromate reductase activity was present in cells exposed to chromate, and cells not expose to chromate during growth do not have chromate reductase activity (**Figure 6.8**). An indication of chromate induced expression of chromate reductases.

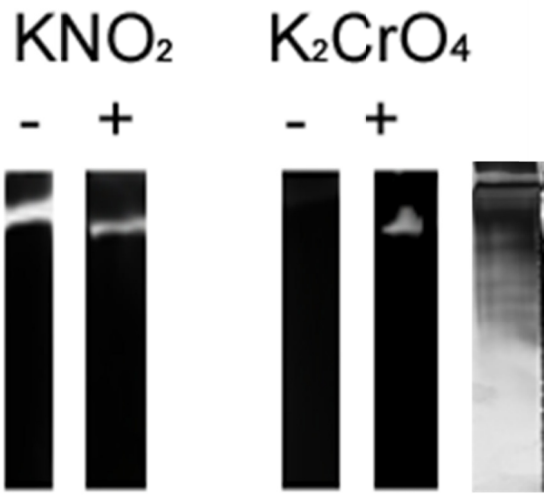

Figure 6.8: *D. desulfuricans* native gel electrophoresis and in-gel nitrate and chromate activity assay. The membrane proteins, collected in the insoluble fraction, were solubilized with 5% CHAPS, then separated via CN-PAGE. The gel was stained with a reduced methyl viologen solution, and then incubated for ~ one minute with substrate, either 0.1 mM potassium nitrite (KNO_2) or 0.1 mM potassium chromate (K_2CrO_4) before transferring to the densitometer to capture this image. The local oxidation of methylviologen is indicative of "active" protein bands; the oxidation of reduced methylviologen in this assay appears as bleaching (white bands). Oxidation occurred in less than 10 minutes, in the case of chromate, and with-in 5 minutes with nitrate. The plus sign (+) indicates the bacteria were grown in the presence of 100 μM potassium chromate, (-) indicates the bacteria were not grown in the presence of chromate. For reference, the coomassie stained gel is provided.

The preparative CN-PAGE separation of *D. desulfuricans* CHAPS soluble fraction revealed the presence of multiple chromophores (**Figure 6.9**). All fractions contain iron sulfur proteins (**Table 6.4**). Fractions four and five contained a high amount of iron sulfur protein content, and are deep green in color and heme stain positive (**Figure 6.9**). Fraction 7 had nitrite reductase activity in the preparative scale in-gel assay (**Figure 6.9**). Fractions one and two were pink, these are the fractions which exhibited nitrite and

chromate reductase activity (**Figure 6.8** and Figure **6.9**). Fraction ten was yellow, this protein was lost during electroelution as the small size of the protein permitted it to travel through the membranes. The SDS-PAGE gel of the fractions purified is in **Figure 6.10**.

Table 6.4: The electronic absorption data of *D. desulfuricans* fractions isolated with preparative CN-PAGE. The ratio of A_{280}/ A_{408} provides an indication of the iron sulfur content in each fraction; as A_{408} is indicative of iron-sulfur proteins.

***D. desulfuricans* Fraction #**	**A_{280}/ A_{408}**
1	0.32
2	0.48
3	0.42
4	**0.64**
5	**0.64**
6	0.21
7	0.63

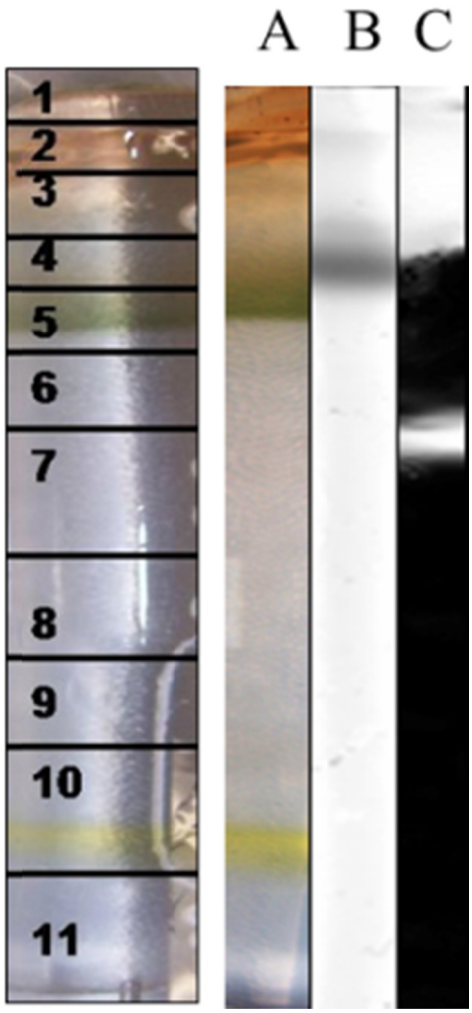

Figure 6.9: The preparative fractionation of the *D. desulfuricans* CHAPS soluble fraction using electrophoresis. The 5% CHAPS soluble fraction was separated using preparative CN-PAGE using a *modified* Model 491 Prep Cell (BioRad). (a) A photograph of the resulting gel, (b) the in-gel nitrite reductase activity assay preformed on a horizontal slice from the tube gel (c) a diagram of the tube gel sectioning. The eight segments were isolated from the acrylamide gel matrix by electroelution.

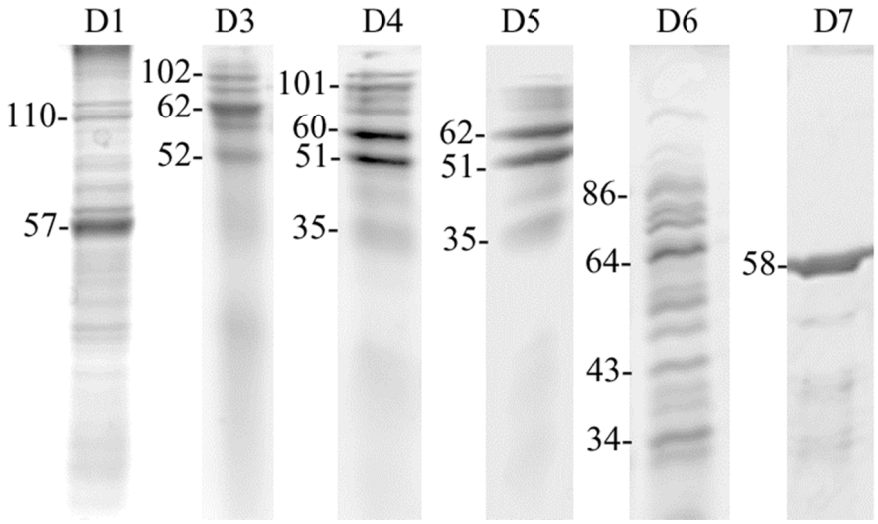

Figure 6.10: SDS-PAGE of *D. desulfuricans* protein fractions isolated with preparative CN-PAGE. A 12 % acrylamide gel was used. After colloidal coomassie blue staining, the gel was scanned with a densitometer (Bio-Rad, GS 800) and the molecular weights calculated (Quanity One, Bio-Rad). D1, fraction 1; D3, fraction 3; D4, fraction 4; D5, fraction 5; D6, fraction 6; D7, fraction 7.

The 62 kDa band from fraction five (**Figure 6.10**) was identified by MALDI-TOF MS as the alpha subunit of dissimilatory sulfite reductase (dSiR). The 51 and 35 kDa bands correspond in size to the beta and gamma subunits of dSiR. *Desulfovibrio* dSiR, also called desulfoviridin, is reported to catalyze the six electron reduction of sulfite. The *Desulfovibrio vulgaris* dSiR[261] protein has been studied for a number of years and has been reported to reduce nitrite and hydroxylamine. The electronic absorption spectra of the fraction five, the *D. desulfuricans* dSiR enriched fraction (**Figure 6.11**), confirms the presence of the siroheam protein. The 630 nm band is indicative of sirohemes, like desulfoviridin. **Figure 6.9** shows the characteristic green color of desulfoviridin in the tube gel (post separation). Fraction five had nitrite reductase activity, and chromate inhibited the transformation of nitrite (data not included).

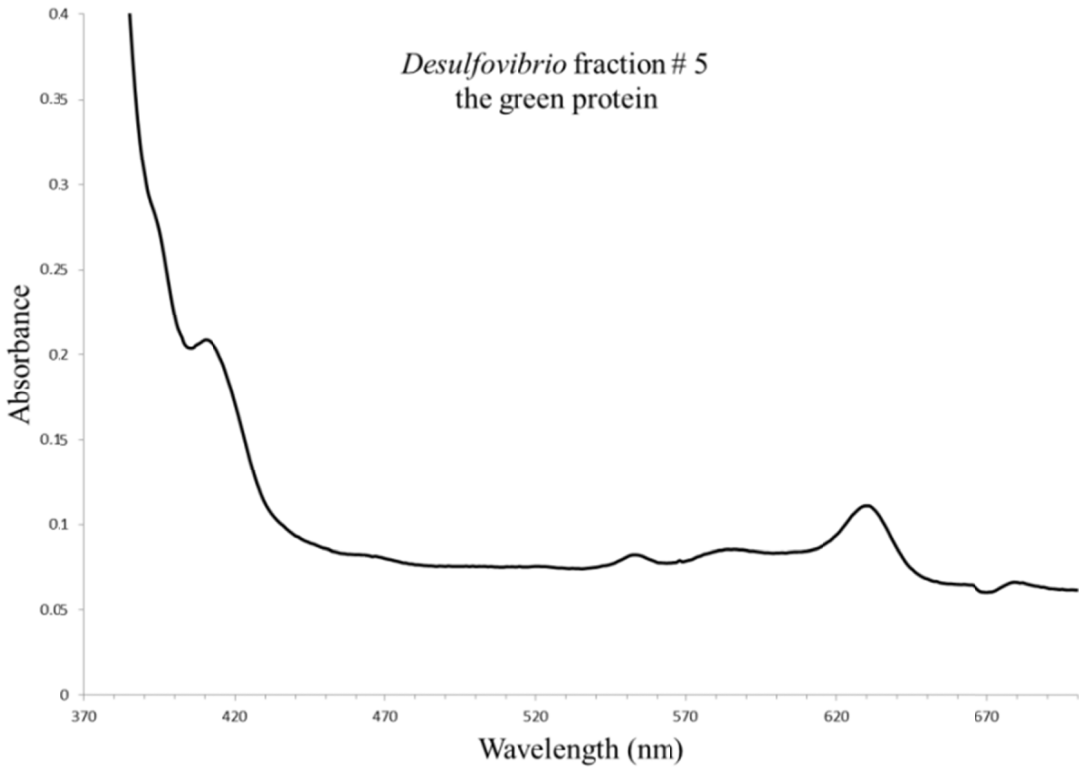

Figure 6.11 The electronic absorption spectra of the desulfoviridin enriched fraction from *D. desulfuricans.*

The electronic absorption spectra collect from the as-isolated and dithionite reduced *D. desulfuricans* fraction # 1 reveals the presence of a c-type cytochrome (**Figure 6.12**). Fraction one displays the most in-gel nitrite and chromate reductase activity.

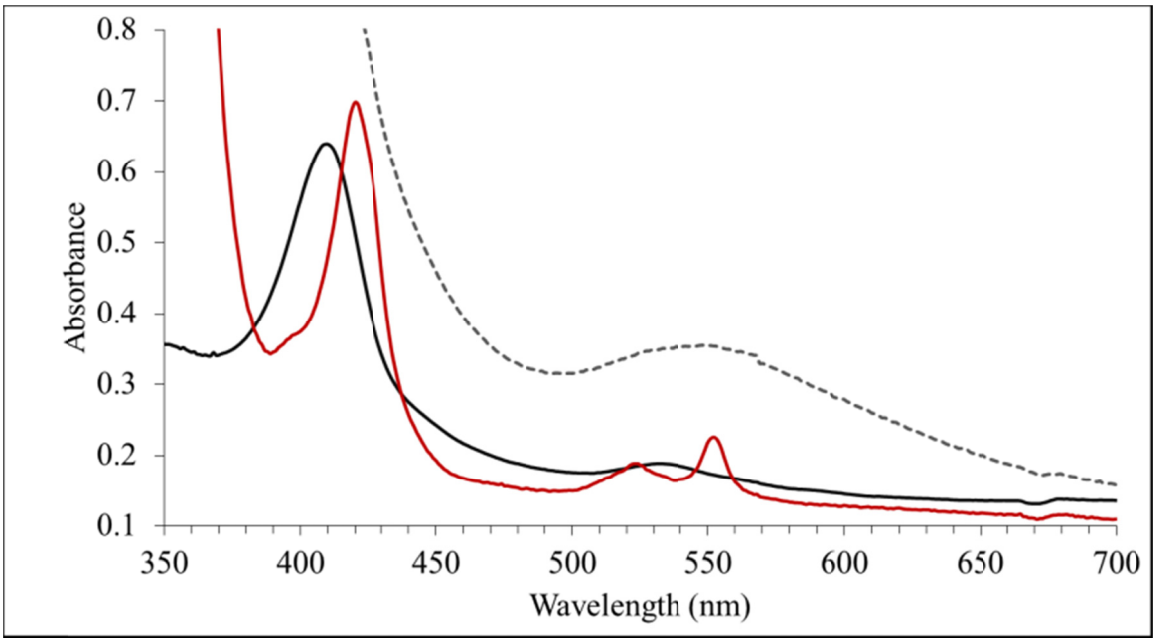

Figure 6.12: The electronic absorption spectra of nitrite reductase activity fraction from *D. desulfuricans.* The as- isolated protein (black line), dithionite reduced (red line), and chromate oxidized (grey dashed line). The cytochrome protein (400 uL) was reduced after the addition of 60 uL of 0.1 M sodium dithionite, then re-oxidized by adding 20 uL 0.1M potassium chromate.

6.3.3. The isolation of a multiheme protein from G. metallireducens nitrate and nitrite reductase activity.

The preparative CHAPS native polyacrylamide gel electrophoresis (CN-PAGE) procedure used to in the purification of *S. barnesii* proteins (**Section 6.3.1**) was repeated for *G. metallireducens*. Unlike *D. desulfuricans* and *S. barnesii*, the CHAPS soluble fraction from *G. metallireducens* did not display any in-gel chromate reductase activity (data not included). Two fractions, fractions three and four had elevated levels of iron sulfur content (**Table 6.5**), these samples were a vivid pink color (**Figure 6.13**). After SDS-PAGE separation (**Figure 6.14**), the 34 kDa band was identified as a hypothetical *G. metallireducens* protein (accession number 78222133). The sequence of the hypothetical *G. metallireducens* protein indicated that is contains nine heme binding motifs. The electronic spectrum also indicates the presence of c- type cytochromes (**Figure 6.15**).

Table 6.5: The electronic absorption data of *G. metallireducens* fractions isolated with preparative CN-PAGE. The ratio of A_{280}/ A_{408} provides an indication of the iron sulfur content in each fraction; as A_{408} is indicative of iron-sulfur proteins.

***G. metallireducens* Fraction #**	**A_{280}/ A_{408}**
3	0.95
4	**1.16**

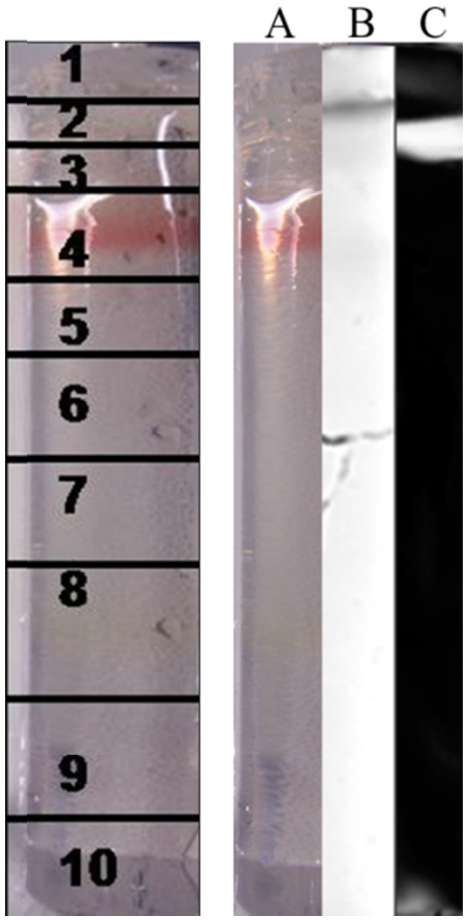

Figure 6.13: The preparative fractionation of the *G. metallireducens* CHAPS soluble fraction using electrophoresis. 1% CHAPS soluble fraction was separated using preparative CN-PAGE using a *modified* Model 491 Prep Cell (BioRad). A diagram of the tube gel sectioning is provided in the left panel. A) a photograph of the resulting gel, B) the heme stained tube gel C) the in-gel nitrite reductase activity assay preformed on a horizontal slice from the tube gel. The eight segments were isolated from the acrylamide gel matrix by electroelution.

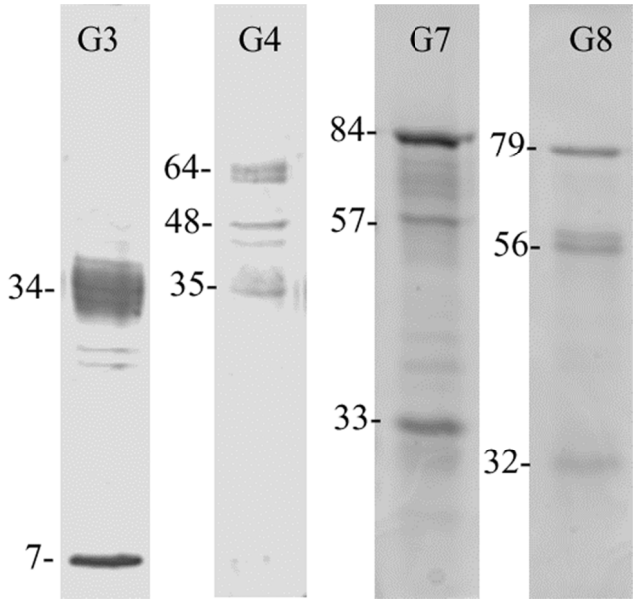

Figure 6.14: SDS-PAGE of *G. metallireducens* protein fractions isolated with preparative CN-PAGE. A 12 % acrylamide gel was used. After colloidal coomassie blue staining, the gel was scanned with a densitometer (Bio-Rad, GS 800) and the molecular weights calculated (Quanity One, Bio-Rad). G3, fraction 3; D4, fraction 4; D7, fraction 7; D8, fraction 8.

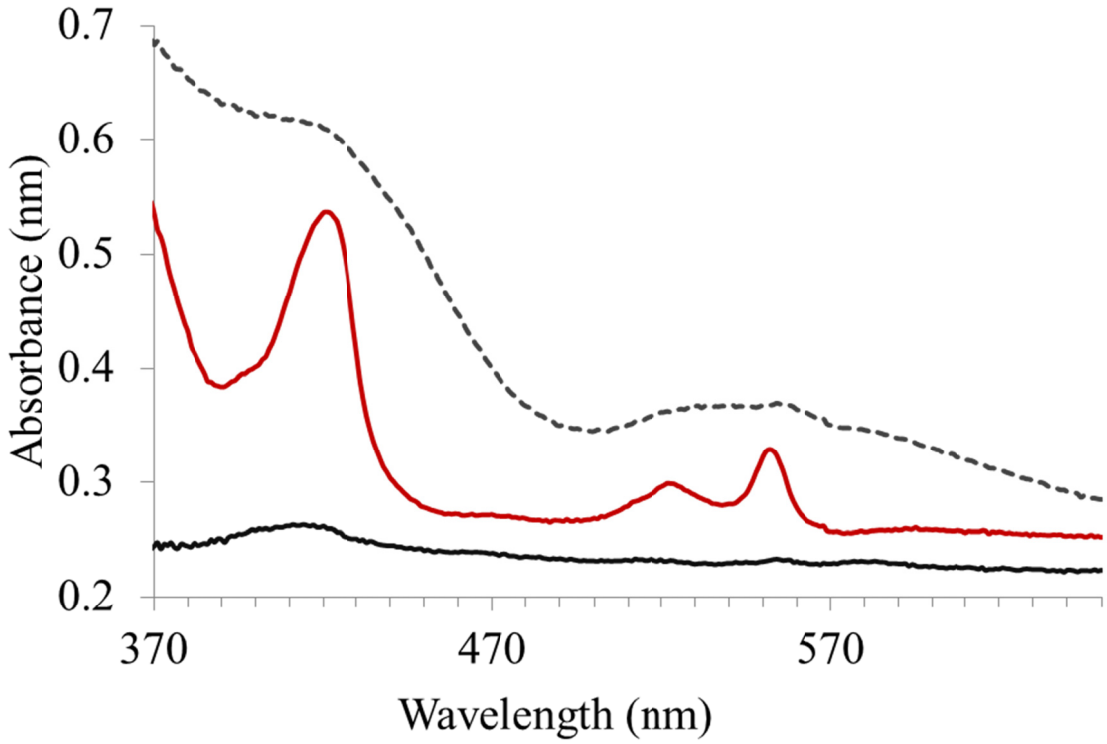

Figure 6.15: The electronic absorption spectra of the *G. metallireducens* pink heme enriched fraction. The as- isolated protein (black line), dithionite reduced (red line), and chromate oxidized (grey dashed line). The cytochrome protein (400 uL) was reduced after the addition of 60 uL of 0.1 M sodium dithionite, then re-oxidized by adding 20 uL 0.1M potassium chromate.

6.4. Conclusions

Nitrite reduction by the *S. barnesii* cell lysate was inhibited by chromate, but nitrate reduction was not inhibited, indicating that NrfA may be oxidized by chromate. *S. barnesii* is capable of reducing chromate. The in-gel chromate reductase assay indicates that a protein reduces chromate. The chromate reducing protein complex can also reduce nitrite. The protein complex was isolated using preparative CN-PAGE, and multiple proteins are present. The complex is more abundant in cells exposed to chromate during growth.

Several nitrite reducing proteins were separated from the CHAPS solubilized *D. desulfuricans* fraction. The major nitrite reductase was a c-type cytochrome, which can be monitored with in-gel activity assays. Similar to the *S. barnesii* nitrite reductase protein complex, the *D. desulfuricans* protein complex reduced nitrite and chromate, and is overexpressed in cells exposed to chromate during growth.

A siroheam containing, green protein was isolated from *D. desulfuricans*; the protein was identified as *Desulfovibrio vulgaris* dSiR, known as desulfoviridin. As reported in *D. vulgaris, D. desulfuricans* dSiR can reduce nitrite, and nitrite reduction is inhibited by chromate.

A "hypothetical" multi-heme cytochrome protein was isolated from *G. metallireducens*; the protein also can reduce nitrite.

Appendix V: Reagents and Protocols

Media

SES-3 nitrate medium (1 L):

- 980 ml distilled water (dH_2O)
- 0.23 g K_2HPO_4 (dibasic)
- 0.23 g KH_2PO_4 (monobasic)
- 0.46 g NaCl
- 0.23 g $(NH_4)_2SO_4$
- 0.12 g $MgSO_4$& $7H_2O$
- 10 g yeast extract
- 2.8 ml sodium lactate (60 % Solution)
- 4.2 g $NaHCO_3$
- 0.5 g cysteine
- 2 ml 500x trace elements (recipe below)
- 2 ml 500x vitamin mix (recipe below)
- 1.7 g Na NO^-_3

Vitamin Mix (500x)

- 980 mL of dH2O
- 0.01 g biotin
- 0.01 g folic acid
- 0.05 g pyridoxine hydrochloride
- 0.025 g riboflavin
- 0.025 g thiamine
- 0.025 g nicotinic acid
- 0.025 g pantothenic acid
- 0.025 g p-aminobenzoic acid
- 0.025 g thioctoc acid
- 0.0005 g vitamin B-12

Trace Elements (500x)

- 980 mL of d.H2O
- 7.55 g nitrilotriacectic acid (NTA)
- 15.0 g magnesium sulfate ($MgSO_4$)
- 2.55 g manganese chloride ($MnSO_4$)
- 5.0 g sodium chloride (NaCl)
- 0.5 g ferric sulfate ($FeSO_4$)
- 0.5 g calcium chloride ($CaCl_2$)
- 0.5 g cobalt chloride ($CoCl_2$)
- 0.5 g zinc sulfate ($ZnSO_4$)
- 0.05 g cupric sulfate ($CuSO_4$)
- 0.05 g aluminum potassium sulfate (Al K SO_4)
- 0.05 g boric acid (H_3BO_3)
- 0.25 g sodium molybdate (Na_2MoO_4)
- 0.12 g nickel chloride ($NiCl_2$)

LB media (1L)

- 10 g trypton
- 5 g yeast extract
- 5 g sodium chloride

LB Expression media (1L)

- LB media
- 1mM sodium molybdate (Na_2MoO_4)
- 25 μg/mL Kanamycin
- 100 μg/mL Ampicillin

Buffers

SES-3 lysis buffer
- 100 mM Tris-HCl pH 7.6
- 300 mM NaCl

Buffer A
- 10 mM Tris HCl
- 0.1% CHAPS
- Adjust to pH 7.5 with HCl

Buffer B
- 250 mM Tris HCl
- 0.1% CHAPS
- 300 mM NaCl
- Adjust to pH 7.5 with HCl

Ni-lysis buffer
- 50 mM KPO_4
- 300 mM NaCl
- 10 mM Imidazole
- pH 8.0

Ni-wash buffer
- 50 mM KPO_4
- 300 mM NaCl
- 30 mM Imidazole
- pH 7.0

Ni-elution buffer
- 50 mM KPO_4
- 300 mM NaCl
- 400 mM Imidazole
- pH 7.5

Electrophoresis

Protein electrophoresis

Sodium dodecyl sulfate-polyacrylamide gel electrophoresis (SDS/PAGE)

Resolving gel (10% acrylamide)
- 3.3 mL 30 % acrylamide (Bio Rad)
- 4.2 mL dH_2O
- 2.5 mL gel buffer (1.5 M Tris-HCl + 0.4% SDS pH 8.8)
- 10 uL Tetramethylethylenediamine (TEMED)
- 60 uL 10% Ammonium persulfate (AP)

Stacker gel (4% acrylamide)
- 670 uL 30% acrylamide (Bio Rad)
- 3.09 mL dH_2O
- 1.25 mL gel buffer (1.5 M Tris-HCl + 0.4% SDS pH 6.8)
- Add 5 uL TEMED
- 50 uL AP

Colloidal coomassie blue G-250 stain
- 0.1% coomassie G-250
- 2% H_3PO_4
- 5% methanol
- 10% $(NH_4)_2(SO_4)$

* Tris- glycine running buffer and Laemmli sample buffer were purchased from Bio-Rad laboratories.

CHAPS native-polyacrylamide gel electrophoresis (CN-PAGE)

Resolving gel (10% acrylamide)
- 3.3 mL 30 % acrylamide (Bio Rad)
- 4.2 mL dH_2O
- 2.5 mL gel buffer (1.5 M Tris-HCl pH 8.8 + 0.5% CHAPS)
- 10 uL Tetramethylethylenediamine (TEMED)
- 60 uL 10% Ammonium persulfate (AP)

Stacker gel (4% acrylamide)
- 670 uL 30% acrylamide (Bio Rad)
- 3.09 mL dH_2O
- 1.25 mL gel buffer (1.5 M Tris-HCl pH 6.8 + 0.5% CHAPS)
- Add 5 uL TEMED
- 50 uL AP

Cathode buffer (1L)
- 3 g Tris base
- 14.4 g glycine

Anode buffer
- 250 mL cathode buffer
- 0.25 g CHAPS

Preparative CN-PAGE sample buffer
- Dilute protein sample to 5.0 mL final volume with Tris-HCL (pH6.8)
- 3 mL glycerol
- 0.12 g CHAPS
- 1.0 mL dH_2O

DNA agarose gel electrophoresis

50x TAE DNA electrophoresis buffer (1L)

- 242 g Tris base
- 57.1 mL acetic acid
- 100 mL 0.5 M EDTA
- pH 8

1x TAE DNA electrophoresis gel

- 1% agarose
- 1x TAE buffer
- Ethidium bromide

Polymerase chain reaction (PCR)

Preparative PCR reaction mixture:

- 25 µL 2 x Ready mix (Sigma 098K6076: Tag poly, NT & buffer)
- 2.5 µL of forward primer stock [20 µM] (1 µM in final reaction)
- 2.5 µL of reverse primer stock [20 µM] (1 µM in final reaction)
- 0.5 µL PWO DNA polymerase 1 unit/ µL
- 10-50 ng DNA
- Dilute to 50 µL with PCR grade sterile water

PCR thermo cycling parameters:
Elongation time = X_t
Annealing Temp = X_T

1. Heated lid $110^{O}C$
2. 94 ^{o}C 4 min
3. 94 ^{o}C 45 sec
4. X_t ^{o}C 45 sec
5. 72 ^{o}C X_T sec
6. 25 cycles of steps 3- 5
7. 72 ^{o}C 41 sec
8. 4 ^{o}C final/ hold

Cloning protocols

Ligation reaction
- 10x T4 ligase buffer with 10 mM ATP (BioLabs, #B0202S)
- T4 DNA ligase (BioLabs, #M0202L)
- 1:4 ratio of vector to insert in 8 uL total
- 0.5 µL of 20 mM ATP

Colony PCR
- 10 µL 2 x Ready mix (Sigma 098K6076: Tag poly, NT & buffer)
- µL PCR grade sterile water
- 1 µL of forward primer stock [20 µM]
- 1 µL of reverse primer stock [20 µM]

Preparative restriction assay
- 48 µL DNA
- 14 µL Tango buffer
- 0.25 - 0.5 µL* RE Enzyme 1
- 0.25 - 0.5 µL * RE Enzyme 2
- Fill to 65 µL final volume with sterile water

* 0.25 µL XhoI, NcoI, EcoRI and BglII
*0.5 µL NdeI

Test restriction assay
- 1 µL buffer
- 2 µL plasmid
- 0.2 – 0.5 µL RE Enzyme
- Fill to 10 µL final volume with sterile water

Protein assays

Griess assay
- 100 µL sample
- 100 µL 1% sulfanilamide in 3N HCl
- 100 µL 0.02% N-(1-napthyl) ethylenediamine hydrochloride (NED) in H_2O

Methyl viologen coupled nitrate reductase assay
- 80-100 µg of protein
- 0.8 µM methylviologen
- 10 µM KNO_3^-

Assay buffer
- 100 mM TrisHCl adjusted to pH 8 with HCl
- 0.1mM CHAPS
- 1mM Na_2MoO_4
- Purged with N_2 gas

Sodium dithionite stock
- 60 mM sodium dithionite
- 100 mM Tris-HCl (pH 8), purged with N_2 gas

Methyl viologen stock
- 50 mL assay buffer, purged with N_2 gas
- 0.1 g methyl viologen (Sigma- Aldrich)
- Titrate with sodium dithionite stock solution to yield a final absorbance of 1.2– 1.6 at 630 nm

Mass spectroscopy techniques

Moco oxidation

Oxidation to FormA

- Dilute protein sample to a final volume of 140 µl with 100 mM Tris HCl (pH 7.2)
- add 17.5 µl of the following reagent: 1.5 % I_2, 2.0% KI-solution + 0.1 % HCl
- Incubate in the dark overnight at room temperature
- Centrifuge at 15000 rpm for 5 min at room temperature
- Remove the supernatant

Dephosphorylation

- add the supernatant to 20 µl freshly prepared 1% ascorbic acid
- add 70 µl of un-buffered Tris [1 M]
- add 5 µl 1 M $MgCl_2$
- add 5 µl alkaline phosphatase (1 to 10 dilution in 20 mM Tris pH 8.3)
- incubate in the dark for 30 min at room temperature
- Centrifuge at 15000 rpm for 5 min at room temperature
- Dilute 1 to 10 in fresh filtered water

Moco content determination:

To quantify molybdenum cofactor (Moco) content in the NapA protein, the molybdopterin molecule was converted to an oxidized form, dephospho-Form A, which can be detected by it characteristic emission spectra, as originally described by Johnson et al. [262]. (see oxidation protocol) The oxidized Form A was immediately separated via HPLC (Agilent 1200 rapid Resolution) at room temperature and detected fluorimetrically. The sample separation was performed on C4 reverse-phase column (4.6-mm inner diameter by 12.5 cm; 5-um particle size). The samples were eluted after applying a methanol gradient from 10 to 23 % at 2 ml min^{-1} in 10 mM Phosphate buffer. The dephospho-Form A was detected fluorimetrically (excitation, 370 nm; emission, 450 nm). The amount of Form A was quantified by integration of the fluorescent peak and compared with the integrated intensity of a standard compound. The standard Moco solution was purified with the same method from *chlamydomonas rheinharditii.*

Mass spectroscopy details (provided by Peter Chovanec)

Extracted peptides were desalted and concentrated with a ZipTip (Millipore Corporation) and eluted with a 1% formic acid and 50% methanol solution prior to mass spectrometry (MS) analysis. The MS analysis was performed using a quadrupole-time-of-flight (Q-TOF) LC/MS system (Agilent Technologies) equipped with a 1200 Series liquid chromatography, a chipcube MS interface, and a 6530 Q-TOF mass spectrometer. The instrument was operated under the Mass Hunter Data Acquisitions software (version B.02.01, Agilent Technologies). Peptides were separated on a 43 mm C18 chip with a 40 nL trap column (Protein ID chip #; G4240-62005; Agilent Technologies), and gradient elution was performed from 3% acetonitrile to 97% acetonitrile in 0.1% formic acid using a flow rate of 600 nL/min. Fragmentor voltage, skimmer voltage and OCT RF Vpp were set to 175 V, 65 V and 750 V, respectively. The following MS settings used were the: precursor ion selection, medium (4 m/z); mass range, 400−1500 m/z; acquisition rate MS, 3 scans/sec; acquisition rate MS/MS, 3 scans/s (m/z 50-3200); collision energy, 3 V/100 Da; offset, 2 V. Reference mass correction was activated using reference mass of 922.0098. All MS/MS raw spectra were processed by Qualitative analyses software version B.03.01 (Agilent Technologies) to generate peak lists (.mgf) and exported files were analyzed against the bacterial subset in the NCBI database using the Mascot program v2.3 (www.matrixscience.com). The MASCOT parameters were: enzyme: trypsine, fixed modification: carbamidomethyl (C), variable modification: oxidation (M), mass tolerance for the peptides was set to ±1 Da and ± 0.5 Da for MS/MS, 'max missed cleavages' set to 1 and peptide charge set at ´2+ and 3+´. Only proteins with 2 and more peptides with a $P < 0.05$ in search algorithm were reported.

Works cited

1. ChemicalComputingGroup: **Molecular Operating Environment (MOE)**. In., 2010.10 edn. Quebec, Canada; 2010.

2. Nicholas KB, NIcholas HB: **GeneDoc: multiple sequence alignment editor and shading utility**. In., 2.7.000 edn; 2006.

3. Key J, Hefti M, Purcell EB, Moffat K: **Structure of the redox sensor domain of *Azotobacter vinelandii* NifL at atomic resolution: Signaling, dimerization, and mechanism**. *Biochemistry* 2007, **46**(12):3614-3623.

4. Food and Nutrition Board IoM: **Molybdenum**. In: *Dietary reference intakes for vitamin A, vitamin K, boron, chromium, copper, iodine, iron, manganese, molybdenum, nickel, silicon, vanadium, and zinc.* Edited by Food and Nutrition Board IoM. Washington, D.C.: National Academy Press; 2001: 420-441.

5. Mendel RR, Bittner F: **Cell biology of molybdenum**. *Biochimica et Biophysica Acta* 2006, **1763**:621-635.

6. Mendel RR: **Molybdenum: biological activity and metabolism**. *Dalton Transactions* 2005(21):3404-3409.

7. Havemeyer A, Grünewald S, Wahl B, Bittner F, Mendel R, Erdélyi P, Fischer J, Clement B: **Reduction of N-hydroxy-sulfonamides, including N-hydroxy-valdecoxib, by the molybdenum-containing enzyme mARC**. *Drug Metabolism and Disposition* 2010, **38**(11):1917-1921.

8. Kotthaus J, Wahl B, Havemeyer A, Kotthaus J, Schade D, Garbe-Schönberg D, Mendel R, Bittner F, Clement B: **Reduction of Nω-hydroxy-L-arginine by the mitochondrial amidoxime reducing component (mARC)**. *Biochemical Journal* 2010, **433**(2):383-391.

9. Dekker M: **Molybdenum and Tungsten: Their Roles in Biological Processes**, vol. 39. New York; 2002.

10. Cvetkovic A, Menon AL, Thorgersen MP, Scott JW, Poole Ii FL, Jenney Jr FE, Lancaster WA, Praissman JL, Shanmukh S, Vaccaro BJ *et al*: **Microbial metalloproteomes are largely uncharacterized**. *Nature* 2010, **466**(7307):779-782.

11. Mendel RR: **Biology of the molybdenum cofactor**. *Journal of Experimental Botany* 2007, **58**(9):2289-2296.

12. Boll M, Schink B, Messerschmidt A, Kroneck PMH: **Novel bacterial molybdenum and tungsten enzymes: three-dimensional structure,**

spectroscopy, and reaction mechanism. *Biological Chemistry* 2005, **386**(10):999-1006.

13. Moura J, Brondino C, Trincão J, Romão M: **Mo and W *bis*-MGD enzymes: nitrate reductases and formate dehydrogenases**. *Journal of Biological Inorganic Chemistry* 2004 **9**(7):791-799.

14. Rothery RA, Workun GJ, Weiner JH: **The prokaryotic complex iron-sulfur molybdoenzyme family**. *Biochimica et Biophysica Acta (BBA) - Biomembranes* 2008, **1778**(9):1897-1929.

15. Hille R: **The Mononuclear Molybdenum Enzymes**. *Chemical Reviews* 1996, **96**(7):2757-2816.

16. Wahl B, Reichmann D, Niks D, Krompholz N, Havemeyer A, Clement B, Messerschmidt T, Rothkegel M, Biester H, Hille R *et al*: **Biochemical and Spectroscopic Characterization of the Human Mitochondrial Amidoxime Reducing Components hmARC-1 and hmARC-2 Suggests the Existence of a New Molybdenum Enzyme Family in Eukaryotes**. *Journal of Biological Chemistry* 2010, **285**(48):37847-37859.

17. Romão MJ: **Molybdenum and tungsten enzymes: a crystallographic and mechanistic overview**. *Dalton Transactions* 2009, **21**:4041-4260.

18. Schwarz G, Mendel RR, Ribbe MW: **Molybdenum cofactors, enzymes and pathways**. *Nature* 2009, **460**(7257):839-847.

19. Pushie MJ, George GN: **Spectroscopic studies of molybdenum and tungsten enzymes**. *Coordination Chemistry Reviews* 2011, **255**(9-10):1055-1084.

20. Schwarz G, Mendel RR: **Molybdenum cofactor biosynthesis and molybdenum enzymes**. *Annual Review of Plant Biology* 2006, **57**:623-647.

21. Noriega C, Hassett DJ, Rowe JJ: **The mobA gene is required for assimilatory and respiratory nitrate reduction but not xanthine dehydrogenase activity in *Pseudomonas aeruginosa***. *Current Microbiology* 2005, **51**(6):419-424.

22. Schwarz G, Santamaria-Araujo JA, Wolf S, Lee H-J, Adham IM, Grone H-J, Schwegler H, Sass JO, Otte T, Hanzelmann P *et al*: **Rescue of lethal molybdenum cofactor deficiency by a biosynthetic precursor from *Escherichia coli***. *Human Molecular Genetics* 2004, **13**(12):1249-1255.

23. Hine FJ, Taylor AJ, Garner CD: **Dithiolene complexes and the nature of molybdopterin**. *Coordination Chemistry Reviews* 2010, **254**(13-14):1570-1579.

24. Boyington JC, Gladyshev VN, Khangulov SV, Stadtman TC, Sun PD: **Crystal Structure of Formate Dehydrogenase H: Catalysis Involving Mo,**

Molybdopterin, Selenocysteine, and an Fe4S4 Cluster. *Science* 1997, **275**(5304):1305-1308.

25. Fischer B, Enemark JH, Basu P: **A chemical approach to systematically designate the pyranopterin centers of molybdenum and tungsten enzymes and synthetic models**. *Journal of Inorganic Biochemistry* 1998, **72**(1-2):13-21.

26. Hettmann T, Siddiqui RA, Langen Jv, Frey C, Romão MJ, Diekmann S: **Mutagenesis study on the role of a lysine residue highly conserved in formate dehydrogenases and periplasmic nitrate reductases**. *Biochemical and Biophysical Research Communications* 2003, **310**:40-47.

27. Enemark JH, Garner CD: **The coordination chemistry and function of the molybdenum centres of the oxomolybdoenzymes**. *Journal of Biological Inorganic Chemistry* 1997, **2**(6):817-822.

28. Kloer DP, Hagel C, Heider J, Schulz GE: **Crystal structure of ethylbenzene dehydrogenase from *Aromatoleum aromaticum***. *Structure* 2006, **14**(9):1377-1388.

29. Bertero MG, Rothery RA, Palak M, Hou C, Lim D, Blasco F, Weiner JH, Strynadka NCJ: **Insights into the respiratory electron transfer pathway from the structure of nitrate reductase A**. *Nature Structural Biology* 2003, **10**(9):681-687.

30. McEwan AG, Ridge JP, McDevitt CA, Hugenholtz P: **The DMSO reductase family of microbial molybdenum enzymes: Molecular properties and role in the dissimilatory reduction of toxic elements**. *Geomicrobiology Journal* 2002.

31. Bray RC, Adams B, Smith AT, Richards RL, Lowe DJ, Bailey S: **Reactions of Dimethylsulfoxide Reductase in the Presence of Dimethyl Sulfide and the Structure of the Dimethyl Sulfide-Modified Enzyme**. *Biochemistry* 2001, **40**(33):9810-9820.

32. Li H-K, Temple C, Rajagopalan KV, Schindelin H: **The 1.3 Å crystal structure of *Rhodobacter sphaeroides* dimethyl sulfoxide reductase reveals two distinct molybdenum coordination environments**. *Journal of the American Chemical Society* 2000, **122**(32):7673-7680.

33. Messerschmidt A, Niessen H, Abt D, Einsle O, Schink B, Kroneck PMH: **Crystal structure of pyrogallol–phloroglucinol transhydroxylase, an Mo enzyme capable of intermolecular hydroxyl transfer between phenols**. *Proceedings of the National Academy of Sciences of the United States of America* 2004, **101**(32):11571-11576.

34. Czjzek M, Dos Santos J-P, Pommier J, Giordano G, Méjean V, Haser R: **Crystal structure of oxidized trimethylamine N-oxide reductase from *Shewanella massilia* at 2.5 å resolution**. *Journal of Molecular Biology* 1998, **284**(2):435-447.

35. Ellis PJ, Conrads T, Hille R, Kuhn P: **Crystal Structure of the 100 kDa Arsenite Oxidase from *Alcaligenes faecalis* in Two Crystal Forms at 1.64 Å and 2.03 Å**. *Structure* 2001, **9**(2):125-132.

36. Raaijmakers H, Romão M: **Formate-reduced *E. coli* formate dehydrogenase H: the reinterpretation of the crystal structure suggests a new reaction mechanism**. *Journal of Biological Inorganic Chemistry* 2006, **11**(7):849-854.

37. Raaijmakers H, Macieira S, Dias JM, Teixeira S, Bursakov S, Huber R, Moura JJG, Moura I, Romão MJ: **Gene Sequence and the 1.8 Å Crystal Structure of the Tungsten-Containing Formate Dehydrogenase from *Desulfovibrio gigas***. *Structure* 2002, **10**(9):1261-1272.

38. Najmudin S, González P, Trincão J, Coelho C, Mukhopadhyay A, Cerqueira N, Romão C, Moura I, Moura J, Brondino C *et al*: **Periplasmic nitrate reductase revisited: a sulfur atom completes the sixth coordination of the catalytic molybdenum**. *Journal of Biological Inorganic Chemistry* 2008.

39. Dias JM, Than ME, Humm A, Huber R, Bourenkov GP, Bartunik HD, Bursakov S, Calvete J, Caldeira J, Carneiro C *et al*: **Crystal structure of the first dissimilatory nitrate reductase at 1.9 Å solved by MAD methods**. *Structure* 1999, **7**:65-79.

40. Coelho C, González PJ, Moura JJG, Moura I, Trincão J, João Romão M: **The Crystal Structure of *Cupriavidus necator* Nitrate Reductase in Oxidized and Partially Reduced States**. *Journal of Molecular Biology* 2011, **In Press, Uncorrected Proof**.

41. Arnoux P, Sabaty M, Alric J, Frangioni B, Guigliarelli B, Adriano J-M, Pignol D: **Structural and redox plasticity in the heterodimeric periplasmic nitrate reductase**. *Nature Structural Biology* 2003, **10**(11):928-924.

42. Jepson BJN, Mohan S, Clarke TA, Gates AJ, Cole JA, Butler CS, Butt JN, Hemmings AM, Richardson DJ: **Spectropotentiometric and structural analysis of the periplasmic nitrate reductase from *Escherichia coli*.** . *Journal of Biological Chemistry* 2007, **282**(9):6425-6437.

43. Jormakka M, Yokoyama K, Yano T, Tamakoshi M, Akimoto S, Shimamura T, Curmi P, Iwata S: **Molecular mechanism of energy conservation in polysulfide respiration**. *Nature Structural and Molecular Biology* 2008, **15**(7):730-737.

44. Jormakka M, Törnroth S, Byrne B, Iwata S: **Molecular basis of proton motive force generation: structure of formate dehydrogenase-N.** . *Science* 2002, **295**(5561):1863-1868.

45. Jormakka M, Richardson D, Byrne B, Iwata S: **Architecture of NarGH reveals a structural classification of Mo-*bis*MGD enzymes.** . *Structure* 2004, **12**(1):95-104.

46. Magalon A, Fedor JG, Walburger A, Weiner JH: **Molybdenum enzymes in bacteria and their maturation**. *Coordination Chemistry Reviews* 2011, **255**:1159-1178.

47. Richardson DJ, Berks BC, Russell DA, Spiro S, Taylor CJ: **Functional, biochemical and genetic diversity of prokaryotic nitrate reductases**. *Cellular and Molecular Life Sciences* 2001, **58**(2):165-178.

48. Zhang L, Nelson KJ, Rajagopalan KV, George GN: **Structure of the Molybdenum Site of Escherichia coli Trimethylamine N-Oxide Reductase**. *Inorganic Chemistry* 2007, **47**(3):1074-1078.

49. Stewart LJ, Bailey S, Bennett B, Charnock JM, Garner CD, McAlpine AS: **Dimethylsulfoxide reductase: an enzyme capable of catalysis with either molybdenum or tungsten at the active site**. *Journal of Molecular Biology* 2000, **299**(3):593-600.

50. Gates AJ, Hughes RO, Sharp SR, Millington PD, Nilavongse A, Cole JrA, Leach E-R, Jepso B, Richardson DJ, Butler CS: **Properties of the periplasmic nitrate reductases from *Paracoccus pantotrophus* and *Escherichia coli* after growth in tungsten-supplemented media**. *FEMS Microbiology Letters* 2003, **220**:261-269.

51. Dennis MJ, Wilson LA: **Nitatres and nitrites**. In: *Encyclopedia of Food Sciences and Nutrition.* Edited by Benjamin C. Oxford: Academic Press; 2003: 4136-4141.

52. Doel JJ, Nigel Benjamin, Hector MP, Michael Rogers, Allaker RP: **Evaluation of bacterial nitrate reduction in the human oral cavity.** . *European J Oral Sci* 2005, **113**(1):14-19.

53. Li H, Thompson I, Carter P, Whiteley A, Bailey M, Leifert C, Killham K: **Salivary nitrate - an ecological factor in reducing oral acidity.** . *Oral Microbiol Immunol* 2007, **22**(1):67-71.

54. Li H, Thompson I, Carter P, Whiteley A, Bailey M, Leifert C, Killham K: **Salivary nitrate - an ecological factor in reducing oral acidity.** . *Oral Microbiology and Immunology* 2007, **22**(1):67-71.

55. Parham NJ, Gibson GR: **Microbes involved in dissimilatory nitrate reduction in the human large intestine**. *FEMS Microbiology Ecology* 2000, **31**:21-28.

56. Forsythe SJ, Cole JA: **Nitrite accumulatin during anaerobic nitrate reduction by binary suspensions of bacteria isolated from the achlorhydric stomach**. *Journal of General Microbiology* 1987, **133**(7):1845-1849.

57. Forsythe SJ, Cole JA: **Nitrite accumulation during anaerobic nitrate reduction by binary suspensions of bacteria isolated from the achlorhydric stomach**. *J Gen Microbiol* 1987, **133**:1845-1849.

58. Allison C, Macfarlane GT: **Effect of nitrate on methane production and fermentation by slurries of human faecal bacteria**. *J Gen Microbiol* 1988, **134**:1397-1405.

59. Forsythe SJ, Dolby JM, Webster ADB, Cole JA: **Nitrate- and nitrite-reducing bacteria in the achlorhydric stomach**. *The Pathological Society of Great Britain and Ireland* 1998, **25**:253-259.

60. Duncan C, Li H, Dykhuizen R, Frazer R, Johnston P, MacKnight G, Smith L, Lamza K, McKenzie H, Batt L *et al*: **Protection against oral and gastrointestinal diseases: importance of dietary nitrate intake, oral nitrate reduction, and enterosalivary nitrate circulation**. *Comparative Biochemistry and Physiology - Part A: Molecular & Integrative Physiology* 1997, **118**:939-948.

61. Sellars MJ, Hall SJ, Kelly DJ: **Growth of *Campylobacter jejuni* supported by respiration of fumarate, nitrate, nitrite, trimethylamine-N-oxide, or dimethyl sulfoxide requires oxygen**. *Journal of Bacteriology* 2002, **184**(15):4187–4196.

62. Pittman MS, Kelly DJ: **Electron transport through nitrate and nitrite reductases in *Campylobacter jejuni***. *Biochemical Society Transactions* 2005, **33**(1):190-192.

63. Ward MH, Mark SD, Cantor KP, Weisenburger DD, Correa-Villaseor A, Zahn SH: **Drinking Water Nitrate and the Risk of Non-Hodgkin's Lymphoma**. *Epidemiology* 1996, **7**:465-471.

64. Hughes R, Rowland IR: **Metabolic activities of the gut microflora in relation to cancer**. *Microbial Ecology in Health and Disease* 2000, **12**(1):179 - 185.

65. Rowland RHaIR: **Metabolic activities of the gut microfora in relation to cancer**. *Microbial Ecology in Health and Disease* 2000, **Suppl 2**:179-185.

66. Griesenbeck J, Brender J, Sharkey J, Steck M, Huber J, Rene A, McDonald T, Romitti P, Canfield M, Langlois P *et al*: **Maternal characteristics associated with the dietary intake of nitrates, nitrites, and nitrosamines in women of child-bearing age: a cross-sectional study**. *Environmental Health* 2010, **9**(1):1-17.

67. Ward MH: **Too Much of a Good Thing? Nitrate from Nitrogen Fertilizers and Cancer**. *Reviews on Environmental Health* 2009, **24**(4):357-363.

68. Hord NG, Tang Y, Bryan NS: **Food sources of nitrates and nitrites: the physiologic context for potential health benefits**. *The American Journal of Clinical Nutrition* 2009, **90**(1):1-10.

69. Lundberg JO, Weitzberg E, Cole JA, Benjamin N: **Nitrate, bacteria and human health**. *Nature Reviews Microbiology* 2004, **2**:593-602.

70. Gladwin MT, Raat NJH, Shiva S, Dezfulian C, Hogg N, Kim-Shapiro DB, Patel RP: **Nitrite as a vascular endocrine nitric oxide reservoir that contributes to hypoxic signaling, cytoprotection, and vasodilation.** . *American Journal of Physiology* 2006, **291**(5):H2026-H2035.

71. Lundberg JO, Weitzberg E, Gladwin MT: **The nitrate-nitrite-nitric oxide pathway in physiology and therapeutics**. *Nature Reviews Drug Discovery* 2008, **7**(2):156-167.

72. Gladwin MTR, Nicolaas J. H.; Shiva, Sruti; Dezfulian, Cameron; Hogg, Neil; Kim-Shapiro, Daniel B.; Patel, Rakesh P. : **Nitrite as a vascular endocrine nitric oxide reservoir that contributes to hypoxic signaling, cytoprotection, and vasodilation.** . *Am J Physiol* 2006, **291**(5):H2026-H2035.

73. Claus SP, Ellero SL, Berger B, Krause L, Bruttin A, Molina J, Paris A, Want EJ, de Waziers I, Cloarec O *et al*: **Colonization-Induced Host-Gut Microbial Metabolic Interaction**. *mBio* 2011, **2**(2).

74. O'Hara AM, Shanahan F: **The gut flora as a forgotten organ**. *EMBO Reports* 2006, **7**(7):688-693.

75. Stolz JF, Basu P: **Evolution of nitrate reductase: molecular and structural variations on a common function.** *Chembiochem* 2002, **3**(2-3):198-206.

76. Zumft WG: **Cell Biology and Molecular Basis of Denitrification**. *MIcrobial and Molecular Biology Reviews* 1997, **61**(4):533-616.

77. Maria R, Martinez-Espinosa, Dridge EJ, Bonete MJ, Butt JN, Butler CS, Sargent F, Richardson DJ: **Look on the positive side! The orientation, identification and bioenergetics of 'Archaeal' membrane-bound nitrate reductases**. *FEMS Microbiology Letters* 2007, **276**(2):129-139.

78. Kern M, Simon J: **Electron transport chains and bioenergetics of respiratory nitrogen metabolism in *Wolinella succinogenes* and other Epsilonproteobacteria**. *Biochimica et Biophysica Acta - Bioenergetics* 2009, **1787**(6):646-656.

79. Sears HJ, Ferguson SJ, Richardson DJ, Spiro S: **The identification of a periplasmic nitrate reductase in *Paracoccus denitrificans***. *FEMS Microbiology Letters* 1993, **113**(1):107.

80. Tamegai H, Ikeda E, Kato C, Horikoshi K: **Identification of the functional periplasmic nitrate reductase (*nap*) gene cluster from the deep-sea denitrifier *Pseudomonas* sp. strain MT-1.** *Bioscience, Biotechnology, and Biochemistry* 2007, **71**(8):2041-2045.

81. Cruz-García C, Murray AE, Klappenbach JA, Stewart V, Tiedje JM: **Respiratory nitrate ammonification by *Shewanella oneidensis* MR-1**. *Journal of Bacteriology* 2007, **189**(2):656–662.

82. Richardson DJ: **Bacterial respiration: a flexible process for a changing environment**. *Microbiology* 2000, **146**(3):551-571.

83. Potter LC, Cole JA: **Essential roles for the products of the *napABCD* genes, but not *napFGH*, in periplasmic nitrate reduction by *Escherichia coli* K-12**. *Biochemical Journal* 1999, **344**:69-76.

84. Simon J, van Spanning RJM, Richardson DJ: **The organisation of proton motive and non-proton motive redox loops in prokaryotic respiratory systems**. *Biochimica et Biophysica Acta (BBA) - Bioenergetics* 2008, **1777**(12):1480-1490.

85. Delgado MJ, Bonnard N, Tresierra-Ayala A, Bedmar EJ, Muller P: **The *Bradyrhizobium japonicum napEDABC* genes encoding the periplasmic nitrate reductase are essential for nitrate respiration**. *Microbiology* 2003, **149**(12):3395-3403.

86. Kern M, Mager AM, Simon J: **Role of individual nap gene cluster products in NapC-independent nitrate respiration of *Wolinella succinogenes***. *Microbiology* 2007, **153**(Pt 11):3739-3747.

87. Cooksley C, Jenks PJ, Green A, Cockayne A, Logan RPH, Hardie KR: **NapA protects *Helicobacter pylori* from oxidative stress damage, and its production is influenced by the ferric uptake regulator**. *Journal of Medical Microbiology* 2003, **52**:461-469.

88. Weingarten RA, Grimes JL, Olson JW: **Role of *Campylobacter jejuni* Respiratory Oxidases and Reductases in Host Colonization**. *Applied and Environmental Microbiology* 2008, **74**(5):1367-1375.

89. Vegge CS, Brondsted L, Li Y-P, Bang DD, Ingmer H: ***Campylobacter jejuni* is driven by energy taxis towards the most favorable conditions for growth**. *Applied and Environmental Microbiology* 2009:AEM.00287-00209.

90. Spiro S: **Regulators of bacterial responses to nitric oxide**. *FEMS Microbiology Reviews* 2007, **31**(2):193-211.

91. Taveirne ME, Sikes ML, Olson JW: **Molybdenum and tungsten in *Campylobacter jejuni*: their physiological role and identification of separate transporters regulated by a single ModE-like protein**. *Molecular Microbiology* 2009, **74**(3):758-771.

92. Schwintner C, Sabaty M, Berna B, Cahors S, Richaud P: **Plasmid content and localization of the genes encoding the denitrification enzymes in two strains of *Rhodobacter sphaeroides***. *FEMS Microbiology Letters* 1998, **165**(2):313-321.

93. Siddiqui RA, Warnecke-Eberz U, Hengsberger A, Schneider B, Kostka S, Friedrich B: **Structure and function of a periplasmic nitrate reductase in *Alcaligenes eutrophus* H16**. *Journal of Bacteriology* 1993, **175**(18):5867-5876.

94. Coelho C, González PJ, Trincão J, Carvalho AL, Najmudin S, Hettman T, Dieckman S, Moura JJG, Moura I, Romão MJ: **Heterodimeric nitrate reductase (NapAB) from *Cupriavidus necator* H16: purification, crystallization and preliminary X-ray analysis**. *Crystallization Communications* 2007, **63**(6):516-519.

95. Simpson PJ, Richardson DJ, Codd R: **The periplasmic nitrate reductase in *Shewanella*: the resolution, distribution and functional implications of two NAP isoforms, NapEDABC and NapDAGHB**. *Microbiology* 2010, **156**(Pt 2):302-312.

96. Simpson PJ, McKinzie AA, Codd R: **Resolution of two native monomeric 90kDa nitrate reductase active proteins from *Shewanella gelidimarina* and the sequence of two napA genes**. *Biochemical and biophysical research communications* 2010, **398**(1):13-18.

97. Marietou A, Richardson DJ, Cole J, Mohan S: **Nitrate reduction by *Desulfovibrio desulfuricans*: a periplasmic nitrate reductase system that lacks NapB, but includes a unique tetraheme c-type cytochrome, NapM**. *FEMS Microbiology Letters* 2005, **248**:217-225.

98. González PJ, Correia C, Moura I, Brondino CD, Moura JJG: **Bacterial nitrate reductases: Molecular and biological aspects of nitrate reduction**. *Journal of Inorganic Biochemistry* 2006, **100**(5-6):1015-1023.

99. Stewart V: **Nitrate regulation of anaerobic respiratory gene expression in *Escherichia coli***. *Molecular Mircobiology* 1993, **9**(3):425-434.

100. Stewart V: **Regulation of nitrate and nitrite reductase synthesis in enterobacteria**. *Antonie van Leeuwenhoek* 1994, **66**(1):37-45.

101. Rabin VSaRS: **Dual sensors and dual response regulators interact to control nitrate- and nitrite- responsive gene expression in *Esherichia coli***. In: *Two-Component Signal Transduction.* Edited by James A. Hoch TJS: ASM Press; 1995.

102. Teixidó L, Pilar Cortés, Anna Bigas, Gerard Àlvarez, Jordi Barbé, Campo S: **Control by Fur of the nitrate respiration regulators NarP and NarL in *Salmonella enterica***. *International microbiology* 2010, **13**:33-39.

103. Wang H, Tseng C-P, Gunsalus RP: **The *nap*F and *nar*G nitrate reductase operons in *Escherichia coli* are differentially expressed in response to submicromolar concentrations of nitrate but not nitrite**. *Journal of Bacteriology* 1999, **181**:5303-5308.

104. Potter LC, Millington P, Griffiths L, Thomas GH, Cole JA: **Competition between *Escherichia coli* strains expressing either a periplasmic or a membrane-bound nitrate reductase: does Nap confer a selective advantage during nitrate-limiting growth?** *Biochem J* 1999, **344**:77- 84.

105. Stewart V, Lu Y, Darwin AJ: **Periplasmic nitrate reductase (Nap ABC Enzyme) supports anaerobic respiration by *Escherichia coli* K-12**. *Journal of Bacteriology* 2002, **184**:1314-1323.

106. Thomas GH: **New roles for nitrate reductases**. *Trends In Microbiol* 2000, **8**:15.

107. Robles EF, Sanchez C, Bonnard N, Delgado MJ, Bedmar EJ: **The *Bradyrhizobium japonicum napEDABC* genes are controlled by the FixLJ-FixK(2)-NnrR regulatory cascade**. *Biochemical Society Transactions* 2006, **34**(Pt 1):108-110.

108. Mesa S, Hauser F, Friberg M, Malaguti E, Fischer H-M, Hennecke H: **Comprehensive assessment of the regulons controlled by the FixLJ-FixK,-FixK1 cascade in *Bradyrhizobium japonicum***. *Journal of Bacteriology* 2008, **190**(20):12.

109. Sears HJ, Sawers G, Berks BC, Ferguson SJ, Richardson DJ: **Control of periplasmic nitrate reductase gene expression (*napEDABC*) from *Paracoccus pantotrophus* in response to oxygen and carbon substrates**. *Microbiology* 2000, **146 (Pt 11)**:2977-2985.

110. Gavira M, RoldÃ¡n MD, Castillo F, Moreno-ViviÃ¡n C: **Regulation of nap gene expression and periplasmic nitrate reductase activity in the phototrophic bacterium *Rhodobacter sphaeroides* DSM158**. *Journal of Bacteriology* 2002, **184**(6).

111. Ellington MJ, Bhakoo KK, Sawers G, Richardson DJ, Ferguson SJ: **Hierarchy of carbon source selection in *Paracoccus pantotrophus*: strict correlation between reduction state of the carbon substrate and aerobic expression of the *nap* operon**. *Journal of Bacteriology* 2002, **184**(17):4767-4774.

112. Ellington MJ, Fosdike WL, Sawers RG, Richardson DJ, Ferguson SJ: **Regulation of the *nap* operon encoding the periplasmic nitrate reductase of *Paracoccus pantotrophus*: delineation of DNA sequences required for redox control**. *Archives of Microbiology* 2006, **184**(5):298-304.

113. Rabin RS, Stewart V: **Dual response regulators (NarL and NarP) interact with dual sensors (NarX and NarQ) to control nitrate- and nitrite-regulated gene expression in *Escherichia coli* K-12**. *Journal of Bacteriology* 1993, **175**(11):3259-3268.

114. Stewart V, Bledsoe PJ, Chen L-L, Cai A: **Catabolite Repression Control of napF (Periplasmic Nitrate Reductase) Operon Expression in *Escherichia coli* K-12**. *Journal of Bacteriology* 2009, **191**(3):996-1005.

115. Giel JL, Rodionov D, Liu M, Blattner FR, Kiley PJ: **IscR-dependent gene expression links iron-sulphur cluster assembly to the control of O2-regulated genes in *Escherichia coli***. *Molecular Microbiology* 2006, **60**(4):1058-1075.

116. Anderson LA, McNairn E, Leubke T, Pau RN, Boxer DH: **ModE-Dependent Molybdate Regulation of the Molybdenum Cofactor Operon moa in *Escherichia coli***. *Journal of Bacteriology* 2000, **182**(24):7035-7043.

117. Mouncey NJ, Mitchenall LA, Pau RN: **The *modE* gene product mediates molybdenum-dependent expression of genes for the high-affinity molybdate transporter and *modG* in *Azotobacter vinelandii***. *Microbiology* 1996, **142**(8):1997-2004.

118. Stewart V, Bledsoe PJ, Williams SB: **Dual overlapping promoters control *napF* (periplasmic nitrate reductase) operon expression in *Escherichia coli* K-12**. *Journal of Bacteriology* 2003, **185**(19):5862-5870.

119. McNicholas PM, Gunsalus RP: **The molybdate-responsive *Escherichia coli* ModE transcriptional regulator coordinates periplasmic nitrate reductase (*napFDAGHBC*) operon expression with nitrate and molybdate availability**. *Journal of Bacteriology* 2002, **184**(12):3253-3259.

120. Palyada K, Threadgill D, Stintzi A: **Iron acquisition and regulation in *Campylobacter jejuni***. *Journal of Bacteriology* 2004, **186**(14):4714-4729.

121. Holmes K, Mulholland F, Pearson BM, Pin C, McNicholl-Kennedy J, Ketley JM, Wells JM: ***Campylobacter jejuni* gene expression in response to iron limitation and the role of Fur**. *Microbiology* 2005, **151**(1):243-257.

122. Sampathkumar B, Napper S, Carrillo CD, Willson P, Taboada E, Nash JHE, Potter AA, Babiuk LA, Allan BJ: **Transcriptional and translational expression patterns associated with immobilized growth of *Campylobacter jejuni***. *Microbiology* 2006, **152**(2):567-577.

123. Woodall CA, Jones MA, Barrow PA, Hinds J, Marsden GL, Kelly DJ, Dorrell N, Wren BW, Maskell DJ: ***Campylobacter jejuni* Gene Expression in the Chick Cecum: Evidence for Adaptation to a Low-Oxygen Environment**. *Infection and Immunity* 2005, **73**(8):5278-5285.

124. Stintzi A: **Gene expression profile of *Campylobacter jejuni* in response to growth temperature variation**. *Journal of Bacteriology* 2003, **185**(6):2009-2016.

125. Pignol D, Adriano J-M, Fontecilla-Camps J-C, Sabaty M: **Crystallization and preliminary X-ray analysis of the periplasmic nitrate reductase (NapA & NapB complex) from *Rhodobacter sphaeroides* f. sp. *denitrificans***. *Acta Crystallographica Section D* 2001, **57**(12):1900-1902.

126. Jepson BJN, Marietout A, Mohan S, Cole JA, Butler CS, Richardson DJ: **Evolution of the soluble nitrate reductase: defining the monomeric periplasmic nitrate reductase subgroup.** *Biochemical Society Transactions* 2006, **36**(1):122-126.

127. Reyes F, Gavira M, Castillo F, Moreno-Vivián C: **Periplasmic nitrate-reducing system of the phototrophic bacterium *Rhodobacter sphaeroides* DSM 158: transcriptional and mutational analysis of the *napKEFDABC* gene cluster**. *Biochemical Journal* 1998, **331**(3):897-904.

128. Ilbert M, Méjean V, Giudici-Orticoni M-T, Samama J-P, Iobbi-Nivol C: **Involvement of a mate chaperone (TorD) in the maturation pathway of molybdoenzyme TorA**. *Journal of Biological Chemistry* 2003, **278**(31):28787-28792.

129. Hatzixanthis K, Clarke TA, Oubrie A, Richardson DJ, Turner RJ, Sargent F: **Signal peptide–chaperone interactions on the twin-arginine protein transport pathway**. *Proceedings of the National Academy of Sciences of the United States of America* 2005, **102**(24):8460-8465.

130. Buchanan G, Maillard J, Nabuurs SB, Richardson DJ, Palmer T, Sargent F: **Features of a twin-arginine signal peptide required for recognition by a Tat proofreading chaperone**. *FEBS Letters* 2008, **582**(29):3979-3984.

131. Maillard J, Spronk CAEM, Buchanan G, Lyall V, Richardson DJ, Palmer T, Vuister GW, Sargent F: **Structural diversity in twin-arginine signal peptide-binding proteins**. *Proceedings of the National Academy of Sciences* 2007, **104**(40):15641-15646.

132. Thyssen A, Grisez L, Van Houdt R, Ollevier F: **Phenotypic characterization of the marine pathogen *Photobacterium damselae* subsp. *piscicida***. *International Journal of Systematic Bacteriology* 1998, **48**(4):1145-1151.

133. Alfredsson GA, Kristjansson JK, Hjorleifsdottir S, Stetter KO: ***Rhodothermus marinus*, gen. nov., sp. nov., a Thermophilic, Halophilic Bacterium from Submarine Hot Springs in Iceland**. *Journal of General Microbiology* 1988, **134**(2):299-306.

134. Knauber T, Doss SD, Gerth K, Perlova O, Müller R, Treuner-Lange A: **Mutation in the *rel* gene of *Sorangium cellulosum* affects morphological and physiological differentiation**. *Molecular Microbiology* 2008, **69**(1):254-266.

135. Sanford RA, Cole JR, Tiedje JM: **Characterization and description of *Anaeromyxobacter dehalogenans* gen. nov., sp. nov., an aryl-halorespiring facultative anaerobic myxobacterium**. *Applied and Environmental Microbiology* 2002, **68**(2):893-900.

136. Kern M, Mager AM, Simon J: **Role of individual *nap* gene cluster products in NapC-independent nitrate respiration of *Wolinella succinogenes***. *Microbiology* 2007, **153**:3739–3747.

137. Brondijk TH, Fiegen D, Richardson DJ, Cole JA: **Roles of NapF, NapG and NapH, subunits of the Escherichia coli periplasmic nitrate reductase, in ubiquinol oxidation**. *Molecular Microbiology* 2002, **44**(1):245-255.

138. Nilavongse A, Brondijk THC, Overton TW, Richardson DJ, Leach ER, Cole JA: **The NapF protein of the *Escherichia coli* periplasmic nitrate reductase system: demonstration of a cytoplasmic location and interaction with the catalytic subunit, NapA**. *Microbiology* 2006, **152**:3227-3237.

139. Kern M, Simon J: **Periplasmic nitrate reduction in *Wolinella succinogenes*: cytoplasmic NapF facilitates NapA maturation and requires the menaquinol dehydrogenase NapH for membrane attachment**. *Microbiology* 2009, **155**(Pt 8):2784-2794.

140. Olmo-Mira MF, Gavira M, Richardson DJ, Castillo F, Moreno-Vivian C, Roldan MD: **NapF Is a cytoplasmic iron-sulfur protein required for Fe-S cluster assembly in the periplasmic nitrate reductase**. *The Journal of Biological Chemistry* 2004, **279**(48):49727-49735.

141. Pittman MS, Elvers KT, Lee L, Jones MA, Poole RK, Park SF, Kelly DJ: **Growth of *Campylobacter jejuni* on nitrate and nitrite: electron transport to NapA and NrfA via NrfH and distinct roles for NrfA and the globin Cgb in protection against nitrosative stress**. *Molecular Microbiology* 2007, **63**(2):575-590.

142. Marietou A, Griffiths L, Cole J: **Preferential reduction of the thermodynamically less favorable electron acceptor, sulfate, by a nitrate-reducing strain of the sulfate-reducing bacterium *Desulfovibrio desulfuricans* 27774**. *Journal of Bacteriology* 2009, **191**(3):882-889.

143. Brigé A, Leys D, Meyer TE, Cusanovich MA, Beeumen JJV: **The 1.25 Å resolution structure of the diheme NapB subunit of soluble nitrate reductase reveals a novel cytochrome c fold with a stacked heme arrangement**. *Biochem* 2002, **41**:4827-4836.

144. Brigé A, Cole JA, Hagen WR, Guisez Y, Van Beeumen JJ: **Overproduction, purification and novel redox properties of the dihaem cytochrome c, NapB, from *Haemophilus influenzae***. *Biochemical Journal* 2001, **356**(Pt 3):851-858.

145. Berks BC, Richardson DJ, Reilly A, Willis AC, Ferduson SJ: **The *napEDABC* gene cluster encoding the periplasmic nitrate reductase system of *Thiosphaera pantotropha***. *Biochemical Journal* 1995, **309**:983-992.

146. Arnoux P, Sabaty M, Alric J, Frangioni B, Guigliarelli B, Adriano J-M, Pignol D: **Structural and redox plasticity in the heterodimeric periplasmic nitrate reductase,"** *Nature Struct Biol* 2003, **10**(11):928-924.

147. Jepson BJN, Mohan S, Clarke TA, Gates AJ, Cole JA, Butler CS, Butt JN, Hemmings AM, Richardson DJ: **Spectropotentiometric and structural analysis of the periplasmic nitrate reductase from *Escherichia coli.*** . *J Biol Chem* 2007, **282**(9):6425-6437.

148. Wooldridge KG, Vliet AHMv: **Iron Transport and Regulation**. In: *Campylobacter: molecular and cellular biology*. Edited by K. ME, Ketley JM. Wymondham, UK: Horizon Scientific Press; 2005.

149. Cartron ML, Roldán MD, Ferguson SJ, Berks BC, Richardson DJ: **Identification of two domains and distal histidine ligands to the four haems in the bacterial c-type cytochrome NapC; the prototype connector between quinol/quinone and periplasmic oxido-reductases**. *Biochemical Journal* 2002, **368**:425-432.

150. Gross R, Eichler R, Simon J: **Site-directed modifications indicate differences in axial haem c iron ligation between the related NrfH and NapC families of multihaem c-type cytochromes**. *Biochemical Journal* 2005, **390**(3):689-693.

151. Simon J, Gross R, Einsle O, Kroneck PMH, Kröger A, Klimmek O: **A NapC/NirT-type cytochrome c (NrfH) is the mediator between the quinone pool and the cytochrome c nitrite reductase of Wolinella succinogenes**. *Molecular Microbiology* 2000, **35**(3):686-696.

152. Myers C, Myers J: **Cloning and sequence of cymA, a gene encoding a tetraheme cytochrome c required for reduction of iron(III), fumarate, and nitrate by *Shewanella putrefaciens* MR-1**. *Journal of Bacteriology* 1997, **179**(4):1143-1152.

153. Brondijk THC, Nilavongse A, Filenko N, Richardson DJ, Cole JA: **NapGH components of the periplasmic nitrate reductase of *Escherichia coli* K-12: location, topology and physiological roles in quinol oxidation and redox balancing**. *Biochemical Journal* 2004, **379**(Pt 1):47-55.

154. Kern M, Simon J: **Characterization of the NapGH quinol dehydrogenase complex involved in *Wolinella succinogenes* nitrate respiration**. *Molecular Microbiology* 2008, **69**(5):1137-1152.

155. Oremland RS, Blum JS, Culbertson CW, Visscher PT, Miller LG, Dowdle P, Strohmaier FE: **Isolation, growth, and metabolism of an obligately anaerobic,**

selenate-respiring bacterium, strain SES-3. *Applied Environmental Microbiology* 1994, **60**(8):3011-3019.

156. Oremland RS, Hollibaugh JT, Maest AS, Presser TS, Miller LG, Culbertson CW: **Selenate reduction to elemental selenium by anaerobic bacteria in sediments and culture: Biogeochemical significance of a novel, sulfate-independent respiration**. *Applied and Environmental Microbiology* 1989, **55**(9):2333-2343.

157. Laverman AM, Switzer Blum J, Schaefer JK, Phillips EJP, Lovley DR, Oremland RS: **Growth of strain SES-3 with arsenate and other diverse electron acceptors**. *Applied and Environmental Microbiology* 1995, **61**:3556-3561.

158. Stolz JF, Oremland RS, Paster BJ, Dewhirst FE, VanDamme P: **Genus *Sulfurospirillum***. *Bergey's Manual of Systematic Bacteriology* 2002, **2**.

159. Stolz JF, Basu P, Santini JM, Oremland RS: **Arsenic and selenium in microbial metabolism**. *Annual Review of Microbiology* 2006, **60**(1):107-130.

160. Stolz J, Oremland R, Paster B, Dewhirst F, Vandamme P: **Genus III. *Sulfurospirillum*** In: *Bergey's Manual® of Systematic Bacteriology*. 2005: 1165-1168.

161. Oremland RS, Blum JS, Bindi AB, Dowdle PR, Herbel M, Stolz JF: **Simultaneous reduction of nitrate and selenate by cell suspensions of selenium-respiring bacteria**. *Applied and Environmental Microbiology* 1999, **65**(10):4385-4392.

162. Hubert C, Voordouw G: **Oil Field Souring Control by Nitrate-Reducing *Sulfurospirillum* spp. That Outcompete Sulfate-Reducing Bacteria for Organic Electron Donors**. *Applied and Environmental Microbiology* 2007, **73**(8):2644-2652.

163. Lenz M, Enright A, O'Flaherty V, van Aelst A, Lens P: **Bioaugmentation of UASB reactors with immobilized *Sulfurospirillum barnesii*; for simultaneous selenate and nitrate removal**. *Applied Microbiology and Biotechnology* 2009, **83**(2):377-388.

164. Stolz JF, Basu P: **Evolution of nitrate reductase: molecular and structural variations on a common theme.** 2002, **3**:198-206.

165. Richardson DJ, Berks BC, Russell DA, Spiro S, Taylor CJ: **Functional, biochemical and genetic diversity of prokaryotic nitrate reductase.** *Cell Mol Life Sci* 2001, **58**:165-178.

166. Sadana JC, McElroy WD: **Nitrate reductase from *Achromobacter fischeri*. Purification and properties: Function of flavines and cytochrome**. *Archives of Biochemistry and Biophysics* 1957, **67**(1):16-34.

167. Berks BC, Richardson DJ, Robinson C, Reilly A, Aplin RT, Ferguson SJ: **Purification and characterization of the periplasmic nitrate reductase from *Thiosphaera pantotropha***. *European Journal of Biochemistry* 1994, **220**(1):117-124.

168. Bursakov S, Liu M-Y, Paynel WJ, LeGall J, Moura I, Moura JJG: **Isolation and preliminary characterization of a soluble nitrate reductase from the sulfate reducing organism *Desulfovibrio desulfuricans* ATCC 27774**. *Anaerobe* 1995, **1**:55-60.

169. Stolz JF, Gugliuzza T, Blum JS, Oremland R, Murillo FM: **Differential cytochrome content and reductase activity in *Geospirillum barnesii* strain SeS3**. *Archives of microbiology* 1997, **167**(1):1-5.

170. Scopes RK: **Proteins Purification: Principles and Practice**, 3rd edn. New York, NY: Springer Science + Business Media, LLC; 1993.

171. Dementin S, Arnoux P, Frangioni B, Grosse S, Léger C, Burlat B, Guigliarelli B, Sabaty M, Pignol D: **Access to the Active Site of Periplasmic Nitrate Reductase: Insights from Site-Directed Mutagenesis and Zinc Inhibition Studies**. *Biochemistry* 2007, **46**(34):9713-9721.

172. Ridley H, Watts CA, Richardson DJ, Butler CS: **Development of a viologen-based microtiter plate assay for the analysis of oxyanion reductase activity: Application to the membrane-bound selenate reductase from *Enterobacter cloacae* SLD1a-1**. *Analytical biochemistry* 2006, **358**(2):289-294.

173. Watanabe T, Honda K: **Measurement of the extinction coefficient of the methyl viologen cation radical and the efficiency of its formation by semiconductor photocatalysis**. *The Journal of Physical Chemistry* 1982, **86**(14):2617-2619.

174. Motulsky HJ: **Prism v 5.01**. In. San Diego CA: GraphPad Software; 2007.

175. Griess P: **Bemerkungen zu der Abhandlung der HH. Weselsky und Benedikt Ueber einige Azoverbindungen**. *Berichte der deutschen chemischen Gesellschaft* 1879, **12**(1):426-428.

176. Laemmli UK: **Cleavage of structural proteins during the assembly of the head of bacteriophage T4**. *Nature* 1970, **227**(5259):680-685.

177. Watts CA, Ridley H, Dridge EJ, Leaver JT, Reilly AJ, Richardson DJ, Butler CS: **Microbial reduction of selenate and nitrate: common themes and variations**. In: *10th Nitrogen Cycle Meeting 2004: Feb , 2005 2005*; 2005: 173-175.

178. Stolz JF, Oremland RS: **Bacterial respiration of arsenic and selenium**. *FEMS Microbiology Reviews* 1999, **23**(5):615-627.

179. Sabaty M, Avazari C, Pignol D, Vermeg A: **Characterization of the reduction of selenate and tellurite by nitrate reductases**. *Applied and environmental microbiology* 2001, **11**.

180. Mayhew SG: **The redox potential of dithionite and SO^{-2} from equilibrium reactions with flavodoxins, methyl viologen and hydrogen plus hydrogenase**. *European Journal of Biochemistry* 1978, **85**(2):535-547.

181. Jordan A, Reichard P: **Ribonuleotide reductases** *Annual Review of Biochemistry* 1998, **67**(1):71-98.

182. Nakamura R, Ishii K, Hashimoto K: **Electronic absorption spectra and redox properties of *c*-type cytochromes in living microbes**. *Angewandte Chemie International Edition* 2009, **48**(9):1606-1608.

183. Sellars MJ, Hall SJ, Kelly DJ: **Growth of *Campylobacter jejuni* supported by respiration of fumarate, nitrate, nitrite, trimethylamine-N-oxide, or dimethyl sulfoxide requires oxygen**. *J Bacteriol* 2002, **184**(15):4187-4196.

184. Reid AN, Pandey R, Palyada K, Naikare H, Stintzi A: **Identification of *Campylobacter jejuni* Genes Involved in the Response to Acidic pH and Stomach Transit**. *Applied and Environmental Microbiology* 2008, **74**(5):1583-1597.

185. Bedzyk L, Wang T, Ye RW: **The periplasmic nitrate reductase in *Pseudomonas* sp. strain G-179 catalyzes the first step of denitrification**. *Journal of Bacteriology* 1999, **181**(9):2802-2806.

186. Sambrook J, Fritsch EF, Maniatis T: . In: *Molecular Cloning, A Laboratory Manual.* 2nd edn. New York; 1989.

187. Fouts DE, Mongodin EF, Mandrell RE, Miller WG, Rasko DA, Ravel J, Brinkac LM, DeBoy RT, Parker CT, Daugherty SC *et al*: **Major structural differences and novel potential virulence mechanisms from the genomes of multiple campylobacter species**. *PLoS Biol* 2005, **3**:72-85.

188. Stolz JF, Ellis DJ, Blum JS, Ahmann D, Lovley DR, Oremland RS: ***Sulfurospirillum barnesii* sp. nov. and *Sulfurospirillum arsenophilum* sp. nov., new members of the *Sulfurospirillum* clade of the epsilon Proteobacteria.** *International Journal of Systematic Bacteriology* 1999, **49**:1177-1180.

189. Vogelstein B, Gillespie D: **Prepartive and analytical purification of DNA from agarose**. *Proceedings of the National Academy of Sciences* 1979, **76**:615-619.

190. Manske M: **GENtle**. In.; 2004-2008.

191. French C, Keshavarz-Moore E, Ward JM: **Development of a simple method for the recovery of recombinant proteins from the *Escherichia coli* periplasm**. *Enzyme and Microbial Technology* 1996, **19**(5):332-338.

192. Shevchenko A, Tomas H, Havlis J, Olsen JV, Mann M: **In-gel digestion for mass spectrometric characterization of proteins and proteomes**. *Nat Protoc* 2006, **1**(6):2856-2860.

193. Johnson LJ, Hainline BE, Arison BH, Rajagopalan KV: *J Biol Chem* 1984, **259**:5414–5422.

194. Sargent F, Berks B, Palmer T: **Assembly of membrane-bound respiratory complexes by the Tat protein-transport system**. *Archives of Microbiology* 2002, **178**(2):77-84.

195. van Mourik A, Bleumink-Pluym NM, van Dijk L, van Putten JP, Wosten MM: **Functional analysis of a *Campylobacter jejuni* alkaline phosphatase secreted via the Tat export machinery**. *Microbiology* 2008, **154**(Pt 2):584-592.

196. Cotter PA, Gunsalus RP: **Oxygen, nitrate, and molybdenum regulation of *dmsABC* gene expression in *Escherichia coli***. *Journal of Bacteriology* 1989, **171**(7):3817-3823.

197. Pollock VV, Barber MJ: **Biotin Sulfoxide Reductase**. *The Journal of Biological Chemistry* 1997, **272**(6):3355-3362.

198. Lindenstrauß U, Brüser T: **Tat transport of linker-containing proteins in *Escherichia coli***. *FEMS Microbiology Letters* 2009, **295**(1):135-140.

199. Lanciano P, Vergnes A, Grimaldi S, Guigliarelli B, Magalon A: **Biogenesis of a respiratory complex is orchestrated by a single accessory protein**. *The Journal of Biological Chemistry* 2007, **282**(24):17468-17474.

200. Vergnes A, Pommier J, Toci R, Blasco F, Giordano G, Magalon A: **NarJ chaperone binds on two distinct sites of the aponitrate reductase of *Escherichia coli* to coordinate molybdenum cofactor insertion and assembly**. *The Journal of Biological Chemistry* 2005, **281**(4):2170-2176.

201. Marietou A, Richardson D, Cole J, Mohan S: **Nitrate reduction by *Desulfovibrio desulfuricans*: a periplasmic nitrate reductase system that lacks NapB, but includes a unique tetraheme *c*-type cytochrome, NapM**. *FEMS Microbiology Letters* 2005, **248**(2):217-225.

202. Taoka A, Yoshimatsu K, Kanemori M, Fukumori Y: **Nitrate Reductase from the magnetotactic bacterium *Magnetospirillum magnetotacticum* MS-1 : purification and sequemce analysis**. *Canadian Journal Microbiology* 2003, **49**:197-206.

203. Craske A, Ferguson SJ: **The respiratory nitrate reductase from *Paracoccus denitrificans***. *European Journal of Biochemistry* 1986, **158**(2):429-436.

204. Moura I, Bursakov S, Costa C, Moura JJG: **Nitrate and nitrite utilization in sulfate-reducing bacteria**. *Anaerobe* 1997, **3**(5):279-290.

205. Bursakov SA, Carneiro C, Almendra MJ, Duarte RO, Caldeira J, Moura I, Moura JJG: **Enzymatic Properties and Effect of Ionic Strength on Periplasmic Nitrate Reductase (NAP) from *Desulfovibrio desulfuricans* ATCC 27774**. *Biochemical and Biophysical Research Communications* 1997, **239**:816-822.

206. Bird L: **Cloning and Heterologous Expression of the *napA* gene from *Sulfurospirillum barnesii***. Pittsburgh, PA Duquesne University 2007.

207. Altekruse SF, Stern NJ, Fields PI, Swerdlow DL: ***Campylobacter jejuni*—An emerging foodborne pathogen**. *Emerging Infectious Diseases* 1999, **5**(1).

208. Marshall B, Warren JR: **Unidentified curved bacilli in the stomach of patients with gastritis and peptic ulceration** *The Lancet* 1984, **323**(8390):1311-1315.

209. Tabata A, Yamamoto I, Matsuzaki M, Satoh T: **Differential regulation of periplasmic nitrate reductase gene (*napKEFDABC*) expression between aerobiosis and anaerobiosis with nitrate in a denitrifying phototroph *Rhodobacter sphaeroides* f. sp. *denitrificans***. *Archives of Microbiology* 2005, **184**(2):108-116.

210. Visiers I, Ballesteros JA, Weinstein H, Ravi Iyengar and John DH: **Three-dimensional representations of G protein-coupled receptor structures and mechanisms**. In: *Methods in Enzymology*. vol. Volume 343: Academic Press; 2002: 329-371.

211. Indarte M, Madura JD, Surratt CK: **Dopamine transporter comparative molecular modeling and binding site prediction using the LeuT(Aa) leucine transporter as a template.** . *Proteins* 2008, **70**(3):1033-1046.

212. Esposito EX, Tobi D, Madura JD: **Comparative Protein Modeling**, vol. 22. Hoboken NJ: J Wiley and Sons, Inc. ; 2006.

213. Seto M, Whitlow M, McCarrick MA, Srinivasan S, Zhu Y, Pagila R, Mintzer R, Light D, Johns A, Meurer-Ogden JA: **A model of the acid sphingomyelinase phosphoesterase domain based on its remote structural homolog purple acid phosphatase**. *Protein Sci* 2004, **13**(12):3172-3186.

214. Tamura K, Dudley J, Nei M, Kumar S: **MEGA4: Molecular Evolutionary Genetics Analysis (MEGA) Software Version 4.0**. *Molecular Biology and Evolution* 2007, **24**(8):1596-1599.

215. Arnoux P, Sabaty M, Alric J, Frangioni B, Guigliarelli B, Adriano J-M, Pignol D: **Structural and redox plasticity in the heterodimeric periplasmic nitrate reductase,"** *Nature Structural Biology* 2003, **10**(11):928-924.

216. Henikoff S, Henikoff JG: **Amino acid substitution matrices from protein blocks**. In: *Proceedings of the National Academy of Science: 1992; USA*; 1992: 10915.

217. Humphrey W, Dalke A, Schulten K: **VMD - Visual Molecular Dynamics**. *J MolecGraphics* 1996, **14**(1):33-38.

218. Jones S, Thornton JM: **Principles of protein-protein interactions**. *Proceedings of the National Academy of Sciences* 1996, **93**(1):13-20.

219. Jepson BJN, Marietout A, Mohan S, Cole JA, Butler CS, Richardson DJ: **Evolution of the soluble nitrate reductase: defining the monomeric periplasmic nitrate reductase subgroup.** *Biochem Soc Trans* 2006, **36**(1):122-126.

220. Gao H, Yang ZK, Barua S, Reed SB, Romine MF, Nealson KH, Fredrickson JK, Tiedje JM, Zhou J: **Reduction of nitrate in *Shewanella oneidensis* depends on atypical NAP and NRF systems with NapB as a preferred electron transport protein from CymA to NapA**. *The ISME Journal* 2009, **3**: 966-976.

221. Kinoshita K, Nakamura H: **Identification of protein biochemical functions by similarity search using the molecular surface database eF-site**. *Protein Science* 2003 **12**:1589-1595.

222. Sabaty M, Avazeri C, Pignol D, Vermeglio A: **Characterization of the reduction of selenate and tellurite by nitrate reductases**. *Appl Environ Microbiol* 2001, **67**(11):5122-5126.

223. Food and Nutrition Board IoM: **Chromium**. In: *Dietary reference intakes for vitamin A, vitamin K, boron, chromium, copper, iodine, iron, manganese, molybdenum, nickel, silicon, vanadium, and zinc.* Edited by Food and Nutrition Board IoM. Washington, D.C.: National Academy Press; 2001: 197-223.

224. Singh J, Pritchard DE, Carlisle DL, McLean JA, Montaser A, Orenstein JM, Patierno SR: **Internalization of carcinogenic lead chromate particles by cultured normal human lung epithelial cells: formation of intracellular lead-inclusion bodies and induction of apoptosis**. *Toxicology and Applied Pharacology* 1999, **161**(3):240-248.

225. Gaggelli E, Berti F, D'Amelio N, Gaggelli N, Valensin G, Bovalini L, Paffetti A, Trabalzini L: **Metabolic pathways of carcinogenic chromium**. *Environmental Health Perspectives* 2002, **110** (5):733-738.

226. Anderson RA: **Chromium, glucose intolerance and diabetes.** *Journal of the American College of Nutrition* 1998 **17**(6):548-555.

227. Mertz W: **Chromium in human nutrition: A review**. *The Journal of Nutrition* 1993, **123**(4):626-633.

228. Levina A, Lay PA: **Chemical properties and toxicity of chromium(III) nutritional supplements**. *Chemical Research in Toxicology* 2008, **21**(3):563-571.

229. Vincent JB: **The Biochemistry of Chromium**. *The Journal of Nutrition* 2000, **130**(4):715-718.

230. Stearns DM: **Is chromium a trace essential metal?** *BioFactors* 2000, **11**(3):149-162.

231. Lamson DS, Plaza SM: **The safety and efficacy of high-dose chromium**. *Alternative Medicine Review* 2002, **7**(3):218.

232. Vincent J: **Recent developments in the biochemistry of chromium(III)**. *Biological Trace Element Research* 2004, **99**(1):1-16.

233. Rai D, Eary LE, Zachara JM: **Environmental chemistry of chromium**. *Science of The Total Environment* 1989, **86**(1-2):15-23.

234. **Search Superfund Site Information**. In., July 16, 2010 edn: Environmental protection agency; 2011.

235. Middleton SS, Latmani RB, Mackey MR, Ellisman MH, Tebo BM, Criddle CS: **Cometabolism of Cr(VI) by *Shewanella oneidensis* MR-1 produces cell-associated reduced chromium and inhibits growth**. *Biotechnology and Bioengineering* 2003, **83**(6):627-637.

236. Kourtev PS, Nakatsu CH, Konopka A: **Inhibition of nitrate reduction by chromium(VI) in anaerobic soil microcosms**. *Applied and Environmental Microbiology* 2009, **75**(19):6249-6257.

237. Ishibashi Y, Cervantes C, Silver S: **Chromium reduction in *Pseudomonas putida***. *Applied and Environmental Microbiology* 1990, **56**(7):2268-2270.

238. Park CH, Keyhan M, Wielinga B, Fendorf S, Matin A: **Purification to homogeneity and characterization of a novel *Pseudomonas putida* chromate reductase**. *Applied and Environmental Microbiology* 2000, **66**(5):1788-1795.

239. Ramírez-Díaz M, Díaz-Pérez C, Vargas E, Riveros-Rosas H, Campos-García J, Cervantes C: **Mechanisms of bacterial resistance to chromium compounds**. *BioMetals* 2008, **21**(3):321-332.

240. Opperman DJ, Piater LA, Heerden Ev: **A novel chromate reductase from *Thermus scotoductus* SA-01 related to old yellow enzyme**. *Journal of Bacteriology* 2008, **190**(8):3076-3082.

241. Mohammad Zubair Alam AM: **Chromate resistance, transport and bioreduction by *Exiguobacterium* sp. ZM-2 isolated from agricultural soil irrigated with tannery effluent**. *Journal of Basic Microbiology* 2008, **48**(5):416-420.

242. Gonzalez CF, Ackerley DF, Lynch SV, Matin A: **ChrR, a soluble quinone reductase of *Pseudomonas putida* that defends against H_2O_2**. *Journal of Biological Chemistry* 2005, **280**(24):22590-22595.

243. Barak Y, Ackerley DF, Dodge CJ, Banwari L, Alex C, Francis AJ, Matin A: **Analysis of novel soluble chromate and uranyl reductases and generation of an improved enzyme by directed evolution**. *Applied and Environmental Microbiology* 2006, **72**(11):7074-7082.

244. Sedlácek V, Spanning RJMv, Kucera I: **Characterization of the quinone reductase activity of the ferric reductase B protein from *Paracoccus denitrificans***. *Archives of Biochemistry and Biophysics* 2009, **483**(1):29-36.

245. Kwak YH, Lee DS, Kim HB: ***Vibrio harveyi* nitroreductase is also a chromate reductase**. *Applied and Environmental Microbiology* 2003, **69**(8):4390-4395.

246. Lovley DR, Phillips EJP: **Reduction of chromate by *Desulfovibrio vulgaris* and its c3 cytochrome**. *Applied and Environmental Microbiology* 1994, **60**(2):726-728.

247. Chardin B, Giudici-Orticoni MT, De Luca G, Guigliarelli B, Bruschi M: **Hydrogenases in sulfate-reducing bacteria function as chromium reductase**. *Applied Microbiology and Biotechnology* 2003 **63**(3):315-321.

248. Lovley DR, Giovannoni SJ, White DC, Champine JE, Phillips EJP, Gorby YA, Goodwin S: ***Geobacter metallireducens* gen. nov. sp. nov., a microorganism capable of coupling the complete oxidation of organic compounds to the reduction of iron and other metals**. *Archives of Microbiology* 1993, **159**(4):336-344.

249. Lopes FA, Morin P, Oliveira R, Melo LF: **Interaction of *Desulfovibrio desulfuricans* biofilms with stainless steel surface and its impact on bacterial metabolism**. *Journal of Applied Microbiology* 2006 **101**(5):1087-1095.

250. Murillo F, Stolz JF: **Preparative Native PAGE Purification of Membrane Bound Active Nitrate Reductases**. In: *US/EG Bulletin 2028*. Edited by Bio-Rad.

251. Martínez Murillo F, Gugliuzza T, Senko J, Basu P, Stolz JF: **A heme-C-containing enzyme complex that exhibits nitrate and nitrite reductase**

activity from the dissimilatory iron-reducing bacterium *Geobacter metallireducens*. *Archives of Microbiology* 1999, **172**(5):313-320.

252. Jones RW, Garland PB: **Sites and specificity of the reaction of bipyridylium compounds with anaerobic respiratory enzymes of *Escherichia coli***. *Biochemical Journal* 1977, **164**:199-211.

253. Bueno E, Bedmar EJ, Richardson DJ, Delgado MJ: **Role of *Bradyrhizobium japonicum* cytochrome c550 in nitrite and nitrate respiration**. *FEMS Microbiology Letters* 2008, **279**(2):188-194.

254. Wang T-H, Fu H, Shieh Y-J: **Monomeric NarB Is a Dual-Affinity Nitrate Reductase, and Its Activity Is Regulated Differently from That of Nitrate Uptake in the Unicellular Diazotrophic Cyanobacterium *Synechococcus* sp. Strain RF-1**. *Journal of Bacteriology* 2003, **185**(19):5838-5846.

255. Borcherding H, Leikefeld S, Frey C, Diekmann S, cke PS: **Enzymatic Microtiter Plate-Based Nitrate Detection in Environmental and Medical Analysis**. *Analytical Biochemistry* 2000, **282**:1-9.

256. Fry IV, Cammack R, Hucklesby DP, Hewitt EJ: **Kinetics of leaf nitrite reductase with methyl viologen and ferredoxin under controlled redox conditions**. *Biochemical Journal* 1982, **205**(1):235-238.

257. Loach PA: **Oxidation-reduction potentials, absorbance bands and molar absorbance of compounds used in biochemical studies**. In: *Physical and Chemical Data.* vol. I, 3 edn: CRC Press; 2000: 122-130.

258. Saha R, Nandi R, Saha B: **Sources and toxicity of hexavalent chromium**. *Journal of Coordination Chemistry* 2011, **64**(10):1782 - 1806.

259. Garg BS, Mehta YL, Katyal M: **Sensitive tests for nitrite through azo-dye formation**. *Talanta* 1976, **23**(1):71-71.

260. Einsle O, Messerschmidt A, Stach P, Bourenkov GP, Bartunik HD, Huber R, Kroneck PMH: **Structure of cytochromec nitrite reductase**. *Nature* 1999, **400**:476-480.

261. Seki Y, Nagai Y, Ishimoto M: **Characterization of a Dissimilatory-Type Sulfite Reductase, Desulfoviridin, from Desulfovibrio africanus Benghazi**. *Journal of Biochemistry* 1985, **98**(6):1535-1543.

262. Johnson JL, Hainline BE, Rajagopalan KV, Arison BH: **The pterin component of the molybdenum cofactor. Structural characterization of two fluorescent derivatives**. *Journal of Biological Chemistry* 1984, **259**(9):5414-5422.